

Neuroarchitecture and central regulation
of peptidergic systems in the ventral ganglion of
Drosophila melanogaster

(Neuroarchitektur und zentrale Regulation von peptidergen Systemen
im Ventralganglion von *Drosophila melanogaster*)

Dissertation zur Erlangung des Doktorgrades
der Naturwissenschaften (Dr. rer. nat.)

dem Fachbereich Biologie
der Philipps-Universität Marburg
vorgelegt von

Matthias Vömel
aus Seeheim-Jugenheim.

Marburg/Lahn, Mai 2008

Vom Fachbereich Biologie der Philipps-Universität Marburg
als Dissertation am angenommen.

Erstgutachter: Prof. Dr. Uwe Homberg

Zweitgutachter: Prof. Dr. Joachim Schachtner

Tag der mündlichen Prüfung am

Contents

Erklärung: Eigene Beiträge und veröffentlichte Teile der Arbeit.....	1
Zusammenfassung.....	3
Introduction.....	9
I. Neuroarchitecture of peptidergic systems in the larval ventral ganglion of <i>Drosophila melanogaster</i>	27
II. Neuroarchitecture of aminergic systems in the larval ventral ganglion of <i>Drosophila melanogaster</i>	47
III. Neurotransmitter-induced changes in the intracellular calcium concentration suggest a differential central modulation of CCAP neuron subsets in <i>Drosophila</i>	67
IV. A method for the synaptic isolation of CCAP neurons during calcium imaging experiments in the intact central nervous system of <i>Drosophila</i>	87
V. A method for the genetic silencing of nicotinic acetylcholine receptors on the CCAP neurons of <i>Drosophila</i>	95
VI. Venus-tagged peptides for the visualization of neuropeptide transport and release in <i>Drosophila</i>	103

Erklärung: Eigene Beiträge und veröffentlichte Teile der Arbeit

Laut Promotionsordnung der Philipps-Universität Marburg (in der Fassung vom 12.4.2000) müssen bei Teilen der Dissertation, die aus gemeinsamer Forschungsarbeit entstanden sind, „die individuellen Leistungen des Doktoranden deutlich abgrenzbar und bewertbar sein.“ Da dies alle Kapitel meiner Dissertation betrifft, werde ich meinen individuellen Beitrag zu jedem dieser Kapitel im Folgenden erläutern:

Kapitel I: „Neuroarchitecture of peptidergic systems in the larval ventral ganglion of *Drosophila melanogaster*.“

- Durchführung und Auswertung von etwa einem Drittel der Experimente.
- Entwicklung der standardisierten schematischen Präsentation und Beschreibung von 3D-kartieren Neuronen in der anterior-posterior Achse des larvalen Ventralganglions.
- Verfassen der Veröffentlichung in Zusammenarbeit mit den Mitautoren.
- Veröffentlichung: Santos JG, Vömel M, Struck R, Homberg U, Nässel DR, Wegener C. (2007). PLoS ONE 2(8): e695.
Das vorliegende Kapitel entspricht der Veröffentlichung.

Kapitel II: „Neuroarchitecture of aminergic systems in the larval ventral ganglion of *Drosophila melanogaster*.“

- Planung der Experimente in Zusammenarbeit mit Dr. Christian Wegener.
- Durchführung und Auswertung aller Experimente.
- Verfassen der Veröffentlichung in Abstimmung mit Dr. Christian Wegener.
- Veröffentlichung: Vömel M, Wegener C. (2008). PLoS ONE 3(3): e1848.
Das vorliegende Kapitel entspricht der Veröffentlichung.

Kapitel III: „Neurotransmitter-induced changes in the intracellular calcium concentration suggest a differential central modulation of CCAP neuron subsets in *Drosophila*.“

- Planung der Experimente in Zusammenarbeit mit Dr. Christian Wegener.
- Entwicklung und Umsetzung der Methoden zum Ca²⁺-Imaging mit genetisch kodierten Calcium-Indikatoren in Zellkultur und im intakten Ventralganglion von *Drosophila*.
- Durchführung und Auswertung aller Experimente.
- Verfassen der Veröffentlichung in Abstimmung mit Dr. Christian Wegener.
- Veröffentlichung: Vömel M, Wegener C. (2007). Dev Neurobiol 67: 792-809.
Das vorliegende Kapitel entspricht der Veröffentlichung.

Kapitel IV: „A method for the synaptic isolation of CCAP neurons during calcium imaging experiments in the intact central nervous system of *Drosophila*.“

- Herstellen der transgenen Fliegenstämme in Zusammenarbeit mit Dr. Christian Wegener.
- Durchführung und Auswertung aller Experimente.
- Verfassen des Manuskripts in Abstimmung mit Dr. Christian Wegener.

Kapitel V: „A method for the genetic silencing of nicotinic acetylcholine receptors on the CCAP neurons of *Drosophila*.“

- Planung der Experimente in Zusammenarbeit mit Dr. Christian Wegener.
- Durchführung und Auswertung aller Experimente.
- Verfassen des Manuskripts in Abstimmung mit Dr. Christian Wegener.

Kapitel VI: „Venus-tagged peptides for the visualization of neuropeptide transport and release in *Drosophila*.“

- Planung der Experimente.
- Herstellen der DNA-Konstrukte und transgenen Fliegen.
- Durchführung und Auswertung aller Experimente.
- Verfassen des Manuskripts in Abstimmung mit Dr. Christian Wegener.

Über diese Arbeiten hinaus habe ich im Rahmen meiner Doktorarbeit noch an thematisch verwandten Projekten mitgewirkt, die für weitere Studien der AG Wegener von Bedeutung sind, aber nicht Teil meiner Dissertation sind. Diese Projekte befassen sich mit der enzymatischen Prozessierung des CAPA-Präpropeptids und der Spezifität verschiedener Prohormonkonvertasen von *Drosophila*. Die Ergebnisse dieser Projekte liegen bereits teilweise vor, sind momentan aber noch nicht zur Veröffentlichung vorgesehen.

Außerdem habe ich die Arbeitsgruppe von Prof. Dr. Joachim Schachtner in einem Projekt unterstützt, das zum Ziel hatte, die Expression des Neuropeptids Mas-Allatotropin im Geruchssystem des Tabakswärmers *Manduca sexta* zu untersuchen. Die Ergebnisse dieses Projektes wurden bereits veröffentlicht, sind aber ebenfalls nicht Bestandteil meiner Dissertation:

- Veröffentlichung: Utz S, Huetteroth W, Vömel M, Schachtner J. (2008). Mas-allatotropin in the developing antennal lobe of the sphinx moth *Manduca sexta*: distribution, time course, developmental regulation, and colocalization with other neuropeptides. *Dev Neurobiol* 68: 123-142.

Die Abfassung der Dissertation in englischer Sprache wurde vom Dekan des Fachbereichs Biologie am 09.04.2008 genehmigt.

Zusammenfassung

Neurone kommunizieren mit ihren Zielzellen über Botenstoffe, die man im allgemeinen drei Hauptgruppen zuordnen kann, klassischen Neurotransmittern, Neuropeptiden und unkonventionellen Transmittern (wie z.B. gasförmige Signalstoffe). Klassische Neurotransmitter sind typischerweise Aminosäuren oder Aminosäurederivate, die in der Nähe der Präsynapse synthetisiert und in den synaptischen Spalt freigesetzt werden. Dementsprechend dienen klassische Neurotransmitter meistens der lokalen Signalübertragung über kurze Distanzen hinweg. Im Vergleich zu den klassischen Neurotransmittern sind Neuropeptide komplexere Signalmoleküle, die im Zellkörper synthetisiert und sowohl an Synapsen als auch an nicht-synaptischen Bereichen freigesetzt werden können. Werden Neuropeptide in den Blutkreislauf sekretiert, wirken sie häufig als Neurohormone, die die Aktivität von entfernt gelegenen Zielzellen beeinflussen.

Da Neuropeptide in Wirbeltieren wie in Wirbellosen eine Vielzahl von essentiellen physiologischen Vorgängen regulieren wie z.B. Lernen, Reproduktion und Wachstum, gibt es zahlreiche Untersuchungen darüber, wo bestimmte Neuropeptide synthetisiert und ausgeschüttet werden, welche Zielzellen sie beeinflussen und welche physiologische Funktion sie dabei erfüllen. Relativ unbekannt ist allerdings, wie die neuronale Aktivität von peptidergen Neuronen und damit die Peptidfreisetzung vom zentralen Nervensystem kontrolliert wird.

Die vorliegende Dissertation hatte deshalb zum Ziel, die zentrale Regulation von peptidergen Systemen im ventralen Nervensystem der *Drosophila* Larve zu untersuchen. Die Arbeit besteht aus sechs Kapiteln, die zu drei Themenkomplexen gehören:

- Beschreibung der Morphologie und Neuroarchitektur von peptidergen und potentiell interagierenden aminergen Systemen im ventralen Nervensystem der *Drosophila* Larve mit Hilfe von Immunzytochemie, zell-spezifischer Expression von Markerproteinen, konfokaler Laser-Rastermikroskopie und 3D-Rekonstruktion (Kapitel I und II).
- Identifizierung von Neurotransmittern, die an der zentralen Regulation der häutungs-relevanten CCAP Neurone beteiligt sind (Kapitel III), durch „Calcium Imaging“. Entwicklung von Methoden zur transienten synaptischen Isolierung von CCAP Neuronen in „Calcium Imaging“-Experimenten (Kapitel IV) bzw. zur zell-spezifischen Inhibierung von nikotinischen Acetylcholin-Rezeptoren (Kapitel V).
- Herstellung und Charakterisierung von Fluorophor-gekoppelten Peptiden zur Messung der Peptidfreisetzung aus peptidergen *Drosophila* Neuronen; hier kamen molekularbiologische und proteinbiochemische Techniken zum Einsatz.

Kapitel I: Neuroarchitektur von peptidergen Systemen im larvalen Ventralganglion von *Drosophila melanogaster*

Santos JG, Vömel M, Struck R, Homberg U, Nässel DR, Wegener C. (2007). Neuroarchitecture of peptidergic systems in the larval ventral ganglion of *Drosophila melanogaster*. PLoS ONE 2(8): e695.

Um zu verstehen, wie das zentrale Nervensystem die Aktivität von peptidergen Neuronen kontrolliert, ist es essentiell, die Neurone zu identifizieren, die mit peptidergen Neuronen interagieren. Das ventrale Nervensystem der *Drosophila* Larve („larval ventral ganglion“, LVG) bietet dafür ideale Voraussetzungen, da es genetisch zugänglich und mit seinen ca. 10.000 Neuronen und dem segmentalen Aufbau vergleichsweise übersichtlich ist (- das Gehirn von *Drosophila* besteht beispielsweise aus mehr als 50.000 Neuronen). Im LVG können darüberhinaus identifizierte Neurone und ihre Projektionen in einem Landmarkensystem dreidimensional kartiert werden. Dieses Landmarkensystem, das mit einem kommerziell erhältlichen Antikörper gegen das Zelladhäsionsmolekül Fasciclin2 (Fas2) markiert werden kann, ist zwischen verschiedenen Larven und während der Larvalentwicklung konstant und erlaubt somit einen schnellen und räumlich genauen Abgleich von Projektionsmustern verschiedener Neurone. Da bereits diverse sensorische Neurone und Motoneurone im Fas2 Landmarkensystem kartiert wurden, besteht ferner die Möglichkeit, über den Vergleich von „Fas2-Koordinaten“ potenzielle Netzwerkkontakte von peptidergen Neuronen zu identifizieren. Vermutete synaptische Kontakte können dann in weiterführenden Experimenten z.B. auf elektronen-mikroskopischer Ebene genauer analysiert werden.

Mittels Immunzytochemie und zell-spezifischer Expression von fluoreszierenden Markerproteinen konnten 12 peptiderge Neuronengruppen im Fas2 Landmarkensystem des LVG kartiert werden. Diese Neuronengruppen exprimieren die folgenden Präpropeptid-Gene: *Ast* (CG13633), *capa* (CG15520), *Ccap* (CG4910), *Crz* (CG3302), *Eh* (CG5400), *Fmrf* (CG2346), *hug* (CG6371), *IFa* (CG33527), *Leucokinin* (CG13480), *Mip* (CG6456), *Pdf* (CG6496) und *Tk* (CG14734). Abgesehen von den *Mip*-exprimierenden Neuronen zeigten die beschriebenen peptidergen Neuronengruppen keine serielle Homologie, sondern eine Segment-spezifische Verteilung. Peptiderge Neurite projizieren häufig entlang Fas2-immunreaktiver Fasern und verzweigen im medianen Neuropil. Die Analyse von ektopisch exprimierten prä- und postsynaptischen Markerproteinen deutet darauf hin, dass peptiderge Neurone definierte Ein- und Ausgangsregionen besitzen: Peptiderge Verzweigungen im medianen Neuropil scheinen vor allem dendritische Kompartimente (- also Eingangsregionen -) zu bilden. Einige absteigende Neurite im medianen Neuropil könnten aber auch Ausschüttungszonen für bestimmte Peptide wie z.B. CCAP, EH und Leucokinin (- also Ausgangsregionen -) sein. Das letzte abdominale Segment, der sogenannte „terminale Plexus“ zeigte eine besonders dichte Innervierung mit Neuriten verschiedener peptiderger Neuronengruppen und enthält vermutlich sowohl dendritische Kompartimente als auch Ausschüttungszonen. Weitere putative Ausschüttungszonen für Peptide befinden sich an absteigenden Neuriten im intermedialen und lateralen Neuropil. Da diese absteigenden Neurite eine starke Peptid-Immunreaktivität in vielen kurzen Varikositäten aufwiesen, scheinen Neuropeptide im LVG häufig abseits von Synapsen freigesetzt zu werden.

Die dreidimensionale Kartierung erlaubt es nun, die Verteilungs- und Projektionsmuster der verschiedenen peptidergen Neuronengruppen mit denen anderer Neuronengruppen zu vergleichen und potentielle Netzwerkkontakte und co-exprimierte Proteine (z.B. Peptidrezeptoren) zu identifizieren.

Kapitel II: Neuroarchitektur von aminergen Systemen im larvalen Ventralganglion von *Drosophila melanogaster*

Vömel M, Wegener C. (2008). Neuroarchitecture of aminergic systems in the larval ventral ganglion of *Drosophila melanogaster*. PLoS ONE 3(3): e1848.

Nachdem wir die meisten peptidergen Neurone des LVG im Fas2 Landmarkensystem kartiert hatten, ging es nun darum, Neurotransmitter-synthetisierende Neurone zu identifizieren, die mit peptidergen Neuronen interagieren könnten. Neurotransmitter wie Acetylcholin (ACh) oder γ -Aminobuttersäure (GABA) werden in mehreren hundert Neuronen des LVG synthetisiert und regulieren sehr wahrscheinlich zumindest einige peptiderge Neurone. Aufgrund der großen Anzahl von cholinergen/GABAergen Neuriten im zentralen Neuropil ist es jedoch mittels konfokaler Laser-Rastermikroskopie nicht möglich, diejenigen Neurone zu identifizieren, die mit einer bestimmten peptidergen Neuronengruppe in synaptischem Kontakt stehen. Deshalb beschlossen wir, die aminergen Neurone des LVG im Fas2 Landmarkensystem zu kartieren, da diese nur in vergleichsweise geringer Zahl in den Segmenten des LVG vorkommen, stereotype Verteilungsmuster zeigen und individuell identifizierbar sind.

Mittels Immunzytochemie und zell-spezifischer Expression von fluoreszierenden Markerproteinen wurden serotonerge, dopaminerge und tyraminerge/octopaminerge Neurone kartiert und ihre neuronalen Kompartimente mit ektopisch exprimierten prä- und postsynaptischen Markern charakterisiert. Unsere Ergebnisse deuten darauf hin, dass serotonerge und dopaminerge Neurone hauptsächlich bei der Verarbeitung sensorischer Information und der Regulation zentraler Netzwerke beteiligt sind, während tyraminerge/octopaminerge Neurone vor allem Prozesse in der Peripherie zu beeinflussen scheinen. Im Gegensatz zu den serotonergen Neuronen, die eine homogene Gruppe bilden, gehören die dopaminergen und tyraminergen/octopaminergen Neurone des LVG verschiedenen Untergruppen an, die sich vermutlich nicht nur morphologisch, sondern auch funktionell unterscheiden.

Der Vergleich der Projektionsmuster von putativen aminergen Neuronen mit denen der peptidergen Neurone erbrachte außerdem die überraschende Erkenntnis, dass einige DOPA-Decarboxylase exprimierende Neurone des LVG - zumindest im dritten Larvenstadium - keine biogenen Amine, sondern stattdessen die Neuropeptide CCAP, MIP oder Corazonin synthetisieren. Dies zeigt, wie ein Fas2-basierter Vergleich von dreidimensionalen Projektionsmustern zur Identifizierung von co-lokalisierten Signalsubstanzen führen kann.

Kapitel III: Neurotransmitter-induzierte Veränderungen in der intrazellulären Calcium-Konzentration lassen auf eine differentielle, zentrale Modulation der CCAP Neuronen von *Drosophila* schließen

Vömel M, Wegener C. (2007). Neurotransmitter-induced changes in the intracellular calcium concentration suggest a differential central modulation of CCAP neuron subsets in *Drosophila*. Dev Neurobiol 67: 792-809.

Die Fas2-basierten morphologischen Analysen legten nahe, dass peptiderge Neurone im LVG Eingang von Neurotransmitter-synthetisierenden Neuronen erhalten. Weitgehend unbekannt war allerdings, ob peptiderge Neurone überhaupt Neurotransmitterrezeptoren exprimieren und auf bestimmte Neurotransmitter reagieren können. Um diese Frage zu beantworten untersuchten wir in Calcium Imaging-Experimenten, ob verschiedene Neurotransmitter die intrazelluläre Calcium-Konzentration ($[Ca^{2+}]_i$) von „Crustacean cardioactive peptide“-

Zusammenfassung

synthetisierenden Neuronen (N_{CCAP}) beeinflussen. Da Peptidausschüttung von einem Anstieg der $[Ca^{2+}]_i$ abhängt, müssen potentiell regulierende Neurotransmitter dazu fähig sein, die $[Ca^{2+}]_i$ der N_{CCAP} zu verändern.

In einer ersten Serie von Calcium Imaging-Experimenten wurde ein grün-fluoreszierendes Protein (GFP) in den N_{CCAP} ektopisch exprimiert und anschließend die Neurone des Ventralganglion der entsprechenden Larve in primäre Zellkultur überführt. Die kultivierten Neurone wurden dann mit dem synthetischen, Calcium-sensitiven Farbstoff Fura-2 beladen, und ein in der Kultur isoliert liegendes N_{CCAP} anhand seiner GFP-Fluoreszenz identifiziert. In dem darauffolgenden Experiment wurde das N_{CCAP} transient verschiedenen Neurotransmittern ausgesetzt und gleichzeitig die $[Ca^{2+}]_i$ des N_{CCAP} gemessen. Es zeigte sich, dass fast alle N_{CCAP} in Zellkultur mit einem starken Anstieg der $[Ca^{2+}]_i$ auf ACh und Nikotin antworteten, während nur wenige N_{CCAP} auf den muskarinischen ACh-Rezeptor-Agonist Pilocarpin reagierten. Glutamat und der AMPA/Kainat-Rezeptor Agonist Quisqualat bewirkten einen Anstieg der $[Ca^{2+}]_i$ in etwa einem Drittel der N_{CCAP} . Der inhibitorische Transmitter GABA blockierte oder reduzierte in etwa der Hälfte der N_{CCAP} den ACh-vermittelten Anstieg der $[Ca^{2+}]_i$. Diese Ergebnisse deuten darauf hin, dass die meisten N_{CCAP} funktionelle nikotinische ACh-Rezeptoren (nAChRs) exprimieren, aber nur definierte N_{CCAP} Untergruppen Glutamat- oder GABA-Rezeptoren tragen.

Um herauszufinden, welche N_{CCAP} welchen Neurotransmitter-Rezeptor besitzen, wurde in den N_{CCAP} gezielt der genetisch-kodierte Calcium Indikator GCaMP 1.6 exprimiert und das Antwortverhalten der N_{CCAP} auf Neurotransmitter-Applikation im intakten larvalen und adulten Gehirn gemessen. Erstaunlicherweise reagierten nur wenige N_{CCAP} auf cholinerge Agonisten mit einem Anstieg der $[Ca^{2+}]_i$ oder $[Ca^{2+}]_i$ -Oszillationen. Die wenigen reagierenden N_{CCAP} gehörten zu einer definierten Neuronengruppe, die neurohämale Ausschüttungszonen an der Körperwandmuskulatur besitzen. Die meisten N_{CCAP} zeigten einen ausgeprägten Abfall der $[Ca^{2+}]_i$ nach Applikation von cholinergen Agonisten, der möglicherweise auf die Aktivierung von präsynaptischen, inhibitorischen Neuronen zurückzuführen ist. Zusammengefasst lassen unsere Calcium Imaging-Experimente den Schluss zu, dass verschiedene Neurotransmitter bei der Regulation von spezifischen N_{CCAP} -Neuronengruppen beteiligt sein.

Kapitel IV: Eine Methode zur synaptischen Isolierung von CCAP Neuronen in Calcium Imaging-Experimenten am intakten Nervensystem von *Drosophila*

Vömel M, Wegener C. (2008). A method for the synaptic isolation of CCAP neurons during calcium imaging experiments in the intact CNS of *Drosophila*.

Unsere Calcium Imaging-Experimente deuteten darauf hin, dass N_{CCAP} im intakten Nervensystem nicht nur direkt auf systemische Neurotransmitter Applikation reagieren, sondern auch zeitgleich synaptischen Eingang von afferenten Neuronen bekommen. Um in Calcium Imaging-Experimenten die N_{CCAP} identifizieren zu können, die einen bestimmten Neurotransmitter-Rezeptor besitzen, müssen alle N_{CCAP} im intakten LVG von etwaigen afferenten Neuronen synaptisch isoliert werden.

Zu diesem Zweck erzeugten wir transgene Fliegen, die spezifisch in den N_{CCAP} den genetisch kodierten Calcium Indikator GCaMP 1.6 exprimieren und außerdem im gesamten Nervensystem das temperatursensitive Dynamin-Protein Shibire (Shi^{ts}) synthetisieren. Shi^{ts} ist eine GTPase, die bei permissiver Temperatur für das Recycling von synaptischen Vesikeln zuständig ist. Bei restriktiver Temperatur wird Shi^{ts} funktionsunfähig und

blockiert die synaptische Übertragung. Mit den erzeugten Fliegen wird es in zukünftigen Calcium Imaging-Experimenten möglich sein, die Signalübertragung von präsynaptischen Neuronen auf alle N_{CCAP} transient auszuschalten und gleichzeitig die Wirkung von systemisch applizierten Neurotransmittern auf die $[Ca^{2+}]_i$ identifizierter N_{CCAP} zu untersuchen. Damit erhoffen wir uns, alle N_{CCAP} identifizieren zu können, die beispielsweise GABA-Rezeptoren besitzen.

Kapitel V: Eine Methode zur Inhibierung der nikotinischen Acetylcholin-Rezeptoren der CCAP Neurone von *Drosophila*

Vömel M, Wegener C. (2008). A method for the genetic silencing of nicotinic acetylcholine receptors on the CCAP neurons of *Drosophila*.

Unsere Calcium Imaging-Experimente deuteten an, dass die meisten N_{CCAP} im LVG von *Drosophila* von cholinergen Neuronen Eingang erhalten. Ob dieser cholinerge Eingang für die sekretorische Aktivität der N_{CCAP} von Bedeutung ist, blieb allerdings unbeantwortet. Um dieser Frage nachzugehen, beschlossen wir, die nAChR der N_{CCAP} auszuschalten. Da die nAChRs von *Drosophila* aus strukturell unterschiedlichen Untereinheiten bestehen, und die genaue Zusammensetzung der nAChRs unbekannt ist, fällt es äußerst schwer, die nAChRs der N_{CCAP} mit genetischen oder molekularbiologischen Standardmethoden (wie z.B. „knock-down“ oder „knock-out“) auszuschalten. Darum versuchten wir in Calcium Imaging-Experimenten Antagonisten von nAChRs zu identifizieren, die dazu in der Lage sind, die nAChRs der N_{CCAP} permanent zu inhibieren. In einem zweiten Schritt sollten dann solche Antagonisten gezielt in den N_{CCAP} exprimiert werden, um die cholinerge Aktivierung der N_{CCAP} zu verhindern.

Mittels Fura-2-basiertem Calcium Imaging konnten wir zeigen, dass das natürlich vorkommende Peptidtoxin α -Bungarotoxin die cholinerge Aktivierung von N_{CCAP} blockieren kann. In Kooperation mit Justin Blau (New York University, NY) wurden anschließend transgene Fliegen hergestellt, die es ermöglichen, ein membranverankertes α -Bungarotoxin gezielt in den N_{CCAP} zu exprimieren. Mit diesen Fliegen wollen wir in zukünftigen Experimenten untersuchen, ob die cholinerge Aktivierung für die reguläre sekretorische Aktivität der N_{CCAP} notwendig ist. Leider liegt bislang noch nicht die rechtliche Genehmigung vor, mit den erzeugten transgenen Fliegen an der Philipps-Universität Marburg zu arbeiten.

Kapitel VI: Venus-gekoppelte Peptide zur Messung von Neuropeptid-Transport und -Freisetzung in *Drosophila*

Vömel M, Wegener C. (2008). Venus-tagged peptides for the visualization of neuropeptide transport and release in *Drosophila*.

Unsere Calcium Imaging-Experimente zeigten, dass ACh und Glutamat einen Anstieg der $[Ca^{2+}]_i$ in N_{CCAP} auslösen können. Allerdings blieb ungeklärt, ob dieser $[Ca^{2+}]_i$ -Anstieg in den N_{CCAP} zur Ausschüttung von Peptiden führt. Um herauszufinden, ob ACh und Glutamat Ausschüttungsfaktoren der N_{CCAP} sind, stellten wir zwei Fluorophor-gekoppelte Peptide her, die in den N_{CCAP} exprimiert und wie endogene Neuropeptide transportiert und ausgeschüttet werden sollten. Falls ACh und Glutamat tatsächlich eine Peptidausschüttung in den N_{CCAP} induzierten, sollten die Fluorophor-gekoppelten Peptide ebenfalls ausgeschüttet werden, und die Fluoreszenz in den Ausschüttungszonen der N_{CCAP} abnehmen.

Zusammenfassung

Mit molekularbiologischen Standardmethoden wurden zwei verschiedene cDNA Konstrukte hergestellt, die zum einen aus der cDNA des gelb-fluoreszierenden Proteins Venus und zum anderen aus der cDNA eines natürlich vorkommenden Präpropeptids, des präproANF („atrial natriuretic factor“) der Ratte bzw. des präproCAPA-1 von *Drosophila*, bestehen. Nachdem die entsprechenden cDNA-Konstrukte in das Genom von *Drosophila* unter der Kontrolle des UAS („upstream activation sequence“)-Promotors eingebracht worden waren, wurde zunächst mittels konfokaler Laser-Rastermikroskopie untersucht, ob fluoreszierende Fusionsproteine in den peptidergen Neuronen von *Drosophila* synthetisiert werden. Sowohl präproANF- als auch präproCAPA-1-Venus zeigten ein punktförmiges Verteilungsmuster in den Zellkörpern und Neuriten peptiderger Neurone. Dies lässt darauf schließen, dass beide Fusionsproteine in Vesikel verpackt werden. Um zu überprüfen, ob präproANF- und präproCAPA-1-Venus wie endogene *Drosophila*-Peptide prozessiert werden, wurden die jeweiligen Konstrukte gezielt in peptidergen Neuronen exprimiert und anschließend die in den peptidergen Neuronen aufgetretenen Prozessierungsprodukte in Western Blots charakterisiert. Es zeigte sich, dass präproANF-Venus in peptidergen *Drosophila*-Neuronen nicht zu ANF-Venus, sondern nur zu dem Zwischenprodukt proANF-Venus prozessiert wurde. Im Gegensatz dazu schien präproCAPA-1-Venus vollständig zu CAPA-1-Venus prozessiert zu werden. Da die ektopische Expression von präproCAPA-1-Venus zu einem kleineren Fusionsprotein als präproANF-Venus führte, liegt präproCAPA-1-Venus wahrscheinlich in einer vergleichsweise höheren Konzentration in peptidergen Vesikeln vor und eignet sich damit besser zur Messung der Peptidausschüttung. In zukünftigen Experimenten werden wir mit präproANF- und präproCAPA-1-Venus untersuchen, ob ACh und Glutamat die sekretorische Aktivität der N_{CCAP} beeinflussen.

Introduction

Background	11
Neuropeptide biosynthesis and signaling	11
Neuropeptide function in vertebrates and invertebrates	13
<i>Drosophila</i> as a model organism for research into peptidergic networks.....	14
The larval ventral ganglion of <i>Drosophila</i> harbors unique peptidergic networks	15
The regulation of ecdysis in <i>Drosophila</i> – a prime example of how neuropeptides orchestrate behavior.....	16
Aims of my doctoral thesis	17
Results and perspectives	18
Chapter I: Neuroarchitecture of peptidergic systems in the larval ventral ganglion of <i>Drosophila melanogaster</i>	18
Chapter II: Neuroarchitecture of aminergic systems in the larval ventral ganglion of <i>Drosophila melanogaster</i>	19
Chapter III: Neurotransmitter-induced changes in the intracellular calcium concentration suggest a differential central modulation of CCAP neuron subsets in <i>Drosophila</i>	19
Chapter IV: A method for the synaptic isolation of CCAP neurons during calcium imaging experiments in the intact CNS of <i>Drosophila</i>	21
Chapter V: A method for the genetic silencing of nicotinic acetylcholine receptors in the CCAP neurons of <i>Drosophila</i>	21
Chapter VI: Venus-tagged peptides for the visualization of neuropeptide transport and release in <i>Drosophila</i>	22
Conclusions.....	23
References.....	23

Background

The operability of a multi-cellular organism requires that cells communicate with each other in order to coordinate their actions. In the central nervous system (CNS) of metazoans, the communication between neurons and their target cells is based on the transmission of electrical signals and the controlled release of chemical signaling molecules, the so-called transmitters. To generalize, there are three groups of transmitters: Classical neurotransmitters, peptide transmitters, and unconventional transmitters (such as gaseous signaling molecules) [1].

Classical neurotransmitters are acetylcholine (ACh), amino acids like glutamate and glycine, and the glutamate derivate γ -aminobutyric acid (GABA). Other amino acid derivatives like dopamine or serotonin also belong to the group of classical neurotransmitters, but are commonly referred to as biogenic amines [1]. Classical neurotransmitters are of low molecular weight and typically synthesized close to presynaptic endings. After synthesis, classical neurotransmitters are usually packed into small synaptic vesicles and stored in the presynaptic endings. Accordingly, classical neurotransmitters are mainly released at synapses and involved in short-distance signal transmission (“wiring transmission”; [2]). The release of synaptic vesicles requires depolarization and an increase of the intracellular calcium concentration. Following release, classical neurotransmitters are inactivated by specific reuptake mechanisms and/or enzymatic degradation [1].

However, the release/reuptake of certain classical neurotransmitters is not restricted to synapses. Vesicular monoamine transporters, which transport biogenic amines (such as dopamine or norepinephrine) into large dense-core vesicles, reside within neuron somata, axons and dendrites [3,4]. Thus, certain biogenic amines can be packed into both small synaptic vesicles and large dense-core vesicles, and released from presynaptic endings as well as non-synaptic sites [2,5]. When released from non-synaptic sites, biogenic amines may diffuse in the extracellular fluid and modify the excitability of adjacent target neurons (“volume transmission”; [2]). If released into the circulation, biogenic amines may mediate long-distance signal transmission and act as neurohormones. Synaptic/non-synaptic release and neurotransmitter/-hormone action are also characteristics of the most diverse group of chemical transmitters, the peptide transmitters (neuropeptides).

Neuropeptide biosynthesis and signaling

Neuropeptides are small polypeptides of about 3-40 amino acids that occur in all metazoans possessing nervous systems, from the simple nerve nets of the cnidarians to the immensely complex nervous systems of mammals (see e.g. [6–9]). Unlike classical neurotransmitters, neuropeptides are synthesized in the neuron soma as parts of larger precursor proteins, so-called prepropeptides. Structurally diverse prepropeptides may emerge from a common but alternatively spliced RNA transcript. Alternative splicing of the pre-mRNA of the Calcitonin/CGRP gene, for example, gives rise to two prepropeptides with entirely different amino acid sequences, preproCalcitonin and preproCGRP [10].

During translation, the synthesized prepropeptides immediately enter the secretory pathway [11,12]. Nearly all prepropeptides contain a signal sequence of 20-30 amino acids that directs the prepropeptide into the lumen of the endoplasmic reticulum. There, a signal peptidase removes the signal sequence of the prepropeptide (Figure 1).

Introduction

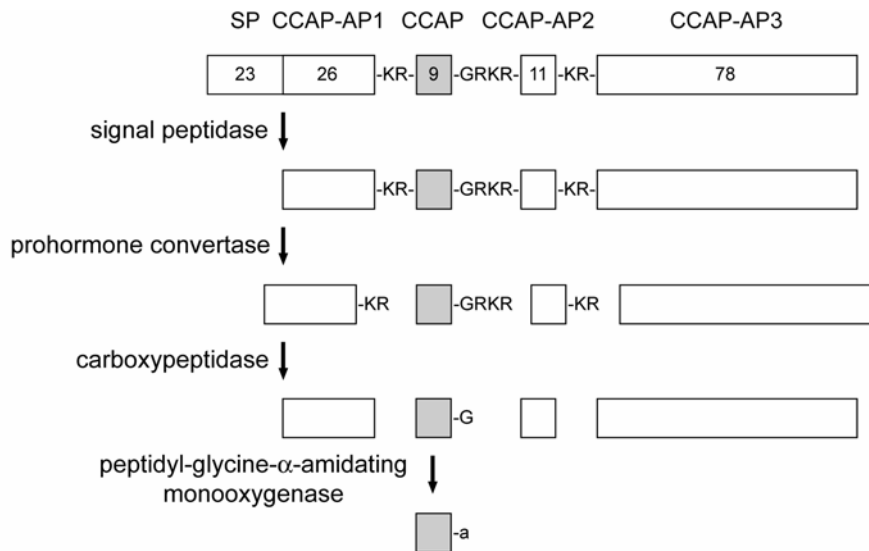


Figure 1: Proteolytical processing of preproCCAP of *Drosophila melanogaster*.

Schematic diagram of preproCCAP and the processing steps to the bioactive CCAP peptide. The grey box represents CCAP (amino acid sequence: PFCNAFTGC), whereas the white boxes represent the signal peptide (SP) and the CCAP-associated peptides (CCAP-AP) 1, 2, and 3, respectively. The numbers in the boxes indicate the amino acid lengths of the corresponding peptides. Amino acids between the boxes indicate proteolytical cleavage (KR, RKR) or amidation (G \rightarrow a) sites. See text for further details (modified from [53]).

The resulting propeptide may fold, form disulfide bonds, and assume its tertiary structure. Some propeptides (e.g. proopiomelanocortin and pro- α -mating factor,) are also glycosylated in the endoplasmic reticulum [12]. Thereafter, the propeptides are transported to the Golgi apparatus.

In the cis-Golgi, the glycosylation of the propeptides proceeds and complex carbohydrates are generated. While the propeptides pass through the Golgi stacks, they can undergo additional modifications such as acetylation, phosphorylation, or tyrosine sulfation [11,12]. Furthermore, calcium-activated endoproteases, so-called prohormone convertases (PCs), cleave the propeptides at specific endoproteolytical cleavage sites ([13]; Figure 1). According to the particular propeptide, endoproteolytical cleavage results either in the release of the contained bioactive neuropeptide(s) or gives rise to an intermediate propeptide molecule that is further processed in the peptidergic vesicle (see below). When the peptides arrive at the trans-Golgi network, they are sorted from lysosomal and constitutively secreted proteins and usually packed into large dense-core vesicles [12]. Intermediate propeptides are packaged together with PCs and other processing enzymes (see below).

While the peptidergic vesicles are transported to their release sites, the contained PCs cleave the bioactive neuropeptides from the intermediate propeptides [11,12]. PCs typically cleave propeptides at paired basic amino acids such as Lys-Arg or Arg-Arg, but mono- or multibasic cleavage sites are used as well ([11,12]; Figure 1). Since propeptides often comprise multiple neuropeptides (- many copies of identical/sequence-related peptides or peptides of different types -) that are flanked by diverse cleavage sites, propeptide processing depends on which PCs are expressed in the particular neuron. Processing of proopiomelanocortin in the anterior pituitary, for example, involves PC1/3 and results in adrenocorticotropin hormone and other peptides, whereas, in the

intermediate pituitary, adrenocorticotropin hormone is further processed to α -melanocyte-stimulating hormone and corticotrophin-like intermediate lobe peptide by PC2 [11,14]. Thus, neurons which produce the same propeptide may express different PCs and, therefore, synthesize diverse bioactive neuropeptides. After a neuropeptide has been cleaved from its propeptide, a carboxypeptidase removes basic amino acids from the carboxy-terminus [11,12]. Subsequently, a peptidyl-glycine- α -amidating monooxygenase may convert carboxy-terminal glycine residues into amides ([15]; Figure 1).

At the release sites, the exocytosis of peptidergic vesicles requires an increase of the intracellular calcium concentration. After exocytosis, neuropeptides typically bind to G-protein-coupled receptors (GPCRs) that interact with different second messenger systems. In the course of the signal transmission, the activated GPCRs are internalized or phosphorylated [16], and the neuropeptide signaling comes to rest. Unlike for classical neurotransmitters, there are no specific reuptake mechanisms for neuropeptides. Peptidases in the extracellular fluid and the cell membranes degrade the remaining neuropeptides [11,12].

Neuropeptide function in vertebrates and invertebrates

Neuropeptides regulate diverse physiological processes such as circadian rhythmicity, growth, ion homeostasis, learning, memory, and reproduction, in both vertebrates and invertebrates [17]. In the vertebrate CNS, the hypothalamus and the pituitary contain a particularly high amount of different neuropeptides [18]. Neurons of the hypothalamus, for example, synthesize several releasing and inhibiting neuropeptides with hormone-like activity and secrete them into a portal venous blood system. The hypothalamic neuropeptides are then transported to the pituitary and cause the pituitary to release its own peptide hormones. The peptide hormones of the pituitary in turn act on a wide range of organs, and hence play important roles in the regulation of multiple physiological processes and behavior [18]. The hierarchic control of neuropeptide secretion in the vertebrate hypothalamus-pituitary system (- discovered by R. Guillemin and A. Schally, who were awarded with the 1977 Nobel Prize for their work -) has its parallel in the regulation of neuropeptide release from the retrocerebral complex of insects:

The retrocerebral complex of insects consists of the corpora cardiaca, the corpora allata, and the nerves that connect these glands with the CNS. Peptidergic neurons in the CNS innervate the corpora cardiaca and secrete several neuropeptides (, e.g. tachykinins and FMRFa-related peptides; [19]) to regulate the release of adipokinetic hormones. The adipokinetic hormones in turn play important roles for the mobilization of stored energy from the fat body during flight [20] and the immune response to pathogenic bacteria and fungi [21]. In some insect species, central neurons also release neuropeptides (allatostatin, allatotropin) to regulate the biosynthesis of juvenile hormone from the corpora allata [22,23]. Other peptidergic neurons in the CNS synthesize prothoracicotropic hormone(s) to control the release of the “molting hormone” ecdysone from the peripherally located prothoracic gland. Juvenile hormone and ecdysone together control vital physiological processes such as development, molting, and reproduction. These examples demonstrate that neurosecretory processes are often similar between vertebrates and insects [18,24]. Since the nervous systems of insects are simpler in terms of neuron number and organization than those of vertebrates, insects are valuable model organisms for studying peptidergic networks and neuropeptide actions on the level of single identifiable neurons.

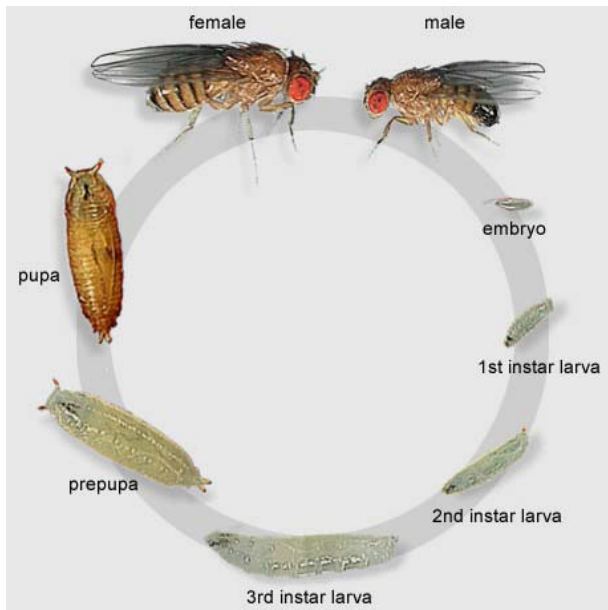


Figure 2: Life cycle of *Drosophila melanogaster*.

The generation time of *Drosophila* is about 14 days at 25° C. The egg develops into a larva within ~ 22 hours. Then, the 1st instar larva hatches and immediately starts feeding. After one day, the 1st instar larva undergoes the first molt. Within the next two days, the 2nd instar larva grows up and molts for the second time. The emerging 3rd instar larva feeds for another three days. In the end, the 3rd instar larva crawls out of the food, stops moving, and builds up an outer pupal case. Within the next ~ 4 hours, the larva undergoes the prepupal molt and enters metamorphosis. After five days, the adult fly emerges from the pupal case. The fly becomes fertile within few hours. After mating, the female fly starts to deposit eggs after two days. The life cycle is complete (modified from the FlyMove website: http://flymove.uni-muenster.de/genetics/flies/lifecycle/lifecyclepict/life_cycle.jpg; [57]).

***Drosophila* as a model organism for research into peptidergic networks**

Among the insects, the fruit fly *Drosophila melanogaster* is the most-studied species. *Drosophila* is used as a genetic model organism since 1910 (, T. H. Morgan received the 1933 Nobel Prize for demonstrating that genes are the mechanical basis of heredity) and in the 1970s also became an important model organism for research into developmental biology (- E. B. Lewis, C. Nüsslein-Volhard, and E. Wieschaus shared the 1995 Nobel Prize for identifying genes that control the embryonic development of *Drosophila*). Although *Drosophila* is small-sized and the dissection/surgery of neural tissues may be more difficult than those in larger insects, *Drosophila* is for several reasons an outstanding model organism for studying how neuropeptide actions integrate into the function of the CNS (“integrative biology”, [25–27]):

1) The genome of *Drosophila* is completely sequenced and, therefore, prepropeptides can be predicted from the DNA sequence *in silico* [28] and subsequently localized on the cellular level by immunocytochemistry or *in situ* hybridization [29,30]. The well-annotated genome also facilitates reverse genetic approaches that allow the identification of specific neuropeptide functions.

2) Virtually any gene of choice can be introduced into the *Drosophila* genome by P-element-mediated transposition and the short life cycle of *Drosophila* allows rapid generation of transgenic flies (Figure 2).

3) Thousands of mutant fly lines have been generated in forward genetic screens to uncover genes that contribute to a particular phenotype. Most of these fly lines can be obtained from public stock centers and at least some of them are probably helpful for the analysis of peptide functions.

4) Selecting *Drosophila* as a model organism gives immediate access to a set of powerful genetic tools: One of the key tools is the GAL4/UAS system ([31]; Figure 3), which provides the opportunity to target the expression of virtually any gene of choice to specific neurons. If the GAL4/UAS system is combined with a ligand- or temperature-inducible gene expression system [32], it is even possible to control both the spatial and temporal expression of the corresponding transgene. During the last years, “combinatorial techniques” have been developed that permit a refined transgene targeting [33].

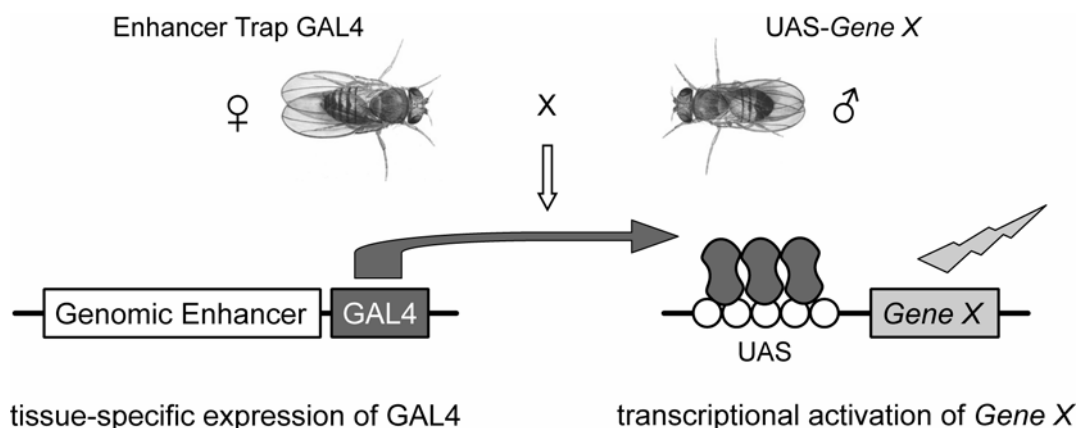


Figure 3: The GAL4/UAS system.

The GAL4/UAS system allows cell-specific and conditional expression of transgenes in *Drosophila*. Transgenic flies which express the yeast transcription factor GAL4 under control of a genomic enhancer are mated with transgenic flies that carry a gene of interest (Gene X) placed behind the upstream activation sequence (UAS) of GAL4. The progeny then express Gene X in the same pattern in which GAL4 is expressed in the parental line (modified from [31]).

5) The physiological roles of peptidergic neurons are at present intensely investigated in *Drosophila*. Particularly, the peptidergic neurons of the ventral nervous system attract much attention, because they are involved in the control of several essential physiological processes such as cardiac activity [34], diuresis [35], ecdysis [36,37], and locomotion [38].

The larval ventral ganglion of *Drosophila* harbors unique peptidergic networks

The ventral nervous system of *Drosophila* consists of three subesophageal, three thoracic and eight abdominal neuromeres, which altogether comprise fewer neurons (~ 10,000; [39]) than the brain (> 50,000; personal communication Kei Ito, University of Tokyo, Japan). In the ventral nervous system of the *Drosophila* larva (referred to as larval ventral ganglion, LVG), all neuron somata locate to an outer cell body layer (cortex) and send projections into the central neuropil ([40]; Figure 4). In the central neuropil, the axons of interneurons and afferent sensory neurons form arborizations and synapses, whereas those of efferent neurons leave the neuropil and project through segmentally repeated nerves to the periphery (Figure 4).

Since the LVG has fewer neurons than the brain and generally shows a homomeric composition, specific peptidergic neurons can be easily identified. Peptidergic neurites can be traced to defined neuropil areas and mapped in a set of three-dimensional landmarks [40]. These landmarks permit to compare the three-dimensional projection patterns of peptidergic neurons with those of candidate pre- and postsynaptic neurons (see below). With the appropriate GAL4 lines, it is also possible to target the expression of pre- and postsynaptic marker proteins to specific peptidergic neurons, and thus reveal the putative in- and output compartments of the respective neurons [41]. Finally, since the lineages of many peptidergic neurons of the LVG are known [39], the LVG provides the unique opportunity to trace the development of peptidergic networks from start to finish.

Taken together, the LVG of *Drosophila* is an ideal model system for studying the interaction between peptidergic neurons and their neural network partners, and the central regulation of neuropeptide release.

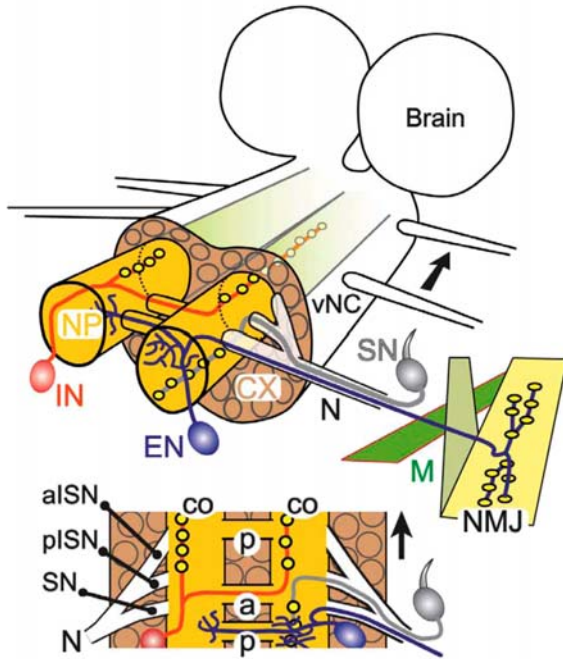


Figure 4: Morphology of the larval CNS.

The larval CNS is composed of the brain and the ventral nerve cord (vNC; referred to as ventral ganglion). In the ventral ganglion, the neuron somata locate to an outer cell body layer (cortex, CX) and send projections into the central neuropil (NP). Both interneurons (IN) and efferent neurons (EN) form arborizations and synapses in the central neuropil. Efferent neurons then project through segmentally repeated nerves (N) to the periphery, where motoneurons form neuromuscular junctions (NMJ) on their target muscles (M). Afferent sensory neurons (SN) project from the periphery into the neuropil. The neuropil is subdivided into longitudinal connectives (co), and anterior (a) and posterior (p) commissures traversing the midline in each segment. The segmental nerves consist of the anterior (a) and posterior (p) roots of the intersegmental nerves and the root of the segmental nerve (SN). Black arrows indicate anterior direction (from [40]).

A prime example of how peptidergic neurons interact and thus ensure the correct expression of behavior is the control of ecdysis. Ecdysis is a vital, stereotyped, and highly conserved behavior that requires the precisely timed concatenation of neurotransmitter signaling and neuroendocrine activity.

The regulation of ecdysis in *Drosophila* – a prime example of how neuropeptides orchestrate behavior

Like all insects, *Drosophila* has an exoskeleton (cuticle) of limited elasticity that needs to be periodically replaced during molts to accommodate growth and changes in morphology. While molting is regulated by 20-hydroxy-ecdysone and juvenile hormone, the timing and execution of ecdysis behavior (the shedding of the old cuticle) is controlled by a series of interacting neuropeptides ([36,37]; Figure 5):

Before the pre-ecdysis onset, peripherally located endocrine cells, the so-called “Inka cells”, secrete ecdysis-triggering hormones (ETHs) into the hemolymph. The ETHs in turn sequentially activate several peptidergic neuron groups in the VG and prompt them to release their peptide contents at key times during the ecdysis sequence. Initially, ETHs seem to induce central secretion of kinin, which presumably initiates pre-ecdysis behavior [42].

After the pre-ecdysis onset, ETH acts on central peptidergic neurons that synthesize FMRFa and eclosion hormone (EH), respectively. While FMRFa appears to regulate muscle activity during the ecdysis sequence [42], EH induces further ETH secretion from the peripherally located Inka cells. Thus, ETH and EH establish a positive feedback pathway. As the ecdysis sequence continues, ETH and EH together induce the release of crustacean cardioactive peptide (CCAP) and myoinhibiting peptides (MIPs) from neurons in the VG.

CCAP inhibits pre-ecdysis behavior and starts the ecdysis motor program. Both CCAP and MIPs also probably participate in the control of post-ecdysis behavior [42]. Since EH, CCAP, and CCAP/MIPs producing neurons respond to ETH with a specific delay, the accurate progress of ecdysis appears to depend not only on neuropeptide actions, but also on precisely timed synaptic input from central neurons [42].

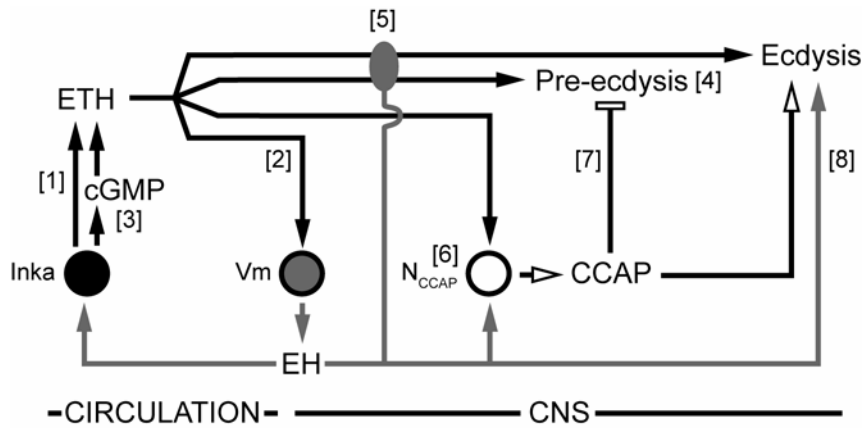


Figure 5: Model for interactions between peptidergic neurons during ecdysis of *Drosophila*.

The ecdysis sequence starts with the release of ETH from peripherally located Inka cells [1]. ETH then induces the release of EH from central Vm neurons [2], which causes further ETH secretion from the Inka cells via increases in cGMP [3]. ETH also appears to activate other peptidergic neurons in the CNS (e.g. kinin and FMRFa producing neurons; not shown) that turn on pre-ecdysis and ecdysis behavior [4]. These actions seem to require EH [5]. Both ETH and EH together induce the central release of CCAP/MIPs from N_{CCAP} [6]. CCAP/MIPs in turn inhibit pre-ecdysis behavior [7] and turn on the ecdysis motor program [8] (modified from [36]).

Aims of my doctoral thesis

Neuropeptide signaling accounts for a large part of the chemical transmission in the *Drosophila* CNS. *In silico* data mining studies suggest that the genome of *Drosophila* encodes up to 120 prepropeptides [28] and approximately 45 G-protein-coupled receptors with neuropeptides as ligands [43,44]. So far, about 40 neuropeptides have been identified by direct mass spectrometric peptide profiling [35,45–47] and many of them have been localized in the *Drosophila* CNS by immunocytochemistry [29,30]. In addition, several molecular and physiological studies have analyzed how particular neuropeptides influence central neural network activity and behavior [29,30,36,37]. It is largely unknown, however, how central neural networks control the neurosecretory activity of peptidergic neurons.

Thus, in my doctoral thesis, I aimed at gaining insights into the neuroarchitecture and the central regulation of peptidergic systems in the LVG of *Drosophila*. In particular, I focused on the central regulation of peptidergic neurons which are involved in the control of ecdysis, because ecdysis is a vital and highly conserved behavior under complex neuroendocrine and central regulation. My dissertation consists of six chapters that address three key aspects:

- Chapter I contains a three-dimensional morphological description of peptidergic systems in the LVG that helps to identify the neural network connections between peptidergic neurons and their pre- and postsynaptic neurons. The ensuing Chapter II then deals with the neuroarchitecture of aminergic neurons in the LVG, because aminergic neurons are likely to interact with peptidergic neurons.

Introduction

- Chapter III focuses on the identification of neurotransmitters that are involved in the central regulation of the ecdysis-relevant CCAP-producing neurons. The subsequent chapters IV and V are concerned with the development of methods for the transient synaptic isolation of CCAP-producing neurons during calcium imaging experiments, and the cell-specific silencing of nicotinic ACh receptors, respectively.
- Chapter VI finally describes the generation and characterization of fluorescent neuropeptide fusion proteins that have been developed to measure neuropeptide release from peptidergic neurons in the intact CNS.

In the following, I will briefly summarize the obtained results and discuss their relevance. Please note that all chapters of this dissertation and additional supporting files can be found on the attached CD.

Results and perspectives

Chapter I: Neuroarchitecture of peptidergic systems in the larval ventral ganglion of *Drosophila melanogaster*

As a first step in the morphological description of peptidergic systems in the LVG of *Drosophila*, we applied GAL4-driven expression of fluorescent marker proteins and immunocytochemistry to map peptidergic neurons and their projections into a set of evenly distributed landmarks. These landmarks, which are labeled by a commercially available monoclonal anti-Fasciclin2 (Fas2) antibody, are constant between individuals and over larval development, and thus allow a comparison of projection patterns of different LVG neurons with high spatial accuracy in three dimensions. Whenever appropriate GAL4 driver lines were available, we also analyzed the distribution of ectopically expressed pre- and postsynaptic marker proteins in peptidergic neurons of the LVG.

In total, we mapped 12 peptidergic neuron groups that express the prepropeptide genes *Ast* (CG13633), *capa* (CG15520), *Ccap* (CG4910), *Crz* (CG3302), *Eh* (CG5400), *Fmrf* (CG2346), *hug* (CG6371), *IFa* (CG33527), *Leucokinin* (CG13480), *Mip* (CG6456), *Pdf* (CG6496), or *Tk* (CG14734). Proteolytical processing of the respective prepropeptides is predicted to give rise to 32 different bioactive neuropeptides. This approximates 75 % of the so far chemically detected neuropeptides in the *Drosophila* CNS.

Our morphological analyses demonstrate that peptidergic neuron groups in the LVG typically localize to specific neuromeres and do not show a segmentally reiterated distribution pattern. Thus, most peptidergic neurons seem to have neuromere-specific functions. Peptidergic neurites often ramify in the median neuropil between the dorso-medial and ventro-medial Fas2 tracts. Since the median peptidergic neurites generally showed weak neuropeptide immunoreactivity and presynaptic marker labeling, they appeared to be mostly dendritic compartments. Some peptidergic projections, however, also seemed to form presynaptic compartments or neuropeptide release sites in the median neuropil. The last abdominal neuromere of the LVG contained a particularly dense network of peptidergic neurites, which probably comprises both dendritic and presynaptic compartments. Putative neuropeptide release sites primarily located to descending neurites that project along intermediate or lateral Fas2 tracts. These descending neurites lacked pronounced arborizations, but often formed

multiple short varicosities with particularly high peptide immunoreactivity. Thus, within the LVG, most neuropeptides seem to act via paracrine release and volume transmission, and not via synaptic release.

The three-dimensional mapping of peptidergic neurons now facilitates the identification of co-expressed proteins and potential neural network contacts.

Chapter II: Neuroarchitecture of aminergic systems in the larval ventral ganglion of *Drosophila melanogaster*

When we mapped the peptidergic neurons into the Fas2 landmark system, we also intended to identify putative pre- and postsynaptic network contacts. Most likely, certain peptidergic neurons interact with ACh- or γ -aminobutyric acid (GABA)-producing neurons, because several hundreds of these neurons locate to the LVG and project to the central neuropil [48–50]. However, the dense network of cholinergic and GABAergic neurites in the LVG complicates the identification of neurons that provide synaptic input to a particular peptidergic neuron group. Thus, we decided to focus on neurotransmitter-producing neurons that may be involved in the central regulation of peptidergic networks and are individually traceable. Ideal candidates were the aminergic neurons, because these neurons can be assigned to defined neuron groups, which all exhibit a stereotypic distribution pattern in the LVG and consist of a small number of neurons (~ 30-60; [51]). Furthermore, aminergic neurons are known to influence endocrine activity [52].

We used GAL4-driven marker gene expression and immunocytochemistry to map the presumed serotonergic, dopaminergic and tyraminerpic/octopaminergic neurons of the LVG into the Fas2 landmark system. With appropriate GAL4 and UAS lines, we also analyzed the distribution of pre- and postsynaptic compartment markers in dopaminergic and tyraminerpic/octopaminergic neurons.

Our morphological data suggest that serotonergic and dopaminergic neurons are involved in the transmission of sensory information and the modulation of central neural networks, while tyraminerpic/octopaminergic neurons primarily appear to control processes in the periphery. Serotonergic neurons probably form a homogenous neuron group, whereas both dopaminergic and tyraminerpic/octopaminergic neurons are separated into distinct neuron subsets that innervate specific neuropil areas in the LVG and presumably have different physiological functions.

By comparing the three-dimensional distribution patterns of peptidergic neurons with those of presumed aminergic neurons, we found that some DOPA decarboxylase-expressing neurons in the LVG appear to synthesize neither serotonin nor dopamine, but instead produce the neuropeptides CCAP, MIPs or corazonin. This example demonstrates how Fas2-based mapping can facilitate the identification of co-localized signaling molecules.

Chapter III: Neurotransmitter-induced changes in the intracellular calcium concentration suggest a differential central modulation of CCAP neuron subsets in *Drosophila*

Our Fas2-based mapping indicated that dendritic compartments of peptidergic neurons frequently overlap with presynaptic compartments of neurotransmitter-synthesizing neurons. It remained unclear, however, whether specific peptidergic neurons actually express the appropriate receptor to respond to a particular input transmitter.

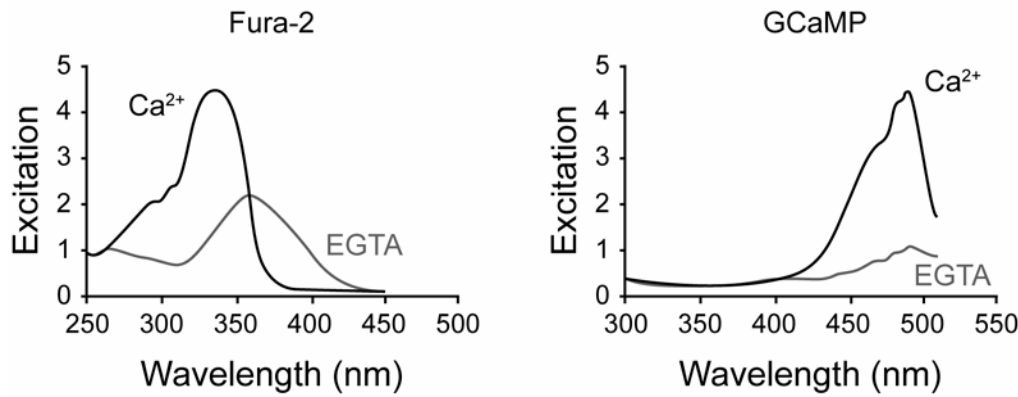


Figure 6: The calcium indicators Fura-2 and GCaMP.

Fluorescence excitation spectra of Fura-2 and GCaMP in the presence of 1mM Ca^{2+} and 5 mM EGTA (ethyleneglycol tetraacetic acid - a Ca^{2+} -chelant). In the presence of Ca^{2+} , Fura-2 shows maximal excitation at ~ 340 nm, but in the presence of EGTA, Fura-2 is maximally excited at ~ 360 nm. For ratiometric calcium imaging, Fura-2 is successively excited at 340 and 380 nm, and relative fluorescence is calculated as the quotient of the corresponding emission intensities ($F = F_{340}/F_{380}$). GCaMP shows maximal excitation at ~ 480 nm, irrespective of the actual Ca^{2+} -concentration. Thus, GCaMP is used for non-ratiometric calcium imaging (modified from the web edition of “The Handbook – A Guide to Fluorescent Probes and Labeling Technologies” by Molecular Probes: <http://probes.invitrogen.com/handbook/figures/0554.html> and [58]).

Thus, we set out to characterize the neurotransmitter receptor complement of peptidergic neurons. For several reasons, we focused on the CCAP-producing neurons (N_{CCAP}): 1) N_{CCAP} ensure the correct execution and circadian timing of ecdysis behavior (see above) and are crucial for proper pupal ecdysis (“head eversion”; [53]). 2) The population of N_{CCAP} consists of morphologically diverse subsets that synthesize not only CCAP, but also differentially produce MIPs or bursicon. These distinct N_{CCAP} subsets act coordinately in a common neural network, but appear to be differentially regulated. At pupal ecdysis, particular N_{CCAP} do not respond to systemic application of ETH, although all N_{CCAP} obviously express the ETH receptor A [42]. After eclosion, a defined N_{CCAP} subset provides synaptic input to the remaining N_{CCAP} to regulate the release of bursicon [54]. Thus, at least some N_{CCAP} are likely to receive neurotransmitter input at particular times of development. 3) Previous findings in the moth *Manduca sexta* also suggest that descending inhibitory neurons from the subesophageal and thoracic ganglia transiently suppress the activation of certain N_{CCAP} [55]. Thus, the stage-specific activity of distinct N_{CCAP} subsets of *Drosophila* [42] may be based on precisely-timed neurotransmitter inputs. 4) The CCAP-GAL4 driver [53] provided the opportunity to genetically manipulate the N_{CCAP} .

Since neuropeptide release from the N_{CCAP} is triggered by an increase of the intracellular calcium concentration ($[\text{Ca}^{2+}]_i$), we applied a combination of GAL4-driven gene expression and non-invasive calcium imaging to identify the input transmitters of the N_{CCAP} . In a first set of experiments, we loaded cultured isolated N_{CCAP} with the synthetic dye Fura-2 (Figure 6), and monitored their $[\text{Ca}^{2+}]_i$ in the absence and presence of different neurotransmitters. Nearly all N_{CCAP} showed $[\text{Ca}^{2+}]_i$ -increases upon application of ACh and nicotine, while only few N_{CCAP} responded to the muscarinic ACh receptor agonist pilocarpine. Glutamate induced $[\text{Ca}^{2+}]_i$ -increases in about one third of N_{CCAP} , and the glutamate receptor agonist quisqualate mimicked this effect.

The principal inhibitory transmitter GABA decreased or blocked the ACh-mediated $[Ca^{2+}]_i$ -increases in about half the N_{CCAP} . These results suggest that most N_{CCAP} express nicotinic ACh receptors (nAChRs), while only some N_{CCAP} possess glutamate or GABA receptors.

In the following experiments, we compared the response behavior of cultured isolated N_{CCAP} with that of N_{CCAP} in the intact CNS. Furthermore, we intended to identify the N_{CCAP} that express a specific neurotransmitter receptor. Thus, we targeted the genetically encoded calcium indicator GCaMP 1.6 ([56]; Figure 6) to the N_{CCAP} , and subsequently monitored the transmitter-induced $[Ca^{2+}]_i$ -responses of N_{CCAP} in the intact larval and adult CNS. Surprisingly, application of cholinergic agonists caused pronounced $[Ca^{2+}]_i$ -decreases in most N_{CCAP} . Only few N_{CCAP} responded with transient $[Ca^{2+}]_i$ -rises or $[Ca^{2+}]_i$ -oscillations. In the LVG, the responding N_{CCAP} belonged to a distinct neuron subset that forms neurohemal release sites at the body wall muscles.

Taken together, our findings suggest that N_{CCAP} belong to different neuron subsets that receive differential synaptic input from cholinergic, GABAergic and glutamatergic neurons besides the known input by neuropeptides. The concerted action of both neurotransmitters and neuropeptides could provide means for a context-dependent activation of specific N_{CCAP} subsets and a fine-tuning of CCAP release.

Chapter IV: A method for the synaptic isolation of CCAP neurons during calcium imaging experiments in the intact CNS of *Drosophila*

Our calcium imaging experiments indicated that N_{CCAP} receive synaptic input from different neurotransmitter-synthesizing neurons. Consequently, when neurotransmitters are systemically applied to the intact CNS during calcium imaging experiments, they may directly and/or indirectly (, i.e. through the activation/inhibition of afferent neurons,) influence the $[Ca^{2+}]_i$ of N_{CCAP} . Because direct and indirect effects may coincide, it is difficult to evaluate by calcium imaging whether a particular N_{CCAP} of the LVG expresses a certain neurotransmitter receptor or not. To identify all N_{CCAP} that express a specific neurotransmitter receptor, the N_{CCAP} need to be transiently separated from their presynaptic network contacts during the calcium imaging experiments.

For this reason, we generated transgenic flies that express CCAP-GAL4 or UAS-GCaMP 1.6 with the temperature-sensitive dynamin protein shibire (shi^{ts}). At permissive temperatures, shi^{ts} acts as a GTPase that mediates membrane recycling following synaptic vesicle release. At restrictive temperatures, shi^{ts} becomes dysfunctional and disrupts synaptic transmission. Thus, in shi^{ts} ; CCAP-GAL4/UAS-GCaMP 1.6 expressing flies, it should be possible to transiently block the synaptic input onto all N_{CCAP} and at the same time monitor the $[Ca^{2+}]_i$ in particular N_{CCAP} . In future experiments, we will use the shi^{ts} ; CCAP-GAL4/UAS-GCaMP 1.6 expressing flies to map the receptor complement of identified N_{CCAP} by calcium imaging.

Chapter V: A method for the genetic silencing of nicotinic acetylcholine receptors in the CCAP neurons of *Drosophila*

Our calcium imaging experiments suggested that most N_{CCAP} receive cholinergic input via nAChRs. It remained unknown, however, whether cholinergic input is actually necessary for a regular neurosecretory activity of N_{CCAP} . To approach this question, we decided to genetically silence the nAChRs of the N_{CCAP} . Since the nAChRs of *Drosophila* consist of structurally diverse subunits, it is difficult to specifically eliminate the

Introduction

nAChRs of the N_{CCAP} by standard genetic tools (such as “*knock-down*” or “*knock-out*”). Thus, we set out to identify peptide toxins that block the nAChRs of cultured N_{CCAP} . Appropriate toxins should then be placed under control of the UAS promotor and ectopically expressed in the N_{CCAP} to inhibit their cholinergic activation.

By Fura-2 based calcium imaging, we found that the naturally occurring peptide toxin α -bungarotoxin (α -BgT; a potent antagonist of nAChRs,) can prevent the cholinergic activation of at least some N_{CCAP} . In collaboration with Justin Blau from New York University we generated transgenic flies that express a membrane-tethered α -BgT under control of UAS. With the respective flies, we plan to examine whether nAChRs are necessary for regular neuropeptide release from N_{CCAP} . Unfortunately, up to now, we do not have the legal permission to use the α -BgT expressing flies at the Philipps-University of Marburg.

Chapter VI: Venus-tagged peptides for the visualization of neuropeptide transport and release in *Drosophila*

Our calcium imaging experiments showed that ACh and glutamate induce $[Ca^{2+}]_i$ -increases in distinct N_{CCAP} subsets. It remained unknown, however, if neurotransmitter-induced $[Ca^{2+}]_i$ -increases trigger neuropeptide release from the N_{CCAP} . To examine whether the putative releasing transmitters influence the secretory activity of N_{CCAP} , we decided to visualize and monitor the peptidergic vesicles of the N_{CCAP} during transmitter application.

We generated two cDNA constructs that encode the improved yellow fluorescent protein variant Venus fused to either the rat atrial natriuretic factor (ANF) or the *Drosophila* CAPA-1 prepropeptide. When targeted to peptidergic neurons, the peptide-Venus fusion proteins were presumed to be transported and released like endogenous *Drosophila* peptides. Accordingly, the peptide-Venus fusion proteins should allow the visualization of neuropeptide release as a decrease in the amount of fluorescent vesicles.

After the generation of transgenic flies expressing preproANF- or preproCAPA-1-Venus under control of UAS, we analyzed whether the respective fusion proteins emit fluorescence and are packaged into vesicles in peptidergic neurons. Both preproANF- and preproCAPA-1-Venus localized in punctate patterns to somata and neurites, and thus the fusion proteins appear to be channeled into the regulated secretory pathway. To investigate whether preproANF- and preproCAPA-1-Venus are processed like endogenous *Drosophila* neuropeptides, we performed Western Blots with CNS extracts from larvae that synthesize the respective fusion proteins in peptidergic neurons. While preproANF-Venus appeared to be processed only to proANF-Venus, preproCAPA-1-Venus seemed to be completely processed to CAPA-1-Venus. Thus, preproCAPA-1-Venus gives rise to a smaller neuropeptide fusion than preproANF-Venus, and accordingly may be better suited for the visualization of vesicle release. To examine if peptidergic vesicles with preproANF- and preproCAPA-1-Venus are transported to secretory sites, we targeted both fusion proteins to the N_{CCAP} . As expected, preproANF- and preproCAPA-1-Venus were transported like endogenous *Drosophila* neuropeptides and accumulated at the putative neurohemal sites of the N_{CCAP} . In future experiments, we will use preproANF- and preproCAPA-1-Venus to visualize vesicle release from peptidergic neurons.

Conclusions

Here, we mapped peptidergic and aminergic neurons in the LVG of *Drosophila* into a three-dimensional landmark system and characterized their pre- and postsynaptic compartments to analyze potential neuronal network relationships. We then applied calcium imaging to identify neurotransmitters that influence the neural activity of the ecdysis-relevant N_{CCAP} . Finally, we developed and described methods for the transient synaptic isolation of N_{CCAP} in the intact *Drosophila* CNS during calcium imaging experiments, the genetic silencing of nAChRs of N_{CCAP} , and the visualization of neuropeptide transport and release in peptidergic *Drosophila* neurons.

References

1. Deutch AY, Roth RH (2003) Neurotransmitters. In: Squire LR, Bloom FE, McConnell SK, Roberts JL, Spitzer NC et al., editors. *Fundamental Neuroscience*. London: Academic Press. pp. 163-196.
2. Agnati LF, Zoli M, Strömberg I, Fuxe K (1995) Intercellular communication in the brain: wiring versus volume transmission. *Neuroscience* 69: 711-726.
3. Hoffman BJ, Hansson SR, Mezey É, Palkovits M (1998) Localization and dynamic regulation of biogenic amine transporters in the mammalian central nervous system. *Front Neuroendocrinol* 19: 187-231.
4. Nirenberg MJ, Liu Y, Peter D, Edwards RH, Pickel VM (1995) The vesicular monoamine transporter 2 is present in small synaptic vesicles and preferentially localizes to large dense core vesicles in rat solitary tract nuclei. *Proc Natl Acad Sci U S A* 92: 8773-8777.
5. Torrealba F, Carrasco MA (2004) A review on electron microscopy and neurotransmitter systems. *Brain Res Brain Res Rev* 47: 5-17.
6. Bechtold DA, Luckman SM (2007) The role of RFamide peptides in feeding. *J Endocrinol* 192: 3-15.
7. Grimmelikhuijzen CJ, Leviev I, Carstensen K (1996) Peptides in the nervous systems of cnidarians: structure, function, and biosynthesis. *Int Rev Cytol* 167: 37-89.
8. Kah O, Lethimonier C, Somoza G, Guilgur LG, Vaillant C, Lareyre JJ (2007) GnRH and GnRH receptors in metazoa: a historical, comparative, and evolutive perspective. *Gen Comp Endocrinol* 153: 346-364.
9. Lovejoy DA, Jahan S (2006) Phylogeny of the corticotropin-releasing factor family of peptides in the metazoa. *Gen Comp Endocrinol* 146: 1-8.
10. Lou H, Gagel RF (2001) Alternative ribonucleic acid processing in endocrine systems. *Endocr Rev* 22: 205-225.
11. Hook V, Funkelstein L, Lu D, Bark S, Wegrzyn J, Hwang SR (2008) Proteases for processing proneuropeptides into peptide neurotransmitters and hormones. *Annu Rev Pharmacol Toxicol* 48: 393-423.
12. Sossin WS, Fisher JM, Scheller RH (1989) Cellular and molecular biology of neuropeptide processing and packaging. *Neuron* 2: 1407-1417.
13. Seidah NG, Chretien M (1999) Proprotein and prohormone convertases: a family of subtilases generating diverse bioactive polypeptides. *Brain Res* 848: 45-62.
14. Nillni EA (2007) Regulation of prohormone convertases in hypothalamic neurons: implications for prothyrotropin-releasing hormone and proopiomelanocortin. *Endocrinology* 148: 4191-4200.
15. Prigge ST, Mains RE, Eipper BA, Amzel LM (2000) New insights into copper monooxygenases and peptide amidation: structure, mechanism and function. *Cell Mol Life Sci* 57: 1236-1259.
16. Hanyaloglu AC, von Zastrow M (2008) Regulation of GPCRs by endocytic membrane trafficking and its potential implications. *Annu Rev Pharmacol Toxicol* 48: 537-568.
17. Strand FL (1999) *Neuropeptides: Regulators of Physiological Processes*. Cambridge: MIT Press.
18. Klowden MJ (2003) Contributions of insect research toward our understanding of neurosecretion. *Arch Insect Biochem Physiol* 53: 101-114.

Introduction

19. Vullings HG, Diederer JH, Veelaert D, Van der Horst DJ (1999) Multifactorial control of the release of hormones from the locust retrocerebral complex. *Microsc Res Tech* 45: 142-153.
20. Gäde G, Auerswald L (2003) Mode of action of neuropeptides from the adipokinetic hormone family. *Gen Comp Endocrinol* 132: 10-20.
21. Mullen LM, Goldsworthy GJ (2006) Immune responses of locusts to challenge with the pathogenic fungus *Metarhizium* or high doses of laminarin. *J Insect Physiol* 52: 389-398.
22. Elekonich MM, Horodyski FM (2003) Insect allatotropins belong to a family of structurally-related myoactive peptides present in several invertebrate phyla. *Peptides* 24: 1623-1632.
23. Stay B, Tobe SS (2007) The role of allatostatins in juvenile hormone synthesis in insects and crustaceans. *Annu Rev Entomol* 52: 277-299.
24. De Loof A (2008) Ecdysteroids, juvenile hormone and insect neuropeptides: Recent successes and remaining major challenges. *Gen Comp Endocrinol* 155: 3-13.
25. Dow JA (2007) Integrative physiology, functional genomics and the phenotype gap: a guide for comparative physiologists. *J Exp Biol* 210: 1632-1640.
26. Dow JA (2007) Model organisms and molecular genetics for endocrinology. *Gen Comp Endocrinol* 153: 3-12.
27. Dow JT, Davies SA (2003) Integrative physiology and functional genomics of epithelial function in a genetic model organism. *Physiol Rev* 83: 687-729.
28. Liu F, Baggerman G, D'Hertog W, Verleyen P, Schoofs L, Wets G (2006) *In silico* identification of new secretory peptide genes in *Drosophila melanogaster*. *Mol Cell Proteomics* 5: 510-522.
29. Nässel DR (2002) Neuropeptides in the nervous system of *Drosophila* and other insects: multiple roles as neuromodulators and neurohormones. *Prog Neurobiol* 68: 1-84.
30. Nässel DR, Homberg U (2006) Neuropeptides in interneurons of the insect brain. *Cell Tissue Res* 326: 1-24.
31. Brand AH, Perrimon N (1993) Targeted gene expression as a means of altering cell fates and generating dominant phenotypes. *Development* 118: 401-415.
32. McGuire SE, Roman G, Davis RL (2004) Gene expression systems in *Drosophila*: a synthesis of time and space. *Trends Genet* 20: 384-391.
33. Luan H, White BH (2007) Combinatorial methods for refined neuronal gene targeting. *Curr Opin Neurobiol* 17: 572-580.
34. Dulcis D, Levine RB, Ewer J (2005) Role of the neuropeptide CCAP in *Drosophila* cardiac function. *J Neurobiol* 64: 259-274.
35. Wegener C, Reinl T, Jänsch L, Predel R (2006) Direct mass spectrometric peptide profiling and fragmentation of larval peptide hormone release sites in *Drosophila melanogaster* reveals tagma-specific peptide expression and differential processing. *J Neurochem* 96: 1362-1374.
36. Ewer J (2005) Behavioral actions of neuropeptides in invertebrates: insights from *Drosophila*. *Horm Behav* 48: 418-429.
37. Žitňan D, Kim YJ, Žitňanova I, Roller L, Adams ME (2007) Complex steroid-peptide-receptor cascade controls insect ecdysis. *Gen Comp Endocrinol* 153: 88-96.
38. Winther AM, Acebes A, Ferrús A (2006) Tachykinin-related peptides modulate odor perception and locomotor activity in *Drosophila*. *Mol Cell Neurosci* 31: 399-406.
39. Bhat KM (1998) Cell-cell signaling during neurogenesis: some answers and many questions. *Int J Dev Biol* 42: 127-139.
40. Landgraf M, Sánchez-Soriano N, Technau GM, Urban J, Prokop A (2003) Charting the *Drosophila* neuropile: a strategy for the standardised characterisation of genetically amenable neurites. *Dev Biol* 260: 207-225.
41. Löhner R, Godenschwege T, Buchner E, Prokop A (2002) Compartmentalization of central neurons in *Drosophila*: a new strategy of mosaic analysis reveals localization of presynaptic sites to specific segments of neurites. *J Neurosci* 22: 10357-10367.
42. Kim YJ, Žitňan D, Galizia CG, Cho KH, Adams ME (2006) A command chemical triggers an innate behavior by sequential activation of multiple peptidergic ensembles. *Curr Biol* 16: 1395-1407.
43. Hauser F, Williamson M, Cazzamali G, Grimmelikhuijzen CJ (2006) Identifying neuropeptide and protein hormone receptors in *Drosophila melanogaster* by exploiting genomic data. *Brief Funct Genomic Proteomic* 4: 321-330.
44. Hewes RS, Taghert PH (2001) Neuropeptides and neuropeptide receptors in the *Drosophila melanogaster* genome. *Genome Res* 11: 1126-1142.

45. Baggerman G, Boonen K, Verleyen P, De Loof A, Schoofs L (2005) Peptidomic analysis of the larval *Drosophila melanogaster* central nervous system by two-dimensional capillary liquid chromatography quadrupole time-of-flight mass spectrometry. *J Mass Spectrom* 40: 250-260.
46. Predel R, Wegener C, Russell WK, Tichy SE, Russell DH, Nachman RJ (2004) Peptidomics of CNS-associated neurohemal systems of adult *Drosophila melanogaster*: a mass spectrometric survey of peptides from individual flies. *J Comp Neurol* 474: 379-392.
47. Taghert PH, Veenstra JA (2003) *Drosophila* neuropeptide signaling. *Adv Genet* 49: 1-65.
48. Küppers B, Sánchez-Soriano N, Letzkus J, Technau GM, Prokop A (2003) In developing *Drosophila* neurones the production of gamma-amino butyric acid is tightly regulated downstream of glutamate decarboxylase translation and can be influenced by calcium. *J Neurochem* 84: 939-951.
49. Salvaterra PM, Kitamoto T (2001) *Drosophila* cholinergic neurons and processes visualized with Gal4/UAS-GFP. *Brain Res Gene Expr Patterns* 1: 73-82.
50. Yasuyama K, Salvaterra PM (1999) Localization of choline acetyltransferase-expressing neurons in *Drosophila* nervous system. *Microsc Res Tech* 45: 65-79.
51. Monastirioti M (1999) Biogenic amine systems in the fruit fly *Drosophila melanogaster*. *Microsc Res Tech* 45: 106-121.
52. Rauschenbach IY, Chentsova NA, Alekseev AA, Gruntenko NE, Adonyeva NV, Karpova EK, Komarova TN, Vasiliev VG, Bownes M (2007) Dopamine and octopamine regulate 20-hydroxyecdysone level *in vivo* in *Drosophila*. *Arch Insect Biochem Physiol* 65: 95-102.
53. Park JH, Schroeder AJ, Helfrich-Förster C, Jackson FR, Ewer J (2003) Targeted ablation of CCAP neuropeptide-containing neurons of *Drosophila* causes specific defects in execution and circadian timing of ecdysis behavior. *Development* 130: 2645-2656.
54. Luan H, Lemon WC, Peabody NC, Pohl JB, Zelensky PK, Wang D, Nitabach MN, Holmes TC, White BH (2006) Functional dissection of a neuronal network required for cuticle tanning and wing expansion in *Drosophila*. *J Neurosci* 26: 573-584.
55. Fuse M, Truman JW (2002) Modulation of ecdysis in the moth *Manduca sexta*: the roles of the suboesophageal and thoracic ganglia. *J Exp Biol* 205: 1047-1058.
56. Reiff DF, Ihring A, Guerrero G, Isacoff EY, Joesch M, Nakai J, Borst A (2005) *In vivo* performance of genetically encoded indicators of neural activity in flies. *J Neurosci* 25: 4766-4778.
57. Weigmann K, Klapper R, Strasser T, Rickert C, Technau G, Jäckle H, Janning W, Klämbt C (2003) FlyMov--a new way to look at development of *Drosophila*. *Trends Genet* 19: 310-311.
58. Nakai J, Ohkura M, Imoto K (2001) A high signal-to-noise Ca(2+) probe composed of a single green fluorescent protein. *Nat Biotechnol* 19: 137-141.

I. Neuroarchitecture of peptidergic systems in the larval ventral ganglion of *Drosophila melanogaster*

Santos JG, Vömel M, Struck R, Homberg U, Nässel DR and Wegener C. (2007). PLoS ONE 2(8): e695.

Abstract.....	29
Introduction.....	29
Results	30
Morphology of AST-A neurons	31
Morphology of capa and hugin neurons	33
Morphology of CCAP neurons.....	34
Morphology of corazonin neurons	35
Morphology of eclosion hormone neurons.....	36
Morphology of FMRFamide neurons.....	36
Morphology of IFamide neurons.....	37
Morphology of leucokinin neurons	37
Morphology of MIP neurons	38
Morphology of PDF neurons.....	38
Morphology of TRP neurons.....	38
Distribution of ectopical c929-GAL4-driven SYB.EGFP and RDL.HA.....	39
Discussion	39
Serial homology	39
SYB.EGFP and RDL.HA as compartment markers in peptidergic neurons	39
Many peptidergic neurons are concentrated around the ganglion midline and might define a dendritic neuropil compartment of peptidergic neurons.....	40
The neuropil of a9 is densely supplied by peptidergic neurites and might serve as in- and output-site for peptidergic neurons	40
Possible overlap of peptidergic and sensory projections.....	40
Possible overlap of peptidergic and motor neuron projections.....	41
Possible overlap of peptidergic and interneuron projections.....	41
Conclusions.....	41
Materials and Methods.....	42
Fly stocks	42
Immunostaining.....	42
Confocal microscopy.....	42
Mapping of immunostaining patterns.....	42
Supporting information (- corresponding files can be found on CD -).....	42
References.....	43

Neuroarchitecture of Peptidergic Systems in the Larval Ventral Ganglion of *Drosophila melanogaster*

Jonathan G. Santos^{1,2}, Matthias Vömel^{1,2}, Rafael Struck^{1,2}, Uwe Homberg², Dick R. Nässel³, Christian Wegener^{1,2*}

1 Emmy Noether Neuropeptide Group, Animal Physiology, Department of Biology, Philipps-University, Marburg, Germany, **2** Animal Physiology, Department of Biology, Philipps-University, Marburg, Germany, **3** Department of Zoology, Stockholm University, Stockholm, Sweden

Recent studies on *Drosophila melanogaster* and other insects have revealed important insights into the functions and evolution of neuropeptide signaling. In contrast, in- and output connections of insect peptidergic circuits are largely unexplored. Existing morphological descriptions typically do not determine the exact spatial location of peptidergic axonal pathways and arborizations within the neuropil, and do not identify peptidergic in- and output compartments. Such information is however fundamental to screen for possible peptidergic network connections, a prerequisite to understand how the CNS controls the activity of peptidergic neurons at the synaptic level. We provide a precise 3D morphological description of peptidergic neurons in the thoracic and abdominal neuromeres of the *Drosophila* larva based on fasciclin-2 (Fas2) immunopositive tracts as landmarks. Comparing the Fas2 “coordinates” of projections of sensory or other neurons with those of peptidergic neurons, it is possible to identify candidate in- and output connections of specific peptidergic systems. These connections can subsequently be more rigorously tested. By immunolabeling and GAL4-directed expression of marker proteins, we analyzed the projections and compartmentalization of neurons expressing 12 different peptide genes, encoding approximately 75% of the neuropeptides chemically identified within the *Drosophila* CNS. Results are assembled into standardized plates which provide a guide to identify candidate afferent or target neurons with overlapping projections. In general, we found that putative dendritic compartments of peptidergic neurons are concentrated around the median Fas2 tracts and the terminal plexus. Putative peptide release sites in the ventral nerve cord were also more laterally situated. Our results suggest that i) peptidergic neurons in the *Drosophila* ventral nerve cord have separated in- and output compartments in specific areas, and ii) volume transmission is a prevailing way of peptidergic communication within the CNS. The data can further be useful to identify colocalized transmitters and receptors, and develop peptidergic neurons as new landmarks.

Citation: Santos JG, Vömel M, Struck R, Homberg U, Nässel DR, et al (2007) Neuroarchitecture of Peptidergic Systems in the Larval Ventral Ganglion of *Drosophila melanogaster*. PLoS ONE 2(8): e695. doi:10.1371/journal.pone.0000695

INTRODUCTION

Neuropeptides are neuronal signaling molecules that are involved in the regulation of diverse processes such as development and growth, metabolism, reproduction, ion homeostasis, circadian rhythms and behavior. Neuropeptides can be produced by neurosecretory cells (secretory neurons) as well as interneurons, and are released as hormones into the circulation, or locally within the CNS. When released within the CNS, neuropeptides might act as “local hormones” via volume transmission (signal substance diffusion in a three-dimensional fashion within the extracellular space—also termed paracrine signaling), or as co-transmitters that act at or nearby synapses. In rare cases, neuropeptides have been identified in sensory cells and motor neurons of insects [1,2].

Insect studies have revealed important insights into how neuropeptides and peptide hormones orchestrate behavior and integrate body functions [1–4]. In contrast, the role of direct synaptic input in the control of activity of peptidergic insect neurons is largely unexplored. This also applies to the fruit fly *Drosophila melanogaster*, although it has been shown that peptidergic *Drosophila* neurons express functional receptors for various neurotransmitters and biogenic amines [5–8]. The afferent pathways forming synaptic inputs on peptidergic neurons are still unidentified. The situation is similar regarding the output of peptidergic neurons. Although our knowledge on the behavioral or physiological effects of insect neuropeptides is steadily increasing (see [1–3]), the identity of targets of peptidergic neurons and the cellular mechanisms behind peptide signaling are commonly unknown, and we do not know whether centrally released peptides act as intrinsic or extrinsic neuromodulators (see [9]).

To answer questions concerning input and output relations of peptidergic systems, it is necessary to unravel the underlying

neuronal circuitries. *Drosophila* is very well suited for this, owing to its relatively small number of neurons and its genetic amenability. Although the nervous system of *Drosophila* operates with a number of neurons that is around 100,000 times smaller than that of the primate brain, it seems to produce a similar diversity of neuropeptides. 31 neuropeptide genes have been identified so far [10]. These encode more than 60 putative peptides, 41 of which have been chemically identified within the CNS [10–13]. Concomitantly, the number of peptidergic neurons expressing a given peptide gene in the *Drosophila* CNS is very small (anything between two and several dozens of neurons), which allows us to individually identify peptidergic neurons. In combination with the available genetic tools, these features have made the fruit fly an established model organism to study neuropeptide signaling (see [14]).

Since the general organization of ventral ganglia is conserved throughout insects and crustaceans [15], unraveling the neuronal

Academic Editor: Alan Nighorn, University of Arizona, United States of America

Received: April 5, 2007; **Accepted:** June 15, 2007; **Published:** August 1, 2007

Copyright: © 2007 Santos et al. This is an open-access article distributed under the terms of the Creative Commons Attribution License, which permits unrestricted use, distribution, and reproduction in any medium, provided the original author and source are credited.

Funding: This work was supported by the Deutsche Forschungsgemeinschaft (DFG We 2652/2-1,2) to CW.

Competing Interests: The authors have declared that no competing interests exist.

* **To whom correspondence should be addressed.** E-mail: wegener@staff.uni-marburg.de

circuitry of peptidergic systems in the fruit fly can contribute to a general understanding of the architecture of peptidergic systems in the ventral nervous system and its neuroendocrinology in these most diverse animal groups. It may also provide insights into more general evolutionary design principles of neuropeptidergic systems, since recent findings suggest that not only the genetic control of neuroendocrine system development (see [16]), but also several peptide functions and signaling cascades bear significant homologies between *Drosophila* and vertebrates (e.g. [17–22]).

The aim of this study is to provide a detailed spatial description of the processes of peptidergic neurons in *Drosophila* and to identify possible in- and output compartments. By immunolabeling and GAL4/UAS-directed expression [23] of fluorescent marker proteins, we have analyzed the morphology and projections of neurons expressing 12 different peptide precursor genes. Our analysis focuses on the thoracic and abdominal neuromeres of the larva (for the sake of simplicity referred to as the larval ventral ganglion, which strictly speaking also comprises the suboesophageal neuromeres that are ignored here). This is mainly for two reasons, which may facilitate the identification of afferents and targets of peptidergic neurons: 1) evenly distributed landmarks of Fasciclin2 (Fas2) immunopositive tracts exist within the ventral ganglion neuropil that are constant between specimens and larval stages [24]. These landmarks allow us to describe projection patterns with high spatial accuracy in three dimensions. Since the Fas2 landmarks are used by several research groups to characterize neurite projections of e.g. sensory (e.g. [25,26]) or motor (e.g. [24]) neurons, a comparison of the Fas2 “coordinates” of peptidergic processes with the projections of those neurons can provide a rationale to identify candidate afferents to or targets of peptidergic neurons, which in a second step can then be more rigorously analyzed. 2) The larval ventral ganglion is less complex than the brain, consists of a smaller number of neurons and shows in general a homomeric composition (see [27]). Despite its reduced complexity, the larval ventral ganglion nevertheless possesses peptidergic interneurons as well as neurosecretory cells producing peptide hormones, and receives sensory inputs of different modalities (see [27]).

As a basal step in deciphering peptidergic circuits, the data provides a morphological rationale to help identify candidate pre- and postsynaptic neurons by analysis of overlapping projections. Our results may additionally be useful for the identification of colocalized classical neurotransmitters, biogenic amines, peptides and receptors, and for developmental studies that rely on peptidergic neurons as landmarks.

RESULTS

In total, we have mapped peptidergic neurons expressing 12 different peptide precursor genes: *ast*, *capa*, *Ccap*, *cor*, *eh*, *Fmrf*, *hug*, *IFa*, *leucokinin*, *mip*, *pdf*, and *Dtk* (see table 1–2). This represents 32 processed peptides, or about 75% of the neuropeptides chemically proven to be produced by the CNS [10–13]. The peptide selection focused on neuropeptide hormones stored in thoracic or abdominal neurohemal organs (FMRFa-like peptides, CAPA peptides) or peripheral release sites on body wall muscles or the gut (CCAP, MIPs, leucokinin, PDF), and the availability of specific GAL4-lines. The results are presented in standardized plates (Fig. 1–13). Each plate shows a general overview of the observed immunolabeling or targeted mCD8.GFP expression in whole-mount preparations within the Fas2 landmark system. When considered useful, plates are accompanied by a supporting file (Fig. S1, S2, S3, S4, S5, S6, S7, and S8) which outlines further important details in a less rigorous way, including distribution patterns of ectopically expressed pre- and postsynaptic markers in case appropriate GAL4-drivers were available. The descriptions of

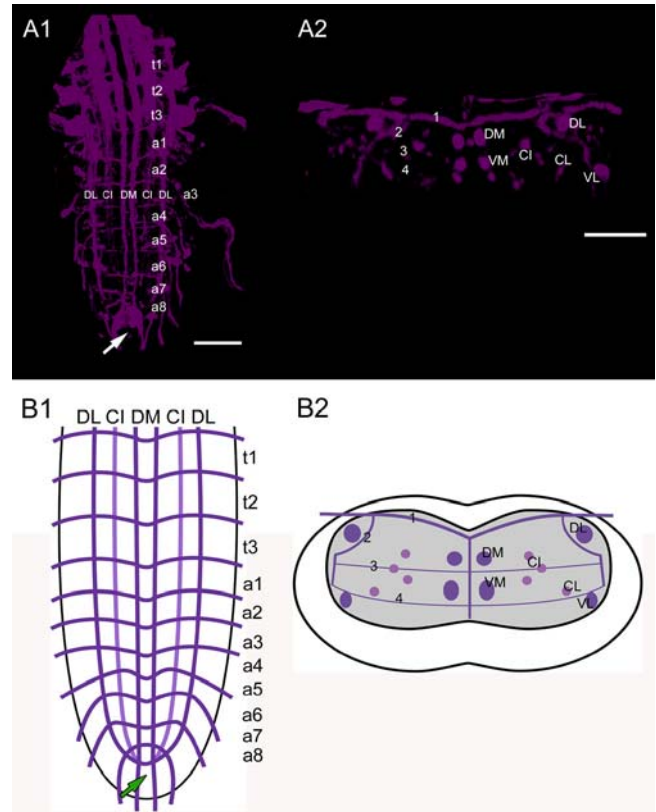


Figure 1. Fasciclin2 labeling. The Fas2 landmark system. A1) Dorsal view of a maximal projection showing longitudinal and transverse Fas2 immunoreactive fascicles. A2) Transversal view at the height of neuromere a3. B1) Idealized dorsal scheme B2) Idealized transverse scheme. Arrows in A1 and B1 show the neuromere a9 (“terminal plexus”). Scale bars: 50 μm in A), 25 μm in B). doi:10.1371/journal.pone.0000695.g001

the individual neuron labeling patterns below include a comprehensive comparison with previous morphological studies. This is preceded by a short summary of the known features of the respective peptides and their genes in *Drosophila*, and a comprehensive citation to published specificity tests of the antisera employed. The described projection patterns were highly constant throughout the preparations, whereas the position of somata was in general somewhat variable.

The neutral nomenclature of the Fas2-positive tracts (Fig. 1, Video S1, S2, and S3) follows Landgraf et al. [24], who also provided a general morphological description. Longitudinal tracts are designated by letters relative to their position in the dorsoventral (D, dorsal; C, central; V, ventral) and mediolateral (M, medial; I, intermediate; L, lateral) position. The five transverse Fas2-positive projections are numbered 1–5 according to their dorsoventral position. The DI and VI tracts were omitted in our schematic diagrams, since they were not always distinguishable and their inclusion would not have added to a more precise localization of peptidergic neurites. The metameric Fas2-staining relates to the segmental neuromeres as follows: each segmental nerve of the abdominal neuromeres a1–7 contains two tracts, the posterior segmental nerve (SN), which originates from the neuropil of the homotopic neuromere, and the anterior intersegmental nerve (ISN). The ISN consists of an anterior root (aISN) originating from the posterior commissure (pC) of the immediately anterior neuromere, and a posterior root (pISN) originating from the anterior commissure (aC) of the homotopic neuromere [27].

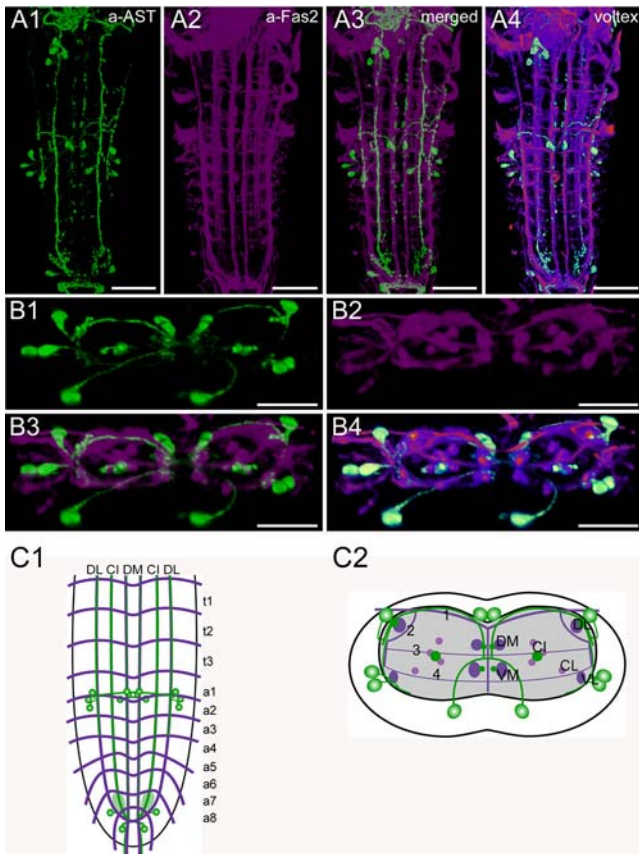


Figure 2. Morphology of AST-A neurons. Mapping of AST-A-IR neurons in whole-mount preparations of the thoracic and abdominal neuromeres of L3 larva in the Fas2 landmark system. A) Dorsal view. B) Transversal view at the height of neuromere a1/a2. C) Idealized dorsal scheme. D) Idealized transverse scheme. Scale bars: 50 μ m in A), 25 μ m in B). Immunostaining is shown in green, Fas2 in magenta. doi:10.1371/journal.pone.0000695.g002

The most prominent Fas2-IR transversal projection visible in the dorsal views is TP-1 which equals the pISN in the late larval stage [24]. Thus, the segmental borders are somewhat anterior to TP-1. Whereas the organization of the thoracic neuromeres t1–3 is very similar to that described for a1–7, there are differences in the segmental nerves of the last two abdominal neuromeres belonging to the tail region. The nerve of a8 only comprises a single fascicle deriving from three roots; the segmental nerve of a9 only has two roots [27].

In the figures, the CNS always appears flattened. This is due to slight compression of the preparations caused by the paraformaldehyde fixation, and due to the shifting light refractive index that is unavoidable during confocal z-scans (see [28]). These effects were not corrected, since they apply alike to Fas2 tracts and peptidergic (and other) neurons and vary depending on the thickness of the preparations. It is thus an advantage of relative landmark systems that these artefacts do not influence the overall results, since the morphological description is only relative to the Fas2 tracts.

Morphology of AST-A neurons (Fig. 2)

In *Drosophila*, three genes [*ast* (CG13633), *mip* (CG6456), *ast2* (CG14919)] encode precursors of peptides that have been designated allatostatins (AST): AST-A, B, and C. This is unfortunate since they do not all display allatostatic activity in a given insect species. AST-B peptides are also commonly referred

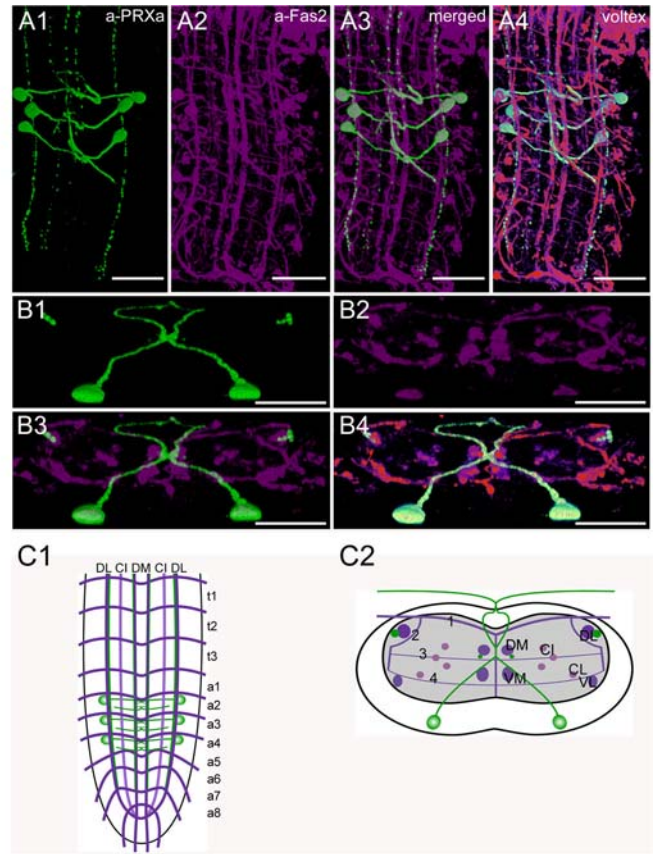


Figure 3. Morphology of CAPA and HUGIN neurons. Mapping of PRXa-IR neurons in whole-mount preparations of the thoracic and abdominal neuromeres of L3 larva in the Fas2 landmark system. A) Dorsal view. B) Transversal view at the height of neuromere a3. C) Idealized dorsal scheme. D) Idealized transverse scheme. Scale bars: 50 μ m in A), 25 μ m in B). Immunostaining is shown in green, Fas2 in magenta. doi:10.1371/journal.pone.0000695.g003

to as myoinhibitory peptides (MIPs) and will be described in a later section. Here, we analyze the distribution of AST-A peptides (Drostatin-A1–4) derived from the *ast* precursor [29]. The four peptides are processed as predicted from the genome in the larval and adult CNS [11,13], but their functions are still unknown. In other insects, Ast-A peptides show either allatostatic or myoinhibitory activity (see [30]).

The distribution pattern of AST-IR neurons (AST neurons) was described by Yoon and Stay [31] with a mouse mAb to *Diploptera* AST-1. We have reproduced this labeling pattern with a polyclonal antiserum against *Diploptera* AST-1 [32] and therefore adopted the nomenclature of Yoon and Stay. Since the polyclonal antiserum recognizes different *Dip*-allatostatins sharing the allatostatin A consensus sequence YXFGLa [32], we assume that the immunoreactivity in *Drosophila* represents at least Drostatin-A1–3 possessing a C-terminal YXFGLa.

The ventral ganglion contains 8 pairs of AST neurons, all located in the abdominal neuromeres. In the first abdominal neuromere (a1), a bilateral pair of AST neurons is located dorsomedially (DMA cells) in the cortex right above the DM tracts and the bifurcation point of transversal projection TP1 (1). Another pair of AST neurons resides in the ventromedial cortex (VMA cells); the position of their somata varies between the VM and the CI tracts. Furthermore, three pairs of neurons are arranged laterally in a1–2. One pair of somata resides dorsally

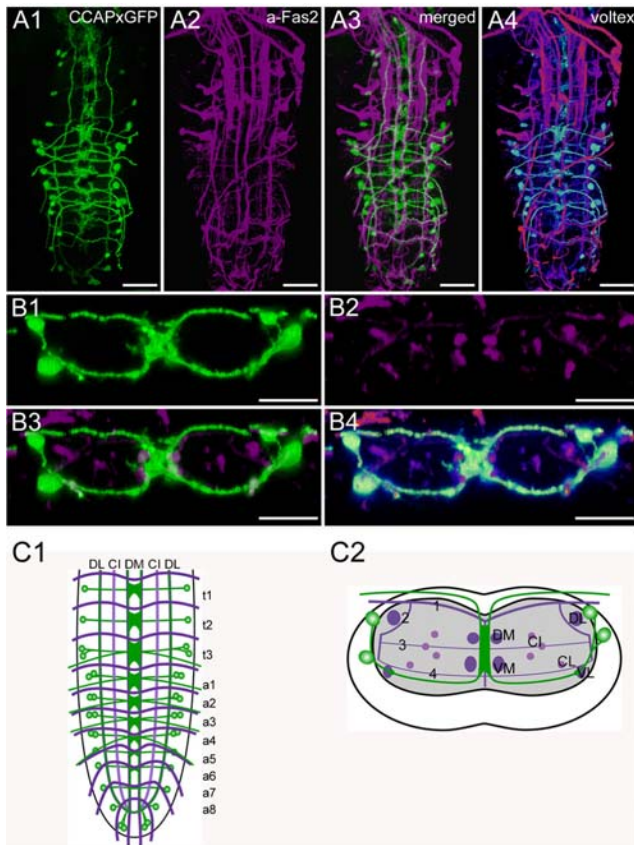


Figure 4. Morphology of CCAP neurons. Mapping of *Ccap-GAL4xUAS-cd8.gfp* expressing neurons in whole-mount preparations of the thoracic and abdominal neuromeres of L3 larva in the Fas2 landmark system. A) Dorsal view. B) Transversal view at the height of neuromere a3. C) Idealized dorsal scheme. D) Idealized transverse scheme. Scale bars: 50 μ m in A), 25 μ m in B). Marker protein expression is shown in green, Fas2 in magenta.
doi:10.1371/journal.pone.0000695.g004

nearly at the height of the DL tract (DLA cells); the other two adjacent pairs are located more ventrally at the height of the VL tract (VLA cells). The last abdominal neuromeres (a8/9) include three pairs of AST neurons (DLAa cells). One pair is located laterally in a8, whereas the other two are arranged more medially in a9, nearly at the tip of the ventral ganglion.

Longitudinal axonal projections of AST neurons are adjacent to the DM, VM, CI and DL tracts. The AST projections close to the DM, VM and DL tracts are poorly stained in a4–8, whereas those close to the CI tracts are most prominently stained. The longitudinal axon projections adjacent to the CI tracts converge in the neuropil of a8, where they give rise to arborizations with pronounced varicosities. Due to the strong staining of the axon projections following the CI tracts, and their varicose endings in a8, it seems likely that these structures represent a major release site of AST peptides, whereas the weaker stained AST projections close to the DM and VM tracts might represent dendritic areas containing fewer peptidergic vesicles.

In the neuropil, the axons of the DMA, VMA, DLA, VLA and DLAa cells converge closely with longitudinal AST projections, which made it impossible to follow their individual paths in detail. The DMA neurons project ventrally and seem to join longitudinal AST projections between the DM and the VM tracts. Each VMA cell sends a single axon dorsomedially, first passing between the

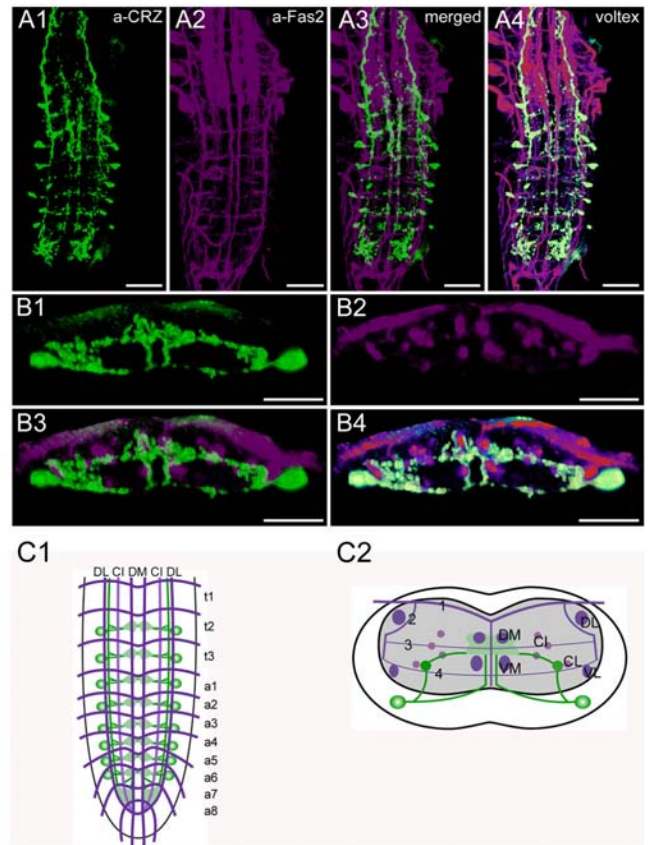


Figure 5. Morphology of corazonin-IR neurons. Mapping of corazonin-IR neurons in whole-mount preparations of the thoracic and abdominal neuromeres of L3 larva in the Fas2 landmark system. A) Ventral view. B) Transversal view at the height of neuromere a6. C) Idealized dorsal scheme. D) Idealized transverse scheme. Scale bars: 50 μ m in A), 25 μ m in B). Immunostaining is shown in green, Fas2 in magenta.
doi:10.1371/journal.pone.0000695.g005

DM and VM tract, and then joining with the contralateral neurite in the midline somewhat below the TP3 tract. There, the axons appear to cross to the contralateral side and continue together dorsally before they diverge in the neuropil beneath the DMA cells and project laterally above the TP1 tract. In the direct neighborhood of the DL tract, the VMA axons bilaterally join the

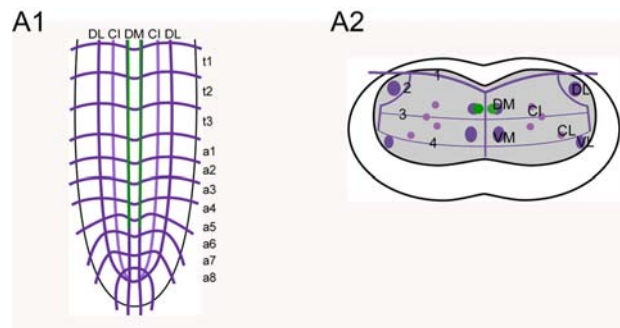


Figure 6. Morphology of eclosion hormone neurons. Mapping of *eh-GAL4xUAS-cd8.gfp* expressing neurons in whole-mount preparations of the thoracic and abdominal neuromeres of L3 larva in the Fas2 landmark system. A1) Idealized dorsal scheme. A2) Idealized transverse scheme.
doi:10.1371/journal.pone.0000695.g006

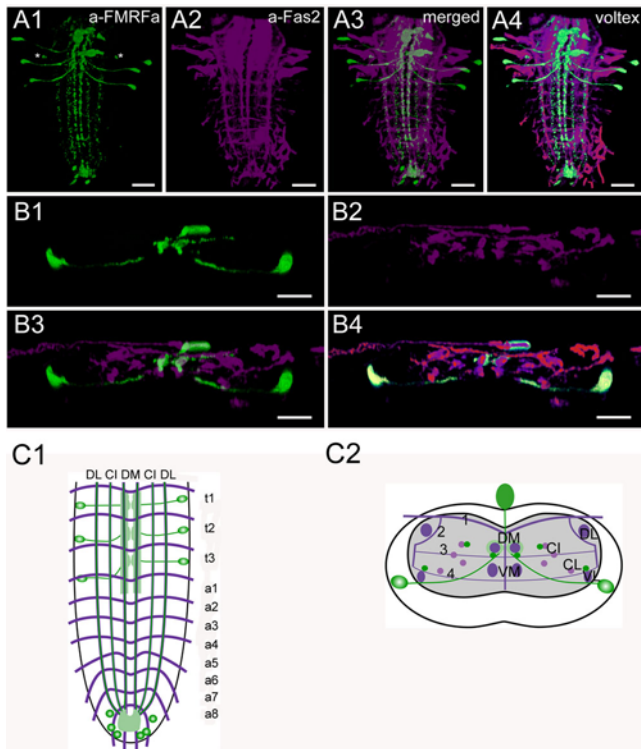


Figure 7. Morphology of FMRFamide neurons. Mapping of FMRFa-IR neurons in whole-mount preparations of the thoracic and abdominal neuromeres of L3 larva in the Fas2 landmark system. A) Dorsal view. B) Transversal view at the height of neuromere t2. C) Idealized dorsal scheme. D) Idealized transverse scheme. Scale bars: 50 μ m in A), 25 μ m in B). Immunostaining is shown in green, Fas2 in magenta. doi:10.1371/journal.pone.0000695.g007

longitudinal AST projections. These longitudinal AST projections are also connected to the DLA and VLA cells. Whereas each of the short axons of the DLA cells forms a small ventral loop before contacting the longitudinal AST projection close to the DL tract, the axons of the VLA cells project dorsally and join the same longitudinal AST projections behind the axons of the VMA and DLA cells. The DLAA cells of a8/9 extend their axons medio-anteriorly where they join with the longitudinal AST projections along CI and proceed posteriorly to exit in the last segmental nerve. These efferent axons innervate the surface of the hindgut [31].

Morphology of *capa* and *hugin* neurons (Fig. 3, S1)

The *hugin* (*hug*) precursor gene (CG6371) encodes a pyrokinin (HUG-PK [33]). The *capability* (*capa*) gene (CG15520) encodes a prepropeptide containing two periviscerokinins (CAPA-PVKs) and one pyrokinin (CAPA-PK) [34]. All of these peptides share the C-terminal sequence PRXa and are processed as predicted from the genome; CAPA-PK also occurs in a shortened form CAPA-PK²⁻¹⁵ in the suboesophageal neuromeres and in the ring gland [11–13]. A further potential PRXa (HUG- γ) is encoded by the HUGIN prepropeptide, but has not been shown to be processed. The *hug* gene has been implicated in regulation of feeding behavior in relation to chemosensory and nutritional signals [35] and CAPA-PVKs display diuretic activity on Malpighian tubules [34].

The pattern of PRXa-expressing neurons (PRXa neurons) in *Drosophila* was described using polyclonal antisera raised against Hez-pheromone biosynthesis activating neuropeptide, *Aplysia* myomodulin, and Pea-CAPA-PVK-2 [36–38]. The distribution of HUG-PK was studied by *in situ*-hybridization and by *hug*-GAL4-

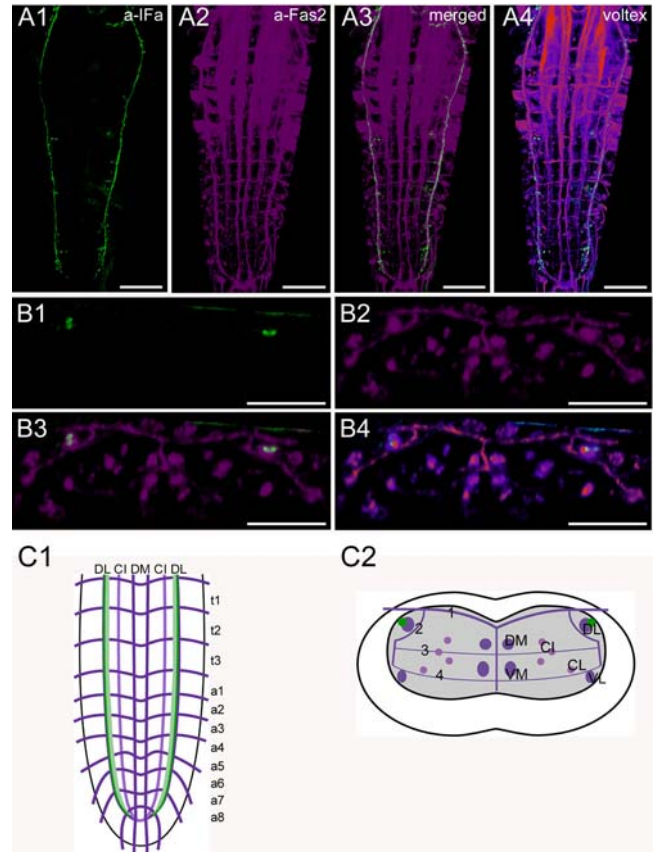


Figure 8. Morphology of IFamide neurons. Mapping of IFa-IR neurons in whole-mount preparations of the thoracic and abdominal neuromeres of L3 larva in the Fas2 landmark system. A) Dorsal view. B) Transversal view at the height of neuromere a3. C) Idealized dorsal scheme. D) Idealized transverse scheme. Scale bars: 50 μ m in A), 25 μ m in B). Immunostaining is shown in green, Fas2 in magenta. doi:10.1371/journal.pone.0000695.g008

directed GFP-expression [35]. The expression of CAPA was described by *in situ* hybridization and a precursor-specific antiserum [34]. In this study, we have used a polyclonal antiserum against Pea-PVK-2, which specifically recognizes the C-terminus PRXa ([39]) shared by the CAPA and HUGIN peptides, as well as marker molecule expression driven by Va-GAL4 (see below, [40]) and *hug*-GAL4 [35]. The ventral ganglion contains 3 pairs of strong PRXa-IR neurons (Va neurons): a bilateral pair of these Va neurons is located ventrally in each of the first three abdominal neuromeres. The Va neurons express *capa* and process all three CAPA peptides [12,34]. The position of the Va somata varied between preparations from a more median to a more lateral ventral position close to the ventral lateral (VL) tract. Typically, the somata on each side are arranged in a row. Each cell body sends a single axon dorsomedially through the neuropil, first passing below the central intermediate (CI) longitudinal Fas2-IR tracts, and then below the dorsal median (DM) tracts. Each axon reaches the midline at about transverse projection 3, where it joins with the axon of the contralateral Va neuron. The axons subsequently project together a short distance dorsally before they diverge and form a loop inside the neuropil and dorsal cortex. The loop closes just before the neurites leave the ventral ganglion and pass through the median nerve to finally enter the transverse nerves, where they end blindly. The median nerve and the innervated proximal part of the transverse nerves in a1–3 are

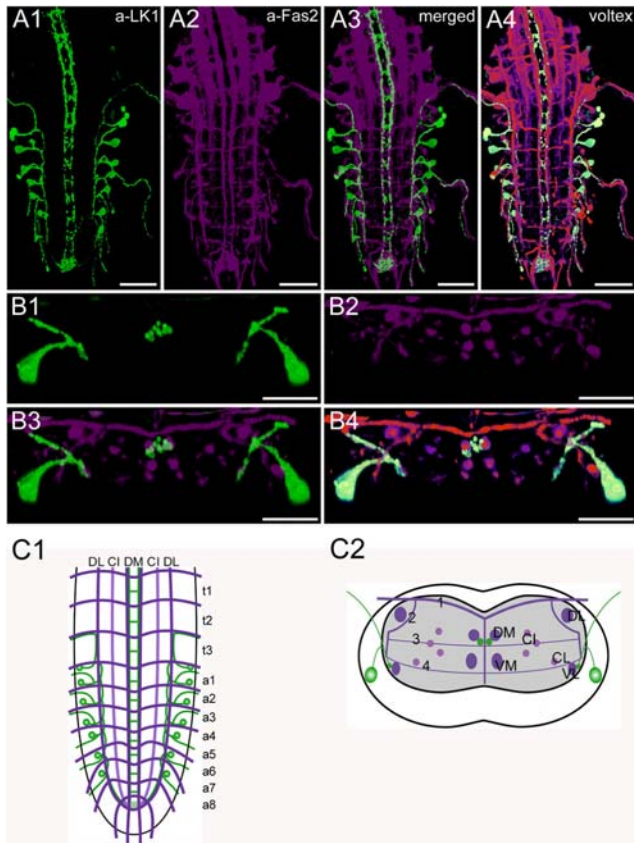


Figure 9. Morphology of leucokinin-IR neurons. Mapping of leucokinin-IR neurons in whole-mount preparations of the thoracic and abdominal neuromeres of L3 larva in the Fas2 landmark system. A) Dorsal view. B) Transversal view at the height of neuromere a3. C) Idealized dorsal scheme. D) Idealized transverse scheme. Scale bars: 50 μm in A), 25 μm in B). Immunostaining is shown in green, Fas2 in magenta. doi:10.1371/journal.pone.0000695.g009

neurohemal release sites (perisymphetic organs) for the CAPA peptides [38]. Va-GAL4-driven SYB.EGFP only labels the Va somata where the protein is produced, as well as the median nerve and the proximal part of the transverse nerves, but not the Va axons (Fig. S1). The accumulation of the vesicle marker SYB.EGFP fits well with the neurohemal function of the perisymphetic organs. Interestingly, we could not find morphological correlates for arborizations within the CNS by either PRXa immunostainings, or by GFP-expression and subsequent anti-GFP staining.

Descending PRXa-IR neurites run along each DM and DL tract and terminate in a7 around the border to a8. These neurites contain HUG-PK as shown by PRXa immunostaining of *hug-GAL4xUAS-GFP* flies.

Morphology of CCAP neurons (Fig. 4, S2)

The CCAP prepropeptide is encoded by the *Ccap* gene (CG4910). In *Drosophila*, CCAP has not been detected biochemically so far. In *Drosophila*, CCAP has an important role in the regulation of heart beat and ecdysis-related behaviors [41,42].

The distribution pattern of CCAP neurons has been described by immunostainings with a polyclonal antiserum produced by HJ Agricola [42,43], and by *in situ* hybridization as well as a specific *Ccap-GAL4*-line [42]. In our study, we relied on a specific polyclonal antiserum produced and characterized by H Dirksen [44] as well as the *Ccap-GAL4* line.

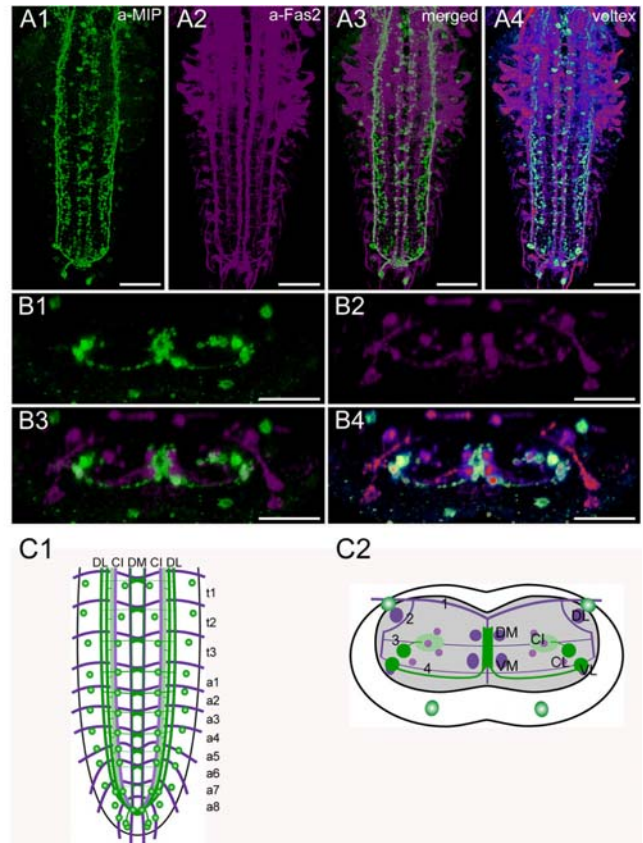


Figure 10. Morphology of MIP neurons. Mapping of Pea-MIP-IR neurons in whole-mount preparations of the thoracic and abdominal neuromeres of L3 larva in the Fas2 landmark system. A) Dorsal view. B) Transversal view at the height of neuromere a2. C) Idealized dorsal scheme. D) Idealized transverse scheme. Scale bars: 50 μm in A), 25 μm in B). Immunostaining is shown in green, Fas2 in magenta. doi:10.1371/journal.pone.0000695.g010

The observed pattern of *Ccap-GAL4*-driven GFP-expressing neurons (CCAP neurons) matched generally that of the known patterns of CCAP-immunoreactivity [43] and *Ccap*-expression [42], though there are a few differences in the number of neurons and in the extent of GFP-expressing neurites [8]. In t1 and t2, a bilateral pair of CCAP neurons is located ventrolaterally, i.e. nearly at the height of the VL tract. In contrast, t3 and a1–4 each contain two pairs of CCAP neurons. These neurons are also located laterally. The position of their somata in a1–4 varied in the dorso-ventral axis from a more median to a more dorsal position, i.e. between the height of the VL and the DL tract, whereas the pairs in t3 are ventrally located (Fig. S2). In a5–7, only one pair of lateral neurons expresses *Ccap-GAL4*-driven GFP; their somata reside between the height of the VL and the DL tract. We could however visualize single additional CCAP neurons by immunostaining in a5–7. Thus it seems likely that also a5–7 contain two pairs of CCAP neurons. The last abdominal neuromeres a8–9 contain three pairs of CCAP neurons, one is located laterally, whereas the other two are arranged more medially, nearly at the tip of the ventral ganglion. In many preparations, GFP-expression in these CCAP neurons of a8–9 is weak. Single descending CCAP neurites project very close to the VL tracts on both sides and coincide in the terminal plexus of a9. Further descending neurons, most probably originating in the brain, run along the DM fascicles (Fig. S2).

Each CCAP neuron in t1–3 and a1–7 sends a neurite beneath the transversal projection 4 ventromedially, where the neurites

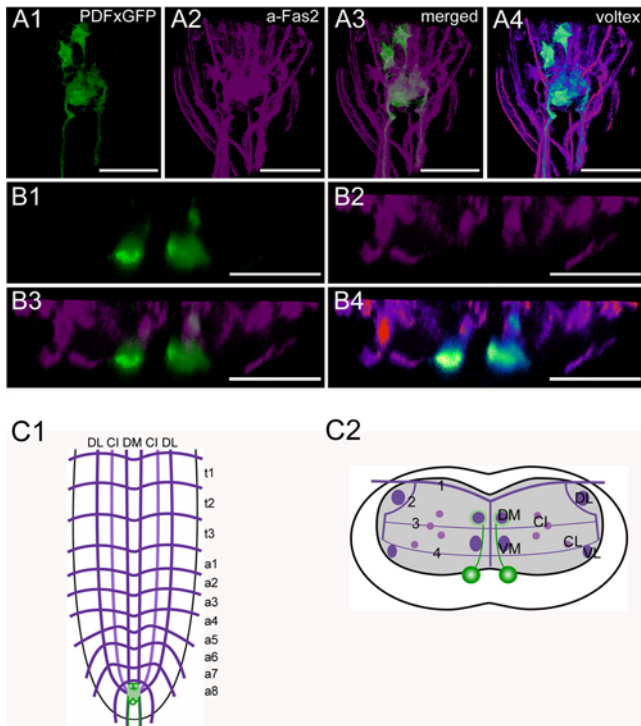


Figure 11. Morphology of PDF neurons. Mapping of *pdf-GAL4xUAS-cd8.gfp* expressing neurons in whole-mount preparations of the thoracic and abdominal neuromeres of L3 larva in the Fas2 landmark system. A) Dorsal view of the posterior part of the VNC. B) Transversal view at the height of neuromere a8. C) Idealized dorsal scheme. D) Idealized transverse scheme. Scale bars: 50 μ m in A), 25 μ m in B). Marker protein expression is shown in green, Fas2 in magenta. doi:10.1371/journal.pone.0000695.g011

from both sides join in proximity to the VM tracts. These joining CCAP neurites form extensive arborizations along the midline between the DM and VM tracts, which are most prominent in t3. In t3 and a1–4, the medially joined neurites of at least one neuron pair project further dorsally until they leave the central neuropil. These neurites diverge in the dorsal cortex, project via the segmental nerves to the periphery, and form type III terminals on body wall muscles M12 and M13 [8].

Based on release studies with a peptide-GFP construct, the descending neurites along the VL tract have been suggested to be central CCAP release sites [45]. This suggestion is supported by the accumulation of CCAP-IR material and *ccap-GAL4*-driven SYB.EGFP in these descending neurites. Furthermore, both CCAP-IR and SYB.EGFP, but not GFP, strongly label median descending neurites with pronounced varicosities along the DM fascicles. This suggests that CCAP is also released along the DM tract.

In contrast, the putative postsynaptic marker RDL.HA (see discussion) is exclusively present between the DM and VM tracts at the region of the extensive arborizations of the thoracic and abdominal CCAP neurons (Fig. S2). These arborizations are strongly labeled by GFP, only faintly labeled by SYB.EGFP, and unlabeled in CCAP immunostainings (Fig. S2). We thus assume that the median arborizations around the DM and VM tracts represent a dendritic compartment, whereas CCAP release mostly occurs from descending neurites along the VL and DM tracts as well as from peripheral release sites on muscle M12 and M13 [8].

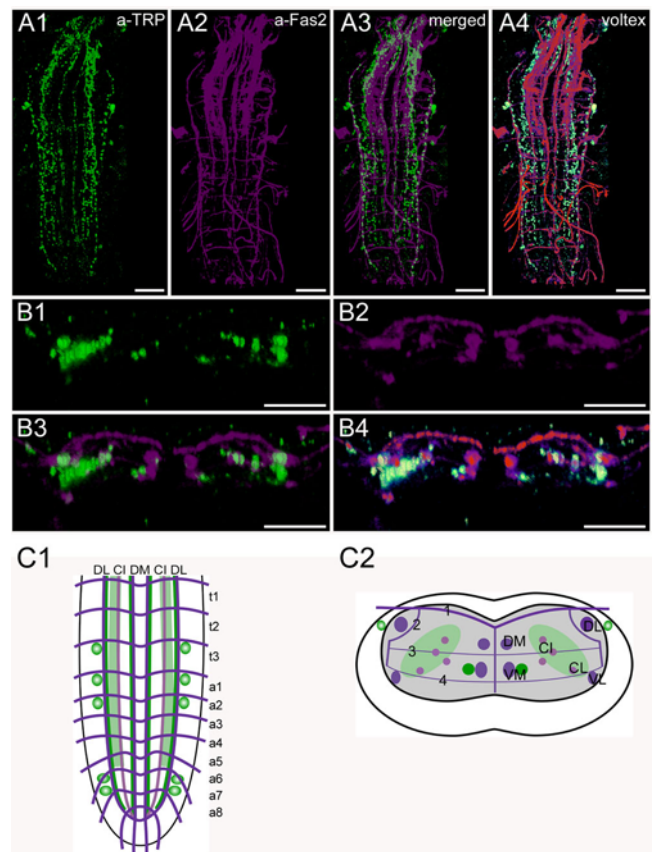


Figure 12. Morphology of tachykinin-related peptide-expressing neurons. Mapping of TRP-IR neurons in whole-mount preparations of the thoracic and abdominal neuromeres of L3 larva in the Fas2 landmark system. A) Dorsal view. B) Transversal view at the height of neuromere a1. C) Idealized dorsal scheme. D) Idealized transverse scheme. Scale bars: 50 μ m in A), 25 μ m in B). Immunostaining is shown in green, Fas2 in magenta. doi:10.1371/journal.pone.0000695.g012

Morphology of corazonin neurons (Fig. 5, S3)

The *Drosophila* corazonin prepropeptide is encoded by the *crz* gene [46,47]. Corazonin occurs in full length, but also in a shortened form, corazonin³⁻¹¹ [11–13]. The function of corazonin in *Drosophila* is so far unknown, although it might be associated with the circadian clock and the control of ecdysis [47,48].

The pattern of corazonin-IR neurons (corazonin neurons) in *Drosophila* was described by Choi et al. [47] with a specific polyclonal antiserum as well as *in situ* hybridization, and by Landgraf et al. [24] with a polyclonal antiserum produced by J Veenstra [49]. In this study, the Veenstra antiserum was used and yielded results identical to those previously described.

In total, 16 corazonin neurons are located in the ventral ganglion. In t2–3, and a1–6, one bilaterally symmetric pair of strongly stained neurons was observed. Each soma is located ventro-laterally approximately below the VL tract. It sends a neurite towards the midline which bifurcates shortly after leaving the soma. The lower branch projects ventrally towards the midline, then bends dorsally and enters the neuropil below and slightly medial to the VM tract. At the dorsal height of the VM tracts, it enters a medial varicose region located between the DM and VM tracts. The upper branch first projects dorsally until it reaches a longitudinal corazonin-IR tract that runs along the inner side of the CL tract. It then bends medially between the CI tracts

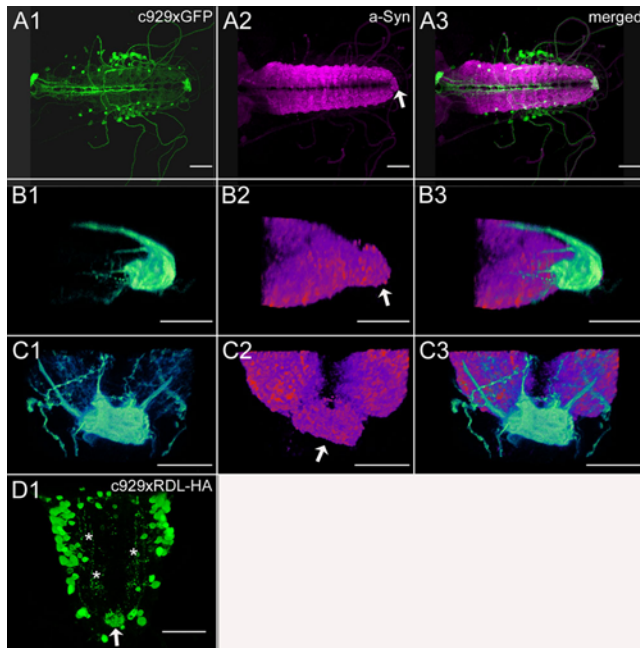


Figure 13. Distribution of c929-GAL4 driven expression of synaptic markers. A) Dorsal view of the VNC of a c929-GAL4xUAS-GFP larva, voltex projection. B) Lateral view of a8–9 of a c929-GAL4xUAS-GFP larva, voltex projection. C) Dorsal view of a8–9 of a c929-GAL4xUAS-GFP larva, voltex projection. Note the reduced morphology of the neuropil in a9 (= the terminal plexus), immunolabeled against the synaptic marker protein synapsin (arrow) in A–C). D) Dorsal view of a c929-GAL4xUAS-RDL.HA larva, maximum projection. RDL.HA immunostaining labels the cell bodies, descending neurites (asterisks) and the terminal plexus (arrow). Scale bars: 100 μ m in A), 20 μ m in B–C), 50 μ m in D). HA-immunostaining or GFP expression is shown in green, synapsin-IR in magenta. doi:10.1371/journal.pone.0000695.g013

until it reaches the varicose region between the DM and VM tracts. This varicose region seems to be formed by endings of both upper and lower branches. The longitudinal corazonin-IR tract along the CL tract extends posteriorly until a7, and anteriorly into the brain. At both endings, the tract arborizes and forms a varicose field. In the ventral ganglion, this field fills the neuropil between DL/VL and DM/VM tracts of a7–8, is strongly immunoreactive and extends ventrally from an intermediate position to the VM

Table 1. Employed fly lines

Lines	Donor [Reference]
<i>pdf-Gal4</i>	Jeff Hall [119]
<i>Ccap-Gal4</i>	John Ewer [42]
<i>Eh-Gal4</i>	John Ewer [51]
<i>Va-Gal4</i>	Stefan Thor [40]
<i>hug-Gal4</i>	Michael Pankratz [35]
<i>c929-Gal4</i>	Paul Taghert [78]
<i>fmr-Gal4</i>	Paul Taghert
<i>UAS-cd8.gfp</i>	Bloomington Stock Center, Tzumin Lee and Liqun Luo [120]
<i>UAS</i>	Bloomington Stock Center, Jim Posakony
<i>nls.RedStinger</i>	
<i>UAS-n-syb.egfp</i>	Bloomington Stock Center, Kendal Broadie [88]
<i>UAS-rdl.HA</i>	Andreas Prokop [89]

doi:10.1371/journal.pone.0000695.t001

tracts (see also Fig. S3). The longitudinal corazonin-IR fascicle appears to be formed by neurites of the corazonin neurons in the ventral ganglion. It was, however, impossible to distinguish whether only some or all corazonin neurons contribute to it. Whereas the complete fascicle could be visualized with the corazonin antiserum in the thoracic neuromeres, staining broke up into varicosities in the abdominal neuromeres. Since varicosities are putative peptide release sites, it appears that corazonin is released from the longitudinal corazonin-IR fascicle along the CL tract in the abdominal neuromeres, the median neuropil between the DM and VM tracts, and especially within the neuropil of a7/a8.

Morphology of eclosion hormone neurons (Fig. 6)

The eclosion hormone (EH) is encoded by the *Drosophila* gene *Eh* (CG5400 [50]) and plays an important role in the regulation of ecdysis behavior [51]. It has so far not been chemically characterized in *Drosophila*.

The morphology has been described by immunostaining [50], and with an *Eh*-GAL4 line [51] that was also used in this study.

EH is exclusively expressed in a single pair of neurons with somata in the ventromedial brain. Their axons (one per hemisegment) descend along, and to some extent overlap, the DM tract and terminate at segment a5/a6. In our hands, the *Eh*-GAL4 line was only a weak driver for marker molecules, and we could only label somata by ectopic expression of RDL.HA or SYB.EGFP.

Morphology of FMRFa neurons (Fig. 7, S4)

The *Drosophila* *Fmr*f precursor gene (CG2346) encodes eight different FMRFa-like neuropeptides [52–54], all of which have been chemically identified in the CNS [11–13]. In *Drosophila*, FMRFa-like peptides may play a role as hormones during ecdysis and myomodulators on body wall muscles and the heart [55–57].

The larval pattern of FMRFa-IR neurons (FMRFa neurons) was described with different polyclonal antisera raised against FMRFa [53,54,58–60], and by *in situ* hybridization [53,61]. In this study, we employed a *fmr*f-GAL4 driver [62] to express GFP, and a polyclonal anti-RFamide serum [63] that is expected to label FMRFa-like peptide 2–7 and probably also other peptides containing RFamide in its C-terminus in *Drosophila*.

The overall pattern of the 14 FMRFa-IR neurons is basically similar to that described in earlier studies [53,54,58,59], although several median FMRFa-IR neurons reported in these studies could not be found in our immunostainings. The nomenclature of neurons follows [54]. In each of the thoracic neuromeres, one pair of strongly staining Tv neurons could be visualized, which were also included in the *fmr*f-GAL4 driver line. Their somata are quite large and elongated, located very close to the lateral border of the neuromeres ventrolaterally to the VL tracts. Each Tv neuron sends a single axon toward the midline. It first projects below the VL tract, bends upward below the CL and CI tracts, and approaches the DM tract from below. Strongly GFP-labeled arborizations were visible around the DM tract. These arborizations are probably dendritic input areas, since they were not marked by *fmr*f-GAL4-driven expression of SYB.EGFP (Fig. S4). In the anterior-posterior axis, the dendritic areas of the three pairs of Tv neurons form a continuous band from t1 to about half the way between a1 and a2. The axon of each Tv neuron then fasciculates with that of the contralateral Tv neuron and projects into the respective neurohemal thoracic perisymphathetic organ (tPSO) where strong arborizations and varicose structures were visible. The tPSOs exhibited a strong accumulation of *fmr*f-GAL4-driven SYB.EGFP (Fig. S4), indicating that FMRFa-like peptides are stored and released from the tPSOs. One smaller neuron in the

Table 2. Employed antisera

Antisera/mAb	(Dilution)	
	Source	Donor [Reference]
Anti-CRZ	(1:2000) rabbit	Jan Veenstra [49]
Anti-CCAP	(1:1000) rabbit	Heinrich Dirksen [44]
Anti-FMRFa	(1:4000) rabbit	Eve Marder [63]
Anti-IFa	(1:500) rabbit	Peter Verleyen & Liliane Schoofs [65]
Anti-LK-1	(1:2000) rabbit	[68]
Anti-MIP	(1:4000) rabbit	Manfred Eckert [71]
Anti-PDF	(1:4000) rabbit	[76]
Anti-PRXa	(1:4000) rabbit	Manfred Eckert [39]
Anti-TRP	(1:4000) rabbit	[121]
Anti-allatostatin-A	(1:5000) rabbit	Hans Agricola [32]
Anti-Fas2 mAb 1D4	(1:75) mouse	Developmental Study Hybridoma Bank, Corey Goodman
Anti-HA mAb 3F10	(1:75) rat	Roche Diagnostics, Mannheim, Germany

doi:10.1371/journal.pone.0000695.t002

second thoracic neuromere near each Tv soma was also FMRFa-IR (asterisk in A1); its neurite could however not be visualized. In the terminal abdominal neuromere a9, six At1 cells could be stained. Again, their neurites could not be visualized.

On each side of the ventral ganglion, three descending varicose FMRFa-IR neurites run medial along the CI tract, ventral to the DM tract, and dorsal to the VL tract. These FMRFa-IR neurites terminated in the neuropil of the terminal abdominal neuromere which showed strong FMRFa-immunoreactivity.

Morphology of IFamide neurons (Fig. 8)

The *IFa* gene (CG33527) of *Drosophila* encodes one IFamide (IFa) which is processed as predicted from the genome [11,13]. IFa is a potent modulator of sexual behavior in the fruit fly [64].

The pattern of IFa-IR neurons (IFa neurons) has been described with a polyclonal antiserum against the LFamide of the flesh fly *Neobellieria bullata* [65], and by immunostaining and *in situ* hybridization [64]. In this study, the *Neobellieria* LFamide antiserum was used and yielded results identical to those described.

In the ventral ganglion, IFa-IR somata (IFa somata) are absent. However, two pairs of IFa somata are strongly stained in the anterior medial region of the larval brain. These neurons send descending axons (one in each hemisphere) along the DL fascicles through the complete ventral ganglion. These IFa axons end abruptly in a8/9, just before the longitudinal Fas2 fascicles terminate at the border of the terminal plexus of a9. Arborizations within the terminal plexus were never observed. Varicosities are pronounced along short side-branches oriented medially towards the neuropil in each of the thoracic and abdominal neuromeres. These varicosities suggest that IFa is released along the whole DL tract within the thoracic and abdominal neuromeres.

Morphology of leucokinin neurons (Fig. 9, S5)

The *Drosophila* *Leucokinin* precursor gene (CG1 3480) encodes one leucokinin [66], which is processed as predicted from the genome [11,13,66]. Leucokinin acts as a diuretic hormone on the Malpighian tubules [66].

The pattern of leucokinin-IR neurons (LK neurons) was described in *Drosophila* [24,67] with a polyclonal antiserum raised against *Leucophaea leucokinin* I [68]. In this study, we reproduced this pattern using the same antiserum.

Table 3. Peptidergic projections in relation to Fas2 tracts Assignment of putative main compartment identities as suggested by morphology, immunolabeling intensities and distribution of synaptic markers

Fas2 tract	peptide projection	putative compartment identity
DM/VM	AST-A	input
	CCAP	input (and non-peptidergic output?)
	corazonin	in?- and output
	MIP	in- and output
	EH	output
DM	c929	in- and output
	HUG-PK	output
	FMRFa	input (Tv neurons), output (descending neurons)
	leucokinin	output (descending neurons)
VM	PDF	input
	Dtk	n.d.
DL	AST-A	n.d.
	HUG-PK	output
	IFa	output
	c929	in- and output
	leucokinin	input?
VL	CCAP	output
	c929	in- and output
	leucokinin	input?
CI	AST-A	n.d.
	MIP	output
	Dtk	output
	c929	input
CL	corazonin	output
	MIP	output
	Dtk	output
	c929	in- and output
neuropil a8	corazonin	output
	c929	output
neuropil a9	FMRFa	n.d.
	leucokinin	output (descending neurons)
	c929	in- and output

doi:10.1371/journal.pone.0000695.t003

In each of the first seven abdominal neuromeres, one bilateral pair of strongly stained neurons was observed. In general, the most anterior neurons appeared to be gradually larger and were placed closer to the external cortex border than the posterior neurons. Each soma is located ventro-laterally in each hemi-neuromere approximately at the height of the VL tract. It sends a neurite dorsomedially that divides into two branches just before or when entering the neuropil at the height of the lower CI fascicles. The dorsal branch projects further dorso-anteriorly, leaves the ventral ganglion through the segmental nerve of the next anterior segment (segmental nerves of t3 and a1–6), and forms peripheral release sites on body wall muscle M8 [67].

The second branch turns ventrally until it reaches the VL tract where it seems to become a part of a descending leucokinin fascicle along the VL tract from a1 to a8. The leucokinin-fascicle enters the neuropil of a9 (the “terminal plexus” [24]), where it strongly arborizes. The terminal plexus is also innervated by two

descending varicose leucokinin fascicles that are associated with the DM tracts. These descending neurites seem to originate from somata in the first suboesophageal ganglion [24,67].

Based on the distribution of varicosities, two putative release areas of leucokinin can be postulated: peripheral release sites of the abdominal leucokinin neurons mostly on muscle M8 [67], and central release sites along the DM tract throughout the whole ventral ganglion originating from leucokinin neurons in the first suboesophageal neuromere.

Morphology of MIP neurons (Fig. 10)

The *Mip* prepropeptide gene (CG6456) of *Drosophila* encodes 5 putative myoinhibiting peptides (MIPs [69], also designated AST-B-1-5 [70]). Three of these have been chemically characterized within the CNS [11,13]. The functions of MIPs in *Drosophila* are unknown, although they are likely to play a role during ecdysis [57].

The distribution of MIP-expressing neurons (MIP neurons) has been studied by *in situ* hybridization and by immunostaining [57,70]. Kim et al. [57] assigned two pairs of MIP neurons co-expressing CCAP to the abdominal neuromeres a1–4 and a8/9, whereas MIP neurons seemed to be absent in a5–7. Neurons that lacked CCAP-expression but showed MIP-IR (e.g. in the thoracic neuromeres and in a8/9) were not described. We have employed a polyclonal antiserum directed against Pea-MIP (GWQDLQGGWa) [71], yielding slightly different results. We assume that the polyclonal antiserum recognizes MIP-1 (AWGSLQSSWa) and MIP-5 (DQWQKLHGGWa), if not all *Drosophila* MIPs which share the C-terminal Wamide.

Two Pea-MIP IR neurons (Pea-MIP neurons) are arranged at each side in two different bilateral symmetric rows in neuromeres t1–a7. The first row of Pea-MIP neurons is located dorso-laterally nearly at the height of the DL tract (at least some of these neurons co-express CCAP), the second row resides ventromedially at the width of the CI tracts. In a8/9, four pairs of Pea-MIP neurons are grouped at the tip of the ventral ganglion. Longitudinal projections of Pea-MIP neurons are adjacent to the DM, VM and VL tracts, and above the CI tract. All longitudinal Pea-MIP projections coincide in the terminal plexus of a9, forming a small terminal area with many varicosities. The Pea-MIP longitudinal projection adjacent to the CI tract innervates an area with many varicosities around the CI tracts. Transversal projections of Pea-MIP neurons reside ventro-medially at the height of the transverse tract 4. The transversal Pea-MIP neurites from both sides join with the central longitudinal Pea-MIP projections in proximity to the VM tracts and establish extensive arborizations in the midline of the central neuropil between the DM and VM tracts.

Morphology of PDF neurons (Fig. 11, S6)

In *Drosophila*, pigment-dispersing factor (PDF) is encoded on the *Pdf* gene (CG6496, [72]) and processed as predicted from the genome. In the brain, PDF has important roles within the circadian system (e.g. [73]).

The pattern of larval PDF-IR neurons (PDF neurons) was described with a polyclonal antiserum raised against crustacean β -PDH [44,74,75]). In this study, we could reproduce this pattern using a characterized polyclonal antiserum produced against *Drosophila* PDF [76,77], with hitherto undescribed dendritic arborizations that were visualized by *pdf*-GAL4-directed GFP-expression as described below.

PDF neurons occur in two groups: one consisting of 3–4 somata in a8, and another consisting of 4 somata in a9. These numbers are based on the *pdf*-GAL4-driven expression of a nucleus-targeted

dsRed-variant, since the cell number was difficult to assess with immunolabelings or membrane-targeted GFP. The somata in a8 are located ventrally directly below the neuropil region, slightly lateral below the VM tracts. Neuromere a9 does not show the typical Fas2-positive pattern. Therefore, a scheme is not given, and positions are described with reference to the Fas2-positive tracts in a8. The somata in a9 are more dorsally located than those in a8, just behind the prominent posterior neuropil at about the height of the DM tracts. The medio-lateral position of the somata in a9 is similar to that in a8, i.e. slightly lateral of the DM/VM tracts. Unlike other peptidergic cell bodies, the PDF somata show a rhombic or polygonal shape. The PDF neurons send immunostained axons through the 8th abdominal segmental nerve into the periphery. Closer analysis of the distribution of *pdf*-GAL4 driven mCD8-GFP reveals pronounced arborizations in the terminal plexus, the neuropil of a9. Anterior to the terminal plexus, *pdf*-GAL4-driven GFP was also visible along the DM tracts in a8. Since these arborizations in the terminal plexus and along the DM tracts are not labeled by different antisera against PDF ([74], this study) and *pdf*-GAL4-driven SYB.EGFP (Fig. S6), we regard these arborizations to be the PDF neuron dendrites. Although PDF is an amidated peptide, the abdominal PDF neurons are not included in L3 larvae of the c929-GAL4 line specific for neurons expressing the amidating enzyme PHM ([78], not shown).

Besides neuromeres a8 and 9, PDF labeling is absent from the rest of the VNC, descending projections from the suboesophageal ganglion or the brain were not observed.

Morphology of TRP neurons (Fig. 12, S7)

The *Drosophila* gene *Dtk* (CG14734) encodes a prepropeptide containing 5 tachykinin-related peptides, DTK1-5 [79], all of which are expressed in the brain [80]. In the fruit fly, DTKs have a modulatory role in olfactory perception and locomotor activity [81].

The distribution of tachykinin-related peptide-IR neurons (TRP neurons) has been described by *in situ* hybridization and immunostaining with a polyclonal antiserum against the cockroach LemTRP-1 (APSGFLGVRamide) [79,80]. We used the same antiserum and found a pattern similar to that described in [80], although the reported weakly TRP-IR neurons expressing *Dtk* could not be visualized in our immunostainings. We assume that the immunoreactivity recognizes all DTKs which share the C-terminal sequence FXGXRamide with LemTRP-1.

In the ventral ganglion, five pairs of neurons were immunostained: one pair in t3, and one pair each in a1, a2, a6 and a7. As in the earlier studies, we could not visualize the neurites of these neurons.

Several TRP-IR neurites with prominent varicosities descend from the brain and suboesophageal ganglion. One pair of TRP-IR neurites descend along the midline parallel to the lateral side of the DM tracts until t3. In some cases, these TRP-IR neurites extended as far as a2, or even further. In most preparations, a second neurite descends from t3 along the outer side of the VM tracts up to a8 on each side. In a few cases, these longitudinal neurites descended from t2. Moreover, a broad varicose region is formed by descending neurites from the brain that are situated mostly between the VL and the CI tracts up to a8. Further lateral TRP-IR neurites descend along the DL tract and terminate in a7 or a8.

On each side in T3, a TRP-IR fascicle runs transversely ventral from the DL tract, continues through the CI tracts and meets the fascicle from the other side at the midline between the DM and

VM tracts (Fig. S7). These fascicles seem to originate from the TRP-IR somata in T3.

Based on the assumption that strongly varicose regions indicate peptide release sites, all the described descending neurites might represent peptide release sites with a particular concentration in the area between the CI and VL tracts.

Distribution of ectopical c929-GAL4-driven SYB.EGFP and RDL.HA (Fig. 13, S8)

The c929-GAL4 line (*dimmed*) is specific for peptidergic neurons and specifies around 200 neuroendocrine cells/neurons, i.e. a large proportion of the peptidergic neurons [78]. c929-GAL4-driven expression of GFP, the presynaptic marker SYB.EGFP, and the postsynaptic marker RDL.HA labeled the same peptidergic neuron somata, and matched the previously described pattern [78]. In contrast, differences in the distribution of the marker proteins were found within neuropil areas (Fig. S8). GFP fluorescence was most intense in the terminal plexus of a9, median fascicles around the DM tracts in the thoracic and the first 3–4 abdominal neuromeres, and lateral fascicles along the DL/VL tract. SYB.EGFP fluorescence occurred in a punctate fashion, in accordance with its suspected localization in the membrane of peptidergic vesicles accumulating at release sites. Spots of high SYB.EGFP fluorescence are thus likely to represent vesicle storage or release sites. SYB.EGFP fluorescence was most intense in the thoracic PSOs, the lateral fascicles and throughout the neuropil of a7/8, suggesting these structures as prominent peptide release sites. The terminal plexus of a9, and the median fascicles contained lesser amounts of SYB.EGFP fluorescence, but also here SYB.EGFP presence suggests that peptides are released at these structures. Noteworthy, also an intermediate fascicle expressing SYB.EGFP was visible, a structure that could also be labeled with lacZ [78], but was not prominently labeled by GFP. The most restricted distribution pattern in the neuropil was found for c929-GAL4-driven RDL.HA, which was concentrated within the terminal plexus of a9 (Fig. 13). Strong contrast enhancement of the vortex projections revealed further RDL.HA localization at lateral, intermediate and median projections (Fig. 13). These results suggest that the terminal plexus contains a higher density of peptidergic postsynaptic sites of peptidergic neurons than any other neuropil area. Postsynaptic compartments of peptidergic neurons appear, however, also to be located at lateral, intermediate and median peptidergic fascicles. Since the anti-RDL.HA staining intensity in general was very weak, areas with a low density of peptidergic postsynapses might have escaped our analysis.

DISCUSSION

Based on our comparative analysis of the projection patterns of processes from different peptidergic neuron types within the Fas2 landmark scaffold, some broader generalizations about the morphological organization of peptidergic systems within the ventral ganglion can be made. These are discussed in the following sections.

Serial homology

As in other eumetazoans, the insect body is segmentally organized. The general organization of thoracic and abdominal ganglia is similar and well preserved throughout the insects and crustaceans [15]. Serial homology (i.e. segmental reiteration) in insect ventral ganglia has been found for aminergic, sensory, motor and interneurons, and to some extent also for peptidergic neurons (see [82–85]). In contrast, the organization of peptidergic neurons in the ventral ganglion of *Drosophila* larvae does not in general follow a strict segmental reiteration of peptidergic modules

throughout the neuromeres. The only segmentally reiterated distribution throughout all ganglionic neuromeres or within a tagma was found for Pea-MIP neurons in neuromeres t1–a8 (Fig. 10), and the FMRFa-containing Tv neurons in the three thoracic neuromeres (Fig. 7). The Tv neurons innervate the thoracic neurohemal perisymphathetic organs, which have a tagma-specific organization and peptidome and exclusively express FMRFa-like peptides across all insects studied (see [12,13,86]). The segmentally reiterated distribution of leucokinin and CCAP neurons within the abdominal neuromeres was restricted to a1–7 (Fig. 4, 9). Each leucokinin neuron sends a projection to the periphery with terminals on muscle M8 (the segmental border muscle, [67]) which is lacking in a8/9 (see [87]). This might functionally explain the lack of leucokinin neurons in a8/9. The distribution patterns of the other peptidergic neurons with somata in the abdominal neuromeres show even less serial homology. AST neurons are segment-specific and occur only in a1–2 (Fig. 2). Other peptidergic neuron types skip one or several neuromeres, e.g. corazonin neurons only occur in a1–6 (Fig. 5). The lack of a strict segmentally reiterated pattern throughout the thoracic and abdominal neuromeres suggests that the restricted and differential distribution of peptidergic neurons reflects neuromere-specific functional connections. We are, however, not aware of other larval neuron types or circuits that match the observed peptidergic distribution patterns.

The last two abdominal neuromeres a8/9 have a unique pattern of peptidergic somata and projections (e.g. FMRFa, MIP or PDF neurons (Fig. 7, 10, 11)) and show the least serial homology to the more anterior neuromeres of the ventral ganglion. This finding also extends to descending processes. Descending axons may stop before or when reaching the border to a8 (HUG and DTK neurons (Fig. 3, 12)), form extensive varicose ramifications within the neuropil of a8 (AST, corazonin (Fig. 2, S3-C)) or branch extensively in the terminal plexus of a9 (FMRFa, leucokinin, MIP and PDF neurons (Fig. 10, S4-B, S5-B, S6)). Belonging to the tail region, the segments a8/9 differ from the homomeric segments a1–7 with respect to the organization of muscles and sensory neurons (see [27,87]). Furthermore, several unique structures such as the spiracles or the anal pads belong to these terminal segments. Unlike other segmental nerves, the segmental nerve of a9 innervates the hindgut musculature [27]. The unique pattern of peptidergic neurons in a8/9 might thus, at least partially, reflect a segment-specific function related to e.g. control of spiracles or intestinal functions. For example, the PDF neurons innervate the hindgut [74], but their exact function is so far unknown. Similar segmental differences between a8 and the rest of the abdominal neuromeres have been found for neurons expressing biogenic amines [84].

SYB.EGFP and RDL.HA as compartment markers in peptidergic neurons

The fusion construct *syb.egfp* has been developed as a presynaptic marker [88]. Since synaptobrevin (SYB) is an integral membrane protein of small synaptic vesicles and large peptide-containing vesicles alike, SYB.EGFP also labels peptide vesicles and hence peptide accumulation and release sites (varicosities), which typically do not spatially coincide with synapses. Concomitantly, we assume that purely dendritic compartments of peptidergic neurons do not contain vesicles and show no or only weak SYB.EGFP labeling. These assumptions are supported by results obtained for PDF neurons in the brain [6], and the Tv and Va neurons which innervate neurohemal organs (Fig. S1, Fig. S4-A3). Here indeed, SYB.EGFP was only found in the cell bodies (where the protein is made) and in the terminals in the neurohemal organs

(where the peptidergic vesicles are stored and released). The axonal projections as well as the arborizations within the VNC were unlabeled. Nevertheless, when interpreting the SYB.EGFP distribution, it has to be kept in mind that SYB.EGFP might also label presynaptic sites if the peptidergic neurons contain co-localized classical neurotransmitters.

The hemagglutinin-tagged GABA_A receptor subunit RDL.HA has been shown to be a useful specific postsynaptic marker in motor neurons [89]. Since the GABA_A receptor subunit RDL is involved in mediating GABAergic postsynaptic currents [90], we tried whether ectopic RDL.HA expression indicates postsynaptic sites (dendrites) of peptidergic neurons also. The general expression level of RDL.HA was very weak, and we only obtained discernible labeling intensities with two different GAL4-drivers, *Ccap-* and *c929-GAL4* (Fig. 13-D, Fig. S2-C). Nevertheless, the labeling was spatially very confined to neuron compartments that showed no varicosities or only weak SYB.EGFP fluorescence. This suggests that RDL.HA labeled postsynaptic sites in peptidergic neurons.

Many peptidergic arborizations are concentrated around the ganglion midline and might define a dendritic neuropil compartment of peptidergic neurons

Arborizations around the median DM and VM tracts turned out to be a prominent feature of most characterized peptidergic neurons with somata in the ventral ganglion, including the AST, CCAP, corazonin, FMRFa, MIP and PDF neurons (Fig. 2, 4, 5, 7, 10, 11). In contrast to e.g. motor neurons, the prominent midline arborizations of peptidergic neurons were rather short, and did not occupy large areas in the more lateral neuropils between the median and lateral tracts. For the CCAP neurons, ectopically expressed RDL.HA localized exclusively to these median arborizations (Fig. S2-C). In contrast, SYB.EGFP as well as peptide-immunoreactivity was absent or relatively low in these arborizations (Fig. S2, 4, 6). Also in the general peptidergic *c929-GAL4*-line, SYB.EGFP expression was low in the median compared to lateral fascicles (Fig. S8). This might suggest that the median arborizations represent peptidergic dendrites. Descending processes of CCAP, EH, HUG and leucokinin neurons (originating from somata in the suboesophageal ganglion or the brain) all have putative release sites around the DM and VM tracts (Fig. 3, 4, 6, 9). Of the peptidergic neurons with cell bodies in the VNC, only those expressing corazonin were found to have varicosities indicative of release sites around the DM and VM tracts (Fig. 5).

Taken together, these findings suggest that the arborizations around the DM and VM tracts are mainly input compartments for peptidergic VNC neurons, and point to this midline region as a main site for synaptic inputs onto peptidergic neurons including the CCAP neurons. The different putative sites of in- and outputs to peptidergic neurons in the VNC are summarized in Table 3. Peptides released from varicosities of leucokinin, CCAP, HUG, EH and corazonin neurites along the DM tract may modulate synaptic transmission around the DM tracts, or might represent direct input signals to peptidergic neurons. Also, the dorsal ap-let neurons with somata in the ventral ganglion expressing the peptide precursor *Nplp1* appear to have their output sites along the DM tracts as indicated by strong peptide immunoreactivity [91–93]. Unlike any of the peptidergic neurons characterized here, the dorsal ap-let neurons seem to have extensive arborizations within the neuropil of each hemineuromere [91], which appear to contain no or only little peptide immunoreactive material [92,93] and hence might represent dendritic regions. Also the leucokinin neurons with somata in the ventral ganglion do not send

projections towards the midline (Fig. 9). Since leucokinin release is likely to occur at peripheral release sites on body wall muscles [67], it is possible that a synaptic input region is located along the VL tract, the only projection site of abdominal leucokinin neurons within the CNS neuropil.

The neuropil of a9 is densely supplied by peptidergic neurites and might serve as in- and output site for peptidergic neurons

The last abdominal neuromere is only rudimentary [27] and does not display the typical *Fas2* pattern seen in the rest of the ventral ganglion. Instead, the *Fas2* tracts converge in the neuropil of a9 (also termed “terminal plexus” [24]), and seem to fill it completely (Fig. 1, Video S1, S2, and S3). Accordingly, the neuropil of a9 cannot be organized as the other ventral neuromeres. Still, a9 receives sensory afferents and also sends out motor efferents [27]. Based on the distribution pattern of ectopically expressed synaptic markers with the peptidergic *c929-GAL4* driver and the differences in the distribution pattern of PDF immunoreactivity and *pdf-GAL4*-driven SYB.EGFP and CD8.GFP (Fig. 11, S6, S8), the terminal plexus seems to represent a prominent site for converging inputs to several peptidergic neurons. The presence of rather weak SYB.EGFP labeling, and varicose and strongly labeled endings of descending leucokinin neurites (Fig. S5) suggest that the terminal plexus at the same time also serves as an output neuropil for peptidergic neurons.

The termination of several descending peptidergic neurites just anterior to this terminal neuropil demonstrates that the existing peptidergic projections in the terminal plexus are neuromere-specific. The peptidergic innervation of the terminal plexus might thus reflect tail-specific input onto peptidergic neurons, or a functional role of the peptides in tail- or gut-related physiological processes (see above). A comparable terminal neuropil with dense peptidergic innervation appears to be present also in larvae of other fly species (based on leucokinin immunostaining [67]), but has not been described so far in adult flies or other insects with the possible exception of cockroaches. As in fly larvae, descending leucokinin neurites from the brain terminate and branch in a median neuropil in the last abdominal neuromere in the terminal abdominal ganglion of the Madeira cockroach *Leucophaea maderae* [68]. In the American cockroach, *Periplaneta americana*, the median dorso-caudal neuropil of the last abdominal neuromere shows dense pyrokinin- [94], perisulfakinin- [83,95], as well as proctolinergic arborizations [96] which make both pre- and postsynaptic contacts to peptidergic and non-peptidergic neurons [97]. The corresponding posterior proctolinergic neurons of the cockroach send processes to the hindgut musculature [96]. Similar efferent proctolinergic neurons have been demonstrated in the ventral nerve cord of *Drosophila* and a blowfly species [98–100]. In *Periplaneta*, the region of the dorso-caudal neuropil contains a much higher diversity of neuropeptides than any other region in the ventral ganglion chain as shown by mass spectrometric profiling [101]. A similar situation might also apply to phasmids, mantids and isopods [101].

Possible overlap of peptidergic and sensory projections

As outlined above, the area between the DM and VM tracts of each hemineuromere appears to be a main input region for peptidergic neurons of the VNC. This region does not appear to contain sensory projections, which instead are concentrated in the area between the ventrolateral and median tracts in each

hemineuromere [24,102]. Only the terminals of class I multidendritic neurons (vpda, ddaE and vbd neurons) and dbd neurons, multidendritic neurons with bipolar dendrites, are located laterally at the DM tracts [24–26,102] and could thus potentially overlap with CCAP, corazonin, FMRFa or MIP arborizations. Class II–IV multidendritic neurons have been mapped to the ventral CNS [26]. This area is mostly outside the putative input area of peptidergic neurons between the DM and VM tract, only the TRP-neurites running along the VM tract might overlap. The more ventrally located median projections of further multidendritic neurons [24,26] seem not to overlap with peptidergic projections. Neurites of CCAP, FMRFa, leucokinin and MIP neurons along the VL tracts might, however, be close to the terminals of external sense organ and class II multidendritic neurons [26,102].

The projection area of chordotonal organs has been mapped to ventral areas partially overlapping with the CI tracts, and medially extending nearly until the VM tract [24]. This rather large area contains processes of AST, MIP, and DTK neurons.

In insects, cholinergic multidendritic neurons function as touch-, stretch- or proprioceptors that respond to changes in body shape (see [103,104]), but their function in *Drosophila* has not been determined so far. In Heteropterans, the stimulation of abdominal stretch receptors (multiterminal neurons) can trigger the release of diuretic hormone and the peptide hormone PTH, which initiates molting [105,106]; the underlying neuronal pathways are unknown. The CCAP/MIP neurons that possibly overlap with class I multidendritic neurons play an essential role during ecdysis, wing inflation and tanning in *Drosophila* [42,107] and express functional ACh receptors [8]. One might thus speculate that sensory information from multidendritic receptor neurons of the body wall may modulate the release activity of CCAP/MIP neurons in the context of ecdysis, wing inflation or tanning. Obviously, an overlap of multidendritic sensory neurons and peptidergic neurons has to be demonstrated properly, yet this example shows that the morphological mapping of peptidergic neurons can lead to testable functional hypotheses.

The varicose morphology suggests that the processes of AST, MIP and TRP neurons in proximity to projections of class II–IV multidendritic neurons, chordotonal and external sense organs are peptide release sites. It is thus possible that ASTs, MIPs and DTKs modulate sensory inputs onto central neurons. The functions of ASTs and MIPs in *Drosophila* are unknown, but DTKs have been shown to have a modulatory role in sensory processing during olfactory perception [81].

Possible overlap of peptidergic and motor neuron projections

As in other insects, the dendritic compartments of motor neurons in the *Drosophila* larva are located in the dorsal neuropil of the ventral nerve cord. They occupy most of the neuropil area dorsal to the CI tracts, with exception of the area between the DM tracts [24]. Based on the presence of varicosities within the dorsal neuropil, the following peptides might be released within the motor input area: ASTs, FMRFa, IFa, hug-PK and DTKs (Fig. 2, 3, 7, 8). This morphological correlation raises the possibility that these peptides are implicated in the regulation of locomotor activity, which is testable. So far, there is only evidence that DTKs released within the CNS regulate the locomotor activity of adult flies [81].

Possible overlap of peptidergic and interneuron projections

The relative scarcity of potential overlap between sensory and neuropeptide projections found in this study suggests that most

peptidergic neurons of the ventral nerve cord do not receive monosynaptic input from sensory neurons. It is thus likely that peptidergic neurons in the ventral ganglion of *Drosophila* receive polyneuronal inputs of different sensory modalities via interneurons. This assumption is in line with the described association of neurites of the pCC interneuron as well as unspecified non-sensory neurons with the DM tract [24]. Nevertheless, too little information about the morphology and spatial distribution of interneuron projections exists to derive suggestions for neuronal connections with peptidergic neurons. The detailed studies on the organization of thoracic or abdominal ganglia in other insects also do not assign particular neurons or inputs to the region dorsal to the “ventral association center” [108], which corresponds to the region around the *Drosophila* DM tracts. Interestingly, the dense arborizations of the vasopressin-like immunoreactive (VPLI) neurons in the locust suboesophageal ganglion with synaptic contacts to a descending cholinergic interneuron are situated around the ganglion midline [109] between the dorsal and ventral median tract, which relate to the DM and VM tract of *Drosophila* [24]. The VPLI neurons represent, to our knowledge, the only case in which the cellular identity and effect of synaptic input onto a peptidergic insect neuron has been established. The spiking activity of these neurons is indirectly modulated by visual and mechanosensory input via the cholinergic interneuron [110].

The descending leucokinin-, CCAP-, corazonin- and FMRFa-containing axons that run along the median side of the DM tracts (Fig. 4, 5, 7) suggest these peptides as candidate non-synaptic input factors for peptidergic neurons with arborizations around the DM tract.

The longitudinal axons of AST, FMRFa, MIP, and DTK neurons are associated with the CI tracts (Fig. 2, 7, 10, 12), and thus roughly located in an intermediate tier between the dorsal neuropil containing motor neuron dendrites, and the ventral neuropil containing sensory projections. Although it has been questioned whether it indeed reflects a functional organization [111], the middle tier has classically been assigned as “associative” neuropil containing interneurons [112,113]. Peptides released at the CI tract region thus appear well suited to modulate interneurons, which in principle could provide an effective means to achieve wide ranging effects on different (interlinked) neuronal networks [114].

Conclusions

Our mapping of the products of 12 peptide precursor genes suggests that peptidergic neurons in the *Drosophila* VNC typically have separated in- and output compartments in specific areas. Prominent input areas appear to be located around the DM/VM tracts, and in the terminal plexus of a9. Output areas within the VNC are less defined: for some descending and local peptidergic neurons release may be around DM/VM tracts, but others may release their peptides along the CI or lateral tracts.

The neuromere-specific distributions and morphological specializations of many peptidergic neurons indicate that subsets of peptidergic neurons of a given chemical identity may subservise differential and neuromere-specific functions. The prevailing lack of pronounced arborizations at putative output sites within the VNC and the distribution of varicosities and SYB:EGFP along the length of little branched descending fibers suggest that most of the investigated interneuronal peptides act via paracrine release and volume transmission [115]. However, our results cannot exclude more focal actions of peptides. The secretory neurons described here have peripheral release sites in the PSOs, the gut or at muscles.

Chapter I

Based on findings in vertebrates, mollusks and crustaceans (see [116–118]), neuropeptides in insect interneurons are commonly considered to be released as co-transmitters together with classical transmitters or biogenic amines (see [2]). The mapping of peptidergic neurons now allows to compare the distribution of peptides with that of classical neurotransmitters and biogenic amines in order to test the extent of co-transmission in the *Drosophila* ventral ganglion.

MATERIALS AND METHODS

Fly stocks

Wild-type Oregon R (OrR), GAL4 driver fly strains and UAS reporter gene lines (see Table 1) were reared under a (12: 12) L:D cycle at 18°C or 25°C on standard cornmeal agar medium and yeast. GAL4 driver strain flies were crossed with UAS reporter gene fly strains to localize peptidergic neurons in the ventral nerve cord in the offspring.

Immunostaining

CNS from third instar OrR or GAL4xUAS larvae were dissected in standard fly saline, fixed for 2 hours in 4% paraformaldehyde in 0.1M sodium phosphate buffered saline (PBS, pH 7.2), washed in PBS with 1% TritonX (PBT) and incubated for at least 24 h in PBT containing 10% normal goat serum in combination with rabbit anti-peptide or mouse mAbs (see Table 2). The mouse mAbs were obtained from the Developmental Studies Hybridoma Bank under the auspices of the NICHD and maintained by the University of Iowa. Preparations were then washed 5 times during a day with PBT and incubated for at least 24 h in PBT containing 10% normal goat serum with Cy2-, Cy3- or Cy5-conjugated AffiniPure goat anti-mouse or goat anti-rabbit IgG (H+L; Jackson ImmunoResearch, Germany), used at a dilution of 1:2000. Preparations were subsequently washed for about 4 h, and then mounted in 80% glycerol diluted in phosphate buffer. To avoid compression of the preparations, small plastic spacers were placed between the slide and cover glass.

The nomenclature of the Fas2-IR tracts follows [24].

Confocal microscopy

Confocal stacks were acquired in 0.4-0.5 μm steps along the z-axis by a confocal laser scanning microscope (Leica TCS SP2, Leica Microsystems Wetzlar, Germany, equipped with a 40 x HCX PL APO oil immersion objective, n.a. = 1.25) with 8bit intensity resolution. To obtain 3D images for the panels, stacks were subjected to texture-based volume rendering (voltex) using Amira 3.1 software (Mercury Computer Systems GmbH, Berlin, Germany). Otherwise, maximum projections shown are generated by Leica Confocal Software 2.6 (Leica Microsystems Heidelberg GmbH, Germany).

Mapping of immunostaining patterns

Obtained images were assembled using Adobe Photoshop 7.0. Schematic drawings of double labelings (anti-Fas2/anti-Peptide and anti-Fas2/GFP) in the ventral nerve cord were generated using Adobe Illustrator CS 11.0 software. The suboesophageal region of the ventral nerve cord was not considered in the schemes.

SUPPORTING INFORMATION

Figure S1 Detail of CAPA neurons. Dorsal view of a maximum projection of a preparation expressing Va-GAL4-driven SYB.-EGFP. Unlike GFP, SYB.EGFP only labels the somata of the Va neurons (asterisks) and the proximal neurohemal part of the

abdominal transverse nerves 1–3 (arrows). Scale bar = 50 μm . Found at: doi:10.1371/journal.pone.0000695.s001 (0.12 MB TIF)

Figure S2 Details of CCAP neurons. A) Dorsal view of a maximum projection of a larva expressing *Ccap*-GAL4-driven GFP (A1) immunostained against CCAP (A2) and merged image (A3). Median arborizations are only visible by GFP, whereas the immunostaining strongly labels median descending fibers in the suboesophageal ganglion and the thoracic and abdominal neuromeres. B) Dorsal view of a maximum projection of a larva expressing *Ccap*-GAL4-driven SYB.EGFP. The distribution of SYB.EGFP is more similar to that of CCAP-IR (A2) than to that of GFP (A1). C) Dorsal view of maximum projections of larvae expressing *Ccap*-GAL4-driven RDL.HA. Only the cell bodies and distinct staining around the midline are labeled. The linear structures are tracheae detected by their autofluorescence. Due to the weak labeling intensity, the preparation had to be scanned with high sensitivity. D) *Ccap*-GAL4-driven GFP, lateral view of a voltex projection. The CCAP neurons in the suboesophageal (arrowhead) and thoracic neuromeres are ventrally located (asterisks), whereas the abdominal CCAP neurons are in a dorsal position. E) *Ccap*-GAL4-driven GFP, voltex projection of the neuromeres a7–9. The terminal plexus is marked by an arrow. Scale bars = 50 μm , E) 25 μm . RDL.HA immunolabeling and GFP and SYB.EGFP expression is shown in green, CCAP immunolabeling in red, Fas2 in magenta. Found at: doi:10.1371/journal.pone.0000695.s002 (4.29 MB TIF)

Figure S3 Details of corazonin neurons. A) Ventral view of corazonin-IR neurons in t3–a2. A1) Voltex projection, A2) Maximum projection. A3) Detail of the neurite projections of the corazonin neurons in a1, voltex projection. B) Corazonin-IR neurite projections in a4–6, maximum projections. B1–2) Dorsal view. B3) Ventral view of the neurite projections between the VM tracts in the segments a4–5. C1–2) Ventral view of a voltex projection of the abdominal segments a6–8 showing the posterior-most pair of corazonin neurons in a6 and the dense pronounced varicosities in a7 and a8. C3) Posterior view of a cross section of a maximal projection in segment a7. Scale bars = 100 μm , B3) 25 μm . Immunostaining is shown in green, Fas2 in magenta. Found at: doi:10.1371/journal.pone.0000695.s003 (3.23 MB TIF)

Figure S4 Details of FMRFa neurons. A) *fmrfa*-GAL4-driven expression of marker molecules in the Tv neurons. A1) GFP-expression, dorso-lateral view. A2) GFP-expression, lateral view. A3) SYB.EGFP-expression, dorsal view. The pronounced median arborizations in A1-2 (arrows) visualized by GFP are devoid of SYB.EGFP fluorescence in A3. SYB.EGFP is however accumulated in the thoracic PSOs (arrowheads) and the Tv neuron somata (asterisks). B) FMRFa-IR in the posterior abdominal neuromeres, dorsal view. Terminal plexus is marked by an arrow. Scale bars = A) 10 μm , B) 25 μm . Immunostaining or marker protein expression is shown in green, Fas2 in magenta. Found at: doi:10.1371/journal.pone.0000695.s004 (1.41 MB TIF)

Figure S5 Details of leucokinin neurons. A) Ventral view of a voltex projection of leucokinin neurons in a hemineuromere of a1–3. B) Dorsal view of a voltex projection of leucokinin neurons in a5–9 showing dense arborizations in the terminal plexus (arrow). C1–3) Dorsal, posterior and lateral view of the dense arborizations in the terminal plexus. Scale bars = A–B) 30 μm , C) 10 μm . Immunostaining is shown in green, Fas2 in magenta. Found at: doi:10.1371/journal.pone.0000695.s005 (2.45 MB TIF)

Figure S6 Details of the morphology of PDF expressing neurons. PDF-neurons in a8–9, voltex projections. A) Lateral

view. B) Anterio-lateral view. C) Dorso-lateral view. The arborizations in the terminal plexus (arrow) are only labeled by CD8.GFP (A), but not by immunostaining (C1) or SYB.EGFP (C2). Scale bars =20 μm . Immunostaining or marker protein expression is shown in green, Fas2 in magenta.

Found at: doi:10.1371/journal.pone.0000695.s006 (1.10MB TIF)

Figure S7 Details of the morphology of TRP neurons. Voltage projections of TRP-IR varicosities in different neuromeres. A) Dorsal view of a3–4. B) Posterior view of transverse section at the height of t3. C) Dorsal view of a pair of TRP-IR neurons (asterisks) in t2. D) Dorsal view of a3. Scale bars = A) 20 μm , B–D) 30 μm . Immunostaining is shown in green, Fas2 in magenta.

Found at: doi:10.1371/journal.pone.0000695.s007 (2.78 MB TIF)

Figure S8 Distribution of c929-GAL4 driven expression of SYB.EGFP and CD8.GFP. Dorsal view of maximum projections of the VNC in gray scale (GS) or false color coding (FC). In FC, low staining intensity is coded by blue, high staining intensity by red. Each row represents a separate preparation. Strongest accumulation of SYB.EGFP is visible in the thoracic PSOs (arrows) and descending lateral and intermediate fascicles, whereas the terminal plexus (arrowhead) only shows relatively little fluorescence. In contrast, CD8.GFP fluorescence is most intense in the terminal plexus and in median and lateral fascicles, and missing in the thoracic PSOs. Scale bars = 100 μm .

Found at: doi:10.1371/journal.pone.0000695.s008 (4.71 MB TIF)

Video S1 3D reconstruction of the Fas2 landmarks. Movie of a full reconstruction of the Fas2-positive tracts in the ventral nerve cord of a L3 larva.

Found at: doi:10.1371/journal.pone.0000695.s009 (7.81 MB AVI)

Video S2 Moving layer through Fas2 landmarks, dorsoventral axis. Movie of the Fas2-positive tracts in the ventral nerve cord of a L3 larva, from ventral to dorsal.

Found at: doi:10.1371/journal.pone.0000695.s010 (10.02 MB AVI)

Video S3 Moving layer through Fas2 landmarks, anterior-posterior axis. Movie of the Fas2-positive tracts in the ventral nerve cord of a L3 larva.

Found at: doi:10.1371/journal.pone.0000695.s011 (9.27 MB AVI)

ACKNOWLEDGMENTS

We are very grateful to the various donors of fly lines and antisera listed in the tables. We also like to thank Andreas Prokop for valuable advice, Franz Grolig and Joachim Schachtner for maintaining the confocal facility, Ruth Hyland and Renate Renkawitz-Pohl for fly housing, Wolf Huetteroth for valuable advice with the Amira software, and Susanne Neupert, Reinhard Predel and Marta Zlatic for helpful discussions. We are particularly indebted to the authors of previous studies on the morphology of peptidergic neurons in *Drosophila*, whose descriptions have much simplified our task.

Author Contributions

Conceived and designed the experiments: CW JS MV. Performed the experiments: CW JS MV RS. Analyzed the data: CW DN JS MV RS UH. Contributed reagents/materials/analysis tools: CW DN UH. Wrote the paper: CW DN JS MV UH.

REFERENCES

- Nässel DR (2002) Neuropeptides in the nervous system of *Drosophila* and other insects: multiple roles as neuromodulators and neurohormones. *Prog Neurobiol* 68: 1–84.
- Nässel DR, Homberg U (2006) Neuropeptides in interneurons of the insect brain. *Cell Tissue Res* 326: 1–24.
- Ewer J (2005) Behavioral actions of neuropeptides in invertebrates: insights from *Drosophila*. *Horm Behav* 48: 418–429.
- Žitňan D, Adams ME (2004) Neuroendocrine regulation of insect ecdysis. In: Gilbert LI, Iatrou K, Gill SS, eds. *Comprehensive Molecular Insect Science*. Amsterdam: Elsevier. pp 1–59.
- Wegener C, Hamasaka Y, Nässel DR (2004) Acetylcholine increases intracellular Ca^{2+} via nicotinic receptors in cultured PDF-containing clock neurons of *Drosophila*. *J Neurophysiol* 91: 912–923.
- Hamasaka Y, Wegener C, Nässel DR (2005) GABA modulates *Drosophila* circadian clock neurons via GABA_B receptors and decreases in calcium. *J Neurobiol* 65: 225–240.
- Hamasaka Y, Nässel DR (2006) Mapping of serotonin, dopamine, and histamine in relation to different clock neurons in the brain of *Drosophila*. *J Comp Neurol* 494: 314–330.
- Vömel M, Wegener C (2007) Neurotransmitter-induced changes in the intracellular calcium concentration suggest a differential central modulation of CCAP neuron subsets in *Drosophila*. *Devel Neurobiol* 67: 792–809.
- Katz PS, Frost WN (1996) Intrinsic neuromodulation: altering neuronal circuits from within. *Trends Neurosci* 19: 54–61.
- Taghert PH, Veenstra JA (2003) *Drosophila* neuropeptide signaling. *Adv Genetics* 49: 1–65.
- Baggerman G, Boonen K, Verleyen P, De Loof A, Schoofs L (2005) Peptidomic analysis of the larval *Drosophila melanogaster* central nervous system by two-dimensional capillary liquid chromatography quadrupole time-of-flight mass spectrometry. *J Mass Spectrom* 40: 250–260.
- Wegener C, Reinl T, Jansch L, Predel R (2006) Direct mass spectrometric peptide profiling and fragmentation of larval peptide hormone release sites in *Drosophila melanogaster* reveals tagma-specific peptide expression and differential processing. *J Neurochem* 96: 1362–1374.
- Predel R, Wegener C, Russell WK, Tichy SE, Russell DH, et al. (2004) Peptidomics of CNS-associated neurohemal systems of adult *Drosophila melanogaster*: a mass spectrometric survey of peptides from individual flies. *J Comp Neurol* 474: 379–392.
- Johnson EC (2006) Postgenomic approaches to resolve neuropeptide signaling in *Drosophila*. In: Satake H, ed. *Invertebrate neuropeptides and hormones*. Trivandrum: Transworld research network. pp 179–224.
- Mulloney B, Tschuluun N, Hall WM (2003) Architectonics of crayfish ganglia. *Microsc Res Techn* 60: 253–265.
- Hartenstein V (2006) The neuroendocrine system of invertebrates: a developmental and evolutionary perspective. *J Endocrinol* 190: 555–570.
- Claeys I, Simonet G, Poels J, Van Loy T, Vercammen L, et al. (2002) Insulin-related peptides and their conserved signal transduction pathway. *Peptides* 23: 807–816.
- Johnson EC, Shafer OT, Trigg JS, Park J, Schooley DA, et al. (2005) A novel diuretic hormone receptor in *Drosophila*: evidence for conservation of CGRP signaling. *Journal of Experimental Biology* 208: 1239–1246.
- Mertens I, Vandingenen A, Johnson EC, Shafer OT, Li W, et al. (2005) PDF receptor signaling in *Drosophila* contributes to both circadian and geotactic behaviors. *Neuron* 48: 213–219.
- Hyun S, Lee Y, Hong ST, Bang S, Paik D, et al. (2005) *Drosophila* GPCR han is a receptor for the circadian clock neuropeptide PDF. *Neuron* 48: 267–278.
- Melcher C, Bader R, Walther S, Simakov O, Pankratz MJ (2006) Neuromedin U and its putative *Drosophila* homolog hugin. *PLoS Biol* 4: e68.
- Wu Q, Wen T, Lee G, Park JH, Cai HN, et al. (2003) Developmental control of foraging and social behavior by the *Drosophila* neuropeptide Y-like system. *Neuron* 39: 147–161.
- Brand A, Perrimon N (1993) Targeted gene expression as a means of altering cell fates and generating dominant phenotypes. *Development* 118: 401–415.
- Landgraf M, Sánchez-Soriano N, Technau GM, Urban J, Prokop A (2003) Charting the *Drosophila* neuropile: a strategy for the standardised characterisation of genetically amenable neurites. *Devel Biol* 260: 207–225.
- Zlatic M, Landgraf M, Bate M (2003) Genetic specification of axonal arbors: atonal regulates robo3 to position terminal branches in the *Drosophila* nervous system. *Neuron* 37: 41–51.
- Grueber WB, Ye B, Yang CH, Younger S, Borden K, et al. (2007) Projections of *Drosophila* multidendritic neurons in the central nervous system: links with peripheral dendrite morphology. *Development* 134: 55–64.
- Campos-Ortega JA, Hartenstein V (1997) *The embryonic development of Drosophila melanogaster*. Berlin: Springer.
- Ito K, Okada R, Tanaka NK, Awasaki T (2003) Cautionary observations on preparing and interpreting brain images using molecular biology-based staining techniques. *Microsc Res Techn* 62: 170–186.
- Lenz C, Williamson M, Grimmelikhuijzen CJP (2000) Molecular cloning and genomic organization of an allatostatin prohormone from *Drosophila melanogaster*. *Biochem Biophys Res Commun* 273: 1126–1131.
- Gäde G, Hoffmann KH, Spring JH (1997) Hormonal regulation in insects: facts, gaps, and future directions. *Physiol Rev* 77: 963–1032.

31. Yoon JG, Stay B (1995) Immunocytochemical localization of *Diptera punctata* allatostatin-like peptide in *Drosophila melanogaster*. *J Comp Neurol* 363: 475–488.
32. Vitzthum H, Homberg U, Agricola H (1996) Distribution of Dip-allatostatin I-like immunoreactivity in the brain of the locust *Schistocerca gregaria* with detailed analysis of immunostaining in the central complex. *J Comp Neurol* 369: 419–437.
33. Meng X, Wahlström G, Immonen T, Kolmer M, Tirronen M, et al. (2002) The *Drosophila hugin* gene codes for myostimulatory and ecdysis-modifying neuropeptides. *Mech Devel* 117: 5–13.
34. Kean L, Cazenave W, Costes L, Broderick KE, Graham S, et al. (2002) Two nitridergic peptides are encoded by the gene *capability* in *Drosophila melanogaster*. *Am J Physiol* 282: R1297–1307.
35. Melcher C, Pankratz MJ (2005) Candidate gustatory interneurons modulating feeding behavior in the *Drosophila* brain. *PLoS Biol* 3: e305.
36. Choi MY, Rafaeli A, Jurenka RA (2001) Pyrokinin/PBAN-like peptides in the central nervous system of *Drosophila melanogaster*. *Cell Tissue Res* 306: 459–465.
37. O'Brien MA, Taghert PH (1998) A peritachal neuropeptide system in insects: release of myomodulin-like peptides at ecdysis. *J Exp Biol* 210: 193–209.
38. Santos JG, Pollák E, Rexer KH, Molnár L, Wegener C (2006) Morphology and metamorphosis of the peptidergic Va neurons and the median nerve system of the fruit fly, *Drosophila melanogaster*. *Cell Tissue Res* 326: 187–199.
39. Eckert M, Herbert Z, Pollák E, Molnár L, Predel R (2002) Identical cellular distribution of all abundant neuropeptides in the major abdominal neurohemal system of an insect (*Periplaneta americana*). *J Comp Neurol* 452: 264–275.
40. Allan DW, St. Pierre SE, Miguel-Aliaga I, Thor S (2003) Specification of neuropeptide cell identity by the integration of retrograde BMP signaling and a combinatorial transcription factor code. *Cell* 113: 73–86.
41. Dulcis D, Levine RB, Ewer J (2005) Role of the neuropeptide CCAP in *Drosophila* cardiac function. *J Neurobiol* 64: 259–274.
42. Park JH, Schroeder AJ, Helfrich-Förster C, Jackson FR, Ewer J (2003) Targeted ablation of CCAP neuropeptide-containing neurons of *Drosophila* causes specific defects in execution and circadian timing of ecdysis behavior. *Development* 130: 2645–2656.
43. Ewer J, Truman JW (1996) Increases in cyclic 3', 5'-guanosine monophosphate (cGMP) occur at ecdysis in an evolutionarily conserved crustacean cardioactive peptide-immunoreactive insect neuronal network. *J Comp Neurol* 370: 330–341.
44. Dircksen H, Keller R (1988) Immunocytochemical localization of CCAP, a novel crustacean cardioactive peptide, in the nervous system of the shore crab, *Carcinus maenas* L. *Cell Tissue Res* 254: 347–360.
45. Husain QM, Ewer J (2004) Use of targetable GFP-tagged neuropeptide for visualizing neuropeptide release following execution of behavior. *J Neurobiol* 59: 181–191.
46. Veenstra JA (1994) Isolation and structure of the *Drosophila* corazonin gene. *Biochem Biophys Res Commun* 204: 292–296.
47. Choi YJ, Lee G, Hall JC, Park JH (2005) Comparative analysis of Corazonin-encoding genes (Crz's) in *Drosophila* species and functional insights into Crz-expressing neurons. *J Comp Neurol* 482: 372–385.
48. Kim YJ, Spalovská-Valachová I, Cho KH, Žitňanová I, Park Y, Adams ME, Žitňan D (2004) Corazonin receptor signaling in ecdysis initiation. *Proc Natl Acad Sci U S A* 101: 6704–6709.
49. Veenstra JA (1991) Presence of corazonin in three insect species, and isolation and identification of [His⁷]corazonin from *Schistocerca americana*. *Peptides* 12: 1285–1289.
50. Horodyski FM, Ewer J, Riddiford LM, Truman JW (1993) Isolation, characterization and expression of the eclosion hormone gene of *Drosophila melanogaster*. *Eur J Biochem* 215: 221–228.
51. McNabb S, Baker JD, Agapite J, Steller H, Riddiford LM, et al. (1997) Disruption of a behavioral sequence by targeted death of peptidergic neurons in *Drosophila*. *Neuron* 19: 813–823.
52. Schneider LE, Taghert PH (1988) Isolation and characterization of a *Drosophila* gene that encodes multiple neuropeptides related to Phe-Met-Arg-Phe-NH₂ (FMRFamide). *Proc Natl Acad Sci U S A* 85: 1993–1997.
53. Chin A, Reynolds ER, Scheller RH (1990) Organization and expression of the *Drosophila* FMRFamide-related prohormone gene. *DNA Cell Biol* 9: 263–271.
54. Taghert PH, Schneider LE (1990) Interspecific comparison of a *Drosophila* gene encoding FMRFamide-related neuropeptides. *J Neurosci* 10: 1929–1942.
55. Hewes RS, Snowdeal EC, Saitoe M, Taghert PH (1998) Functional redundancy of FMRFamide-related peptides at the *Drosophila* larval neuromuscular junction. *J Neurosci* 18: 1138–1251.
56. Johnson E, Ringo J, Dowse H (2000) Native and heterologous neuropeptides are cardioactive in *Drosophila melanogaster*. *J Insect Physiol* 46: 1229–1236.
57. Kim YJ, Žitňan D, Galizia CG, Cho KH, Adams ME (2006) A command chemical triggers an innate behavior by sequential activation of multiple peptidergic ensembles. *Curr Biol* 16: 1395–1407.
58. White K, Hurteau T, Punsal P (1986) Neuropeptide-FMRFamide-like immunoreactivity in *Drosophila*: development and distribution. *J Comp Neurol* 247: 430–438.
59. Schneider LE, Sun ET, Garland DJ, Taghert PH (1993) An immunocytochemical study of the FMRFamide neuropeptide gene products in *Drosophila*. *J Comp Neurol* 337: 446–460.
60. Lundquist T, Nässel DR (1990) Substance P-, FMRFamide, and gastrin/cholecystokinin-like immunoreactive neurons in the thoraco-abdominal ganglia of the flies *Drosophila* and *Calliphora*. *J Comp Neurol* 294: 161–178.
61. Schneider LE, O'Brien MA, Taghert PH (1991) *In situ* hybridization analysis of the FMRFamide neuropeptide gene in *Drosophila*. I. Restricted expression in embryonic and larval stages. *J Comp Neurol* 304: 608–622.
62. Suster ML, Martin JR, Sung C, Robinow S (2003) Targeted expression of tetanus toxin reveals sets of neurons involved in larval locomotion in *Drosophila*. *J Neurobiol* 55: 233–246.
63. Marder E, Calabrese RL, Nusbaum MP, Trimmer B (1987) Distribution and partial characterization of FMRFamide-like peptides in the stomatogastric nervous system of the rock crab, *Cancer borealis*, and the spiny lobster, *Panulirus interruptus*. *J Comp Neurol* 259: 150–163.
64. Terhzaz S, Rosay P, Goodwin SF, Veenstra JA (2007) The neuropeptide SIFamide modulates sexual behavior in *Drosophila*. *Biochem Biophys Res Commun* 352: 305–310.
65. Verleyen P, Huybrechts J, Baggerman G, van Lommel A, De Loof A, et al. (2004) SIFamide is a highly conserved neuropeptide: a comparative study in different insect species. *Biochem Biophys Res Commun* 320: 334–341.
66. Terhzaz S, O'Connell FC, Pollock VP, Kean L, Davies SA, et al. (1999) Isolation and characterization of a leucokinin-like peptide of *Drosophila melanogaster*. *J Exp Biol* 202: 3667–3676.
67. Cantera R, Nässel DR (1992) Segmental peptidergic innervation of abdominal targets in larval and adult dipteran insects revealed with an antiserum against leucokinin I. *Cell Tissue Res* 269: 459–471.
68. Nässel DR, Cantera R, Karlsson A (1992) Neurons in the cockroach nervous system reacting with antisera to the neuropeptide leucokinin I. *J Comp Neurol* 322: 45–67.
69. Vanden Broeck J (2001) Neuropeptides and their precursors in the fruit fly, *Drosophila melanogaster*. *Peptides* 22: 241–254.
70. Williamson M, Lenz C, Winther ÅME, Nässel DR, Grimmelikhuijzen CJP (2001) Molecular cloning, genomic organization, and expression of B-type (Cricket type) allatostatin prohormone from *Drosophila melanogaster*. *Biochem Biophys Res Commun* 281: 544–550.
71. Predel R, Rapus J, Eckert M (2001) Myoinhibitory neuropeptides in the American cockroach. *Peptides* 22: 199–208.
72. Park J, Hall JC (1998) Isolation and chronobiological analysis of a neuropeptide pigment-dispersing factor gene in *Drosophila melanogaster*. *J Biol Rhythms* 13: 219–228.
73. Renn S, Park JH, Rosbash M, Hall JC, Taghert PH (1999) A pdf neuropeptide gene mutation and ablation of PDF neurons each cause severe abnormalities of behavioral circadian rhythms in *Drosophila*. *Cell* 99: 791–802.
74. Helfrich-Förster C (1997) Development of pigment-dispersing hormone-immunoreactive neurons in the nervous system of *Drosophila melanogaster*. *J Comp Neurol* 380: 335–354.
75. Dircksen H, Zahnaw CA, Gaus G, Keller R, Rao KR, et al. (1987) The ultrastructure of nerve endings containing pigment-dispersing hormone (PDH) in crustacean sinus glands: identification by an antiserum against a synthetic PDH. *Cell Tissue Res* 250: 377–387.
76. Persson M, Eklund MB, Dircksen H, Muren JE, Nässel DR (2001) Pigment-dispersing factor in the locust abdominal ganglia may have roles as circulating neurohormone and central neuromodulator. *J Neurobiol* 48: 19–41.
77. Hamasaka Y, Mohrher CJ, Predel R, Wegener C (2005) Chronobiological analysis and mass spectrometric characterization of pigment-dispersing factor in the cockroach *Leucophaea maderae*. *J Insect Sci* 5: 43.
78. Hewes R, Park D, Sauthier SA, Schaefer AM, Taghert PH (2003) The bHLH protein Dimmed controls neuroendocrine cell differentiation in *Drosophila*. *Development* 130: 1771–1781.
79. Siviter RJ, Coast GM, Winther ÅME, Nachman RJ, Taylor CA, et al. (2000) Expression and functional characterization of a *Drosophila* neuropeptide precursor with homology to mammalian preprotachykinin A. *J Biol Chem* 275: 23273–23280.
80. Winther ÅME, Siviter RJ, Isaac RE, Predel R, Nässel DR (2003) Neuronal expression of tachykinin-related peptides and gene transcript during post-embryonic development of *Drosophila*. *J Comp Neurol* 464: 180–196.
81. Winther ÅME, Acebes A, Ferrús A (2006) Tachykinin-related peptides modulate odor perception and locomotor activity in *Drosophila*. *Molec Cell Neurosci* 31: 399–406.
82. Kutsch W, Breidbach O (1994) Homologous structures in the nervous systems of arthropoda. *Adv Insect Physiol* 24: 1–113.
83. Agricola HJ, Bräunig P (1995) Comparative aspects of peptidergic signaling pathways in the nervous system of arthropods. In: Kutsch W, Breidbach O, eds. *The nervous system of invertebrates: an evolutionary and comparative approach*. Basel: Birkhäuser, pp 303–327.
84. Nässel DR (1996) Neuropeptides, amines and amino acids in an elementary insect ganglion: functional and chemical anatomy of the unfused abdominal ganglion. *Progr Neurobiol* 48: 325–420.
85. Monastiriotti M (1999) Biogenic amine systems in the fruit fly *Drosophila melanogaster*. *Microsc Res Techn* 45: 106–121.
86. Predel R (2001) Peptidergic neurohemal system of an insect: mass spectrometric morphology. *J Comp Neurol* 436: 363–375.
87. Bate M (1993) The mesoderm and its derivatives. In: Bate M, Martínez-Arias A, eds. *The development of Drosophila melanogaster*. Cold Spring Harbor: Cold Spring Harbor Laboratory Press, pp 1013–1090.

88. Estes PS, Ho GLY, Narayanan R, Ramaswami M (2000) Synaptic localization and restricted diffusion of a *Drosophila* neuronal synaptobrevin-green fluorescent protein chimera *in vivo*. *J Neurogenet* 13: 233–255.
89. Sánchez-Soriano N, Bottenberg W, Fiala A, Haessler U, Kerassoviti A, et al. (2005) Are dendrites in *Drosophila* homologous to vertebrate dendrites? *Devel Biol* 288: 126–138.
90. Lee D, Su H, O'Dowd DK (2003) GABA receptors containing Rdl subunits mediate fast inhibitory synaptic transmission in *Drosophila* neurons. *J Neurosci* 23: 4625–4634.
91. Löhr R, Godenschwege T, Buchner E, Prokop A (2002) Compartmentalization of central neurons in *Drosophila*: a new strategy of mosaic analysis reveals localization of presynaptic sites to specific segments of neurites. *J Neurosci* 22: 10357–10367.
92. Baumgardt M, Miguel-Aliaga I, Karlsson D, Ekman H, Thor S (2007) Specification of neuronal identities by feedforward combinatorial coding. *PLoS Biol* 5: e37.
93. Verleyen P, Baggerman G, Wiehart U, Schoeters E, van Lommel A, et al. (2004) Expression of a novel neuropeptide, NVGTLARDFQLPIPamide, in the larval and adult brain of *Drosophila melanogaster*. *J Neurochem* 88: 311–319.
94. Predel R, Eckert M, Pollák E, Molnár L, Scheibner O, et al. (2007) Peptidomics of identified neurons demonstrates a highly differentiated expression pattern of FXPRLamides in the neuroendocrine system of an insect. *J Comp Neurol* 500: 498–512.
95. East PD, Hales DF, Cooper PD (1997) Distribution of sulfakinin-like peptides in the central and sympathetic nervous system of the American cockroach, *Periplaneta americana* (L.) and the field cricket, *Teleogryllus commodus* (Walker). *Tissue Cell* 29: 347–354.
96. Eckert M, Agrícola H, Penzlin H (1981) Immunocytochemical identification of proctolin-like immunoreactivity in the terminal ganglion and hindgut of the cockroach *Periplaneta americana* (L.). *Cell Tissue Res* 217: 663–665.
97. Agrícola H, Eckert M, Ude J, Birkenbeil H, Penzlin H (1985) The distribution of a proctolin-like immunoreactive material in the terminal ganglion of the cockroach, *Periplaneta americana* L. *Cell Tissue Res* 239: 203–209.
98. Nässel DR, Holmqvist BI, Moverus BJ (1989) Vasopressin- and proctolin-like immunoreactive efferent neurons in blowfly abdominal ganglia: development and ultrastructure. *J Comp Neurol* 283: 450–463.
99. Taylor CAM, Winther ÅME, Siviter RJ, Shirras AD, Isaac RE, et al. (2004) Identification of a proctolin prohormone gene (Proct) of *Drosophila melanogaster*: expression and predicted prohormone processing. *J Neurobiol* 58: 379–391.
100. Anderson MS, Halpern ME, Keshishian H (1988) Identification of the neuropeptide transmitter proctolin in *Drosophila* larvae: characterization of muscle fiber-specific neuromuscular endings. *J Neurosci* 8: 242–255.
101. Neupert S, Predel R (2006) Chatroom for neuropeptides-unique accumulation of peptidergic messenger molecules in the terminal ganglion of an insect. In: Nachman RJ, Tobe SS, Heimer de la Cotera E, eds. *Proc Invertebrate Neuropeptide conference Guanajuato, Mexico*.
102. Schrader S, Merritt DJ (2000) Central projections of *Drosophila* sensory neurons in the transition from embryo to larva. *J Comp Neurol* 425: 34–44.
103. McIver SB (1985) Mechanoreception. In: Kerkut GA, Gilbert LI, eds. *Comprehensive insect physiology, biochemistry and pharmacology*. Oxford: Pergamon Press. pp 71–132.
104. Grueber WB, Jan LY, Jan YN (2002) Tiling of the *Drosophila* epidermis by multidendritic sensory neurons. *Development* 129: 2867–2878.
105. Maddrell SHP (1964) Excretion in the blood-sucking bug, *Rhodnius prolixus* STÅL. *J Exp Biol* 41: 459–472.
106. Nijhout HF (2003) The control of body size in insects. *Devel Biol* 261: 1–9.
107. Luan H, Lemon WC, Peabody NC, Pohl JB, Zelensky PK, et al. (2006) Functional dissection of a neuronal network required for cuticle tanning and wing expansion in *Drosophila*. *J Neurosci* 26: 573–584.
108. Pflüger HJ, Bräunig P, Hustert R (1988) The organization of mechanosensory neuropiles in locust thoracic ganglia. *Philos Trans Roy Soc London B* 321: 1–26.
109. Thompson KS, Tyrer NM, May ST, Bacon JP (1991) The vasopressin-like immunoreactive (VLPI) neurons of the locust, *Locusta migratoria*. I. Anatomy. *J Comp Physiol A* 168: 605–617.
110. Thompson KS, Bacon JP (1991) The vasopressin-like immunoreactive (VLPI) neurons of the locust, *Locusta migratoria*. II. Physiology. *J Comp Physiol A* 168: 619–630.
111. Murphey RK, Bacon JP, Johnson SE (1985) Ectopic neurons and the organization of insect sensory systems. *J Comp Physiol A* 156: 381–389.
112. Zawarzin A (1924) Zur Morphologie der Nervenzentren. *Das Bauchmark der Insekten. Z wiss Zool* 122: 323–424.
113. Strausfeld NJ (1976) *Atlas of an insect brain*. Berlin: Springer Verlag.
114. Baraban SC, Tallent MK (2004) Interneuronal neuropeptides - endogenous regulators of neuronal excitability. *Trends Neurosci* 27: 135–142.
115. Agnati LF, Zoli M, Strömberg I, Fuxe K (1995) Intercellular communication in the brain: wiring versus volume transmission. *Neurosci* 69: 711–726.
116. Kupfermann I (1991) Functional studies of cotransmission. *Physiol Rev* 71: 683–732.
117. Strand FL (1999) *Neuropeptides*. Cambridge, MA: MIT Press.
118. Nusbaum MP, Blitz DM, Swensen AM, Wood D, Marder E (2001) The roles of co-transmission in neural network modulation. *Trends Neurosci* 24: 146–154.
119. Park J, Helfrich-Förster C, Lee G, Liu L, Rosbash M, et al. (2000) Differential regulation of circadian pacemaker output by separate clock genes in *Drosophila*. *Proc Natl Acad Sci USA* 97: 3608–3613.
120. Lee T, Luo L (1999) Mosaic analysis with a repressible cell marker for studies of gene function in neuronal morphogenesis. *Neuron* 22: 451–461.
121. Winther ÅME, Nässel DR (2001) Intestinal peptides as circulating hormones: release of tachykinin-related peptide from the locust and cockroach midgut. *J Exp Biol* 204: 1295–1305.

II. Neuroarchitecture of aminergic systems in the larval ventral ganglion of *Drosophila melanogaster*

Vömel M and Wegener C. (2008). PLoS ONE 3(3): e1848.

Abstract.....	49
Introduction.....	49
Methods	50
Fly stocks	50
Immunocytochemistry.....	50
Confocal microscopy and data processing	50
Results	50
5-HT neurons.....	50
Tyrosine hydroxylase neurons.....	52
DOPA decarboxylase neurons.....	55
Tyrosine decarboxylase 2 and tyramine β -hydroxylase neurons.....	57
Fas2-based identification of co-localized signaling molecules	59
Discussion	61
Both interneurons and efferent neurons of the larval VG contain BAs.....	61
Aminergic innervation varies between specific VG neuromeres	61
Ectopically expressed fluorescent fusion proteins as neuronal compartment markers in aminergic neurons	61
Neuronal compartments of 5-HT neurons.....	62
Possible overlap of 5-HT neurons with other neuronal projections	62
Neuronal compartments of dopaminergic TH neurons.....	62
Possible overlap of TH neurons with other neuronal projections.....	63
Neuronal compartments of tyraminerpic/octopaminergic TDC2 neurons.....	63
Possible overlap of TDC2 neurons with other neuronal projections	63
Fas2-based fractionation and definition of the complex <i>Ddc-gal4</i> expression pattern reveals <i>Ddc</i> expression in peptidergic neurons.....	63
Supporting information (- corresponding files can be found on CD -).....	64
References.....	65

Neuroarchitecture of Aminergic Systems in the Larval Ventral Ganglion of *Drosophila melanogaster*

Matthias Vömel, Christian Wegener*

Emmy Noether Neuropeptide Group, Animal Physiology, Department of Biology, Philipps-University Marburg, Marburg, Germany

Abstract

Biogenic amines are important signaling molecules in the central nervous system of both vertebrates and invertebrates. In the fruit fly *Drosophila melanogaster*, biogenic amines take part in the regulation of various vital physiological processes such as feeding, learning/memory, locomotion, sexual behavior, and sleep/arousal. Consequently, several morphological studies have analyzed the distribution of aminergic neurons in the CNS. Previous descriptions, however, did not determine the exact spatial location of aminergic neurite arborizations within the neuropil. The release sites and pre-/postsynaptic compartments of aminergic neurons also remained largely unidentified. We here used *gal4*-driven marker gene expression and immunocytochemistry to map presumed serotonergic (5-HT), dopaminergic, and tyraminerpic/octopaminergic neurons in the thoracic and abdominal neuromeres of the *Drosophila* larval ventral ganglion relying on Fasciclin2-immunoreactive tracts as three-dimensional landmarks. With tyrosine hydroxylase- (TH) or tyrosine decarboxylase 2 (TDC2)-specific *gal4*-drivers, we also analyzed the distribution of ectopically expressed neuronal compartment markers in presumptive dopaminergic TH and tyraminerpic/octopaminergic TDC2 neurons, respectively. Our results suggest that thoracic and abdominal 5-HT and TH neurons are exclusively interneurons whereas most TDC2 neurons are efferent. 5-HT and TH neurons are ideally positioned to integrate sensory information and to modulate neuronal transmission within the ventral ganglion, while most TDC2 neurons appear to act peripherally. In contrast to 5-HT neurons, TH and TDC2 neurons each comprise morphologically different neuron subsets with separated in- and output compartments in specific neuropil regions. The three-dimensional mapping of aminergic neurons now facilitates the identification of neuronal network contacts and co-localized signaling molecules, as exemplified for DOPA decarboxylase-synthesizing neurons that co-express crustacean cardioactive peptide and myoinhibiting peptides.

Citation: Vömel M, Wegener C (2008) Neuroarchitecture of Aminergic Systems in the Larval Ventral Ganglion of *Drosophila melanogaster*. PLoS ONE 3(3): e1848. doi:10.1371/journal.pone.0001848

Editor: Shawn Hochman, Emory University, United States of America

Received: December 7, 2007; **Accepted:** February 12, 2008; **Published:** March 26, 2008

Copyright: © 2008 Vömel, Wegener. This is an open-access article distributed under the terms of the Creative Commons Attribution License, which permits unrestricted use, distribution, and reproduction in any medium, provided the original author and source are credited.

Funding: This work was supported by the Deutsche Forschungsgemeinschaft (DFG We 2652/2-2,3) to CW.

Competing Interests: The authors have declared that no competing interests exist.

* E-mail: wegener@staff.uni-marburg.de

Introduction

Biogenic amines (BAs) originate from the amino acid metabolism and act as important intercellular signaling molecules in both vertebrates and invertebrates. In insects, BAs are often synthesized in interneurons and serve a neuromodulator/-transmitter function within the CNS (see [1,2]). Several efferent neurons also release BAs as neurohormones at peripheral targets like the body wall muscles (see [3]). In *Drosophila melanogaster*, BAs play vital roles in the modulation of many physiological processes such as feeding, learning/memory, locomotor activity, sexual behavior, and sleep/arousal (see e.g. [1,2,4]). However, the specific cellular targets of aminergic neurons largely remain unidentified. The small size and chemical structure of BAs complicates antibody production. BA labeling also typically depends on specific fixation procedures that can impair the simultaneous detection of other proteins in co-labeling experiments. To circumvent these technical difficulties, several studies have focused on the detection of enzymes catalyzing BA production or degradation.

Available morphological studies primarily describe the position of aminergic neuron somata within the CNS, but usually do not characterize finer neuronal projections. Data on the accurate

spatial distribution of most BA receptors within the CNS are missing as well. Out of 21 BA receptors identified *in silico* (see [5,6]), only three dopamine ([7–10]; see [11]) and three serotonin receptors [12–14], and one octopamine receptor ([15]; see [16]) have been localized on a cellular level. Besides this lack of information about the cellular targets of specific aminergic neurons, nothing is known about neurons providing synaptic input to aminergic neurons in *Drosophila*.

We therefore set out to provide a three-dimensional morphological characterization of aminergic neurons in the thoracic and abdominal neuromeres of the *Drosophila* larval ventral ganglion (VG). The VG is particularly suited for the analysis of aminergic networks since it offers several advantages: 1) The VG contains both aminergic interneurons and efferent neurons, but has a simpler architecture and fewer neurons than the brain (see [2]). Nevertheless, the VG receives various sensory inputs and takes part in the regulation of essential physiological processes such as locomotion (see [17]) and ecdysis (see [18]). 2) Several light-optical microscopy studies already described the distribution of aminergic neurons and enzymes catalyzing BA production/degradation. Thus, the total number and soma position of aminergic neurons in the VG is known (see [1]). 3) A set of evenly distributed landmarks permits the accurate three-dimensional charting of aminergic

projections within the VG neuropil [19]. These landmarks, which are labeled by antibodies against the cell adhesion molecule Fasciclin2 (Fas2), remain constant between larvae and throughout the larval stages, and recently served as anatomical coordinates to map motoneurons [19], peptidergic [20] and sensory neurons [21,22].

Our three-dimensional maps of presumed serotonergic, dopaminergic and tyraminerbic/octopaminergic neurons allow the tracing of single aminergic neurites to defined neuropil areas within the VG. Thus, the maps facilitate the comparison of aminergic neuron morphology with e.g. a specific BA receptor expression pattern. We also analyzed the distribution of ectopically expressed neuronal compartment markers in presumed dopaminergic and tyraminerbic/octopaminergic neurons. The respective markers indicated distinct in- and output sites, which can now be compared with high spatial resolution to other charted neuronal projections. Finally, our mapping helps to identify co-localized signaling molecules and receptors in aminergic neurons, and improves the suitability of aminergic neurons as anatomical landmarks within the VG.

Methods

Fly stocks

Wild-type Oregon R (OrR) flies and progeny from crosses of appropriate *gal4* driver lines with UAS-marker gene lines [23] were used for immunocytochemistry (for detailed information on the employed fly lines see references in Table 1). All flies were reared under a 12:12 h light:dark regime at 18 or 25°C on standard cornmeal agar medium and yeast.

Immunocytochemistry

For whole-mount immunostainings, CNS of third instar (L3) larvae were dissected in ice-cold 0.1 M sodium phosphate buffered saline (PBS; pH 7.2) and fixed with 4 % paraformaldehyde in PBS for 2 h at 4°C. After several washes with 0.1 M PBS containing 1 % TritonX (PBT), tissue was incubated with primary antibody (for detailed information on the employed antisera see references in Table 2) and 5 % normal goat serum (NGS) in PBT for 1–3 days at 4°C. The tissue was then washed several times with PBT, followed by overnight incubation with the appropriate secondary antibodies and 1 % NGS in PBT at 4°C. As secondary antibodies, Cy3-conjugated AffiniPure goat-anti-rabbit and goat-anti-rat IgG, and Cy5-conjugated AffiniPure goat-anti-rabbit and goat-anti-mouse IgG (Jackson ImmunoResearch, West Grove, PA) were used at a dilution of 1:300. The following day, tissue was washed several times with PBT, twice with 0.01 M PBS, and then

mounted in glycerol:0.01 M PBS (80:20). To visualize fine neurites and to enhance figure contrast, *gal4*-driven expression of mCD8GFP or GFP-tagged fusion proteins like SybGFP was generally revealed with a commercially available polyclonal rabbit-anti-GFP serum (MBL International, Woburn, MA). This GFP antiserum specifically labeled GFP expressing neurons (Fig. S1).

Confocal microscopy and data processing

Confocal stacks were acquired on a confocal laser scanning microscope (Leica TCS SP2, Leica Microsystems, Wetzlar, Germany) with a 40x objective (HCX PL APO 40x, N.A. 1.25) at 512x512 pixel resolution in 0.5–1 mm steps along the z-axis. For 3D volume-rendering, image stacks were imported into AMIRA 3.1 software (Indeed-Visual Concepts, Berlin, Germany) and processed using the “Voltex” and “ObliqueSlice” module. A false color map was applied to the volume-rendered neurons, and brightness and contrast were adjusted. Snapshots were taken in AMIRA and processed with Adobe Photoshop 7.0 (Adobe Systems Inc., San Jose, CA). A schematic representation of the BA labeling in the Fas2 landmark system was generated using Adobe Illustrator CS 11.0 (Adobe Systems Inc., San Jose, CA). To analyze co-localization between *gal4*-driven mCD8GFP expression and immunolabeling, volume-rendered 3D image stacks were down-sampled to maximum pixel intensity projections and further processed with Adobe Photoshop 7.0 and ImageJ 1.34s (NIH, public domain: <http://rsb.info.nih.gov/ij/>).

Results

We used targeted fluorescent marker protein expression [23] and immunocytochemistry to map aminergic neurons in the thoracic and abdominal neuromeres of the *Drosophila* ventral ganglion (referred to as VG; the subesophageal neuromeres are ignored here since they show a less strict Fas2 labeling pattern than the thoracic and abdominal neuromeres) at the L3 larval stage. Since the immunocytochemical detection of most BAs is complicated (see [24]) we mainly focused on the enzymes involved in BA biosynthesis (for an overview about BA biosynthesis see Fig. 1). Consequently, our data do not chemically proof the presence of BAs in the characterized neurons, but indicate that the respective neurons are able to synthesize BAs. Thus, we mapped presumed serotonergic, dopaminergic, and tyraminerbic/octopaminergic neurons into a set of constant and evenly distributed landmarks of the VG that show Fas2 immunoreactivity (for a description of the Fas2 landmark system see Figure 2). Since we could not simultaneously label histamine and Fas2, histaminergic neurons are omitted in our mapping (see [1]). We adopted the neutral nomenclature of Fas2-positive tracts proposed by Landgraf et al. ([19]; see Figure 2) and present our results on standardized plates. Each plate comprises both dorsal/ventral and transverse views of a typical whole-mount preparation and schematic drawings showing the characteristic distribution of the respective aminergic neurons within the Fas2 landmark system. The corresponding text section contains a detailed morphological description as well as a short overview of the synthesis pathway of the respective BA, its physiological functions, and references to previous morphological studies. In case appropriate *gal4* drivers were available, we also analyzed the distribution of ectopically expressed pre- and postsynaptic markers to reveal putative synaptic in-/output zones of aminergic neurons.

5-HT neurons

General characteristics. In *Drosophila*, the tryptophan hydroxylases DTPH (encoded by CG7399) and DTRHn (encoded

Table 1. Employed fly lines.

Fly Line	Donor [Reference]
<i>Ccap-gal4</i>	John Ewer [111]
<i>Ddc-gal4</i>	Bloomington Stock Center; Jay Hirsh [56]
<i>Tdc2-gal4</i>	Bloomington Stock Center; Jay Hirsh [60]
<i>Th-gal4</i>	Bloomington Stock Center; Serge Birman [49]
<i>UAS-DscamGFP</i>	Tzumin Lee [53]
<i>UAS-mCD8GFP</i>	Bloomington Stock Center; Tzumin Lee and Liqun Luo [112]
<i>UAS-SybGFP</i>	Bloomington Stock Center; Kendal Broadie [50,51]
<i>UAS-SytGFP</i>	Bloomington Stock Center; Kendal Broadie [52]

doi:10.1371/journal.pone.0001848.t001

Table 2. Employed antisera.

Antibody	Dilution	Source	Donor [Reference]
anti-5-HT polyclonal	1:5000	rabbit	Immunostar Inc., Hudson, WI
anti-CCAP polyclonal	1:1000	rabbit	Heinrich Dirksen [111,113,114]
anti-DDC polyclonal	1:5000	rabbit	Ross Hodgetts [55]
anti-Fas2 1D4 monoclonal	1:75	mouse	Developmental Studies Hybridoma Bank, University of Iowa, IA
anti-GFP polyclonal	1:500	rabbit	MBL International, Woburn, MA
anti-T β H polyclonal	1:100	rat	Maria Monastirioti [61]
anti-TH monoclonal	1:1000	mouse	Immunostar Inc., Hudson, WI
anti-MIP	1:3000	rabbit	Manfred Eckert [115]

doi:10.1371/journal.pone.001848.t002

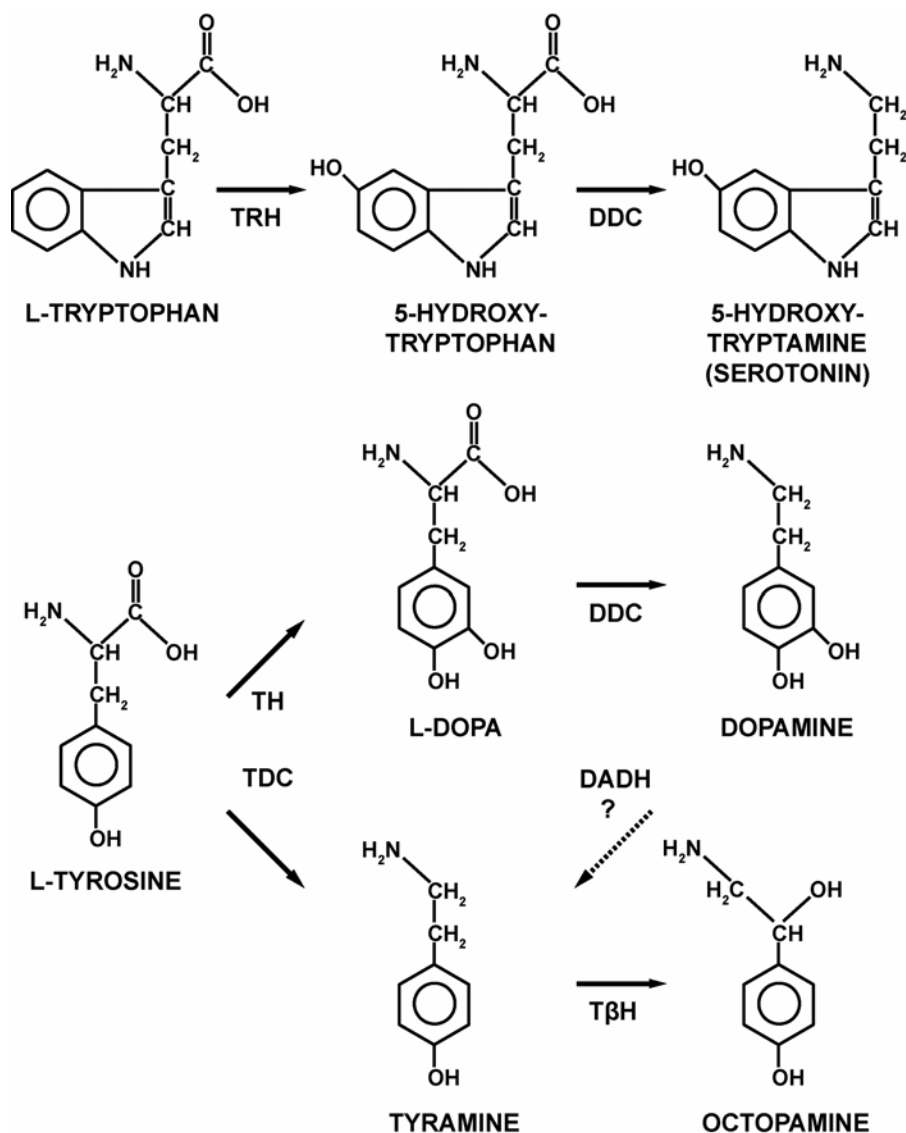


Figure 1. Synthetic pathways for serotonin, dopamine, tyramine, and octopamine. The amino acid tryptophan is the starting point for the synthesis of 5-hydroxytryptamine (5-HT, serotonin), whereas tyrosine is the source for dopamine as well as tyramine and octopamine. An alternative pathway (dotted arrow) via DADH may exist that permits the synthesis of tyramine from dopamine. DADH: dopamine dehydroxylase; DDC: DOPA decarboxylase; T β H: tyramine β -hydroxylase; TDC: tyrosine decarboxylase; TH: tyrosine hydroxylase; TRH: tryptophan hydroxylase.

doi:10.1371/journal.pone.0001848.g001

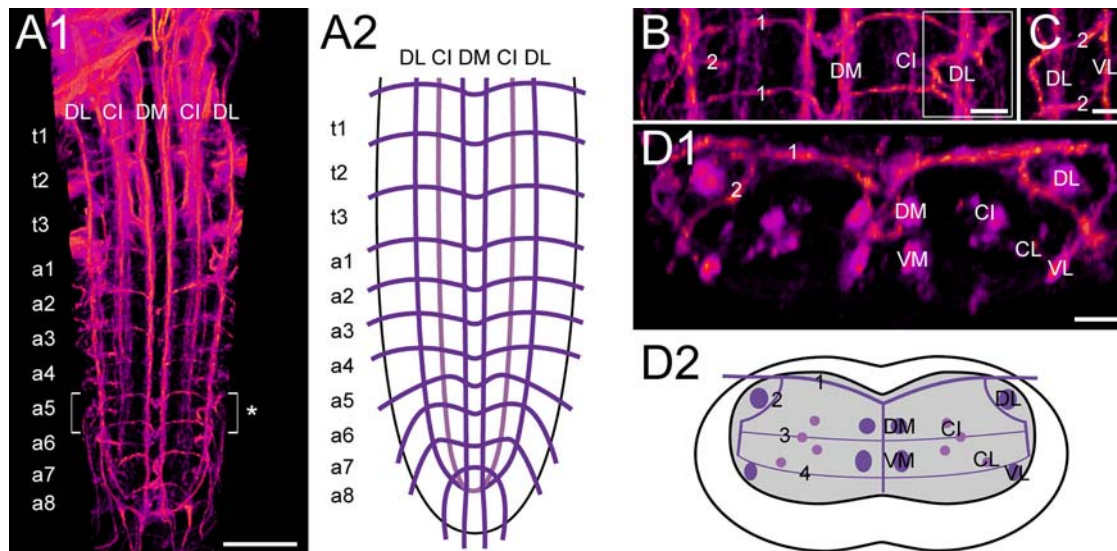


Figure 2. The Fasciclin2 landmark system in the *Drosophila* larval VG. A1) Dorsal view of a 3D image stack showing volume-rendered Fas2-immunoreactive tracts in the thoracic (t1-3) and abdominal neuromeres (a1-8) of the L3 larval VG, and A2) the deduced idealized dorsal scheme. B) Detailed dorsal and C) lateral view of a5 and adjacent neuromeres (* in A1). D1) Transversal view of a5, and D2) the deduced idealized transversal scheme. Longitudinal projections are named according to their relative dorso-ventral (D: dorsal, C: central, V: ventral) and medio-lateral (M: medial, I: intermedial, L: lateral) position. For example, the two dorso-medial Fas2-immunoreactive tracts are referred to as DM tracts. Transversal projections (TP) are numbered according to their relative dorso-ventral position, i.e. “1” represents the topmost TP [19]. Scale bars: 50 μ m in A), 10 μ m in B), C), and D).

doi:10.1371/journal.pone.0001848.g002

by CG9122) catalyze the conversion of tryptophan to 5-hydroxytryptophan [25–27]. DOPA decarboxylase may then metabolize 5-hydroxytryptophan to 5-hydroxytryptamine (5-HT, serotonin). In the larva, 5-HT containing neurons influence endocrine activity, feeding (see [1]), and heart rate [28].

Previous morphological descriptions of 5-HT producing neurons in the larval VG relied on immunostainings [29–31]. We used a commercially available rabbit-anti-5-HT polyclonal antibody (Immunostar Inc.) and observed a staining pattern identical to those previously described.

Morphology (Fig. 3). The VG contains segmentally reiterated bilateral pairs of 5-HT-immunoreactive neurons (5-HT neurons). Typically, two 5-HT neuron pairs reside in each of the thoracic and abdominal neuromeres, with exception of t1 (three pairs) and a8 (one pair). While the somata of thoracic 5-HT neurons reside ventro-medially in the cortex beneath the CI tracts, the somata of abdominal 5-HT neurons lay rather ventro-laterally beneath the VL tracts. In each neuromere, 5-HT neurons project below the transversal projection (TP) 4 ventro-medially until their neurites pass the midline beneath the VM tracts. On the contralateral side, 5-HT neurites bifurcate strongly and innervate the whole neuropil. Thus, we could not trace single 5-HT neurites to separate target sites. Other 5-HT neurites run at the height of TP 3 between the DM and VM tracts and appear to connect the bilateral neuropil parts. Compared to other neuromeres, a7 showed a particularly high concentration of 5-HT neurites. In contrast, a8 and the adjacent “terminal plexus” [19] lacked 5-HT neurite arborizations. The 5-HT neurons of a8 send their primary neurites to the contralateral side, and then appear to supply the neuropil of a7.

Tyrosine hydroxylase neurons

General characteristics. Dopamine (DA) synthesis depends on the concerted action of the enzymes tyrosine hydroxylase (TH) and DOPA decarboxylase. TH catalyzes the first and rate-limiting step in catecholamine biosynthesis and mediates the oxidation of

tyrosine to 3,4-dihydroxy-L-phenylalanine (L-DOPA). DOPA decarboxylase may then metabolize L-DOPA to DA. In *Drosophila*, DA plays a role in various complex neuronal processes such as sleep and arousal [32–34], visual attention [35], stress response [36], learning [37], and sexual behavior [38]. In the larval and adult CNS, DA and TH immunoreactivity appear to localize to the same neurons [29,39,40]. Thus, TH-immunoreactive neurons are commonly referred to as dopaminergic neurons (see [1]). Central TH neurons specifically synthesize only one out of two possible TH splice variants [41,42] from a primary transcript encoded by the *pale* locus (CG10118; [43,44]). The second TH splice variant locates to epidermal cells and serves a vital role in cuticle biosynthesis [45]. Genetic as well as pharmacological inhibition of TH activity suggests that catecholamine loss decreases locomotor activity [46,47].

Previous studies described the morphology of TH-producing neurons (TH neurons) in the VG with immunocytochemistry [29,48] and *Th-gal4*-driven GFP expression [49]. We here used the same *Th-gal4* driver line as well as a commercially available monoclonal mouse-anti-TH antibody. In general, both approaches revealed identical neurons. Ventral midline neurons in a1-7, however, showed very weak or even lacked *Th-gal4*-driven mCD8-GFP expression (Fig. S1), but always immunostained against TH (Fig. S2).

Morphology (Fig. 4). Inferred from *Th-gal4*-driven marker gene expression as well as TH immunostainings, the VG contains two morphologically different TH neuron groups: The first group comprises three ventral median TH neurons (vmTH neurons) in t1, and a single vmTH neuron in each neuromere from t2 to a7. Their cell bodies locate to the midline beneath the VM tracts. The second TH neuron group consists of a bilateral pair of dorso-lateral TH neurons (dlTH neurons) with somata residing at the height of the DL tracts in each neuromere from a1-7. Longitudinal TH projections are adjacent to the VL, beneath the CI, and close to the VM/DM tracts. Neurites of the vmTH neurons project

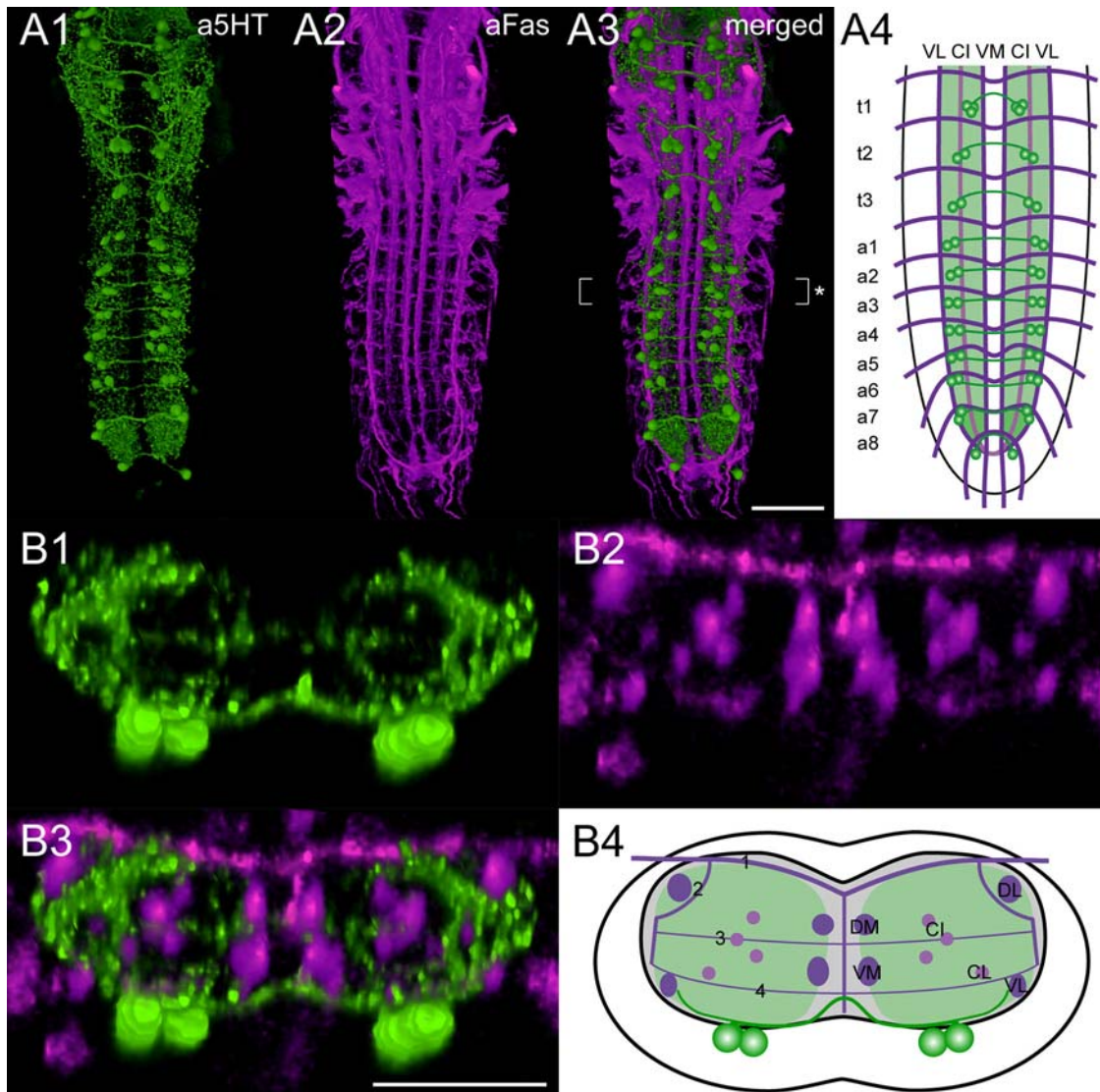


Figure 3. Mapping of 5-HT-immunoreactive neurons. Ventral view of 3D image stacks showing volume-rendered A1) 5-HT-immunoreactive neurons (green) and A2) Fas2-positive tracts (magenta) in a larval VG. The merged image (A3) served for an idealized schematic representation of presumed 5-HT neurons in the Fas2 landmark system (A4). B1-3) Corresponding transversal views of the neuromere a2 (* in A3), and B4) the deduced idealized transversal scheme. Green-shaded areas in the schemes contain a high concentration of 5-HT-immunoreactive arborizations. Scale bars: 50 μ m in A), 25 μ m in B).

doi:10.1371/journal.pone.0001848.g003

dorsally and then appear to join longitudinal TH projections between the DM and VM tracts. The vmTH neurons of t1 also initially project dorsally until their neurites reach the height of the VM tracts. The neurites then diverge and build up a loop enclosing the DM/VM and CI tracts on each side of the neuromere. These neurite loops seem to establish a transversal connection between all longitudinal TH projections within the VG. As opposed to the vmTH neurites, the neurites of the dlTH neurons run ventrally and form fine longitudinal projections along the VL tracts. There, TH neurites divide and proceed in a loop to the median neuropil. Between the CI and the VM tracts, the TH neurites running beneath TP 4 join bilateral fine longitudinal projections somewhat ventro-laterally to the VM tracts. The TH neurites then proceed dorsally until they converge with the upper branch of the TH neurite loop in a prominent longitudinal projection between the DM and VM tracts. TH neurites ramify heavily in the neuropil between the DM/VM and the CI tracts.

Distribution of ectopically expressed markers (Fig. 5).

To identify the in- and output compartments of TH neurons, we ectopically expressed the neuronal compartment markers neuronal synaptobrevin-GFP (SybGFP; [50,51]), synaptotagmin 1-GFP (SytGFP; [52]), and *Drosophila* Down syndrome adhesion molecule [17.1]-GFP (DscamGFP; [53]). *Th-gal4*-driven SybGFP showed a dotted distribution within the VG and largely mimicked the mCD8GFP expression pattern. In t1-3, SybGFP uniformly labeled all TH neurites. The neuromeres a1-5 typically contained less SybGFP than t1-3 and a6-7, since labeling was restricted to TH neuron somata and longitudinal TH projections adjacent to the DM/VM and the VL tracts. Transversal TH neurites appeared to lack SybGFP in a1-5. In a6-7, high amounts of SybGFP accumulated around the DM/VM tracts and also located to transversal TH projections. Particularly, the dorsal branches of the bilateral transversal neurite loops showed intense SybGFP labeling. In contrast to SybGFP, *Th-gal4*-driven SytGFP strongly

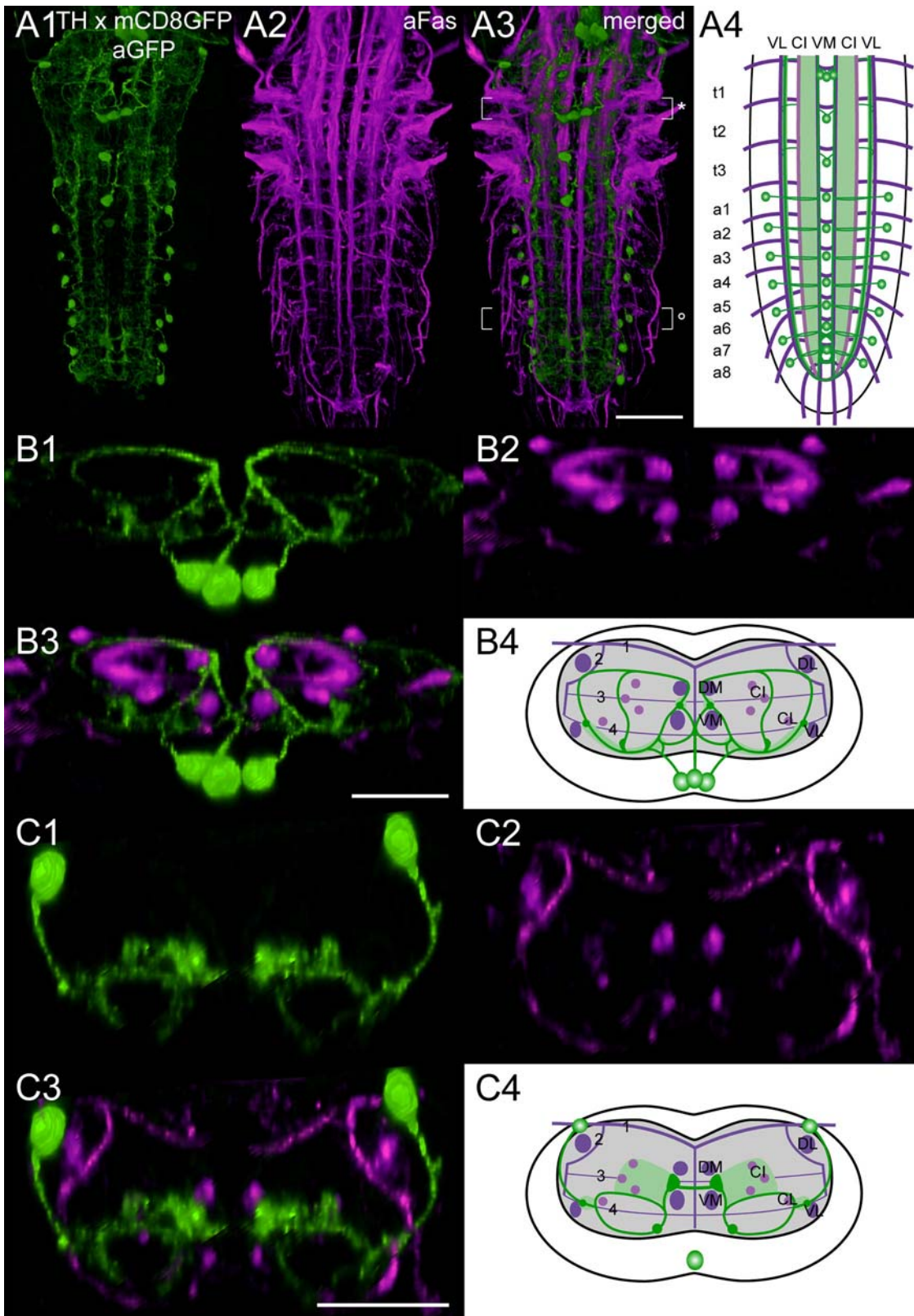


Figure 4. Mapping of *Th-gal4* x mCD8GFP expressing neurons. A1) Ventral view of 3D image stacks showing volume-rendered GFP-immunoreactive neurons (green) and A2) Fas2-positive tracts (magenta) in a larva expressing *Th-gal4*-driven mCD8GFP. The merged image (A3) served for an idealized schematic representation of *Th-gal4* x mCD8GFP expressing neurons in the Fas2 landmark system (A4). B1-3) Corresponding transversal views of the neuromere t1 (* in A3), and B4) the deduced idealized scheme. C1-3) Transversal views, and C4) idealized scheme of a5 (° in A3). Note that the idealized schemes A4) and C4) include the vmTH neurons of a1-7, which often lacked *Th-gal4*-driven mCD8GFP expression. These neurons, however, always showed strong TH immunoreactivity (see Fig. S2). Green-shaded areas in the schemes contain a high concentration of GFP-immunoreactive arborizations. Scale bars: 50 μ m in A), 25 μ m in B) and C).
doi:10.1371/journal.pone.0001848.g004

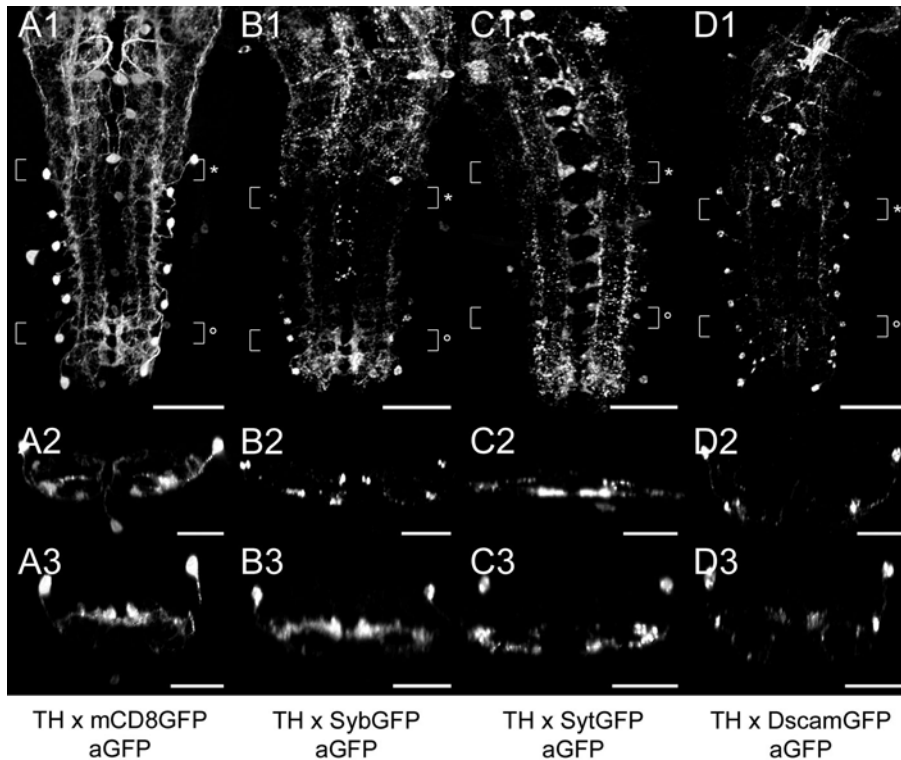


Figure 5. Distribution of ectopically expressed neuronal compartment markers in TH neurons. A1-D1) Dorsal view of GFP immunoreactivity in the VG of larvae expressing *Th-gal4*-driven mCD8GFP (A1-3), SybGFP (B1-3), SytGFP (C1-3), or DscamGFP (D1-3). A2-D2) Corresponding transversal views of the neuromeres t3 or a1 (* in A1-D1). A3-D3) Additional transversal views showing the compartment marker distribution in a5/6 (* in A1-D1). All images are auto-contrasted maximum pixel intensity projections of volume-rendered 3D image stacks. Scale bars: 50 μ m in A1-D1), 25 μ m in A2-D2) and A3-D3). doi:10.1371/journal.pone.0001848.g005

labeled segmentally reiterated neurite arborizations next to the VM tracts. These median arborizations appeared to belong to the transversal TH neurites connecting both neuropil hemispheres. SytGFP further located to longitudinal projections running along the VL tracts and to the neuropil between the CI and VM tracts. Compared to other neuromeres, a6-7 seemed to contain the highest concentration of SytGFP. There, SytGFP particularly accumulated around the longitudinal TH projections adjacent to the VL tracts and in the ventral branches of the transversal TH neurite loops. *Th-gal4*-driven DscamGFP mainly labeled the somata and primary neurites of the dITH neurons and the longitudinal TH projections adjacent to the VL tracts. Furthermore, in a6-7, DscamGFP located to longitudinal TH projections next to the DM tracts and to the ventral parts of the transversal neurite loops. The neuropil between the CI and VM tracts, however, showed only faint DscamGFP labeling.

DOPA decarboxylase neurons

General characteristics. DOPA decarboxylase (DDC) catalyzes the production of DA from L-DOPA, and 5-HT from 5-hydroxytryptophan. The *Drosophila Ddc* gene (CG10697) encodes a primary transcript that is alternatively spliced into two distinct DDC isoforms in the CNS and epidermis. DDC mRNA levels and DDC protein activity peak during development at the end of embryogenesis and at the larval, pupal, and adult molts. DDC-producing neurons (DDC neurons) play a vital role in cuticle biosynthesis and other DA- or 5-HT-mediated processes (see [1,54]).

The distribution of DDC neurons in the VG of *Drosophila* was described with immunocytochemistry [29,43,48]. In addition, Landgraf et al. [19] mapped neurons expressing *Ddc-gal4*-driven

GFP in the Fas2 landmark system. We revealed DDC neurons with a different polyclonal rabbit-anti-DDC serum [55] as well as *Ddc-gal4*-driven mCD8GFP [56]. Although the DDC immunolabeling pattern largely matched the *Ddc-gal4*-driven mCD8GFP expression, we observed some substantial differences in the type and number of labeled neurons (Fig. S3).

Morphology (Fig. 6, 7). Inferred from *Ddc-gal4*-driven marker gene expression (Fig. 6), DDC immunostainings (Fig. 7; Fig. S3), and double labeling experiments with antibodies against 5-HT and TH (Fig. S4), DDC neurons can be categorized into five distinct neuron groups: The first group consists of segmentally reiterated DDC neuron pairs with somata in the ventral cortex below the CI fascicles. These DDC neurons likely represent serotonergic neurons since they showed 5-HT immunoreactivity (Fig. S4; see above for a detailed morphological description). The *Ddc-gal4* driver induced mCD8GFP expression in additional neuron pairs of a3-6 which reside adjacent to the 5-HT neurons in the cortex beneath the CI tracts. These neurons constitute a second distinct DDC neuron group since they obviously synthesize the peptide corazonin [19]. The corazonin-immunoreactive DDC neurons showed faint DDC immunoreactivity in a few preparations, but lacked 5-HT immunoreactivity (Fig. S3, and S4; for a detailed morphological description of corazonin-immunoreactive neurons within the Fas2 landmark system see [20]). The third group of DDC neurons consists of unpaired neurons in the ventral midline of t3 and a1-5, whose somata lay right beneath the DM/VM tracts. Although these neurons typically showed poor *Ddc-gal4*-driven mCD8GFP expression, they always strongly stained with both DDC and TH antisera (Fig. S3, and S4). Thus, these DDC neurons correspond to the presumptive dopaminergic vmTH

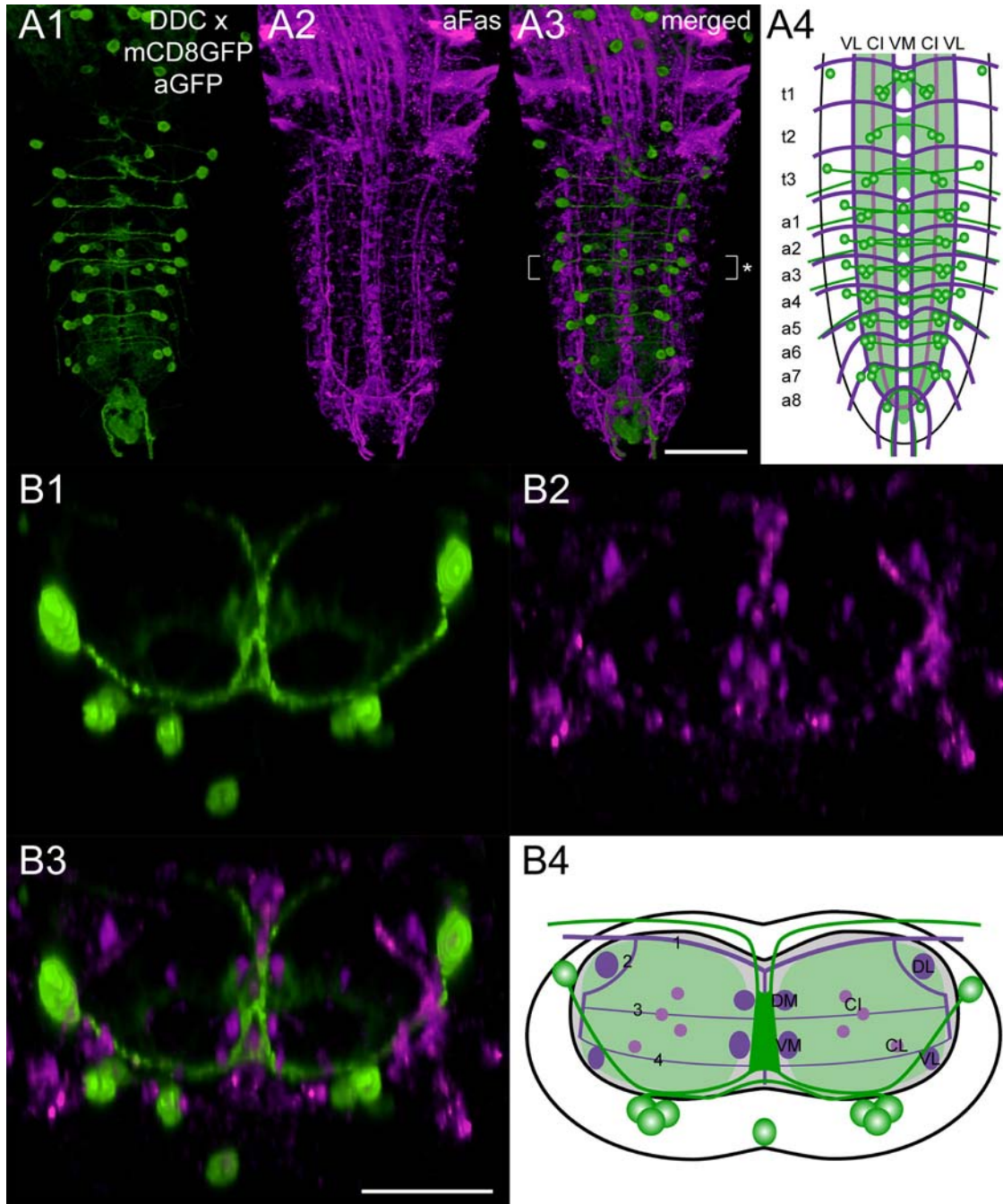


Figure 6. Mapping of *Ddc-gal4* x mCD8GFP expressing neurons. A1) Ventral view of 3D image stacks showing volume-rendered GFP-immunoreactive neurons (green) and A2) Fas2-positive tracts (magenta) in a larva expressing *Ddc-gal4*-driven mCD8GFP. The merged image (A3) served for an idealized schematic representation of *Ddc-gal4* x mCD8GFP expressing neurons in the Fas2 landmark system (A4). B1-3) Corresponding transversal views of the neuromere a4 (* in A3), and B4) the deduced idealized scheme. Note that the *Ddc-gal4* driver typically drives mCD8GFP expression in most, but not all presumed DDC neurons of the VG (see Fig. S3 and S4). Thus, some presumed DDC neurons are not included in the idealized schemes shown here. Green-shaded areas in the schemes contain a high concentration of GFP-immunoreactive arborizations. Scale bars: 50 μ m in A), 25 μ m in B) and C).

doi:10.1371/journal.pone.0001848.g006

neurons (see above). The somata of the fourth and the fifth distinct DDC neuron groups reside dorso-laterally at the height of the DL tracts. The fourth group of DDC neurons showed strong DDC and TH immunolabeling. These DDC neurons, therefore, likely represent the presumptive dopaminergic dITH neurons (Fig. S4; see above), but were usually missing in the *Ddc-gal4* expression pattern. The remaining neurons constitute the fifth distinct DDC

neuron group (VL1 neurons; [19]; see also below) since they neither seem to synthesize 5-HT nor DA (Fig. S4). VL1 neurons showed prominent *Ddc-gal4*-driven mCD8GFP expression, but comparably weak DDC immunoreactivity (Fig. S3). The VL1 neuron somata are typically arranged as segmentally reiterated pairs in t3, a1-4, and a6-7, and reside laterally between the height of the VL and the DL tracts. In t3 and a1-4, VL1 neurites initially

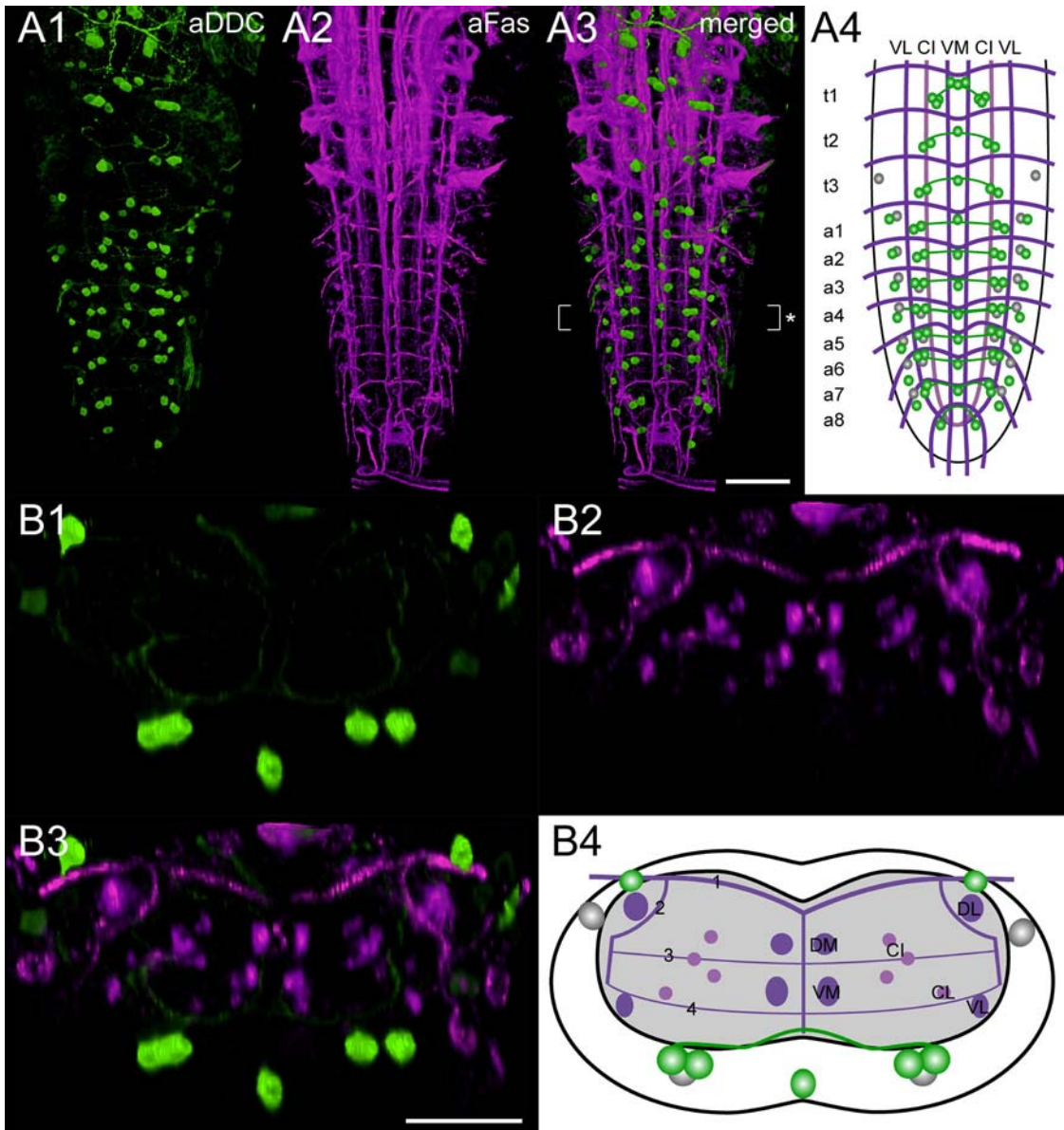


Figure 7. Mapping of DDC-immunoreactive neurons. A1) Ventral view of 3D image stacks showing volume-rendered DDC-immunoreactive neurons (green) and A2) Fas2-positive tracts (magenta) in a larval VG. The merged image (A3) served for an idealized schematic representation of DDC-immunoreactive neurons in the Fas2 landmark system (A4). B1-3) Corresponding transversal views of the neuromere a4 (* in A3), and B4) the deduced idealized scheme. Besides the aminergic neurons, the DDC antiserum also faintly labeled presumed peptidergic neurons, which are shown in gray in the schemes. Noteworthy, these peptidergic neurons are also present in the *Ddc-gal4* expression pattern (see Fig. 6). Scale bars: 50 μ m in A), 25 μ m in B). doi:10.1371/journal.pone.0001848.g007

run ventrally towards the VL tracts, then project beneath the TP 4 ventro-medially until they converge in proximity to the VM tracts. After forming extensive arborizations between the DM and VM tracts, the VL1 neurites proceed dorsally, diverge within the cortex, and project via the segmental nerves to the periphery.

Tyrosine decarboxylase 2 and tyramine β -hydroxylase neurons

General characteristics. Tyrosine decarboxylase (TDC) catalyzes the synthesis of tyramine (TA) from tyrosine. A second enzyme, tyramine β -hydroxylase (T β H), may then convert TA to its metabolite octopamine (OA; see [1,3,4,57–59]). In adult *Drosophila*, two different TDC genes, *Tdc1* (CG30445) and *Tdc2*

(CG30446), show a largely non-overlapping expression pattern: TDC1 is most abundant in non-neural tissue of the abdomen, but also localizes to a few thoracic neurons of the VG [60]. In contrast, TDC2 is primarily expressed within the CNS [60]. Like *Tdc2*, the *Drosophila T β H* gene (CG1543) encodes a single protein that is primarily expressed within CNS neurons. According to the enzymatic function of T β H, T β H-immunoreactive neurons show a similar distribution pattern as OA-immunoreactive neurons in the VG [61]. In *Drosophila*, OA has a multitude of modulatory and hormonal functions (see [1,3,4,57–59]). For example, OA regulates ovulation and egg laying [60,62–64]. Both OA and TA appear to modulate locomotor activity in the larva [65,66] and in the adult fly [67,68]. TA signaling also seems to influence diuresis [69–71] and olfactory behavior [72].

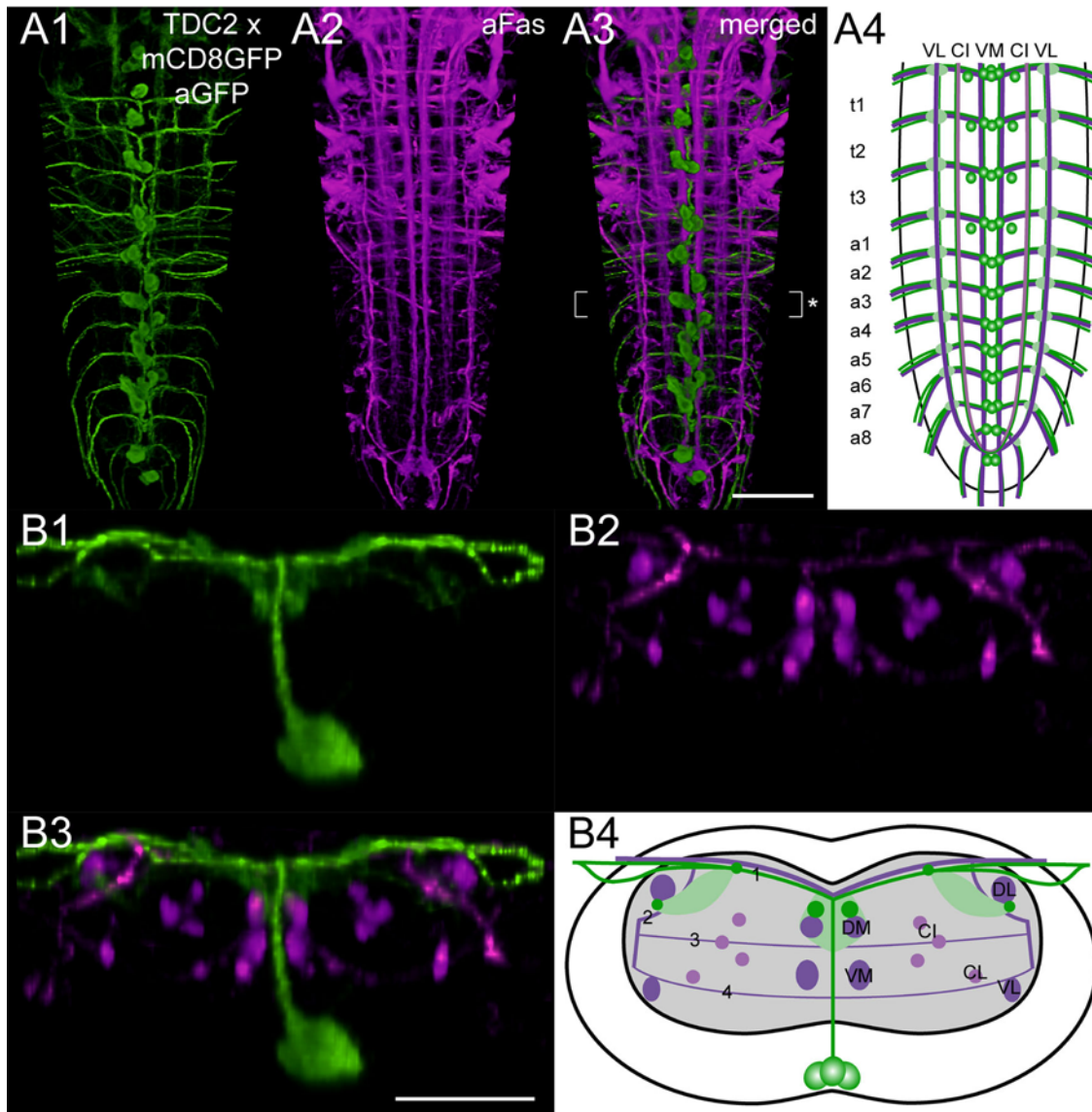


Figure 8. Mapping of *Tdc2-gal4* x mCD8GFP expressing neurons. A1) Ventral view of 3D image stacks showing volume-rendered GFP-immunoreactive neurons (green) and A2) Fas2-positive tracts (magenta) in a larva expressing *Tdc2-gal4*-driven mCD8GFP. The merged image (A3) served for an idealized schematic representation of *Tdc2-gal4* x mCD8GFP expressing neurons in the Fas2 landmark system (A4). B1-3) Corresponding transversal views of the neuromere a3 (* in A3, and B4) the deduced idealized scheme. Note that the idealized scheme A4) includes the pmTDC2 neurons of t1-3 and a1, which often faintly expressed *Tdc2-gal4*-driven mCD8GFP. The pmTDC2 neurons, however, always showed strong TβH immunoreactivity (see Fig. S5). Green-shaded areas in the schemes contain a high concentration of GFP-immunoreactive arborizations. Scale bars: 50 μm in A), 25 μm in B). doi:10.1371/journal.pone.0001848.g008

Previous morphological descriptions of tyraminerpic/octopaminergic neurons in the larval VG relied on immunostainings against TA [73], OA [74], and TβH [61]. In addition, Landgraf et al. [19] mapped the *MzVum-gal4*-expressing neuron group, which appears to include efferent TA-/OA-immunoreactive neurons, in the Fas2 landmark system. We here used a *Tdc2-gal4* line [60] and a polyclonal rat-anti-TβH serum [61] to reveal presumed tyraminerpic/octopaminergic neurons (TDC2 neurons) in the VG. Since all TDC2 neurons showed TβH immunoreactivity (Fig. S5), they likely all produce OA. This opposes the recent assumption that some ventral midline neurons may synthesize only TA and not OA [73]. In general, the distribution of TDC2 neurons resembled the TA immunostaining pattern. We observed additional pairs of paramedial TDC2 neurons and one or two dorsal unpaired

median TDC2 neuron(s) that could not be detected with the TA antiserum [73]. The TA antiserum instead labeled dorso-laterally located neurons (ITA neurons) in a1-7 [73], which appeared to be missing in the *Tdc2-gal4*-driven mCD8GFP expression pattern. Since the ITA neurons also lacked both OA [74] and TβH immunoreactivity (Fig. S5), they possibly synthesize TA, but no OA. Noteworthy, the number and position of ITA neurons highly resembles that of presumptive dopaminergic dITH neurons (see above). Thus, ITA neurons may represent unique TA neurons that synthesize TA from DA via the dopamine dehydroxylase pathway, but do not produce OA (Fig. 1; see [4]).

Morphology (Fig. 8). With respect to their position in the Fas2 landmark system, three distinct TDC2 neuron groups reside in the larval VG: The first group comprises ventral unpaired median

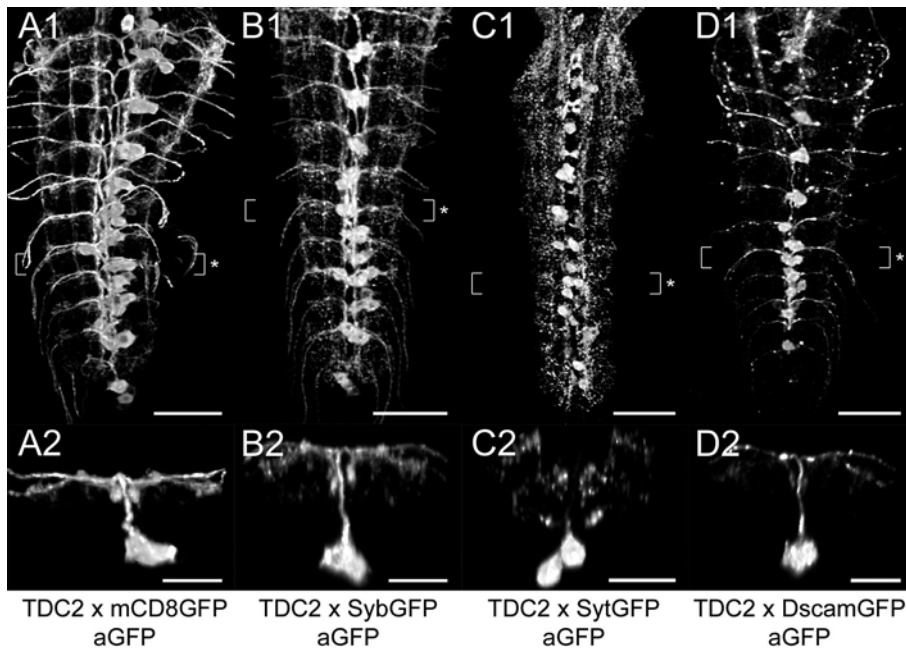


Figure 9. Distribution of ectopically expressed neuronal compartment markers in TDC2 neurons. (A1-D1) Dorsal view of GFP immunoreactivity in the VG of larvae expressing *Tdc2-gal4*-driven mCD8GFP (A1-2), SybGFP (B1-2), SytGFP (C1-2), or DscamGFP (D1-2). (A2-D2) Corresponding transversal views of the neuromeres a3 or a4 (* in A1-D1). All images are auto-contrasted maximum pixel intensity projections of volume-rendered 3D image stacks. Scale bars: 50 μ m in A1-D1), 25 μ m in A2-D2). doi:10.1371/journal.pone.0001848.g009

TDC2 neurons (vumTDC2 neurons) that locate to the cortex beneath the VM tracts. In general, three vumTDC2 neurons compose a neuron cluster in the neuromeres t1-a6, whereas a7 appears to contain only two vumTDC2 neurons. The second group typically consists of two dorso-medial TDC2 neurons (dmTDC2 neuron) residing between the last subesophageal neuromere and t1, and two dmTDC2 neurons of a8. All dmTDC2 neurons localize to the dorsal cortex above the DM tracts. The third distinct TDC2 neuron group in the VG comprises paramedial neuron pairs (pmTDC2 neurons). The pmTDC2 neuron somata lay in the ventral cortex of t1-3 and a1, somewhat ventro-laterally to the VM fascicles. Typically, pmTDC2 neurons showed faint *Tdc2-gal4*-driven mCD8GFP expression, but strong T β H immunoreactivity (Fig. S5). Prominent longitudinal TDC2 neurites project above the DM tracts. Finer longitudinal projections run at the dorsal neuropil rim above the CI fascicles and along the DL tracts. All of these longitudinal neurites appear to originate from descending TDC2 neurons. The descending TDC2 neurites proceed through the whole length of the VG until they coincide at the tip of the VG. In contrast to the descending TDC2 neurons, vumTDC2 neurons project dorsally, where their neurites form extensive arborizations in the neuropil above the DM tracts. The vumTDC2 neurites then diverge in the dorsal cortex and project above TP 1 laterally towards the longitudinal TDC2 neurites at the CI tracts. There, the vumTDC2 neurites may bifurcate again and traverse above or beneath the DL fascicles. Outside of the VG, vumTDC2 neurites join and project together via the segmental nerves to the periphery. We could not trace the projections of the dm- and pmTDC2 neurons since these neurites lacked *Tdc2-gal4*-driven mCD8GFP expression as well as T β H immunoreactivity (Fig. 8, Fig. S5).

Distribution of ectopically expressed markers (Fig. 9). Because *Tdc2-gal4* specifically drove mCD8GFP expression in presumed tyraminergetic/octopaminergic neurons, we used the neuronal compartment markers SybGFP, SytGFP and DscamGFP

to reveal their putative in- and output zones. The distribution of *Tdc2-gal4*-driven SybGFP highly resembled the mCD8GFP expression pattern. SybGFP localized to the neurites of vumTDC2 neurons and to all longitudinal projections of TDC2 neurons. Furthermore, SybGFP accumulated around peripherally projecting vumTDC2 neurites in the dorso-lateral neuropil between the CI and DL tracts. Compared to SybGFP, *Tdc2-gal4*-driven SytGFP showed a different distribution pattern. SytGFP accumulated around the DM/VM tracts and in the dorso-lateral neuropil. The peripheral projections of the vumTDC2 neurons completely lacked SytGFP. Thus, the SytGFP labeling in the VG appears to belong to descending TDC2 neurons. In contrast to SybGFP and SytGFP, DscamGFP almost exclusively localized to vumTDC2 neuron somata and neurites. Only TDC2 neurites in t1-3 and longitudinal TDC2 projections along the DM and DL tracts also showed a dotted DscamGFP labeling pattern.

Fas2-based identification of co-localized signaling molecules

During our morphological characterization of aminergic neurons in the larval VG, we observed two distinct neuron groups within the *Ddc-gal4*-driven mCD8GFP expression pattern that apparently synthesize neither 5-HT nor DA (Fig. S4; see above). While the ventro-medially residing DDC neuron group obviously synthesizes the neuropeptide corazonin [19], the signaling molecules of the other group, the VL1 neurons, have remained unidentified. We hence applied Fas2-based mapping and compared the relative distribution of VL1 neurons in the VG with that of recently mapped peptidergic neurons [20]. Interestingly, the relative position of VL1 neurons in the Fas2 landmark system highly resembled efferent neurons showing crustacean cardioactive peptide (CCAP) and myoinhibiting peptide (MIP; [20]) immunoreactivity. We employed the respective antisera and confirmed that VL1 neurons indeed are CCAP- and MIP-immunoreactive (Fig. 10). Since *Ddc-gal4*-driven

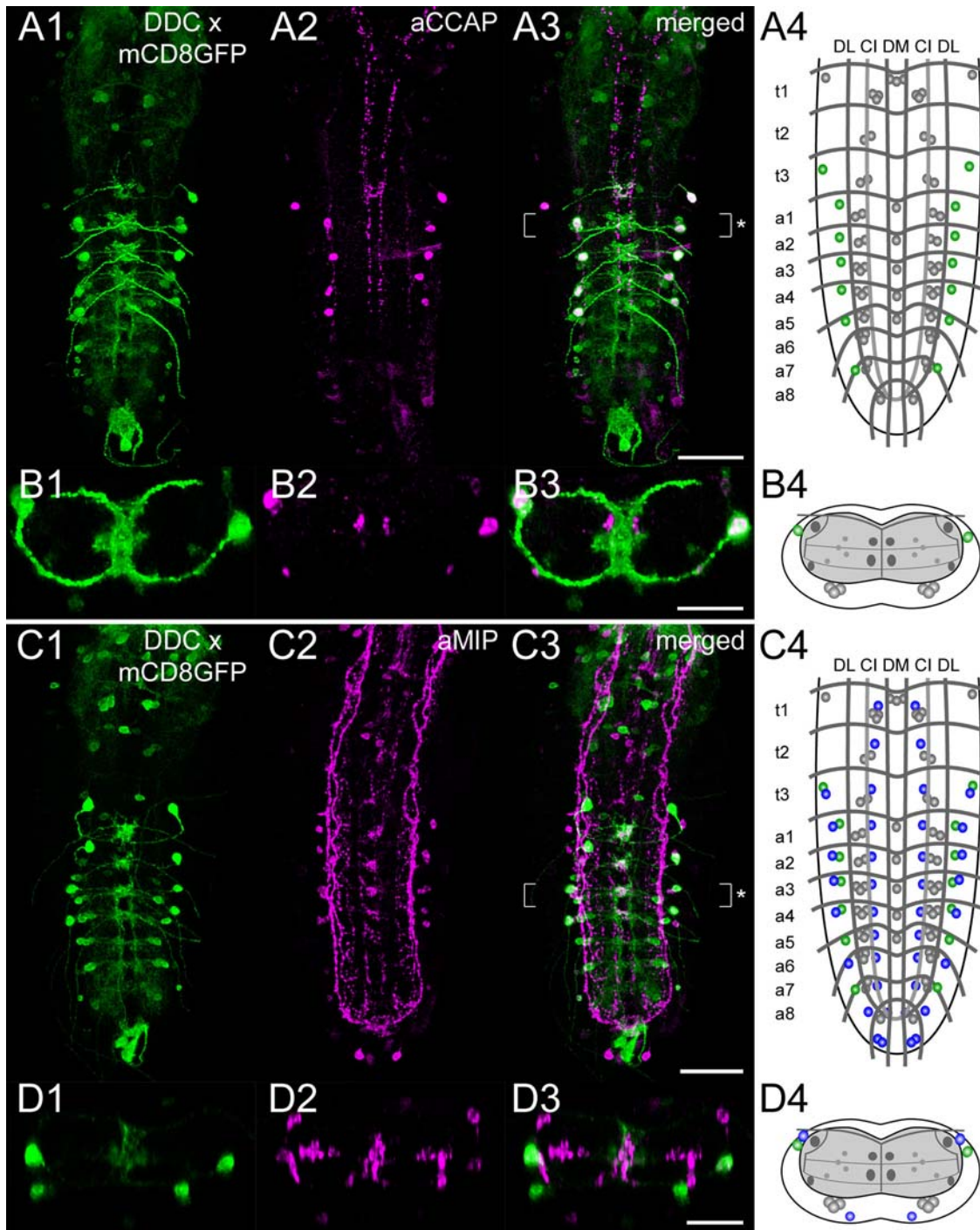


Figure 10. Fas2-based comparison of *Ddc-gal4*-driven mCD8GFP expression and CCAP/MIP immunoreactivity in the larval VG. A1) Dorsal view of *Ddc-gal4* x mCD8GFP expressing neurons (green) and A2) CCAP-immunoreactive neurons (magenta) in a larval VG. The merged image (A3) served for an idealized schematic representation of the respective neuron groups in the Fas2 landmark system (A4). B1-3) Corresponding transversal views of the neuromere a1 (* in A3), and B4) the deduced idealized scheme. C1) Dorsal view of *Ddc-gal4* x mCD8GFP expressing neurons (green) and C2) MIP-immunoreactive neurons (magenta) in a larval VG. The merged image (C3) provided the basis for the scheme shown in (C4). D1-3) Corresponding transversal views of the neuromere a3 (* in C3), and D4) the deduced idealized scheme. In all schemes, neurons showing both *Ddc-gal4*-driven mCD8GFP expression and CCAP/MIP immunoreactivity are green-colored. *Ddc-gal4* x mCD8GFP expressing neurons which lacked CCAP/MIP immunoreactivity are shown in gray. Vice versa, neurons which exclusively showed CCAP/MIP immunoreactivity are blue-colored. Original images are maximum pixel intensity projections of volume-rendered 3D image stacks. Scale bars: 50 μ m in A) and C), 25 μ m in B) and D).
 doi:10.1371/journal.pone.0001848.g010

mCD8GFP was generally missing in dITH neurons, and dITH neurons showed a similar position within the Fas2 landmark system as CCAP/MIP-synthesizing neurons (CCAP/MIP neurons), we finally tested whether any CCAP/MIP neuron co-expresses TH. However, *Ccap-gal4*-driven mCD8GFP expression and TH immunoreactivity did not overlap, but localized to different neuron groups (Fig. S6).

Discussion

We here used *gal4*-driven marker gene expression and immunocytochemistry to three-dimensionally map presumed serotonergic, dopaminergic and tyraminerpic/octopaminergic neurons within the Fas2 landmark system of the larval VG. Furthermore, we employed several ectopically expressed pre- and postsynaptic markers to reveal the in- and output compartments of presumptive dopaminergic TH and tyraminerpic/octopaminergic TDC2 neurons. Our results now allow to compare the segmental distribution patterns of aminergic neurons and to trace aminergic projections to defined neuropil areas within the VG. In the following, we relate the morphology of aminergic neurons to known BA functions and describe putative neuronal network interactions with other VG neurons. We also exemplify how Fas2-based mapping can simplify the identification of co-localized signaling molecules, and allocate all neurons within the complex *Ddc-gal4* expression pattern to distinct neuron subsets.

Both interneurons and efferent neurons of the larval VG contain BAs

Throughout the insects, similar neuron groups synthesize BAs. These groups typically comprise only few neurons with large branching patterns (see [1–3]). In agreement with previous studies [29–31], 5-HT neurons in t1-a8 of the *Drosophila* larval VG represent interneurons with intrasegmental neurites. The 5-HT neurons of a8, however, appear to supply only the neuropil of a7, but not that of a8 and the adjacent “terminal plexus”. Like 5-HT neurons, the presumptive dopaminergic TH neurons lack peripheral projections and appear to exclusively represent interneurons, as previously proposed [39]. In contrast, presumptive tyraminerpic/octopaminergic TDC2 neurons mostly represent efferent vumTDC2 neurons. The vumTDC2 neurons obviously project to larval body wall muscles including M1 and M2 since these muscles showed TA- [73] and OA-immunoreactive type II boutons [74]. In a8, dorsally located dmTDC2 neurons send axons through the associated segmental nerves, and hence are efferent neurons as well. These dmTDC2 neurons probably innervate the reproductive tract in the adult female fly [63]. Besides the dmTDC2 neurons of a8, typically two additional dmTDC2 neurons reside in the dorsal cortex between the last subesophageal neuromere and t1. These dmTDC2 neurons were not described in previous morphological studies on TA- [73] and OA-/TβH-immunoreactive neurons [61,74]. Nevertheless, all dmTDC2 neurons in the VG consistently showed strong *Tdc2-gal4*-driven mCD8GFP expression as well as TβH immunoreactivity. Thus, they likely synthesize both TA and OA. Although we could not trace their neurites, the dmTDC2 neurons resemble a pair of anterior medial neurons in locusts [75] and crickets [76] that localize to t1 and innervate the anterior connectives (see [3]). Alternatively, dmTDC2 neurons may correspond to a single dorsal unpaired median neuron which resides in t1 of the locust and supplies the subesophageal nerves [77]. Like dmTDC2 neurons, pmTDC2 neurons are probably interneurons as well. The soma position of pmTDC2 neurons highly resembles that of descending OA-immunoreactive interneurons detected in the subesophageal

and thoracic neuromeres of bees, crickets, cockroaches, locusts, and moths (see [3,78]).

Aminergic innervation varies between specific VG neuromeres

Within the larval VG of *Drosophila*, aminergic neurons typically show a segmentally reiterated distribution (see [1,2]). The number of aminergic modules, however, often varies between different neuromeres. 5-HT neurons, for instance, typically occur as two bilateral pairs per neuromere. Yet, t1 comprises three 5-HT neuron pairs and a8 only one pair. The presumptive dopaminergic TH neurons also lack a strict serial homology since three vmTH neurons are present in t1, but only one in t2-a7. Furthermore, dITH neurons locate to a1-7, but appear to be missing in t1-3. The neuromere a8 lacks TH neurons. The number of presumptive tyraminerpic/octopaminergic TDC2 neurons differs between various neuromeres as well. Whereas t1 comprises one or two dmTDC2 neurons, comparable neurons are absent in t2-a7. Putative descending pmTDC2 interneurons localize to t1-a1, but appear to be missing in the remaining abdominal neuromeres. Taken together, the number of aminergic modules in t1 and a8 often deviated from that of t2-a7. This difference may at least partially-reflect unique neuronal circuits in t1 and a8. While we are not aware of t1 specific physiological functions in larvae, a8 and the adjacent “terminal plexus” are associated with the tail region, and hence contain a specific set of sensory neurons and motoneurons. The terminal neuromeres also supply several unique structures such as the spiracles or the anal pads (see [79,80]).

Besides the segmental differences in neuron number, the density of aminergic innervation and the amount of immunolabeling/ marker gene expression varies between neuromeres as well. In particular, presumptive dopaminergic TH neurons show a striking neuromere-specific labeling pattern. Whereas a1-5 contain only few labeled TH projections, t1-3 and a6-7 comprise a comparably dense network of TH neurites. Similar to TH neurons, 5-HT neurons most densely innervate the neuropil of a7. Since a high extracellular concentration of 5-HT decreases the density of 5-HT-immunoreactive arborizations within the neuropil [81], a7 may represent a minor 5-HT release site. In contrast to a7, the neuropil of a8 and the adjacent “terminal plexus”(- which receive prominent peptidergic innervation [20] -) typically lack aminergic neurite arborizations. Consequently, larval aminergic neurons may play a subordinate role in tail-related physiological processes.

Ectopically expressed fluorescent fusion proteins as neuronal compartment markers in aminergic neurons

To reveal putative synaptic in- and output zones of aminergic neurons, we employed the neuronal compartment markers neuronal synaptobrevin-GFP, synaptotagmin 1-GFP, and *Drosophila* Down syndrome adhesion molecule [17.1]-GFP. Neuronal synaptobrevin is a vesicle associated membrane protein that plays a role in the SNARE complex during vesicle transport and fusion with the plasma membrane (see [82]). In accordance with this function, ectopically expressed neuronal synaptobrevin-GFP (SybGFP) accumulates at nerve terminals [50,51]. SybGFP therefore served to define the presynaptic compartments of several *Drosophila* neurons, e.g. in the visual system [83–85]. However, neuronal synaptobrevin is not restricted to small synaptic vesicles, but also locates to the membrane of large dense core vesicles, which contain BAs or neuropeptides (see [86–89]). Consequently, in a7, SybGFP localized to putative release sites of presumptive serotonergic DDC neurons [81]. SybGFP was also used to identify non-synaptic release sites in several peptidergic neurons [20,90].

In aminergic neurons, the distribution of *gal4*-driven SybGFP highly resembled the corresponding mCD8GFP expression pattern. SybGFP localized in dotted patterns to aminergic neuron somata and associated neurites. We therefore suggest that SybGFP does not exclusively label the presynaptic compartments of aminergic neurons. This fits to the assumption that ectopically expressed synaptic proteins can either localize to transport vesicles or non-synaptic compartments in peptidergic neurons [91]. On the other hand, the ubiquitous distribution of SybGFP in aminergic neurites may suggest a widespread BA release/recycling from non-synaptic active sites. In mammals, BA release/recycling is not restricted to synapses [92,93]. Vesicular monoamine transporters, which transport BAs into secretory vesicles, reside within neuron somata, axons, and dendrites [92]. In *Drosophila*, the vesicular monoamine transporter DVMAT-A localizes to somata as well as neurites of several aminergic neurons both in the larval [94] and adult CNS [38]. Thus, the widespread distribution of SybGFP and DVMAT-A in aminergic neurons suggests that a considerable amount of aminergic vesicles resides at non-synaptic sites. Non-synaptic BA release/recycling might therefore play a major role for aminergic neuronal network signaling.

Like neuronal synaptobrevin, synaptotagmins also represent integral membrane proteins of both small synaptic and large dense core vesicles (see [86–89]). In *Drosophila*, the products of seven synaptotagmin genes localize to distinct neuronal compartments including the postsynaptic site [95]. At the presynaptic site, synaptotagmin 1 does not participate in the SNARE complex, but acts as a Ca^{2+} -sensor for synaptic vesicle fusion (see [96]). Furthermore, synaptotagmin 1 appears to be the only crucial isoform for synaptic vesicle release [97–99]. Consequently, a synaptotagmin 1-GFP fusion construct (SytGFP) was developed as a synaptic vesicle marker that specifically labels presynaptic sites [52]. In aminergic neurons, the distribution pattern of SytGFP strikingly differed from the observed mCD8GFP and SybGFP labeling. Primary neurites of aminergic neurons always completely lacked SytGFP. Varicose neurite structures which were less evident in the mCD8GFP and SybGFP expression patterns showed strong SytGFP labeling. In agreement with the SytGFP distribution in other *Drosophila* neuron types [52,100,101], SytGFP hence appears to exclusively accumulate at the presynaptic sites of aminergic neurons. Thus, SytGFP represents a valuable marker to separate synapses from other neuronal compartments in aminergic neurons. However, since BA release is not restricted to synapses, SytGFP may not label all BA release sites of aminergic neurons. The sparse co-localization of SytGFP and SybGFP in aminergic neurites in fact suggests that aminergic vesicles-which are located distal to presynaptic sites-generally lack SytGFP. Consequently, non-synaptic BA release appears to be independent of synaptotagmin 1, but may depend on other synaptotagmin isoforms such as synaptotagmin α or β [95]. The differing distribution of SytGFP and SybGFP also suggests that aminergic neurons contain several types of aminergic vesicles which are either associated with presynaptic or non-synaptic BA release. Alternatively, aminergic neurons may synthesize additional non-aminergic neurotransmitters like acetylcholine, GABA, or glutamate. Presumed octopaminergic efferent neurons, for instance, appear to release glutamate from type II terminals at the neuromuscular junction [94]. In such neurons, SytGFP likely labels presynaptically located transmitter vesicles and may not reveal BA release sites.

In contrast to SybGFP and SytGFP, ectopically expressed *Drosophila* Down syndrome adhesion molecule [17.1]-GFP (DscamGFP) localized to postsynaptic compartments and not to axons or presynaptic sites [53]. Consequently, DscamGFP recently served as dendrite marker in mushroom body lobe neurons [101]

and peptidergic neurons [102]. Aminergic neurons showed only weak DscamGFP labeling. DscamGFP primarily localized to neurites that lacked SytGFP labeling. Since SytGFP accumulates at presynaptic sites, DscamGFP appears to represent a valuable marker to define dendritic compartments in aminergic neurons.

Neuronal compartments of 5-HT neurons

In 5-HT neurons, we did not analyze the distribution of ectopically expressed neuronal compartment markers since specific *gal4* drivers are not available. The *Ddc-gal4* driver induces marker gene expression not only in presumed serotonergic, but also in dopaminergic and additional peptidergic neurons (see below). Consequently, neurites of different DDC neuron subsets overlap in specific neuropil areas. Presumptive serotonergic as well as dopaminergic DDC neurites, for instance, localize to the VG neuropil above the CI tracts. These conditions prevent an accurate description and interpretation of the compartment marker distribution in presumptive serotonergic DDC neurons. Thus, appropriate *gal4* drivers (e.g. *Dtph-gal4*) are needed to further analyze 5-HT neuron morphology.

Possible overlap of 5-HT neurons with other neuronal projections

5-HT neurons bifurcate strongly in the whole neuropil of t1-a7, and hence may influence various VG neurons including sensory, inter- as well as motoneurons. However, we did not analyze putative neuronal network contacts of 5-HT neurons since previous morphological studies on *Drosophila* 5-HT receptors [12,13] did not describe the exact spatial location of the respective receptors in the larval VG.

Neuronal compartments of dopaminergic TH neurons

In TH neurons, the distribution of ectopically expressed mCD8GFP, SybGFP, SytGFP, and DscamGFP differed only slightly. This might relate to the fact that the VG contains two different TH neuron groups, the vmTH and dlTH neurons, whose neurites contact each other at longitudinal projections. Consequently, pre- and postsynaptic compartments of both TH neuron groups appeared to overlap, e.g. at longitudinal projections next to the VL tracts. Since additional TH neurons located in the brain or subesophageal ganglia also innervate the VG [1], we could not clarify which TH neuron group attributes to a particular neuronal projection. Several morphological findings, however, suggest that TH neurons possess distinct in- and output sites: Most strikingly, a1-5 contained less TH neurites labeled with mCD8GFP, SybGFP and DscamGFP, as compared to t1-3 and a6-7. In t1-a7, high amounts of SybGFP and SytGFP located to lateral longitudinal projections next to the VL tracts. These longitudinal TH neurites also contained a comparably high amount of DscamGFP, and hence likely represent synaptic in- as well as output compartments of different TH neuron groups. Besides lateral longitudinal TH projections, SybGFP and SytGFP also co-localized to the median neuropil between the DM/VM tracts. At least in a1-5, this neuropil area lacked DscamGFP, and hence probably represents a presynaptic output site of TH neurons. In a6-7, we observed a comparably strong SybGFP and SytGFP labeling in arborizations around transversal TH neurites. Whereas SybGFP mainly located to the dorsal branches of the transversal TH neurite loops, SytGFP and DscamGFP primarily labeled the ventral branches. Thus, the dorsal branches of the transversal TH neurite loops may represent non-synaptic DA release sites, while the ventral branches seem to comprise overlapping synaptic in- and output compartments of different TH neuron groups.

Possible overlap of TH neurons with other neuronal projections

Both vmTH and dlTH neurons innervate distinct neuropil areas within the VG. The vmTH neurons send their primary neurites dorsally and then project through the dorsal part of the neuropil above TP 3. Since the dorsal neuropil comprises the dendritic compartments of most motoneurons [19], vmTH neurites are ideally located to modulate locomotor activity. This fits to the finding that DA application onto intact larval CNS-segmental preparations rapidly decreased the rhythmicity of CNS motor activity and synaptic vesicle release at the neuromuscular junction [103]. Unlike vmTH neurons, dlTH neurons exclusively innervate the ventral part of the VG neuropil beneath TP 3. There, putative dendritic compartments of TH neurons mainly localize to lateral longitudinal and to transversal projections adjacent to the main output site of several afferent sensory neurons, e.g. tactile and proprioceptive neurons [19,21,104]. Thus, some TH neurons may receive synaptic input from specific sensory neurons. On the other hand, TH neurons also seem to have output sites in the ventral part of the neuropil, and hence may influence the signal transmission between sensory neurons and interneurons. This fits to the finding that peptidergic apterous neurons, which appear to transmit sensory input from the VG to the brain [105], express DA receptors [8,106]. Concomitantly, dendritic compartments of apterous neurons [91] seem to reside adjacent to the putative DA release sites of TH neurons at the CI tracts. Besides the overlap between transversal TH neurites and sensory/interneuron projections in the ventral neuropil, TH neurons may influence several neuron groups at other locations within the VG. For instance, the putative synaptic output sites of TH neurons in the median neuropil between the DM/VM tracts overlap with presumptive input compartments of both interneurons and efferent neurons expressing peptides such as CCAP, corazonin, FMRFa, or MIP [20]. Furthermore, the putative output sites at longitudinal TH projections next to the VL tracts lay adjacent to presumptive input compartments of e.g. efferent leucokininergic neurons [20].

Neuronal compartments of tyraminerpic/octopaminergic TDC2 neurons

In the VG, most TDC2 neurons are efferent vumTDC2 neurons and showed a differential distribution of ectopically expressed SybGFP, SytGFP, and DscamGFP. The primary neurites and transversal projections of vumTDC2 neurons were labeled with DscamGFP, but lacked SytGFP. Therefore, these neurites likely represent dendritic input sites. This fits to the finding that vumTDC2 neurons possess output sites at larval body wall muscles [73,74]. However, vumTDC2 neurites within the VG also contained high amounts of SybGFP, and hence may release TA/OA from non-synaptic sites. Besides vumTDC2 neurites, SybGFP strongly labeled longitudinal TDC2 neurites and associated arborizations in the dorso-lateral neuropil between TP 1 and 3. These TDC2 projections showed prominent SytGFP labeling and T β H immunoreactivity, but largely lacked DscamGFP. Thus, the dorsal part of the VG neuropil likely contains output compartments of TDC2 neurons. Since the larval brain seems to contain only tyramine- [73] and no octopamine-immunoreactive neurons [1,61], these output sites likely derive from descending interneurons located in the subesophageal ganglia, dmTDC2, or pmTDC2 neurons. Noteworthy, the strong SybGFP and SytGFP labeling in TDC2 neurites projecting through the dorso-lateral neuropil of the VG overlapped with DscamGFP in transverse vumTDC2 neurites. Thus, descending TDC2 neurons may interact with vumTDC2 neurons.

Possible overlap of TDC2 neurons with other neuronal projections

The VG comprises efferent vumTDC2 neurons as well as several putative TDC2 interneuron groups. Since all vumTDC2 neurons appear to have synapses at peripheral targets [73,74] and dendrites in the dorsal neuropil, they show the typical motoneuron morphology. This corresponds to the finding that OA inhibited synaptic transmission at the neuromuscular junction by affecting both pre- and postsynaptic mechanisms [107]. In addition, T β H mutant larvae, with altered levels of TA and OA, showed severe locomotion defects [66], which seemed to be linked to an imbalance between TA and OA signaling [65]. Hence, vumTDC2 neurons likely regulate peripheral processes such as body wall muscle activity, whereas TDC2 interneurons centrally modulate the neuronal activity of motoneurons and interneurons involved in locomotor control. Interestingly, presumptive presynaptic compartments of descending TDC2 interneurons reside adjacent to transversal vumTDC2 dendrites. Thus, both TDC2 neuron groups may interact to modulate larval locomotor activity. Besides their function for locomotion, descending TDC2 neurons may also influence other neurons which project into the dorsal neuropil between TP 1 and 3. The putative output sites of TDC2 interneurons, for instance, lay adjacent to several peptidergic projections showing allatostatin-A, FMRFa, MIP, or tachykinin immunoreactivity [20]. However, nothing is known about TA/OA receptor distribution in the larval VG.

Fas2-based fractionation and definition of the complex *Ddc-gal4* expression pattern reveals *Ddc* expression in peptidergic neurons

During our morphological analysis of DDC neurons in the L3 larval VG, we identified two DDC neuron groups that obviously synthesize neither 5-HT nor DA. This corresponds to the previous finding that *Ddc-gal4*-driven marker gene expression is not restricted to presumptive serotonergic 5-HT and dopaminergic TH neurons [19]. However, we can not exclude that the putative non-aminergic DDC neurons transiently synthesize BAs during other developmental stages. In our preparations, *Ddc-gal4*-driven mCD8GFP expression never revealed the dlTH neurons. This may relate to the fact that the onset of *Ddc* expression varies between different DDC neuron groups, and high DDC and TH levels do not temporally coincide [29]. Taken together, our results suggest that-at least in the L3 larval VG-the *Ddc-gal4* expression pattern 1) contains additional non-aminergic neurons, and 2) typically comprises most, but not all 5-HT and TH neurons. These particular characteristics of the *Ddc-gal4* driver line should be carefully considered for the interpretation of studies that employed *Ddc-gal4*-driven expression to genetically manipulate serotonergic or dopaminergic neurons. Nevertheless, since all *Ddc-gal4* expressing neurons within the VG showed at least faint DDC immunoreactivity, the *Ddc-gal4* driver appears to restrict ectopical gene expression to DDC neurons. Noteworthy, the DDC neurons which lacked 5-HT and TH immunoreactivity showed corazonin and CCAP/MIP immunoreactivity respectively. In the moth *Manduca sexta*, these peptides play vital roles during ecdysis (see [108]). At least the CCAP/MIP neurons are also necessary for the proper timing and execution of ecdysis behavior in *Drosophila* (see [18]). Since dopaminergic DDC neurons regulate the titers of the molting hormones 20-hydroxyecdysone and juvenile hormone [109], both aminergic and peptidergic DDC neurons may interact to control ecdysis-related events. Recent findings indeed suggest that CCAP/MIP neurons modulate TH activity after eclosion to control the precise onset of tanning [110].

Supporting Information

Figure S1 Comparison of *Th-gal4*-driven mCD8GFP expression and GFP immunoreactivity in the larval VG. A1) Dorsal view of *Th-gal4* x mCD8GFP expressing neurons (green) in a larval VG, and A2) the corresponding GFP immunostaining (magenta). A3) In the merged image, *Th-gal4*-driven mCD8GFP co-localizes with GFP immunoreactivity. B1-3) Corresponding transversal views of the neuromere t1 (* in A3), and C1-3) the neuromere a1 (° in A3). Note that *Th-gal4*-driven mCD8GFP expression usually stayed below the detection threshold in ventral TH neurons of a1-7. These TH neurons, however, could be visualized with the GFP antiserum. All images are maximum pixel intensity projections of volume-rendered 3D image stacks. Scale bars: 50 μ m in A), 25 μ m in B) and C). Found at: doi:10.1371/journal.pone.0001848.s001 (1.67 MB TIF)

Figure S2 Comparison of *Th-gal4*-driven mCD8GFP expression and TH immunoreactivity in the larval VG. A1) Dorsal view of *Th-gal4* x mCD8GFP expressing neurons (green), and A2) TH-immunoreactive neurons (magenta) in a larval VG. A3) In the merged image, *Th-gal4*-driven mCD8GFP largely co-localizes with TH immunoreactivity. A4) Idealized schematic representation of the respective neuron groups in the Fas2 landmark system. B1-3) Corresponding transversal views of the neuromere a2 (* in A3), and B4) the deduced idealized scheme. In the schemes, neurons showing both *Th-gal4*-driven mCD8GFP expression and TH immunoreactivity are green-colored. A few ventral neurons typically showed very faint or even lacked *Th-gal4*-driven mCD8GFP expression, but strongly stained with the TH antiserum (white arrow in B3). These neurons are blue-colored in the schemes. Original images are maximum pixel intensity projections of volume-rendered 3D image stacks. Scale bars: 50 μ m in A), 25 μ m in B). Found at: doi:10.1371/journal.pone.0001848.s002 (1.10 MB TIF)

Figure S3 Comparison of *Ddc-gal4*-driven mCD8GFP expression and DDC immunoreactivity in the larval VG. A1) Ventral view of *Ddc-gal4* x mCD8GFP expressing neurons (green), and A2) DDC-immunoreactive neurons (magenta) in a larval VG. The merged image (A3) served for an idealized schematic representation of the respective neuron groups in the Fas2 landmark system (A4). B1-3) Corresponding transversal views of the neuromere a4 (* in A3), and B4) the deduced idealized scheme. In the schemes, neurons showing both *Ddc-gal4*-driven mCD8GFP expression and DDC immunoreactivity are green-colored. *Ddc-gal4* x mCD8GFP expressing neurons which showed very faint DDC immunoreactivity are shown in gray (white arrows in B3). Vice versa, neurons which appeared to lack *Ddc-gal4* x mCD8GFP expression and showed prominent DDC immunoreactivity are blue-colored (gray arrowhead in B3). Original images are maximum pixel intensity projections of volume-rendered 3D image stacks. Scale bars: 50 μ m in A), 25 μ m in B). Found at: doi:10.1371/journal.pone.0001848.s003 (1.61 MB TIF)

Figure S4 Comparison of *Ddc-gal4*-driven mCD8GFP expression and TH or 5-HT immunoreactivity in the larval VG. A1) Dorsal view of *Ddc-gal4* x mCD8GFP expressing neurons (green), and A2) TH-immunoreactive neurons (magenta) in a larval VG. The merged image (A3) served for an idealized schematic representation of the respective neuron groups in the Fas2 landmark system (A4). B1-3) Corresponding transversal views of the neuromere a4 (* in A3), and B4) the deduced idealized scheme. C1) Dorsal view of *Ddc-gal4* x mCD8GFP expressing neurons (green), and C2) 5-HT-immunoreactive neurons (magenta) in a larval VG. The merged image (C3) provided the basis for the scheme shown in (C4). D1-3) Corresponding transversal views of the

neuromere a3 (* in C3), and D4) the deduced idealized scheme. Note that one of the three *Ddc-gal4* x mCD8GFP expressing neuron pairs which reside in the ventral cortex always lacked 5-HT immunoreactivity (white arrows in D3). In all schemes, neurons showing both *Ddc-gal4*-driven mCD8GFP expression and TH/5-HT immunoreactivity are green-colored. *Ddc-gal4* x mCD8GFP expressing neurons which lacked TH/5-HT immunoreactivity are shown in gray. Vice versa, neurons which exclusively showed TH/5-HT immunoreactivity are blue-colored. Original images are maximum pixel intensity projections of volume-rendered 3D image stacks. Scale bars: 50 μ m in A) and C), 25 μ m in B) and D). Found at: doi:10.1371/journal.pone.0001848.s004 (2.93 MB TIF)

Figure S5 Comparison of *Tdc2-gal4*-driven mCD8GFP expression and T β H immunoreactivity in the larval VG. A1) Ventral view of *Tdc2-gal4* x mCD8GFP expressing neurons (green), and A2) T β H-immunoreactive neurons (magenta) in a larval VG. A3) In the merged image, *Tdc2-gal4*-driven mCD8GFP largely co-localizes with T β H immunoreactivity. A4) Idealized schematic representation of the respective neuron groups in the Fas2 landmark system. B1-3) Corresponding transversal views of the neuromere a1 (* in A3), and B4) the deduced idealized scheme. Due to high T β H background staining, the dorsal half of the VG (dotted line in B3) was omitted in the 3D image stack to reveal co-labeling between *Tdc2-gal4* x mCD8GFP expressing and T β H-immunoreactive neurons. In the schemes, neurons showing both *Tdc2-gal4*-driven mCD8GFP expression and T β H immunoreactivity are green-colored. The paramedial neurons in t2-3 and a1 typically showed very faint or even lacked *Tdc2-gal4*-driven mCD8GFP expression, but strongly stained with the T β H antiserum (white arrows in B3). These neurons are blue-colored in the schemes. Original images are maximum pixel intensity projections of volume-rendered 3D image stacks. Scale bars: 50 μ m in A), 25 μ m in B). Found at: doi:10.1371/journal.pone.0001848.s005 (1.85 MB TIF)

Figure S6 Comparison of *Ccap-gal4*-driven mCD8GFP expression and TH immunoreactivity in the larval VG. A1) Dorsal view of *Ccap-gal4* x mCD8GFP expressing neurons (green), and A2) TH-immunoreactive neurons (magenta) in a larval VG. A3) In the merged image, *Ccap-gal4*-driven mCD8GFP expression and TH immunoreactivity localized to different neuron groups. A4) Idealized schematic representation of the respective neuron groups in the Fas2 landmark system. B1-3) Corresponding transversal views of the neuromere a1 (* in A3), and B4) the deduced idealized scheme. In the schemes, all *Ccap-gal4* x mCD8GFP expressing neurons lacked TH immunoreactivity and are shown in gray. Neurons which only showed TH immunoreactivity are blue-colored. Original images are maximum pixel intensity projections of volume-rendered 3D image stacks. Scale bars: 50 μ m in A), 25 μ m in B). Found at: doi:10.1371/journal.pone.0001848.s006 (1.04 MB TIF)

Acknowledgments

We are very grateful to the various donors of fly lines and antisera listed in the tables. We also thank Franz Grolig for maintenance of the confocal microscope, Renate Renkawitz-Pohl and Ruth Hyland for providing fly housing, and Uwe Homberg for critical reading of the manuscript and general support. We are particularly indebted to the authors of previous studies on the morphology of aminergic neurons in *Drosophila*, whose descriptions facilitated our task.

Author Contributions

Conceived and designed the experiments: CW MV. Performed the experiments: MV. Analyzed the data: MV. Contributed reagents/materials/analysis tools: CW. Wrote the paper: CW MV.

References

- Monastirioti M (1999) Biogenic amine systems in the fruit fly *Drosophila melanogaster*. *Microsc Res Tech* 45: 106–121.
- Nässel DR (1996) Neuropeptides, amines and amino acids in an elementary insect ganglion: functional and chemical anatomy of the unfused abdominal ganglion. *Prog Neurobiol* 48: 325–420.
- Pflüger HJ, Stevenson PA (2005) Evolutionary aspects of octopaminergic systems with emphasis on arthropods. *Arthropod Structure & Development* 34: 379–396.
- Roeder T (2005) Tyramine and octopamine: ruling behavior and metabolism. *Annu Rev Entomol* 50: 447–477.
- Brody T, Cravchik A (2000) *Drosophila melanogaster* G protein-coupled receptors. *J Cell Biol* 150: F83–F88.
- Hauser F, Cazzamali G, Williamson M, Blenau W, Grimmelikhuijzen CJ (2006) A review of neurohormone GPCRs present in the fruit fly *Drosophila melanogaster* and the honey bee *Apis mellifera*. *Prog Neurobiol* 80: 1–19.
- Han KA, Millar NS, Grotewiel MS, Davis RL (1996) DAMB, a novel dopamine receptor expressed specifically in *Drosophila* mushroom bodies. *Neuron* 16: 1127–1135.
- Kim YC, Lee HG, Seong CS, Han KA (2003) Expression of a D1 dopamine receptor dDA1/DmDOP1 in the central nervous system of *Drosophila melanogaster*. *Gene Expr Patterns* 3: 237–245.
- Srivastava DP, Yu EJ, Kennedy K, Chatwin H, Reale V, Hamon M, Smith T, Evans PD (2005) Rapid, nongenomic responses to ecdysteroids and catecholamines mediated by a novel *Drosophila* G-protein-coupled receptor. *J Neurosci* 25: 6145–6155.
- Sugamori KS, Demchynshyn LL, McConkey F, Forte MA, Niznik HB (1995) A primordial dopamine D1-like adenylyl cyclase-linked receptor from *Drosophila melanogaster* displaying poor affinity for benzazepines. *FEBS Lett* 362: 131–138.
- Mustard JA, Beggs KT, Mercer AR (2005) Molecular biology of the invertebrate dopamine receptors. *Arch Insect Biochem Physiol* 59: 103–117.
- Nichols CD (2007) 5-HT₂ receptors in *Drosophila* are expressed in the brain and modulate aspects of circadian behaviors. *Dev Neurobiol* 67: 752–763.
- Yuan Q, Lin F, Zheng X, Sehgal A (2005) Serotonin modulates circadian entrainment in *Drosophila*. *Neuron* 47: 115–127.
- Yuan Q, Joiner WJ, Sehgal A (2006) A sleep-promoting role for the *Drosophila* serotonin receptor 1A. *Curr Biol* 16: 1051–1062.
- Han KA, Millar NS, Davis RL (1998) A novel octopamine receptor with preferential expression in *Drosophila* mushroom bodies. *J Neurosci* 18: 3650–3658.
- Evans PD, Maqueira B (2005) Insect octopamine receptors: a new classification scheme based on studies of cloned *Drosophila* G-protein coupled receptors. *Invert Neurosci* 5: 111–118.
- Landgraf M, Thor S (2006) Development of *Drosophila* motoneurons: specification and morphology. *Semin Cell Dev Biol* 17: 3–11.
- Ewer J (2005) Behavioral actions of neuropeptides in invertebrates: insights from *Drosophila*. *Horm Behav* 48: 418–429.
- Landgraf M, Sánchez-Soriano N, Technau GM, Urban J, Prokop A (2003) Charting the *Drosophila* neuropile: a strategy for the standardised characterisation of genetically amenable neurites. *Dev Biol* 260: 207–225.
- Santos JG, Vömel M, Struck R, Homberg U, Nässel DR, et al. (2007) Neuroarchitecture of peptidergic systems in the larval ventral ganglion of *Drosophila melanogaster*. *PLoS ONE* 2: e695.
- Grueber WB, Ye B, Yang CH, Younger S, Borden K, et al. (2007) Projections of *Drosophila* multidendritic neurons in the central nervous system: links with peripheral dendrite morphology. *Development* 134: 55–64.
- Zlatic M, Landgraf M, Bate M (2003) Genetic specification of axonal arbors: atonal regulates robo3 to position terminal branches in the *Drosophila* nervous system. *Neuron* 37: 41–51.
- Brand AH, Perrimon N (1993) Targeted gene expression as a means of altering cell fates and generating dominant phenotypes. *Development* 118: 401–415.
- Nässel DR (1996) Advances in the immunocytochemical localization of neuroactive substances in the insect nervous system. *J Neurosci Methods* 69: 3–23.
- Coleman CM, Neckameyer WS (2004) Substrate regulation of serotonin and dopamine synthesis in *Drosophila*. *Invert Neurosci* 5: 85–96.
- Coleman CM, Neckameyer WS (2005) Serotonin synthesis by two distinct enzymes in *Drosophila melanogaster*. *Arch Insect Biochem Physiol* 59: 12–31.
- Neckameyer WS, Coleman CM, Eadie S, Goodwin SF (2007) Compartmentalization of neuronal and peripheral serotonin synthesis in *Drosophila melanogaster*. *Genes Brain Behav* 6: 756–769.
- Dasari S, Cooper RL (2006) Direct influence of serotonin on the larval heart of *Drosophila melanogaster*. *J Comp Physiol [B]* 176: 349–357.
- Lundell MJ, Hirsh J (1994) Temporal and spatial development of serotonin and dopamine neurons in the *Drosophila* CNS. *Dev Biol* 165: 385–396.
- Vallés AM, White K (1986) Development of serotonin-containing neurons in *Drosophila* mutants unable to synthesize serotonin. *J Neurosci* 6: 1482–1491.
- Vallés AM, White K (1988) Serotonin-containing neurons in *Drosophila melanogaster*: development and distribution. *J Comp Neurol* 268: 414–428.
- Andretic R, van Swinderen B, Greenspan RJ (2005) Dopaminergic modulation of arousal in *Drosophila*. *Curr Biol* 15: 1165–1175.
- Ganguly-Fitzgerald I, Donlea J, Shaw PJ (2006) Waking experience affects sleep need in *Drosophila*. *Science* 313: 1775–1781.
- Kume K, Kume S, Park SK, Hirsh J, Jackson FR (2005) Dopamine is a regulator of arousal in the fruit fly. *J Neurosci* 25: 7377–7384.
- Ye Y, Xi W, Peng Y, Wang Y, Guo A (2004) Long-term but not short-term blockade of dopamine release in *Drosophila* impairs orientation during flight in a visual attention paradigm. *Eur J Neurosci* 20: 1001–1007.
- Neckameyer WS, Weinstein JS (2005) Stress affects dopaminergic signaling pathways in *Drosophila melanogaster*. *Stress* 8: 117–131.
- Schwarzel M, Monastirioti M, Scholz H, Friggi-Grelin F, Birman S, et al. (2003) Dopamine and octopamine differentiate between aversive and appetitive olfactory memories in *Drosophila*. *J Neurosci* 23: 10495–10502.
- Chang HY, Grygoruk A, Brooks ES, Ackerson LC, Maidment NT, et al. (2006) Overexpression of the *Drosophila* vesicular monoamine transporter increases motor activity and courtship but decreases the behavioral response to cocaine. *Mol Psychiatry* 11: 99–113.
- Budnik V, White K (1988) Catecholamine-containing neurons in *Drosophila melanogaster*: distribution and development. *J Comp Neurol* 268: 400–413.
- Nässel DR, Elekes K (1992) Aminergic neurons in the brain of blowflies and *Drosophila*: dopamine- and tyrosine hydroxylase-immunoreactive neurons and their relationship with putative histaminergic neurons. *Cell Tissue Res* 267: 147–167.
- Birman S, Morgan B, Anzivino M, Hirsh J (1994) A novel and major isoform of tyrosine hydroxylase in *Drosophila* is generated by alternative RNA processing. *J Biol Chem* 269: 26559–26567.
- Vié A, Cigna M, Toci R, Birman S (1999) Differential regulation of *Drosophila* tyrosine hydroxylase isoforms by dopamine binding and cAMP-dependent phosphorylation. *J Biol Chem* 274: 16788–16795.
- Budnik V, White K (1987) Genetic dissection of dopamine and serotonin synthesis in the nervous system of *Drosophila melanogaster*. *J Neurogenet* 4: 309–314.
- Neckameyer WS, White K (1993) *Drosophila* tyrosine hydroxylase is encoded by the *pale* locus. *J Neurogenet* 8: 189–199.
- Friggi-Grelin F, Iché M, Birman S (2003) Tissue-specific developmental requirements of *Drosophila* tyrosine hydroxylase isoforms. *Genesis* 35: 260–269.
- Pendleton RG, Rasheed A, Sardina T, Tully T, Hillman R (2002) Effects of tyrosine hydroxylase mutants on locomotor activity in *Drosophila*: a study in functional genomics. *Behav Genet* 32: 89–94.
- Pendleton RG, Rasheed A, Paluru P, Joyner J, Jerome N, et al. (2005) A developmental role for catecholamines in *Drosophila* behavior. *Pharmacol Biochem Behav* 81: 849–853.
- Konrad KD, Marsh JL (1987) Developmental expression and spatial distribution of dopa decarboxylase in *Drosophila*. *Dev Biol* 122: 172–185.
- Friggi-Grelin F, Coulom H, Meller M, Gomez D, Hirsh J, et al. (2003) Targeted gene expression in *Drosophila* dopaminergic cells using regulatory sequences from tyrosine hydroxylase. *J Neurobiol* 54: 618–627.
- Estes PS, Ho GL, Narayanan R, Ramaswami M (2000) Synaptic localization and restricted diffusion of a *Drosophila* neuronal synaptobrevin–green fluorescent protein chimera *in vivo*. *J Neurogenet* 13: 233–255.
- Ito K, Suzuki K, Estes P, Ramaswami M, Yamamoto D, et al. (1998) The organization of extrinsic neurons and their implications in the functional roles of the mushroom bodies in *Drosophila melanogaster* Meigen. *Learn Mem* 5: 52–77.
- Zhang YQ, Rodesch CK, Brodie K (2002) Living synaptic vesicle marker: synaptotagmin-GFP. *Genesis* 34: 142–145.
- Wang J, Ma X, Yang JS, Zheng X, Zugates CT, et al. (2004) Transmembrane/juxtamembrane domain-dependent Dscam distribution and function during mushroom body neuronal morphogenesis. *Neuron* 43: 663–672.
- Hodgetts RB, O'Keefe SL (2006) Dopa decarboxylase: a model gene-enzyme system for studying development, behavior, and systematics. *Annu Rev Entomol* 51: 259–284.
- Clark WC, Pass PS, Venkataraman B, Hodgetts RB (1978) Dopa decarboxylase from *Drosophila melanogaster*—purification, characterization, and an analysis of mutants. *Molec Gen Metab* 162: 287–297.
- Li H, Chaney S, Roberts IJ, Forte M, Hirsh J (2000) Ectopic G-protein expression in dopamine and serotonin neurons blocks cocaine sensitization in *Drosophila melanogaster*. *Curr Biol* 10: 211–214.
- Blenau W, Baumann A (2001) Molecular and pharmacological properties of insect biogenic amine receptors: lessons from *Drosophila melanogaster* and *Apis mellifera*. *Arch Insect Biochem Physiol* 48: 13–38.
- Farooqui T (2007) Octopamine-mediated neuromodulation of insect senses. *Neurochem Res* 32: 1511–1529.
- Roeder T, Seifert M, Kähler C, Gewecke M (2003) Tyramine and octopamine: antagonistic modulators of behavior and metabolism. *Arch Insect Biochem Physiol* 54: 1–13.
- Cole SH, Carney GE, McClung CA, Willard SS, Taylor BJ, et al. (2005) Two functional but noncomplementing *Drosophila* tyrosine decarboxylase genes: distinct roles for neural tyramine and octopamine in female fertility. *J Biol Chem* 280: 14948–14955.
- Monastirioti M, Linn CE Jr, White K (1996) Characterization of *Drosophila* tyramine beta-hydroxylase gene and isolation of mutant flies lacking octopamine. *J Neurosci* 16: 3900–3911.

62. Lee HG, Seong CS, Kim YC, Davis RL, Han KA (2003) Octopamine receptor OAMB is required for ovulation in *Drosophila melanogaster*. *Dev Biol* 264: 179–190.
63. Middleton CA, Nongthomba U, Parry K, Sweeney ST, Sparrow JC, et al. (2006) Neuromuscular organization and aminergic modulation of contractions in the *Drosophila* ovary. *BMC Biol* 4: 17.
64. Monastirioti M (2003) Distinct octopamine cell population residing in the CNS abdominal ganglion controls ovulation in *Drosophila melanogaster*. *Dev Biol* 264: 38–49.
65. Fox LE, Soll DR, Wu CF (2006) Coordination and modulation of locomotion pattern generators in *Drosophila* larvae: effects of altered biogenic amine levels by the tyramine beta hydroxylase mutation. *J Neurosci* 26: 1486–1498.
66. Saraswati S, Fox LE, Soll DR, Wu CF (2004) Tyramine and octopamine have opposite effects on the locomotion of *Drosophila* larvae. *J Neurobiol* 58: 425–441.
67. Brembs B, Christiansen F, Pflüger HJ, Duch C (2007) Flight initiation and maintenance deficits in flies with genetically altered biogenic amine levels. *J Neurosci* 27: 11122–11131.
68. Hardie SL, Zhang JX, Hirsh J (2007) Trace amines differentially regulate adult locomotor activity, cocaine sensitivity, and female fertility in *Drosophila melanogaster*. *Dev Neurobiol* 67: 1396–1405.
69. Blumenthal EM (2003) Regulation of chloride permeability by endogenously produced tyramine in the *Drosophila* Malpighian tubule. *Am J Physiol Cell Physiol* 284: C718–C728.
70. Blumenthal EM (2005) Modulation of tyramine signaling by osmolality in an insect secretory epithelium. *Am J Physiol Cell Physiol* 289: C1261–C1267.
71. O'Donnell MJ, Leader JP (2006) Changes in fluid secretion rate alter net transepithelial transport of MRP2 and P-glycoprotein substrates in Malpighian tubules of *Drosophila melanogaster*. *Arch Insect Biochem Physiol* 63: 123–134.
72. Kutsukake M, Komatsu A, Yamamoto D, Ishiwa-Chigusa S (2000) A tyramine receptor gene mutation causes a defective olfactory behavior in *Drosophila melanogaster*. *Gene* 245: 31–42.
73. Nagaya Y, Kutsukake M, Chigusa SI, Komatsu A (2002) A trace amine, tyramine, functions as a neuromodulator in *Drosophila melanogaster*. *Neurosci Lett* 329: 324–328.
74. Monastirioti M, Gorczyca M, Rapus J, Eckert M, White K, et al. (1995) Octopamine immunoreactivity in the fruit fly *Drosophila melanogaster*. *J Comp Neurol* 356: 275–287.
75. Stevenson PA, Pflüger HJ, Eckert M, Rapus J (1992) Octopamine immunoreactive cell populations in the locust thoracic-abdominal nervous system. *J Comp Neurol* 315: 382–397.
76. Spörhase-Eichmann U, Vullings HG, Buijs RM, Hörner M, Schürmann FW (1992) Octopamine-immunoreactive neurons in the central nervous system of the cricket, *Gryllus bimaculatus*. *Cell Tissue Res* 268: 287–304.
77. Bräunig P (1988) Identification of a single prothoracic 'dorsal unpaired median' (DUM) neuron supplying locust mouthpart nerves. *J Comp Physiol [A]* 163: 835–840.
78. Stevenson PA, Spörhase-Eichmann U (1995) Localization of octopaminergic neurons in insects. *Comp Biochem Physiol A Physiol* 110: 203–215.
79. Bate M (1993) The mesoderm and its derivatives. In: Bate M, Martinez-Arias A, eds. *The development of Drosophila melanogaster*. Cold Spring Harbor: Cold Spring Harbor Laboratory Press. pp 1013–1090.
80. Campos-Ortega JA, Hartenstein V (1997) *The embryonic development of Drosophila melanogaster*. Berlin: Springer.
81. Sykes PA, Condrón BG (2005) Development and sensitivity to serotonin of *Drosophila* serotonergic varicosities in the central nervous system. *Dev Biol* 286: 207–216.
82. Wojcik SM, Brose N (2007) Regulation of membrane fusion in synaptic excitation-secretion coupling: speed and accuracy matter. *Neuron* 55: 11–24.
83. Hiesinger PR, Scholz M, Meinertzhagen IA, Fischbach KF, Obermayer K (2001) Visualization of synaptic markers in the optic neuropils of *Drosophila* using a new constrained deconvolution method. *J Comp Neurol* 429: 277–288.
84. Otsuna H, Ito K (2006) Systematic analysis of the visual projection neurons of *Drosophila melanogaster*. I. Lobula-specific pathways. *J Comp Neurol* 497: 928–958.
85. Raghu SV, Joesch M, Borst A, Reiff DF (2007) Synaptic organization of lobula plate tangential cells in *Drosophila*: gamma-aminobutyric acid receptors and chemical release sites. *J Comp Neurol* 502: 598–610.
86. Langley K, Grant NJ (1997) Are exocytosis mechanisms neurotransmitter specific? *Neurochem Int* 31: 739–757.
87. Meldolesi J, Chieriegatti E, Luisa MM (2004) Requirements for the identification of dense-core granules. *Trends Cell Biol* 14: 13–19.
88. Meng J, Wang J, Lawrence G, Dolly JO (2007) Synaptobrevin I mediates exocytosis of CGRP from sensory neurons and inhibition by botulinum toxins reflects their anti-nociceptive potential. *J Cell Sci* 120: 2864–2874.
89. Tsuboi T, McMahon HT, Rutter GA (2004) Mechanisms of dense core vesicle recapture following "kiss and run" ("cavicapture") exocytosis in insulin-secreting cells. *J Biol Chem* 279: 47115–47124.
90. Hamasaka Y, Wegener C, Nässel DR (2005) GABA modulates *Drosophila* circadian clock neurons via GABA(B) receptors and decreases in calcium. *J Neurobiol* 65: 225–240.
91. Löhner R, Godenschwege T, Buchner E, Prokop A (2002) Compartmentalization of central neurons in *Drosophila*: a new strategy of mosaic analysis reveals localization of presynaptic sites to specific segments of neurites. *J Neurosci* 22: 10357–10367.
92. Hoffman BJ, Hansson SR, Mezey E, Palkovits M (1998) Localization and dynamic regulation of biogenic amine transporters in the mammalian central nervous system. *Front Neuroendocrinol* 19: 187–231.
93. Nirenberg MJ, Liu Y, Peter D, Edwards RH, Pickel VM (1995) The vesicular monoamine transporter 2 is present in small synaptic vesicles and preferentially localizes to large dense core vesicles in rat solitary tract nuclei. *Proc Natl Acad Sci U S A* 92: 8773–8777.
94. Greer CL, Grygoruk A, Patton DE, Ley B, Romero-Calderon R, et al. (2005) A splice variant of the *Drosophila* vesicular monoamine transporter contains a conserved trafficking domain and functions in the storage of dopamine, serotonin, and octopamine. *J Neurobiol* 64: 239–258.
95. Carr CM, Munson M (2007) Tag team action at the synapse. *EMBO Rep* 8: 834–838.
96. Adolfsen B, Saraswati S, Yoshihara M, Littleton JT (2004) Synaptotagmins are trafficked to distinct subcellular domains including the postsynaptic compartment. *J Cell Biol* 166: 249–260.
97. Geppert M, Goda Y, Hammer RE, Li C, Rosahl TW, et al. (1994) Synaptotagmin I: a major Ca²⁺ sensor for transmitter release at a central synapse. *Cell* 79: 717–727.
98. Yoshihara M, Littleton JT (2002) Synaptotagmin I functions as a calcium sensor to synchronize neurotransmitter release. *Neuron* 36: 897–908.
99. Yoshihara M, Adolfsen B, Littleton JT (2003) Is synaptotagmin the calcium sensor? *Curr Opin Neurobiol* 13: 315–323.
100. Iyengar BG, Chou CJ, Sharma A, Atwood HL (2006) Modular neuropile organization in the *Drosophila* larval brain facilitates identification and mapping of central neurons. *J Comp Neurol* 499: 583–602.
101. Zhang K, Guo JZ, Peng Y, Xi W, Guo A (2007) Dopamine-mushroom body circuit regulates saliency-based decision-making in *Drosophila*. *Science* 316: 1901–1904.
102. Bader R, Wegener C, Pankratz MJ (2007) Comparative neuroanatomy and genomics of hugin and pheromone biosynthesis activating neuropeptide (PBAN). *Fly* 1: 228–231.
103. Cooper RL, Neckameyer WS (1999) Dopaminergic modulation of motor neuron activity and neuromuscular function in *Drosophila melanogaster*. *Comp Biochem Physiol B Biochem Mol Biol* 122: 199–210.
104. Schrader S, Merritt DJ (2000) Central projections of *Drosophila* sensory neurons in the transition from embryo to larva. *J Comp Neurol* 425: 34–44.
105. Soller M, Haussmann IU, Hollmann M, Choffat Y, White K, et al. (2006) Sex-peptide-regulated female sexual behavior requires a subset of ascending ventral nerve cord neurons. *Curr Biol* 16: 1771–1782.
106. Draper I, Kurshan PT, McBride E, Jackson FR, Kopin AS (2007) Locomotor activity is regulated by D2-like receptors in *Drosophila*: an anatomic and functional analysis. *Dev Neurobiol* 67: 378–393.
107. Nishikawa K, Kidokoro Y (1999) Octopamine inhibits synaptic transmission at the larval neuromuscular junction in *Drosophila melanogaster*. *Brain Res* 837: 67–74.
108. Žitňan D, Kim YJ, Žitňanová I, Roller L, Adams ME (2007) Complex steroid-peptide-receptor cascade controls insect ecdysis. *Gen Comp Endocrinol* 153: 88–96.
109. Rauschenbach IY, Chentsova NA, Alekseev AA, Gruntenko NE, Adonyeva NV, et al. (2007) Dopamine and octopamine regulate 20-hydroxyecdysone level *in vivo* in *Drosophila*. *Arch Insect Biochem Physiol* 65: 95–102.
110. Davis MM, O'Keefe SL, Primrose DA, Hodgetts RB (2007) A neuropeptide hormone cascade controls the precise onset of post-eclosion cuticular tanning in *Drosophila melanogaster*. *Development* 134: 4395–4404.
111. Park JH, Schroeder AJ, Helfrich-Förster C, Jackson FR, Ewer J (2003) Targeted ablation of CCAP neuropeptide-containing neurons of *Drosophila* causes specific defects in execution and circadian timing of ecdysis behavior. *Development* 130: 2645–2656.
112. Lee T, Luo L (1999) Mosaic analysis with a repressible cell marker for studies of gene function in neuronal morphogenesis. *Neuron* 22: 451–461.
113. Dircksen H, Keller R (1988) Immunocytochemical localization of CCAP, a novel crustacean cardioactive peptide, in the nervous system of the shore crab, *Carcinus maenas*. *Cell Tissue Res* 254: 347–360.
114. Ewer J, Truman JW (1996) Increases in cyclic 3', 5'-guanosine monophosphate (cGMP) occur at ecdysis in an evolutionarily conserved crustacean cardioactive peptide-immunoreactive insect neuronal network. *J Comp Neurol* 370: 330–341.
115. Predel R, Rapus J, Eckert M (2001) Myoinhibitory neuropeptides in the American cockroach. *Peptides* 22: 199–208.

III. Neurotransmitter-induced changes in the intracellular calcium concentration suggest a differential central modulation of CCAP neuron subsets in *Drosophila*

Vömel M and Wegener C. (2007). Dev Neurobiol 67: 792–809.

Abstract.....	69
Introduction.....	69
Methods	70
Fly strains	70
Cell culture.....	70
Calcium imaging	72
Calcium imaging system and data processing.....	72
Immunocytochemistry.....	72
Confocal laser scanning microscopy	73
Results	73
Morphology of CCAP neurons.....	73
Dissociated CCAP neurons respond to depolarization and cholinergic agonists	74
Dissociated CCAP neurons respond to glutamate and quisqualate	74
Dissociated CCAP neurons respond to GABA	74
<i>In vitro</i> characterization of CCAP neurons expressing genetically encoded Ca ²⁺ -indicators.....	75
CCAP neurons expressing GCaMP 1.6 respond to cholinergic and GABAergic input <i>in vitro</i>	76
CCAP respond to cholinergic input <i>in situ</i>	77
A defined subset of CCAP neurons projects to larval body wall muscles.....	81
Discussion.....	81
Acetylcholine as an input factor of CCAP neurons.....	81
Evidence for a differential activation of CCAP neuron subsets via GABA and glutamate.....	81
CCAP neurons show different Ca ²⁺ -responses to cholinergic agonists between <i>in vitro</i> and <i>in situ</i>	82
Cholinergic agonist-mediated Ca ²⁺ -responses of CCAP neurons change during postembryonic development	82
A distinct CCAP neuron subset forms putative neurohemal zones on larval body wall muscles.....	83
A combination of both <i>in vitro</i> and <i>in situ</i> live cell imaging facilitates studies on the physiology of neuronal networks.....	83
Conclusions.....	83
References.....	84

Neurotransmitter-Induced Changes in the Intracellular Calcium Concentration Suggest a Differential Central Modulation of CCAP Neuron Subsets in *Drosophila*

Matthias Vömel, Christian Wegener

Emmy Noether Neuropeptide Group, Animal Physiology, Department of Biology, Philipps-University Marburg, Karl-von-Frisch-Straße, Marburg D-35032, Germany

Received 1 September 2006; revised 21 December 2006; accepted 5 January 2007

ABSTRACT: The complete sequencing of the *Drosophila melanogaster* genome allowed major progress in the research on invertebrate neuropeptide signaling. However, it is still largely unknown how the insect CNS exerts synaptic control over the secretory activity of peptidergic neurons; afferent pathways and employed chemical transmitters remain largely unidentified. In the present study, we set out to identify neurotransmitters mediating synaptic input onto CCAP-expressing neurons (N_{CCAP}), which play an important role in the regulation of ecdysis-related events. By *in vitro* and *in situ* calcium imaging with synthetic and genetically encoded calcium indicators, we provide evidence that differential neurotransmitter inputs control the activity of N_{CCAP} subsets. In short-term culture, almost all N_{CCAP} showed increases of the free intracellular calcium concentration after application of acetylcholine (ACh) and nicotine, whereas only some N_{CCAP} responded to

glutamate and GABA. In the intact ventral ganglia of both larvae and adults, only few N_{CCAP} showed intracellular calcium-rises or calcium-oscillations after application of cholinergic agonists indicating a prevailing central inhibition of most N_{CCAP} during these developmental stages. In larvae, responding N_{CCAP} were primarily located in the third thoracic neuromere. At least one N_{CCAP} pair in this neuromere belonged to a morphologically distinct subset with neurohemal endings on the body wall muscles. Our results suggest that N_{CCAP} express functional receptors for ACh, glutamate, and GABA, and indicate that these transmitters are involved in a context-dependent regulation of functionally distinct N_{CCAP} subsets. © 2007 Wiley Periodicals, Inc. *Develop Neurobiol* 67: 792–809, 2007

Keywords: crustacean cardioactive peptide; insect ecdysis; neuronal network signaling; calcium imaging; peptide release

INTRODUCTION

Insect development is interrupted by periodic molting of the exoskeleton to accommodate growth and changes in morphology. While molting is regulated

by the titers of the steroid hormone 20-hydroxyecdysone and juvenile hormone, the timing and execution of ecdysis behavior (the shedding of the old cuticle) is controlled by the action of peptide hormones. In *Drosophila melanogaster*, at least three interacting peptide hormones regulate ecdysis behavior (see Žitňan and Adams, 2004; Ewer, 2005): Ecdysis triggering hormone (ETH), eclosion hormone (EH), and crustacean cardioactive peptide (CCAP). ETH and EH form a positive endocrine feedback system and restrict the occurrence of ecdysis to the end of the molt. Whereas ETH appears to be the key regulator of larval ecdysis behavior (Park et al., 2002), EH con-

Correspondence to: C. Wegener (wegener@staff.uni-marburg.de).

Contract grant sponsor: Deutsche Forschungsgemeinschaft (DFG); contract grant number: WE 2652/2-1,2.

© 2007 Wiley Periodicals, Inc.

Published online 21 February 2007 in Wiley InterScience (www.interscience.wiley.com).

DOI 10.1002/dneu.20392

trols at least two different neuron populations. Centrally released EH is believed to activate CCAP-expressing neurons (N_{CCAP}), and the ensuing release of CCAP then initiates the ecdysis motor program (see Žitňan and Adams, 2004; Ewer, 2005). Nevertheless, transgenic flies lacking EH producing cells survive until adulthood, and show normal larval ecdysis behavior (Clark et al., 2004) and only slight defects during adult ecdysis (McNabb et al., 1997). Targeted ablation of N_{CCAP} by the cell death gene reaper demonstrated that these neurons are essential for the normal execution and circadian timing of ecdysis behavior (Park et al., 2003). However, developmental defects were restricted to pupal ecdysis (“head eversion”), whereas larval ecdysis and adult eclosion were less affected. In contrast, flies that lack both EH-expressing neurons and N_{CCAP} showed severe defects at larval ecdysis (Clark et al., 2004). Thus, N_{CCAP} appear to be key regulators only for pupal ecdysis behavior, whereas they rather play a subordinate role during larval and adult ecdysis behavior. Recent studies indicated that this varying importance of N_{CCAP} for ecdysis behavior might be due to a differential participation of distinct N_{CCAP} subsets at a particular ecdysis. In *Drosophila* pharate pupae, application of ETH to the intact ventral ganglion induced characteristic increases of the free intracellular calcium concentration ($[Ca^{2+}]_i$) only in a defined N_{CCAP} subset. Other N_{CCAP} lacked such $[Ca^{2+}]_i$ -responses, although they apparently express the ETH receptor A (Kim et al., 2006). During adult eclosion, one subset of N_{CCAP} seems to release the tanning hormone bursicon into the hemolymph, whereas another N_{CCAP} subset regulates this release (Luan et al., 2006). The finding that some N_{CCAP} co-express myoinhibiting peptides (MIPs), or both MIPs and bursicon, further suggests that the population of N_{CCAP} can be divided into functionally different subsets (Kim et al., 2006). Since peptide hormones seem to act rather stereotypically during each postembryonic ecdysis, the question arises how a differential and stage-dependent activation of specific N_{CCAP} subsets could be achieved. In *Drosophila* and the moth *Manduca sexta*, central excitatory and inhibitory influences play an important role in the determination of ecdysis onset (Ewer and Truman, 1997; Baker et al., 1999; Žitňan and Adams, 2000; Fuse and Truman, 2002). For example, N_{CCAP} in the ventral nerve cord of *Manduca* appear to receive inhibitory input from interneurons located in the subesophageal ganglion and the thoracic ganglia (Žitňan and Adams, 2000). Thus, the activity of N_{CCAP} might be centrally regulated by synaptic input besides the known endocrine control by peptides. It is, however,

unclear which neurotransmitters mediate this central regulation. The widespread expression of neurotransmitters in the CNS of *Drosophila*, the multitude of neurotransmitter receptor subunits, and the uncertainty about the subunit composition of insect neurotransmitter receptors (Yasuyama and Salvaterra, 1999; Sprengel et al., 2001; Buckingham et al., 2005; Sattelle et al., 2005) all greatly complicate genetic approaches. Here, we use live cell Ca^{2+} -imaging to identify putative excitatory and inhibitory input transmitters that might participate in the control of peptide release from the N_{CCAP} .

METHODS

Fly Strains

Fura-2 based imaging experiments were performed with flies of a $w^+;CCAP-gal4$ line specific for N_{CCAP} (Park et al., 2003; kind gift of J. Ewer, Cornell, NY) crossed with either a $w^+;P(w^+mC = UAS-GFP.S65T)T10$ strain (Bloomington Stock Center, donated by C. Goodman) or with $UAS-mCD8-GFP$ flies (Lee and Luo, 1999; Bloomington Stock Center, donated by T. Lee and L. Luo). To determine suitable genetically encoded Ca^{2+} -indicators (GECIs) for *in situ* imaging, flies of the $CCAP-gal4$ line were crossed with $w^{1118};P(w^+mC = UAS-Cameleon\ 2.1)82$ (Diegelmann et al., 2002; Bloomington Stock Center, donated by S. Diegelmann) or $UAS-GCaMP\ 1.6$ flies (Reiff et al., 2005; kind gift of D. Reiff, Martinsried, Germany). Crosses of the $CCAP-gal4$ line with flies of the $UAS-mCD8-GFP$ strain were used for immunocytochemistry. All flies were raised at 18 or 25°C on standard cornmeal agar medium and yeast under a 12:12 h light:dark regime.

Cell Culture

Cell dissociation and culture were modified from Wegener et al. (2004). For each experiment, 7–10 third instar larvae were sterilized in 70% ethanol for ~ 30 s and washed with ddH₂O. Whole larval CNS were dissected out in sterile dissecting saline (Su and O’Dowd, 2003) containing the following (in mM): 126 NaCl, 5.4 KCl, 0.17 NaH₂PO₄, 0.22 KH₂PO₄, 33.3 glucose, 43.8 sucrose, and 9.9 HEPES, pH 7.4. For enzymatic dissociation, 1 mg papain (Sigma-Aldrich, Taufkirchen, Germany) was dissolved in 1 mL sterile dissecting saline containing 1.32 mM L-cysteine and centrifuged at 400 rcf for 3 min. Then, the enzyme solution was transferred to the tube with the CNS and incubated for 10–15 min at 25°C. Thereafter, the tube was centrifuged for 3 min, enzyme solution was pipetted off, and sterile Leibovitz L-15 medium (PAA, Cölbe, Germany) containing 10% heat-treated fetal calf serum and 12 mg/mL mannitol (L-15) was added. After washing three times with L-15, CNS were transferred to a poly-L-lysine-coated cover glass. The cover glass was put into a small plastic cell culture dish and small drops of L-15 were placed at the rim of the dish to prevent

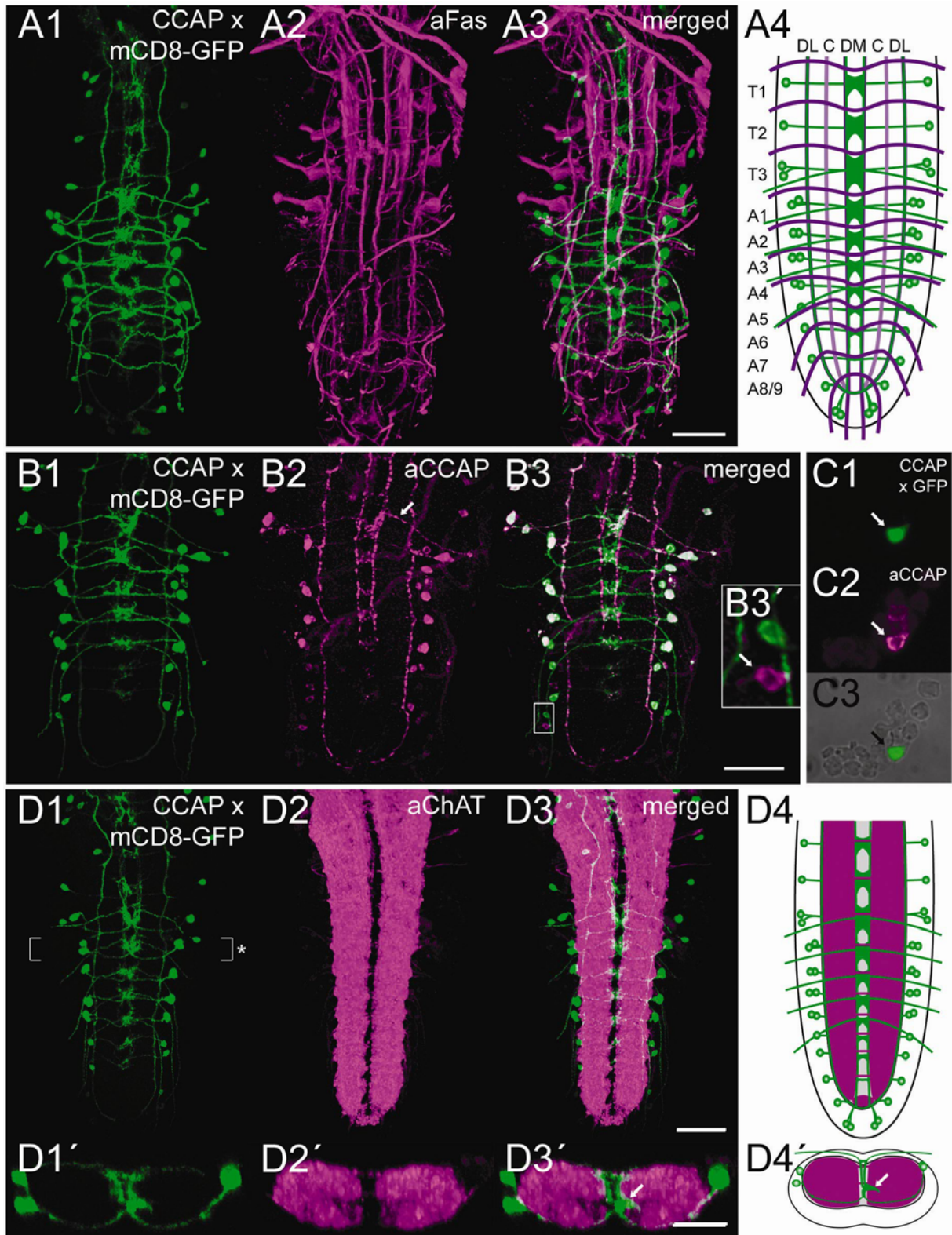


Figure 1

excessive evaporation. Then, CNS were manually dissociated under a microscope using fine tungsten needles. The cell culture dishes were kept in darkness at 20°C in a humidified incubator. Prior to imaging, cells were allowed to attach for at least 2 h.

Calcium Imaging

The cover glass with cells was mounted in an imaging chamber with a volume of 800 μL , sealed with silicon wax. Then, cells were washed with 5 mL L-15. For Fura-2 based Ca^{2+} -imaging, cells were loaded with 2 μM Fura-2 acetoxymethyl ester (Molecular Probes, Leiden, The Netherlands) in 1 mL L-15 for 30 min at room temperature. For *in vitro* imaging with GECIs, the loading step was omitted. Cells were washed with 2 mL standard J+J saline (Jan and Jan, 1976) containing (in mM): 128 NaCl, 2 KCl, 4 MgCl_2 , 1.26 CaCl_2 , 36 Sucrose, and 5 HEPES, pH 7.1. After 5 min, the saline was exchanged for J+J saline containing 0.18 mM CaCl_2 and the cells were left for ~ 35 min in the dark. N_{CCAP} were identified by GFP-expression and imaging was started. During imaging, cells were washed with standard J+J saline. Drugs (purchased from Sigma-Aldrich) were pipetted directly into the bath in a volume of 1–3 mL.

For *in situ* imaging, a whole larval or adult CNS was dissected out in hemolymph-like HL3 saline (HL3; Stewart et al., 1994) containing (in mM): 80 NaCl, 5 KCl, 20 MgCl_2 , 1.5 CaCl_2 , 10 NaHCO_3 , 75 Sucrose, 5 Trehalose, and 5 HEPES, pH 7.2. In some preparations for *in situ* imaging, the larval ventral ganglion was cut at the height of the subesophageal neuromeres to eliminate putative input from the brain. To increase tissue penetration, the CNS was incubated for 7–10 min at room temperature in 1 mL HL3 containing 0.5 mg collagenase and 1 mg dispase. The CNS was then transferred to a small drop of HL3 on a cover glass, which was mounted in the imaging chamber as described. Saline was removed and the tissue was covered with 2% low melting agarose (AppliChem, Darmstadt, Germany) in HL3 warmed to 37°C. Immediately after harden-

ing of the agarose, the imaging chamber was filled with HL3 and imaging was started. All drugs were dissolved in HL3 and bath-applied.

Calcium Imaging System and Data Processing

The imaging system consisted of an Axiovert 200 microscope (Zeiss, Jena, Germany) equipped with a Zeiss 40x Fluor oil immersion objective (NA 1.3), conventional FITC and Fura-2 filter sets (Chroma, Brattleboro, VT), and a cooled CCD camera (Hamamatsu C4742-80-12AG, Hamamatsu Photonics, Herrsching, Germany). For Cameleon 2.1 imaging, a CFP-YFP filter set (Chroma) and an aperture imaging system (Dual-View, Optical Insights, USA) were used. Excitation light was provided by a Polychrome IV system (T.I.L.L. Photonics, Gräfelfing, Germany) equipped with a computer-controlled shutter. Light was attenuated by different quartz neutral density filters (10–50%) to prevent photo-damage of the cells. OpenLab 4.0 software (Improvision, Warwick, UK) on a Macintosh G5 PowerPC was used for system control and image acquisition. Images were typically acquired with an intensity resolution of 12 bit at 0.1 Hz after background subtraction, with 2x2 binning resulting in a pixel resolution of 672 x 512. Data were processed using Microsoft Excel and GraphPad Prism 4 (GraphPad Software, San Diego, CA). For construction of dose-response curves, $[\text{Ca}^{2+}]_i$ -responses were normalized to the maximum ratio obtained after application of ACh receptor agonist which was set to 100%.

Immunocytochemistry

Immunocytochemistry on cultured cells and larval whole-mount CNS was performed using standard procedures. Cultured cells were fixed with 4% PFA for 30 min at 4°C and washed three times for 10 min with phosphate buffered saline (PBS) containing 0.1% TrX (PBT). The cells were blocked with 10% normal goat serum (NGS) in PBT for 1 h

Figure 1 Morphology of N_{CCAP} in the ventral ganglion of *Drosophila*. Larval ventral ganglion of CCAP-gal4 x mCD8-GFP (A1) immunolabeled against Fas (aFas; A2). The merged image (A3) was used to assign N_{CCAP} to a particular neuromere in a scheme of the Fas landmark system (A4). Note that N_{CCAP} lack Fas-IR. Larval ventral ganglion expressing mCD8-GFP in N_{CCAP} (B1) immunolabeled against CCAP (aCCAP; B2). CCAP-IR is visible in transverse projections of N_{CCAP} residing in the last thoracic neuromere (arrow), whereas other N_{CCAP} show weak or lack CCAP-IR in transversal projections. In the merged image (B3), all mCD8-GFP-expressing N_{CCAP} show CCAP-IR. (B3') Enlargement of the boxed area in B3 indicating a CCAP-immunoreactive neuron that lacks mCD8-GFP-expression. A GFP-expressing N_{CCAP} in primary cell culture (arrow; C1) immunolabeled against CCAP (C2). In (C3), the N_{CCAP} as well as adjacent neurons that lack GFP-expression and CCAP-IR are shown. Larval ventral ganglion expressing mCD8-GFP in N_{CCAP} (D1) immunolabeled against choline acetyl transferase (aChAT; D2). The merged image (D3) served for a schematic representation of N_{CCAP} and ChAT-immunoreactive neurites (D4). (D1'-3') show corresponding transverse sections through the first abdominal neuromere as indicated in D1 (asterisk). Note the arborizations of N_{CCAP} in the central neuropil (D3' and D4'; arrow). See text for further details. Images are volume-rendered z-stacks of confocal sections representing dorsal view unless otherwise stated. Scale bars: 50 μm ; in D1'–D3': 25 μm .

at room temperature, followed by overnight incubation at 4°C with primary antibody diluted in PBT and 10% NGS. The next day, cells were washed several times with PBT and incubated with secondary antibody diluted in PBT and 10% NGS for 1 h at room temperature. After several washes with PBT, the cells were washed twice with 0.01 M PBS and mounted in glycerol:PBS (80:20).

For whole-mount immunocytochemistry, CNS of third instar larvae were dissected in ice-cold dissecting saline (Su and O'Dowd, 2003) and fixed with 4% PFA for 2 h at 4°C. After several washes with PBT, tissue was incubated with primary antibody and 5% NGS in PBT for 1–3 days at 4°C. Thereafter, the tissue was washed repeated times with PBT, followed by overnight incubation with secondary antibody and 1% NGS in PBT at 4°C. The following day, tissue was washed and mounted as described. To identify the target areas of N_{CCAP} neurites projecting to the periphery, filleted larvae containing only body wall, body wall muscles, and CNS were fixed with 4% PFA for 2 h at 4°C and processed for immunocytochemistry as described.

The primary antiserum rabbit-anti-*Periplaneta americana* myoinhibiting peptide (aMIP, kind gift M. Eckert, Jena, Germany) was used at a concentration of 1:2000, the rabbit-anti-CCAP antiserum (aCCAP, generously provided by H. Dirksen, Stockholm, Sweden) and mouse monoclonal antibody (mAb) anti-choline acetyl transferase 4B1 (aChAT) were used at 1:1000, the mouse mAb against synapsin (aSyn 3C11, kind gift of E. Buchner, Würzburg, Germany) at 1:100, and the mouse mAb against Fasciclin-2 (aFas) at 1:75. The mAbs aChAT and aFas (1D4) were obtained from the Developmental Studies Hybridoma Bank under the auspices of the NICHD at the University of Iowa, donated by P.M. Salvaterra and C. Goodman. Cy3-conjugated AffiniPure goat-anti-rabbit IgG, and Cy5-conjugated AffiniPure goat-anti-mouse IgG (Jackson ImmunoResearch, West Grove, PA) were used as secondary antibodies at a dilution of 1:300.

Confocal Laser Scanning Microscopy

Confocal stacks were acquired on a confocal laser scanning microscope (Leica TCS SP2, Leica Microsystems, Wetzlar, Germany) with a 40x objective (HCX PL APO 40x, N.A. 1.25) at 512 x 512 or 1024 x 1024 pixel resolution. For 3D volume-rendering, image stacks were imported into AMIRA 3.1 software (Indeed-Visual Concepts, Berlin, Germany) and processed using the "Voltex" and "Oblique-Slice" module. A false color map was applied to the volume-rendered neurons and brightness and contrast were adjusted. Snapshots were taken in AMIRA and finally processed with Adobe Photoshop 7.0 (Adobe Systems, San Jose, CA).

RESULTS

Morphology of CCAP Neurons

To describe the pattern of N_{CCAP} and to assign individual N_{CCAP} to the thoracic or abdominal neuromeres,

we mapped N_{CCAP} in the Fasciclin-2 (Fas) landmark system proposed by Landgraf et al. (2003) [Fig. 1(A1–A4)]. The overall distribution of N_{CCAP} matched with previous descriptions of CCAP-expression (Park et al., 2003) and CCAP-immunoreactivity (CCAP-IR; Ewer and Truman, 1996). We consistently observed CCAP-gal4-driven expression of mCD8-GFP in one pair of laterally located neurons in each of the first two thoracic neuromeres (T1 and T2). The third thoracic neuromere (T3) and each of the first four abdominal neuromeres (A1–A4) contained two pairs of N_{CCAP} . Only one pair of N_{CCAP} resided in the next three abdominal neuromeres (A5–A7), whereas the last abdominal neuromeres A8/9 included three pairs of N_{CCAP} . However, mCD8-GFP-expression in N_{CCAP} of A8/9 was weak in most preparations [Fig. 1(B1,D1)]. Longitudinal projections of N_{CCAP} run along the lateral VL Fas fascicles and along the median DM and VM Fas fascicles, and joined in A8/9. Each N_{CCAP} sent a neurite medially which formed extensive arborizations around the midline between the DM and VM Fas fascicles. In T3 and A1–A4, at least one of two N_{CCAP} at each side projected via the segmental nerves to the periphery. To check the specificity of the CCAP-gal4-driven mCD8-GFP-expression in the ventral ganglion, we immunostained larval CNS with an antiserum against CCAP (aCCAP). In all preparations ($n > 10$), all mCD8-GFP-expressing N_{CCAP} of larval ventral ganglia showed CCAP-IR [Fig. 1(B1–B3)]. However, in some preparations, we observed CCAP-immunoreactive neurons in A5–A7 that lacked mCD8-GFP expression [Fig. 1(B3,B3')]. Thus, not all N_{CCAP} may be included in the CCAP-gal4 expression pattern. All longitudinal mCD8-GFP-expressing N_{CCAP} neurites showed strong CCAP-IR. The transversal projections of N_{CCAP} located in T3 were also strongly immunoreactive for CCAP, whereas those of N_{CCAP} residing in A1–A4 showed only weak or even lacked CCAP-IR [Fig. 1(B2)]. We also fixed dissociated neurons and immunostained them for CCAP to control the specificity of CCAP-gal4-driven GFP-expression *in vitro*. All GFP-expressing neurons stained positive for CCAP, and conversely, all CCAP-immunoreactive neurons expressed GFP [$n > 10$; Fig. 1(C1–C3)].

In *Drosophila*, we found recently that the majority of cultured peptidergic neurons responded to ACh with a transient increase of $[Ca^{2+}]_i$ (Wegener et al., 2004). This study indicated a function of ACh as an input factor of peptidergic neurons in general. Therefore, we stained larval CNS expressing mCD8-GFP in N_{CCAP} with an antiserum against choline acetyl transferase (aChAT), the ACh-producing enzyme. We found ChAT-immunoreactivity (ChAT-IR) widespread over the central neuropil and in close apposi-

tion to CCAP-expressing neurites around the midline of the ventral ganglion [Fig. 1(D1–D4,D1'–D4')].

Dissociated CCAP Neurons Respond to Depolarization and Cholinergic Agonists

In a first set of Ca^{2+} -imaging experiments, we loaded dissociated *Drosophila* CNS cells with the ratiometric Ca^{2+} -sensitive dye Fura-2. Then, we identified the N_{CCAP} *in vitro* by their GFP-expression and monitored the effect of depolarization on their $[\text{Ca}^{2+}]_i$. Application of saline containing 15–100 mM K^+ resulted in a strong rise of $[\text{Ca}^{2+}]_i$ in all N_{CCAP} tested ($n = 9$), demonstrating that dissociated neurons were excitable [Fig. 2(A)]. Since our aChAT immunostainings suggested that ACh might be an input factor of N_{CCAP} , we tested the effect of ACh and other cholinergic agonists on the $[\text{Ca}^{2+}]_i$ of N_{CCAP} at doses commonly used for patch clamp recordings (Albert and Lingle, 1993; Rohrbough and Broadie, 2002) and Ca^{2+} -imaging experiments (Wegener et al., 2004). Application of 10–100 μM ACh induced fast and steep rises of $[\text{Ca}^{2+}]_i$ in 68 of 70 (~97%) N_{CCAP} tested [see e.g. Fig. 2(A)]. To check if ACh acts on the N_{CCAP} via ionotropic nicotinic receptors (nAChRs) or via metabotropic muscarinic receptors (mAChRs), we applied the nAChR agonist nicotine and the mAChR agonist pilocarpine. Application of 10–100 μM nicotine evoked an increase of $[\text{Ca}^{2+}]_i$ in 42 of 45 (~93%) N_{CCAP} [Fig. 2(B 1)], whereas 10–100 μM pilocarpine induced a rise of $[\text{Ca}^{2+}]_i$ in 4 of 14 (~29%) N_{CCAP} tested [Fig. 2(B2)]. Since the majority of N_{CCAP} responded to ACh and nicotine, we constructed dose-response curves for these agonists [Fig. 3 (A1, A2,B1,B2)]. The ACh dose-response curve for N_{CCAP} expressing UAS-GFP showed a threshold concentration of 0.5–1 μM ACh with an EC_{50} of $5.9 \pm 1.8 \mu\text{M}$ [$n = 9$; Fig. 3(A1)]. The threshold concentration for nicotine varied between 0.5 and 1 μM with an EC_{50} of $6.5 \pm 3.9 \mu\text{M}$ [$n = 4$; Fig. 3(B1)]. Typically, we observed a desensitization of the $[\text{Ca}^{2+}]_i$ -response in N_{CCAP} after application of 100 μM nicotine [Fig. 3(B1,B2)].

Dissociated CCAP Neurons Respond to Glutamate and Quisqualate

To screen for further putative input factors, we tested the effects of various transmitters at the fairly high dose of 1 mM on $[\text{Ca}^{2+}]_i$ of N_{CCAP} loaded with Fura-2. Whereas the biogenic amines serotonin ($n = 6$), dopamine ($n = 6$), and octopamine ($n = 7$) did not evoke $[\text{Ca}^{2+}]_i$ -increases (data not shown), application of glutamate induced rises of $[\text{Ca}^{2+}]_i$ in 26 of 74 (~35%) N_{CCAP} tested. The threshold concentration for glutamate was around 100 μM (data not shown). To characterize the involved glutamate receptors, we stimulated

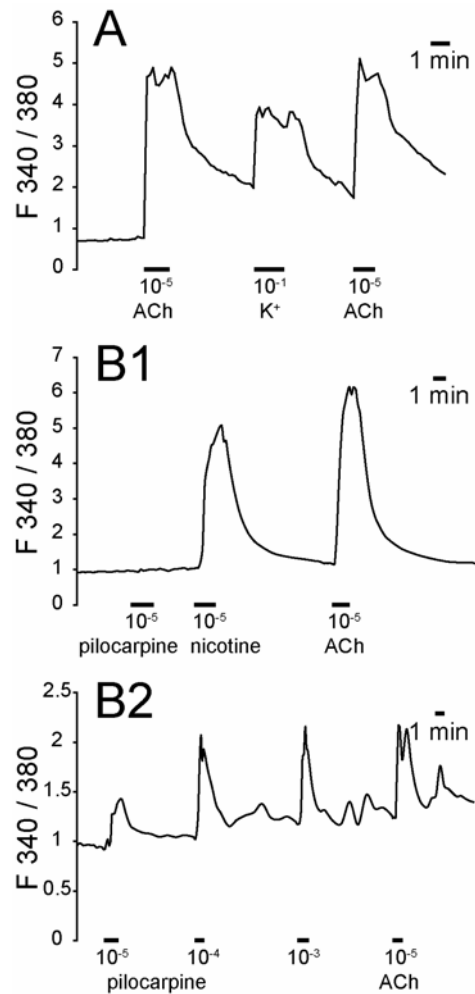


Figure 2 Responses of Fura-2 loaded N_{CCAP} to depolarization and application of cholinergic agonists *in vitro*. Original traces from Ca^{2+} -imaging experiments. Concentrations are given in M. (A) Response of a N_{CCAP} after application of ACh and depolarization with high K^+ . (B1) A N_{CCAP} shows $[\text{Ca}^{2+}]_i$ -increase after application of the nAChR agonist nicotine, but not the mAChR agonist pilocarpine. (B2) Response of a N_{CCAP} to increasing concentrations of pilocarpine and subsequent application of ACh. Bars below the traces indicate the time drugs were present in the bathing solution.

N_{CCAP} with two different glutamatergic agonists, NMDA and quisqualate. Unlike NMDA, which never activated N_{CCAP} [$n = 13$; Fig. 4(A1)], application of 1 mM quisqualate induced $[\text{Ca}^{2+}]_i$ -rises in all N_{CCAP} that responded to glutamate [$n = 6$; Fig. 4(A2)].

Dissociated CCAP Neurons Respond to GABA

To check for inhibitory input, we investigated whether Fura-2 loaded N_{CCAP} respond to GABA, a major inhib-

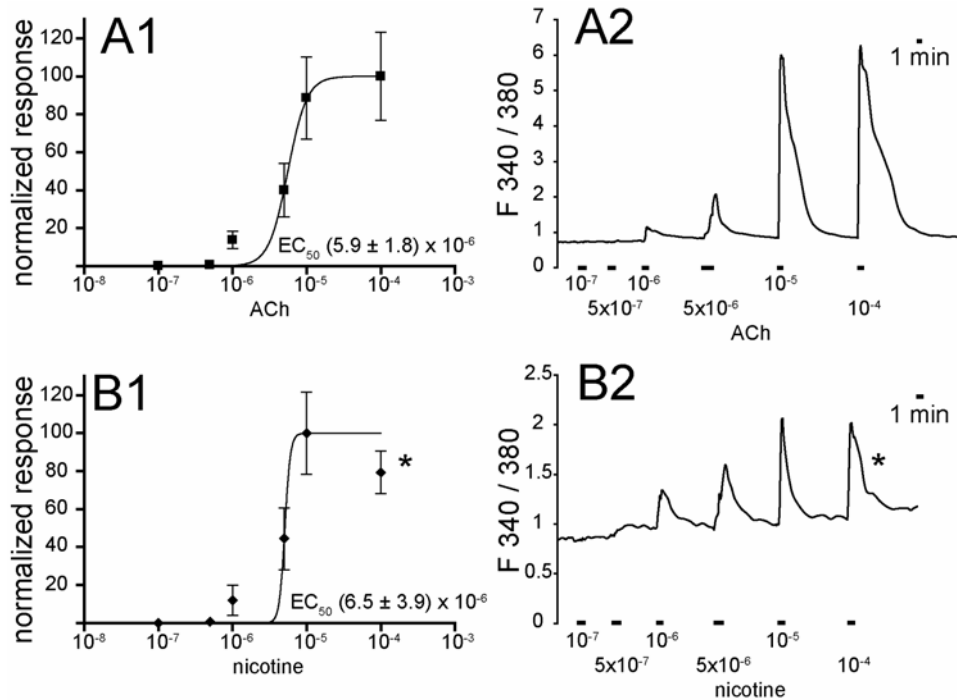


Figure 3 Responses of Fura-2 loaded N_{CCAP} to increasing concentrations of ACh and nicotine *in vitro*. Concentrations are given in M. (A1) Normalized dose-response curve (4-parameter fit) for ACh ($n = 9$); (A2) A representative original trace for ACh-application. (B1) Normalized dose-response curve (4-parameter fit) for nicotine ($n = 5$); (B2) A representative original trace for nicotine-application. Note that the $[Ca^{2+}]_i$ -responses of N_{CCAP} showed desensitization at $100 \mu M$ nicotine (B 1 and B2; asterisks). Error bars represent SEM. Bars below the traces indicate the time drugs were present in the bathing solution.

itory transmitter in the *Drosophila* nervous system (Küppers et al., 2003). Since acutely dissociated N_{CCAP} did neither show elevated levels of $[Ca^{2+}]_i$ nor spontaneous $[Ca^{2+}]_i$ -oscillations, we could not measure $[Ca^{2+}]_i$ -decreases after application of 1 mM GABA. Thus, we tested whether GABA could reduce the ACh-induced $[Ca^{2+}]_i$ -rises. Application of $100 \mu M$ GABA caused a complete block of the ACh-mediated $[Ca^{2+}]_i$ -increases in 3 of 15 (20%) N_{CCAP} tested, i.e. the level of $[Ca^{2+}]_i$ did not change after application of ACh under block conditions [Fig. 4(B1)]. In 4 of 15 (~27%) N_{CCAP} tested, application of GABA led to a reduced ACh-response compared to control, whereas the response to ACh was unaltered by GABA in the remaining 8 (~53%) N_{CCAP} [Fig. 4(B2)].

In Vitro Characterization of CCAP Neurons Expressing Genetically Encoded Ca^{2+} -Indicators

Ca^{2+} -imaging experiments in short term cultures of dissociated neurons loaded with Fura-2 indicated ACh

as a major putative input factor of N_{CCAP} that consistently increased $[Ca^{2+}]_i$. Thus, we asked if ACh also stimulates $[Ca^{2+}]_i$ -rises in the intact nervous system. To specifically monitor $[Ca^{2+}]_i$ of N_{CCAP} *in situ*, we had to use a genetically encoded Ca^{2+} -indicator (GECI). To determine a suitable GECI, we initially imaged N_{CCAP} *in vitro* expressing either the ratiometric Cameleon 2.1 (Diegelmann et al., 2002) or the nonratiometric GCaMP 1.6 (Reiff et al., 2005) under UAS control. We measured the ratio or intensity of fluorescence emission of both GECIs in saline (background signal) and after application of $10 \mu M$ ACh. For comparison, we then calculated the relative signal after ACh-application of each GECI as a multiple of the background signal. Although both Cameleon 2.1 [$n = 7$; Fig. 5(A1,A2)] and GCaMP 1.6 [$n = 9$; Fig. 5 (B)] reliably reported ACh-induced responses in cultured dissociated N_{CCAP} , they showed great differences in the relative ratio or intensity of fluorescence emission after ACh-application. Cameleon 2.1-expressing N_{CCAP} showed a $1.05 (\pm 0.01 \text{ SEM})$ fold higher relative YFP/CFP ratio after ACh-application, whereas the relative intensity after ACh-application

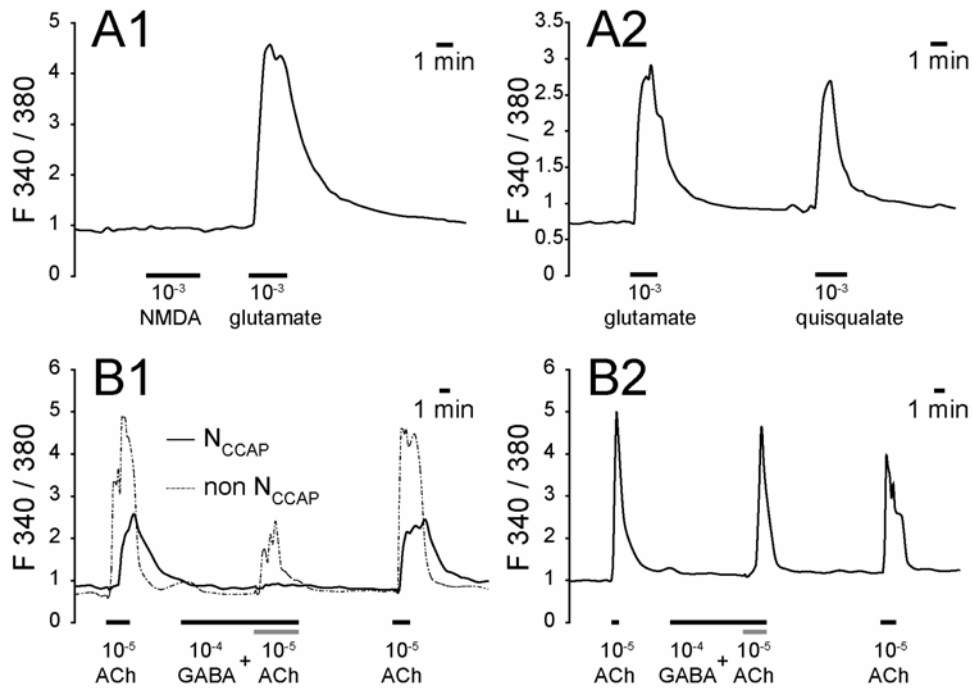


Figure 4 Responses of Fura-2 loaded N_{CCAP} to application of glutamatergic and GABAergic agonists *in vitro*. Original traces from Ca^{2+} -imaging experiments. Concentrations are given in M. (A1) A N_{CCAP} shows $[Ca^{2+}]_i$ -rises after application of glutamate, but does not respond to NMDA. (A2) N_{CCAP} responding to glutamate as well as quisqualate. (B1) In some N_{CCAP} , GABA completely blocks the ACh-mediated $[Ca^{2+}]_i$ -increase (solid line), which is only partly reduced in a non- N_{CCAP} (dashed line). (B2) In other N_{CCAP} GABA does not prevent the ACh-mediated $[Ca^{2+}]_i$ -rise. Bars below the traces indicate the time drugs were present in the bathing solution.

was $1.4 (\pm 0.07 \text{ SEM})$ as high as background intensity in N_{CCAP} expressing GCaMP 1.6. Thus, both GECIs showed an approximately 3- to 4-fold lower relative signal after ACh-application than the synthetic dye Fura-2 [Fig. 5(C)]. Since the relative signal after ACh-application of GCaMP 1.6 was higher than that of Cameleon 2.1 [Fig. 5(C)], we relied on the use of GCaMP 1.6 for the further experiments.

CCAP Neurons Expressing GCaMP 1.6 Respond to Cholinergic and GABAergic Input *In Vitro*

In primary cell culture, 8 out of 11 (~73%) N_{CCAP} expressing GCaMP 1.6 under UAS control responded with $[Ca^{2+}]_i$ -rises after application of $10 \mu\text{M}$ ACh [Fig. 6(A1,A2)]. The three N_{CCAP} that did not respond to ACh were located in not fully dissociated cell clusters. However, these N_{CCAP} showed $[Ca^{2+}]_i$ -increases after application of cholinergic agonists [see Fig. 6(B1)]. Since ACh is rapidly metabolized in the insect nervous system (Treherne and Smith,

1965), we assume that the lack of excitability by ACh was due to ACh-esterase activity. Application of $10\text{--}100 \mu\text{M}$ nicotine induced $[Ca^{2+}]_i$ -rises in 7 of 9 (~78%) N_{CCAP} expressing GCaMP 1.6 [Fig. 6 (B1,B2)]. In one experiment, two neighboring N_{CCAP} residing in a cell cluster both showed transient $[Ca^{2+}]_i$ -increases upon nicotine application [Fig. 6 (B1)]. In contrast, in another experiment two adjacent N_{CCAP} located in a cell cluster responded heterogeneously to application of nicotine [Fig. 6(B2)]. Whereas one of these N_{CCAP} showed transient $[Ca^{2+}]_i$ -oscillations after nicotine application, the associated neuron remained silent. Application of $100 \mu\text{M}$ of the general AChR agonist carbachol induced transient $[Ca^{2+}]_i$ -rises in 10 of 11 N_{CCAP} tested (~91%). The one N_{CCAP} that did not respond to carbachol was located in a not fully dissociated cell cluster. In contrast to nicotine or carbachol, stimulation with the mAChR agonist pilocarpine did not evoke $[Ca^{2+}]_i$ -increases in N_{CCAP} expressing GCaMP 1.6 [$n = 9$; Fig. 6(A1)]. Since our *in vitro* Ca^{2+} -imaging experiments with Fura-2 loaded N_{CCAP} suggested that

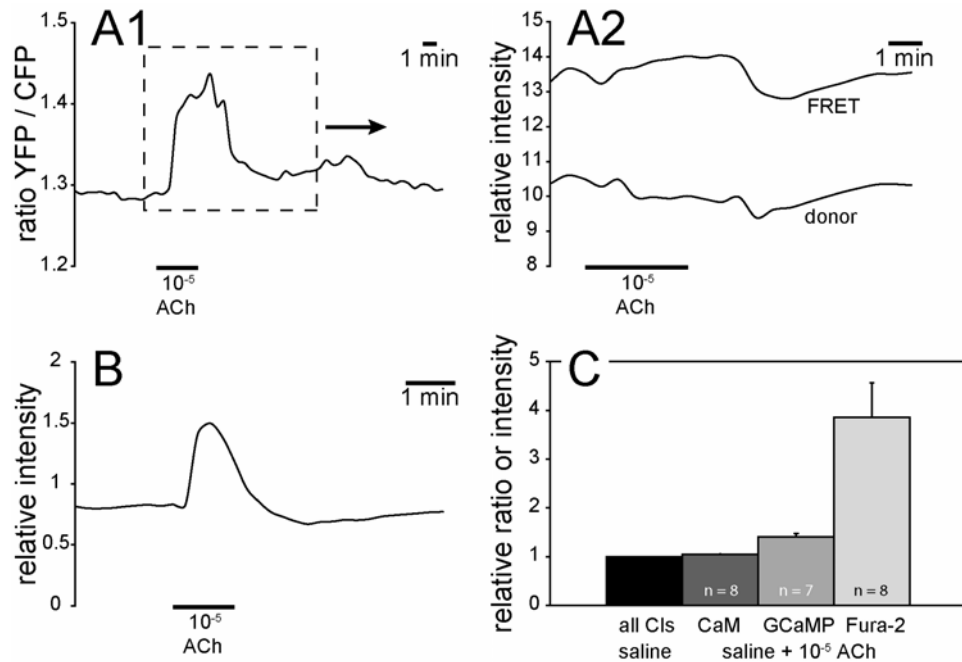


Figure 5 Responses of N_{CCAP} expressing GECIs *in vitro*. Concentrations are given in M. Original traces from Ca^{2+} -imaging experiments. (A1) Response to ACh of a N_{CCAP} expressing the ratiometric Cameleon 2.1; (A2) individual fluorescence emission for the FRET and donor channels of the experiment shown in A1 (dashed box). (B) Response to ACh of a N_{CCAP} expressing the non-ratiometric GCaMP 1.6. (C) Relative ratio or intensity of N_{CCAP} expressing Cameleon 2.1 (CaM) or GCaMP 1.6 (GCaMP), and N_{CCAP} loaded with Fura-2 after ACh-application compared to the background signal of the different $[Ca^{2+}]_i$ -indicators in saline (all CIs). See text for further details. Error bars represent SEM. Bars below the traces indicate the time drugs were present in the bathing solution.

GABA-application could block ACh-mediated $[Ca^{2+}]_i$ -increases, we tested the effect of GABA on N_{CCAP} expressing GCaMP 1.6. Application of $100 \mu M$ GABA induced a decrease of $[Ca^{2+}]_i$ in 1 of 7 (=14%) N_{CCAP} and caused a complete block of the ACh-mediated $[Ca^{2+}]_i$ -increase in this N_{CCAP} [Fig. 6(A2)].

CCAP Neurons Respond to Cholinergic Input *In Situ*

The results described in the previous paragraphs showed that GCaMP 1.6 *in vitro* reliably reported transmitter-induced changes in $[Ca^{2+}]_i$ with a sufficiently large change in fluorescence emission. Thus, we used the intact larval and adult CNS of CCAP-gal4 x UAS-GCaMP 1.6 flies to monitor the effect of cholinergic agonists on N_{CCAP} *in situ*. In third instar larval ventral ganglia, we imaged N_{CCAP} residing in T1–T3 and A1–A6 since GCaMP 1.6-expression was weak or absent in A7–A8/9. Application of $100 \mu M$

nicotine did not induce persistent $[Ca^{2+}]_i$ -increases in 45 N_{CCAP} from 12 different preparations. Instead, we typically observed $[Ca^{2+}]_i$ -decreases after application of nicotine or carbachol which sometimes were preceded by a small and short $[Ca^{2+}]_i$ -increase [Fig. 7 (A1,A2)]. Unlike nicotine, however, carbachol induced transient $[Ca^{2+}]_i$ -oscillations in 29 of 125 (~23%) N_{CCAP} from 22 preparations [Fig. 7 (A1, A2)]. Remarkably, 18 of the 29 N_{CCAP} that showed carbachol-induced $[Ca^{2+}]_i$ -oscillations resided in T3, three responding N_{CCAP} were located both in A1 and A2, four in A3, and one in A4. Thus, N_{CCAP} of T3 consistently responded to carbachol, whereas the N_{CCAP} of A1–A4 showed carbachol-induced $[Ca^{2+}]_i$ -oscillations less frequently. Application of carbachol never caused $[Ca^{2+}]_i$ -oscillations in N_{CCAP} of T1–T2, or A5–A6. We also monitored carbachol-mediated $[Ca^{2+}]_i$ -responses of N_{CCAP} pairs residing in T3 and A1–A4 whenever it was possible to focus on both N_{CCAP} of a particular pair. In these experiments, carbachol-application always induced $[Ca^{2+}]_i$ -oscillation

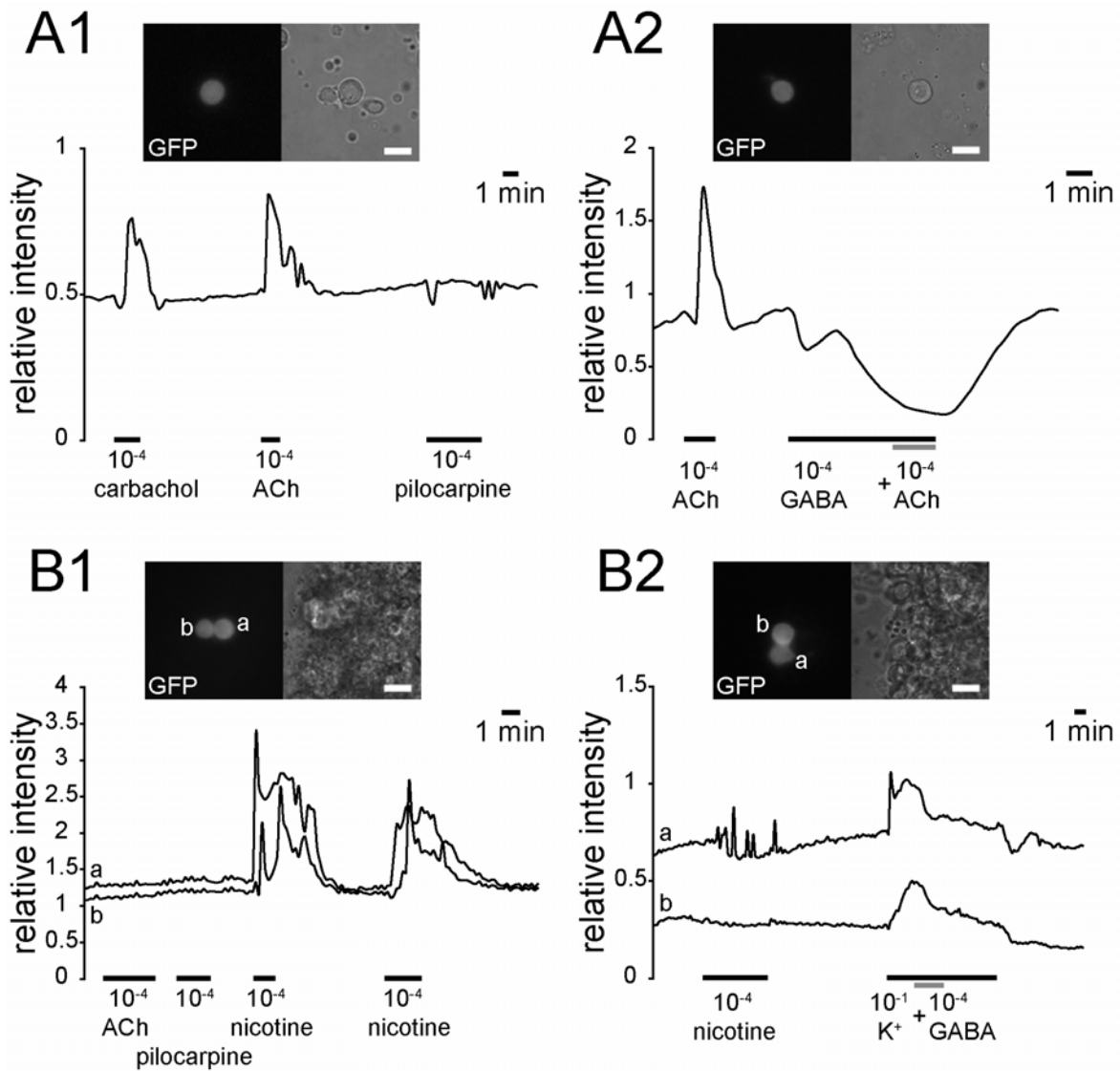


Figure 6 Responses of N_{CCAP} expressing GCaMP 1.6 after application of cholinergic agonists and GABA *in vitro*. Original traces from Ca^{2+} -imaging experiments. Concentrations are given in M. (A1) A N_{CCAP} responds to application of ACh and the general AChR-agonist carbachol, whereas the mAChR-agonist pilocarpine does not induce $[Ca^{2+}]_i$ -increase. (A2) Application of ACh causes a $[Ca^{2+}]_i$ -increase in a N_{CCAP} , whereas GABA induces a decrease of $[Ca^{2+}]_i$ and completely blocks the ACh-mediated $[Ca^{2+}]_i$ -increase. (B1) Two adjacent N_{CCAP} (a, b) located in a not fully dissociated cell cluster show $[Ca^{2+}]_i$ -increases to repetitive application of nicotine, whereas ACh and pilocarpine have no effects. In (B2), two adjacent N_{CCAP} located in a cell cluster respond heterogeneously to application of nicotine but homogeneously to depolarization with high K^+ . One of the N_{CCAP} shows $[Ca^{2+}]_i$ -oscillations (a), whereas the other N_{CCAP} (b) remains quiet. In both N_{CCAP} , application of GABA induces a decrease of $[Ca^{2+}]_i$; despite the high K^+ -induced depolarization. Bars below the traces indicate the time drugs were present in the bathing solution. Insets show the respective N_{CCAP} in primary cell culture. Scale bars: 10 μ m.

in only one N_{CCAP} of the pair, whereas the adjacent neuron remained silent [$n = 16$; nine pairs were located in T3, three in A1, two in A2, and one in A3

and A4, respectively; Fig. 7(A1)]. Carbachol-induced $[Ca^{2+}]_i$ -oscillations were not restricted to the cell body, but could be observed in neurites as well

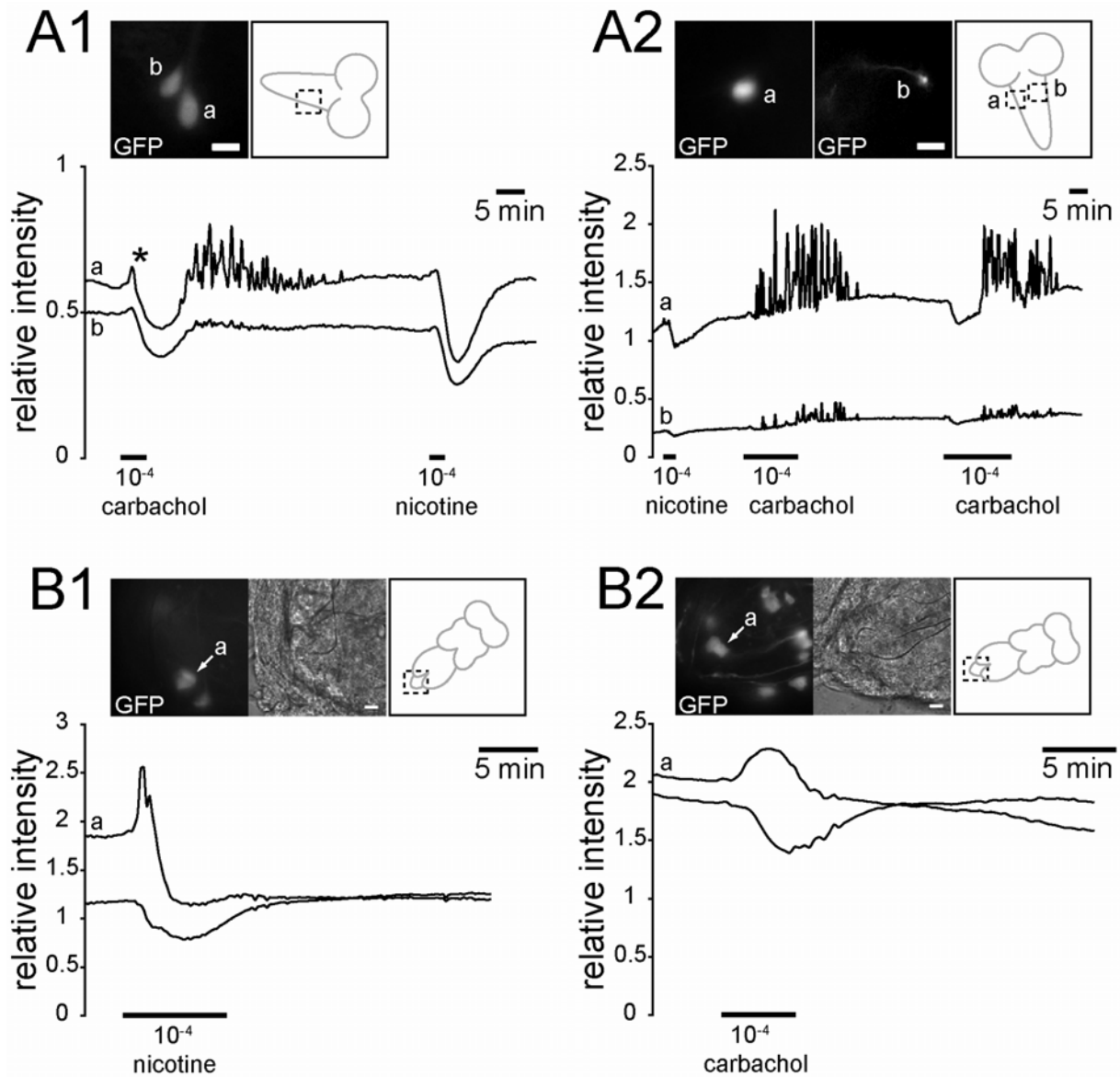


Figure 7 Responses of larval and adult N_{CCAP} expressing GCaMP 1.6 to cholinergic agonists *in situ*. Original traces from Ca^{2+} -imaging experiments. Concentrations are given in M. (A1) Responses of two larval N_{CCAP} of T3 (see inset) to application of different AChR agonists. In both N_{CCAP} , application of carbachol induces a small transient $[Ca^{2+}]_i$ -increase (asterisk), followed by a strong decrease of $[Ca^{2+}]_i$. After wash with saline, the $[Ca^{2+}]_i$ recovers and one N_{CCAP} (a) shows enduring oscillations of $[Ca^{2+}]_i$, whereas the other N_{CCAP} (b) remains quiescent. Application of nicotine causes a rapid and strong decrease of $[Ca^{2+}]_i$ in both N_{CCAP} . (A2) Responses of a larval N_{CCAP} in T3 (a) and in the axon of the corresponding contralateral N_{CCAP} (b) after application of cholinergic agonists (see inset). Application of nicotine induces a small decrease of $[Ca^{2+}]_i$, whereas carbachol causes enduring $[Ca^{2+}]_i$ -oscillations in the N_{CCAP} (a) as well as in the contralateral axon (b) which presumably projects to the periphery. (B1) A N_{CCAP} at the tip of the adult ventral ganglion (a; see inset) shows a transient $[Ca^{2+}]_i$ -increase and a subsequent $[Ca^{2+}]_i$ -decrease after application of nicotine, whereas another N_{CCAP} responds with a decrease only. In (B2), application of carbachol induces a transient $[Ca^{2+}]_i$ -rise in a N_{CCAP} at the tip of the adult ventral ganglion (a; see inset), whereas another N_{CCAP} shows a decrease in $[Ca^{2+}]_i$. Scale bars: $10 \mu\text{m}$. Bars below the traces indicate the time drugs were present in the bathing solution.

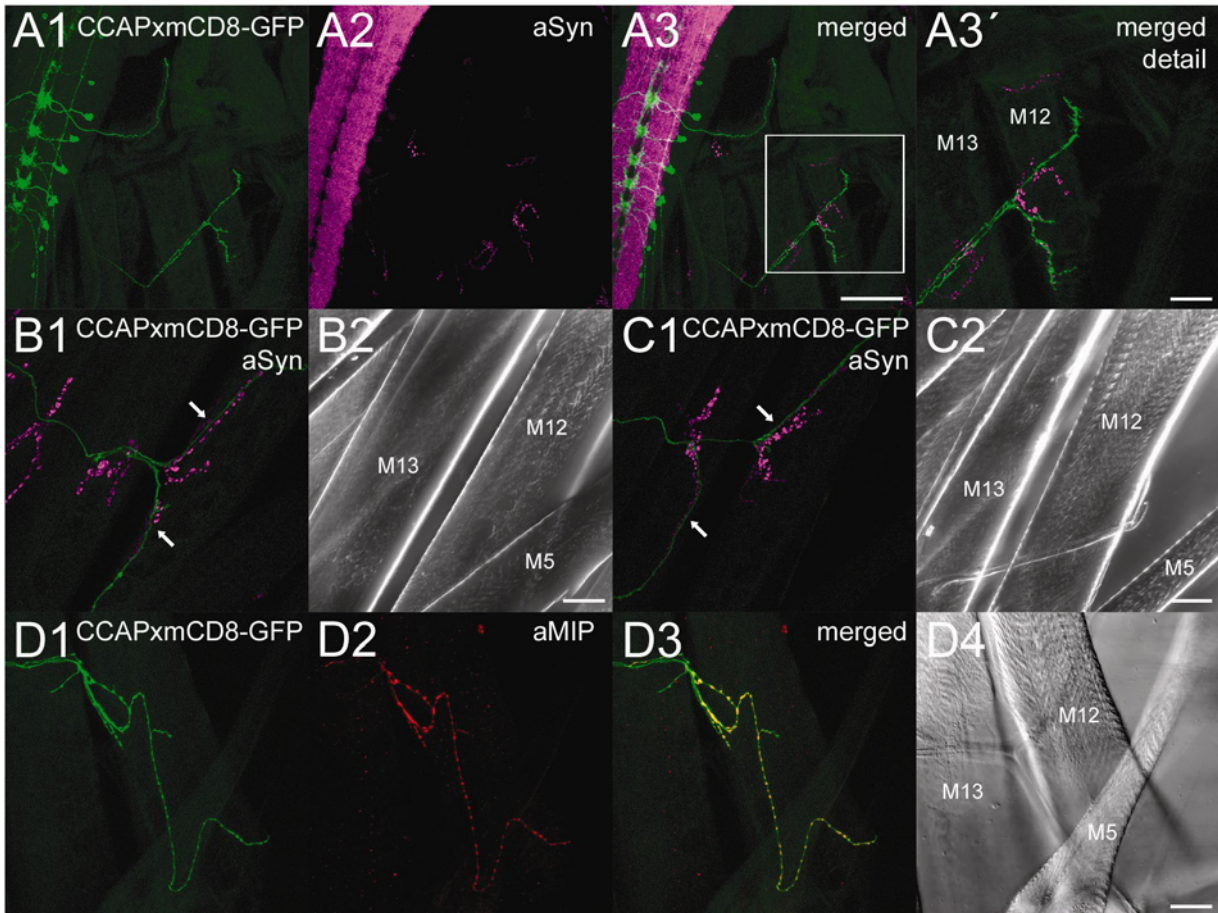


Figure 8 Projections of N_{CCAP} to larval body wall muscles. Filleted larvae of CCAP-gal4 x mCD8-GFP (A1) immunolabeled against the presynaptic protein synapsin (aSyn; A2). A distinct subset of N_{CCAP} projects to the periphery and innervates the larval body wall muscles (A3). (A3') Enlargement of the boxed area in A3 showing mCD8-GFP-expressing projections of N_{CCAP} and adjacent aSyn-positive NMJs on larval muscle M12. (B1-B2) N_{CCAP} typically project to M12, (C1-C2) but the adjacent muscle M13 is also often innervated. Note the close apposition between N_{CCAP} -expressing neurites and NMJs immunolabeled against aSyn (arrows). (D1-D4) Filleted larvae of CCAP-gal4 x mCD8-GFP (A1) immunolabeled against MIP. Peripheral N_{CCAP} -projections at M5, 12, and 13 show strong MIP-IR. See text for further details. Scale bars in A1-A3: 50 μm ; others: 25 μm . [Color figure can be viewed in the online issue, which is available at www.interscience.wiley.com.]

[Fig. 7(A2)]. Application of 100 μM pilocarpine did not evoke $[\text{Ca}^{2+}]_i$ -increases in 16 N_{CCAP} from four different preparations (data not shown). To eliminate putative descending inhibitory input from the brain, we cut the larval ventral ganglion at the height of the subesophageal neuromeres and used only the thoracic and abdominal part of the ventral ganglion for *in situ* Ca^{2+} -imaging. However, this procedure did not eliminate the nicotine-mediated $[\text{Ca}^{2+}]_i$ -decrease of N_{CCAP} in the remaining neuromeres (three different preparations; data not shown). Since most N_{CCAP} in the larval ventral ganglion lacked $[\text{Ca}^{2+}]_i$ -rises after application of cholinergic agonists, we investigated if this situation would change after eclosion. In freshly

ecdysed adults (mostly dissected within 1 h after eclosion, including flies with non-inflated wings), we monitored N_{CCAP} located in the thoracic and the abdominal part of the ventral ganglion. Application of 100 μM nicotine induced transient $[\text{Ca}^{2+}]_i$ -rises in 11 of 69 (~16%) N_{CCAP} from 11 preparations [Fig. 7(B1)]. Application of 100 μM carbachol caused transient $[\text{Ca}^{2+}]_i$ -increases in 12 of 88 (~14%) N_{CCAP} from 11 preparations [Fig. 7(B2)]. As in the larval ventral ganglion, most N_{CCAP} in the adult ventral ganglion remained silent after application of cholinergic agonists. In contrast to the situation in the larval ventral ganglion, we never observed oscillations of $[\text{Ca}^{2+}]_i$ in any adult N_{CCAP} after application of cho-

linergic agonists. All N_{CCAP} that responded to cholinergic agonists resided at the tip of the adult ventral ganglion [see Fig. 7(B1,B2)]. Application of 100 μM pilocarpine did not induce $[Ca^{2+}]_i$ -increases in 33 N_{CCAP} of four preparations (data not shown).

A Defined Subset of CCAP Neurons Projects to Larval Body Wall Muscles

In T3, one N_{CCAP} per pair consistently showed $[Ca^{2+}]_i$ -oscillations upon carbachol application *in situ*. At least some N_{CCAP} in T3, together with N_{CCAP} in A1–A4, constitute a morphologically distinct subset of N_{CCAP} which send efferent projections via the segmental nerves to the periphery. Previously, Hodge et al. (2005) showed that some N_{CCAP} project to the larval body wall. To refine their data, we asked if N_{CCAP} of T3 project to a similar peripheral destination as the N_{CCAP} of A1–A4 and traced the efferent neurites of N_{CCAP} located in T3 and A1–A4 in filleted CCAP-gal4 x mCD8-GFP larvae ($n > 10$). N_{CCAP} projections of both T3 and A1–A4 formed what seemed to be varicose neurohemal endings on the body wall muscles [Fig. 8(A1–A3,A3')]. In accordance with Hodge et al. (2005), the efferent N_{CCAP} neurites primarily ended on the longitudinal muscle M12 [Fig. 8(B1,B2)]. However, we found that adjacent muscles like M13 [Fig. 8(C1,C2)] or M5 [Fig. 8(D1–D4)] were occasionally also innervated (nomenclature following Chiba, 1999). The projections of N_{CCAP} in T3 branched at muscles in proximity to the larval CNS, whereas the N_{CCAP} axons of the neuromeres A1–A4 successively innervated body wall muscles of subsequent body wall segments, i.e. N_{CCAP} axons of the neuromere A4 projected most posteriorly. Thus, we typically observed five putative neurohemal zones at each side of the larval body wall musculature. To check whether N_{CCAP} projections innervate neuromuscular junctions (NMJs), we immunostained filleted larvae expressing mCD8-GFP in N_{CCAP} with an antiserum against the presynaptic marker protein synapsin (aSyn). The projections of the N_{CCAP} built variable—sometimes extensive—arborizations that resided in close proximity to the synapsin-immunoreactive NMJs of the SNb motor neurons. However, we never observed Syn-immunoreactivity (Syn-IR) in the peripheral N_{CCAP} terminals [see Fig. 8(A3', B1,C1)]. Recently, Kim et al. (2006) reported that a subset of N_{CCAP} co-expresses MIPs. To test if MIPs also localize to the putative peripheral release zones of CCAP, we immunostained filleted larvae expressing mCD8-GFP in N_{CCAP} for MIP. In all preparations ($n > 10$), the peripheral endings of

N_{CCAP} located in A1–A4 showed MIP-immunoreactivity [MIP-IR; Fig. 8(D1–D4)]. In contrast, the peripheral endings of N_{CCAP} residing in T3 lacked MIP-IR (data not shown).

DISCUSSION

Acetylcholine as an Input Factor of CCAP Neurons

ACh is the main excitatory transmitter in the CNS of *Drosophila* (Yasuyama and Salvaterra, 1999). Our results provide both immunocytochemical and pharmacological evidence that ACh also plays a role as an input factor of N_{CCAP} . We observed ChAT-IR widespread over the central neuropil of the larval ventral ganglion and projections of N_{CCAP} around the midline between the DM and VM Fas fascicles. Thus, it is likely that N_{CCAP} are contacted by cholinergic neurons. However, the resolution of fluorescence confocal microscopy is not sufficient to prove synaptic contact between ChAT-immunoreactive axon terminals and N_{CCAP} neurites. Our *in vitro* and *in situ* Ca^{2+} -imaging experiments showed that application of ACh as well as nicotine induced $[Ca^{2+}]_i$ -increases in N_{CCAP} . Furthermore, the observed dose-responses of N_{CCAP} for ACh and nicotine are in accordance with those of other larval *Drosophila* neurons measured by Ca^{2+} -imaging (Wegener et al., 2004) or whole-cell patch-clamp recordings (Albert and Lingle, 1993). Thus, N_{CCAP} express functional nAChRs, a feature that appears to be typical for peptidergic neurons (Wegener et al., 2004). In our Ca^{2+} -imaging experiments, the mAChR agonist pilocarpine also induced $[Ca^{2+}]_i$ -rises in some cultured N_{CCAP} . This corresponds to the finding that activation of a cloned *Drosophila* mAChR evoked $[Ca^{2+}]_i$ -increase in a *Drosophila* cell line (Cordova et al., 2003).

Evidence for a Differential Activation of CCAP Neuron Subsets via GABA and Glutamate

The *in vitro* Ca^{2+} -imaging experiments showed that only some N_{CCAP} responded to the candidate input-transmitters GABA or glutamate. Whereas GABA is a major inhibitory neurotransmitter in the insect CNS (Küppers et al., 2003), L-glutamate serves as excitatory as well as inhibitory transmitter (Rohrbough and Broadie, 2002; Daniels et al., 2004; Featherstone et al., 2005). *In vitro*, we found that GABA-application affected ACh-mediated $[Ca^{2+}]_i$ -increases in about half the N_{CCAP} loaded with Fura-2. In addition,

GCaMP 1.6-expressing N_{CCAP} showed GABA-induced $[Ca^{2+}]_i$ -decreases *in vitro*. Thus, we suggest that at least a subset of N_{CCAP} expresses functional GABA receptors, which, however, still need to be characterized. In contrast to GABA, application of glutamate caused increases of $[Ca^{2+}]_i$ in about one third of N_{CCAP} *in vitro*. Application of quisqualate but not NMDA mimicked the glutamate-mediated $[Ca^{2+}]_i$ -rises. Quisqualate is commonly used as an agonist on AMPA/kainate ionotropic glutamate receptors (iGluRs; Usherwood, 1994; Washio, 2002), as well as a specific activator of group I metabotropic glutamate receptors (mGluRs) both in vertebrates and invertebrates (Hinoi et al., 2000; Krenz et al., 2000). However, *Drosophila* apparently expresses only one functional mGluR that shares properties of the vertebrate group II mGluRs with less sensitivity to quisqualate (Bogdanik et al., 2004; Mitri et al., 2004). A recent survey of the *Drosophila* genome indicated that at least 14 of 21 putative iGluRs are of the AMPA (4 genes) or kainate (10 genes) subtype (Sprengel et al., 2001). In the ventral ganglion, a kainate-sensitive iGluR is expressed at high levels throughout the synaptic neuropil (Featherstone et al., 2005). Since application of quisqualate induced rather fast and steep increases of $[Ca^{2+}]_i$ in N_{CCAP} during our Ca^{2+} -imaging experiments, we suggest that at least a subset of N_{CCAP} expresses functional iGluRs of the AMPA/kainate subtype. However, we cannot completely rule out the involvement of an mGluR in the response to glutamate. Taken together, our results indicate that the transmitter-receptor distribution and the corresponding input transmitters probably differ between individual N_{CCAP} providing the opportunity for a central regulation of distinct N_{CCAP} subsets. This assumption is in accordance with the finding that synaptic transmission regulates the activity of a particular N_{CCAP} subset co-expressing the tanning hormone bursicon (Luan et al., 2006).

CCAP Neurons Show Different Ca^{2+} -Responses to Cholinergic Agonists Between *In Vitro* and *In Situ*

The AChR-mediated $[Ca^{2+}]_i$ -signatures differed between fully dissociated N_{CCAP} and N_{CCAP} located in cell clusters or in the intact CNS. Nearly all isolated N_{CCAP} responded to ACh and other cholinergic agonists with fast and steep increases of $[Ca^{2+}]_i$. In contrast, not fully dissociated N_{CCAP} located in cell clusters showed nicotine-mediated transient $[Ca^{2+}]_i$ -rises, transient $[Ca^{2+}]_i$ -oscillations or remained quiescent. Since we never observed ACh- or nicotine-mediated

$[Ca^{2+}]_i$ -oscillations in isolated N_{CCAP} , these $[Ca^{2+}]_i$ -oscillations may only occur in N_{CCAP} receiving input from other neurons. Thus, N_{CCAP} activity may already be modulated at the level of a cell cluster consisting of only few neighboring neurons. In contrast to the situation *in vitro*, most N_{CCAP} in the intact larval or adult CNS responded to application of nicotine and the general AChR agonist carbachol with a pronounced decrease of $[Ca^{2+}]_i$ which was sometimes preceded by a short and small $[Ca^{2+}]_i$ -increase. To our knowledge, there is no report on a nicotine-induced $[Ca^{2+}]_i$ -decrease in neurons. Thus, we assume that the observed $[Ca^{2+}]_i$ -decrease upon systemic application of cholinergic agonists is indirectly caused by activation of as yet unidentified presynaptic inhibitory neurons. Since removal of the brain did not abolish the cholinergic agonist-mediated $[Ca^{2+}]_i$ -decrease in N_{CCAP} , putative inhibitory neurons seem to reside within the larval ventral ganglion. Our results correspond to a previous study in the moth *Manduca sexta* indicating that descending inhibitory input from the subesophageal and thoracic ganglia transiently suppresses the activation of ecdysis-relevant ventral nervous system elements (Žitňan and Adams, 2000; Fuse and Truman, 2002). In *Drosophila*, the inhibition of N_{CCAP} by CNS neurons seems to establish a delay in the onset of ecdysis that allows the completion of EH-activated physiological processes during adult eclosion (Baker et al., 1999). Our Ca^{2+} -imaging studies indicate that GABA may play a role for this inhibitory input, since GABA was able to suppress ACh-induced $[Ca^{2+}]_i$ -increases and evoked a $[Ca^{2+}]_i$ -decrease *in vitro*.

Cholinergic Agonist-Mediated Ca^{2+} -Responses of CCAP Neurons Change During Postembryonic Development

Besides the observed differences in the transmitter-induced responses *in vitro* versus *in situ*, N_{CCAP} responded heterogeneously to cholinergic agonists with respect to their developmental stages. In the intact larval CNS, application of carbachol but not nicotine evoked reproducible $[Ca^{2+}]_i$ -oscillations in N_{CCAP} of T3 and in A1–A4. In contrast to nicotine, carbachol activates both mAChRs and nAChRs. Thus, mAChRs might be responsible for the carbachol-induced $[Ca^{2+}]_i$ -oscillations. However, we also observed $[Ca^{2+}]_i$ -oscillations after application of nicotine in not fully dissociated cultured N_{CCAP} . Furthermore, the specific mAChR agonist pilocarpine never induced $[Ca^{2+}]_i$ -changes in N_{CCAP} *in situ*. We conclude that

application of cholinergic agonists to the entire CNS possibly caused direct as well as indirect effects on the $[Ca^{2+}]_i$ of N_{CCAP} . In contrast to the larva, we never observed $[Ca^{2+}]_i$ -oscillations in the thoracic or abdominal parts of the adult ventral ganglion upon application of carbachol or nicotine. Yet, adult N_{CCAP} in the posterior abdominal neuromeres responded with short and transient $[Ca^{2+}]_i$ -increases to both agonists. These responding N_{CCAP} may belong to a subset of N_{CCAP} showing cGMP-immunoreactivity during eclosion as judged by their localization at the terminal region of the ventral nervous system (Ewer and Truman, 1996; Baker et al., 1999). In general, robust and enduring changes of $[Ca^{2+}]_i$ were restricted to N_{CCAP} of wandering third instar larva, supporting the hypothesis that N_{CCAP} play an essential role primarily at the ecdysis to the pupa (Park et al., 2003). Recently, Kim et al. (2006) showed in comparable Ca^{2+} -imaging experiments that application of ETH to the pharate pupal CNS induced successive activation of distinct N_{CCAP} subsets in the ventral ganglion. The strongest $[Ca^{2+}]_i$ -responses to ETH were observed in N_{CCAP} located in T3, in A1–A4, and in the last abdominal neuromeres (A8/9), whereas other N_{CCAP} showed weak (T1–T2, A7) or completely lacked ETH-induced $[Ca^{2+}]_i$ -responses (A5–A6). The earliest N_{CCAP} responding to ETH just prior to the putative ecdysis onset were located in T3. In exactly these N_{CCAP} , we found that application of carbachol induced reproducible stereotypic $[Ca^{2+}]_i$ -responses. Therefore, a cholinergic input may modulate the activity of N_{CCAP} in T3 which play an important role for the initiation of pupal ecdysis relevant behaviors (Kim et al., 2006). Furthermore, it seems plausible that inhibitory synaptic input affected ETH- or carbachol-mediated $[Ca^{2+}]_i$ -responses in other N_{CCAP} than T3 or A8/9 during the onset of pupal ecdysis.

A Distinct CCAP Neuron Subset Forms Putative Neurohemal Zones on Larval Body Wall Muscles

Apart from the pharmacological evidences for N_{CCAP} subset diversity, we also observed morphological differences between individual N_{CCAP} . In the larval ventral ganglion, the GFP-expressing N_{CCAP} in A5-8/9 seem to have only central projections. In contrast, a particular N_{CCAP} subset located in T3 and A1–A4 projected via the segmental nerves to the periphery. Electron microscopy indicates that nerve branches innervating muscle M12 contain only one peptidergic neurite (Jia et al., 1993). Thus, just one N_{CCAP} of each pair in T3 and A1–A4 apparently possesses a peripheral projection. The N_{CCAP} terminals at the body wall muscles

lacked Syn-IR. Since NMJ with type I terminals typically show Syn-IR (Godenschwege et al., 2004) and type II terminals are very small (Jia et al., 1993), the peripheral N_{CCAP} neurites seem to end in type III terminals as previously suggested by Hodge et al. (2005). Presumably, the N_{CCAP} endings at the larval body wall are identical to the insulin-immunoreactive terminals described by Gorczyca et al. (1993). In our immunostainings of CCAP-gal4 x UAS-mCD8-GFP larvae, only the transversal projections of N_{CCAP} located in T3 showed prominent CCAP-IR (see also Ewer and Truman, 1996). Noteworthy, the peripheral terminals of these N_{CCAP} in T3 lacked MIP-IR, whereas those of N_{CCAP} located in A1-A4 showed strong MIP-IR. Thus, the N_{CCAP} of T3 may play a role for CCAP-release during pupal ecdysis onset, whereas N_{CCAP} in A1-A4 appear to co-release CCAP together with MIP. Peripherally released CCAP may influence heartbeat, body wall, or visceral muscle activity as reported for *Drosophila* and other insects (Dirksen, 1998; Donini et al., 2002; Dulcis et al., 2005).

A Combination of Both *In Vitro* and *In Situ* Live Cell Imaging Facilitates Studies on the Physiology of Neuronal Networks

We applied noninvasive live cell imaging to characterize the effects of various neurotransmitters on $[Ca^{2+}]_i$ of N_{CCAP} *in vitro* and *in situ*. We found that the response behavior of dissociated N_{CCAP} differed considerably from that of N_{CCAP} located within the intact CNS. Although we cannot completely rule out that our *in vitro* results might be influenced by dissociation and culture procedures or that the responsiveness of N_{CCAP} *in situ* might be affected by different diffusion capacities and desensitizing effects of agonists, we suggest that the observed differences between *in vitro* and *in situ* are caused by a complex presynaptic regulation of N_{CCAP} activity *in vivo*. In other words, a neuron within the intact CNS may not necessarily respond to bulk application of a given transmitter although it expresses the appropriate receptor. Thus, a combination of both *in vitro* and *in situ* live cell imaging is necessary for a comprehensive characterization of the receptor complement and the possible input-mediated $[Ca^{2+}]_i$ -responses of specific neurons.

CONCLUSIONS

Our Ca^{2+} -imaging studies suggest a complex and differential central regulation of N_{CCAP} activity by ACh,

glutamate, and GABA. These neurotransmitters are known to influence the secretory activity of peptidergic neurons (Lapchak and Beaudet, 1990; Garside and Mazurek, 1997; Shirai et al., 2001; Engelmann et al., 2004), and may play a similar role in *Drosophila*. The concerted action of both peptide hormones and central transmitters could provide means for a context-dependent activation of distinct N_{CCAP} subsets and a fine-tuning of CCAP-release. An identification of presynaptic neurons would allow the use of cell-specific genetic techniques to test the physiological significance of the proposed neurotransmitter inputs and their effects on $[Ca^{2+}]_i$ of N_{CCAP} .

We thank John Ewer and Dierk Reiff for the kind gift of flies, Erich Buchner, Heiner Dirksen, and Manfred Eckert for the kind gift of antibodies, Ruth Hyland and Renate Renkawitz-Pohl for providing fly housing, and Uwe Homberg and Monika Stengl for general support.

REFERENCES

- Albert JL, Lingle CJ. 1993. Activation of nicotinic acetylcholine receptors on cultured *Drosophila* and other insect neurons. *J Physiol* 463:605–630.
- Baker JD, McNabb SL, Truman JW. 1999. The hormonal coordination of behavior and physiology at adult ecdysis in *Drosophila melanogaster*. *J Exp Biol* 202:3037–3048.
- Bogdanik L, Mohrmann R, Ramaekers A, Bockaert J, Grau Y, Broadie K, Parmentier ML. 2004. The *Drosophila* metabotropic glutamate receptor DmGluRA regulates activity-dependent synaptic facilitation and fine synaptic morphology. *J Neurosci* 24:9105–9116.
- Buckingham SD, Biggin PC, Sattelle BM, Brown LA, Sattelle DB. 2005. Insect GABA receptors: Splicing, editing, and targeting by antiparasitics and insecticides. *Mol Pharmacol* 68:942–951.
- Chiba A. 1999. Early development of the *Drosophila* neuromuscular junction: A model for studying neuronal networks in development. In: Budnik V, Sian Gramates L, editors. *Neuromuscular Junctions in Drosophila*. New York: Academic Press, pp 1–24.
- Clark AC, del Campo ML, Ewer J. 2004. Neuroendocrine control of larval ecdysis behavior in *Drosophila*: Complex regulation by partially redundant neuropeptides. *J Neurosci* 24:4283–4292.
- Cordova D, Delpech VR, Sattelle DB, Rauh JJ. 2003. Spatiotemporal calcium signaling in a *Drosophila melanogaster* cell line stably expressing a *Drosophila* muscarinic acetylcholine receptor. *Invert Neurosci* 5:19–28.
- Daniels RW, Collins CA, Gelfand MV, Dant J, Brooks ES, Krantz DE, DiAntonio A. 2004. Increased expression of the *Drosophila* vesicular glutamate transporter leads to excess glutamate release and a compensatory decrease in quantal content. *J Neurosci* 24:10466–10474.
- Diegelmann S, Fiala A, Leibold C, Spall T, Buchner E. 2002. Transgenic flies expressing the fluorescence calcium sensor Cameleon 2.1 under UAS control. *Genesis* 34:95–98.
- Dirksen H. 1998. Conserved crustacean cardioactive peptide (CCAP) neuronal networks and functions in arthropod evolution. In: Webster SG, Coast GM, editors. *Recent Advances in Arthropod Endocrinology*. Cambridge: Cambridge University Press, pp 302–333.
- Donini A, Ngo C, Lange AB. 2002. Evidence for crustacean cardioactive peptide-like innervation of the gut in *Locusta migratoria*. *Peptides* 23:1915–1923.
- Dulcis D, Levine RB, Ewer J. 2005. Role of the neuropeptide CCAP in *Drosophila* cardiac function. *J Neurobiol* 64:259–274.
- Engelmann M, Bull PM, Brown CH, Landgraf R, Horn TF, Singewald N, Ludwig M, et al. 2004. GABA selectively controls the secretory activity of oxytocin neurons in the rat supraoptic nucleus. *Eur J Neurosci* 19:601–608.
- Ewer J. 2005. Behavioral actions of neuropeptides in invertebrates: Insights from *Drosophila*. *Horm Behav* 48:418–429.
- Ewer J, Truman JW. 1996. Increases in cyclic 3',5'-guanosinemonophosphate (cGMP) occur at ecdysis in an evolutionarily conserved crustacean cardioactive peptide-immunoreactive insect neuronal network. *J Comp Neurol* 370:330–341.
- Ewer J, Truman JW. 1997. Invariant association of ecdysis with increases in cyclic 3',5'-guanosinemonophosphate immunoreactivity in a small network of peptidergic neurons in the hornworm, *Manduca sexta*. *J Comp Physiol [A]* 181:319–330.
- Featherstone DE, Rushton E, Rohrbough J, Liebl F, Karr J, Sheng Q, Rodesch CK, et al. 2005. An essential *Drosophila* glutamate receptor subunit that functions in both central neuropil and neuromuscular junction. *J Neurosci* 25:3199–3208.
- Fuse M, Truman JW. 2002. Modulation of ecdysis in the moth *Manduca sexta*: The roles of the subesophageal and thoracic ganglia. *J Exp Biol* 205:1047–1058.
- Garside S, Mazurek MF. 1997. Role of glutamate receptor subtypes in the differential release of somatostatin, neuropeptide Y, and substance P in primary serum-free cultures of striatal neurons. *Synapse* 27:161–167.
- Godenschwege TA, Reisch D, Diegelmann S, Eberle K, Funk N, Heisenberg M, Hoppe V, et al. 2004. Flies lacking all synapsins are unexpectedly healthy but are impaired in complex behaviour. *Eur J Neurosci* 20:611–622.
- Gorczyca M, Augart C, Budnik V. 1993. Insulin-like receptor and insulin-like peptide are localized at neuromuscular junctions in *Drosophila*. *J Neurosci* 13:3692–3704.
- Hinoi E, Ogita K, Takeuchi Y, Ohashi H, Maruyama T, Yoneda Y. 2000. Direct radiolabeling by [³H]quisqualic acid of group I metabotropic glutamate receptor in rat brain synaptic membranes. *Brain Res* 881:199–203.
- Hodge JJ, Choi JC, O'Kane CJ, Griffith LC. 2005. Shaw potassium channel genes in *Drosophila*. *J Neurobiol* 63:235–254.
- Jan LY, Jan YN. 1976. Properties of the larval neuromuscular junction in *Drosophila melanogaster*. *J Physiol* 262:189–214.

- Jia XX, Gorczyca M, Budnik V. 1993. Ultrastructure of neuromuscular junctions in *Drosophila*: Comparison of wild type and mutants with increased excitability. *J Neurobiol* 24:1025–1044.
- Kim YJ, Žitňan D, Galizia CG, Cho KH, Adams ME. 2006. A command chemical triggers an innate behavior by sequential activation of multiple peptidergic ensembles. *Curr Biol* 16: 1395–1407.
- Krenz WD, Nguyen D, Pérez-Acevedo NL, Selverston AI. 2000. Group I, II, and III mGluR compounds affect rhythm generation in the gastric circuit of the crustacean stomatogastric ganglion. *J Neurophysiol* 83:11 88–1201.
- Küppers B, Sánchez-Soriano N, Letzkus J, Technau GM, Prokop A. 2003. In developing *Drosophila* neurones the production of γ -amino butyric acid is tightly regulated downstream of glutamate decarboxylase translation and can be influenced by calcium. *J Neurochem* 84:939–951.
- Landgraf M, Sánchez-Soriano N, Technau GM, Urban J, Prokop A. 2003. Charting the *Drosophila* neuropile: A strategy for the standardised characterisation of genetically amenable neurites. *Dev Biol* 260:207–225.
- Lapchak PA, Beudet A. 1990. Cholinergic regulation of vasoactive intestinal peptide content and release in rat frontal cortex and hippocampus. *J Neurochem* 55:1340–1345.
- Lee T, Luo L. 1999. Mosaic analysis with a repressible cell marker for studies of gene function in neuronal morphogenesis. *Neuron* 22:451–461.
- Luan H, Lemon WC, Peabody NC, Pohl JB, Zelensky PK, Wang D, Nitabach MN, et al. 2006. Functional dissection of a neuronal network required for cuticle tanning and wing expansion in *Drosophila*. *J Neurosci* 26:573–584.
- McNabb SL, Baker JD, Agapite J, Steller H, Riddiford LM, Truman JW. 1997. Disruption of a behavioral sequence by targeted death of peptidergic neurons in *Drosophila*. *Neuron* 19:813–823.
- Mitri C, Parmentier ML, Pin JP, Bockaert J, Grau Y. 2004. Divergent evolution in metabotropic glutamate receptors. A new receptor activated by an endogenous ligand different from glutamate in insects. *J Biol Chem* 279:9313–9320.
- Park JH, Schroeder AJ, Helfrich-Förster C, Jackson FR, Ewer J. 2003. Targeted ablation of CCAP neuropeptide-containing neurons of *Drosophila* causes specific defects in execution and circadian timing of ecdysis behavior. *Development* 130:2645–2656.
- Park Y, Filippov V, Gill SS, Adams ME. 2002. Deletion of the ecdysis-triggering hormone gene leads to lethal ecdysis deficiency. *Development* 129:493–503.
- Reiff DF, Ihring A, Guerrero G, Isacoff EY, Joesch M, Nakai J, Borst A. 2005. *In vivo* performance of genetically encoded indicators of neural activity in flies. *J Neurosci* 25:4766–4778.
- Rohrbough J, Broadie K. 2002. Electrophysiological analysis of synaptic transmission in central neurons of *Drosophila* larvae. *J Neurophysiol* 88:847–860.
- Sattelle DB, Jones AK, Sattelle BM, Matsuda K, Reenan R, Biggin PC. 2005. Edit, cut and paste in the nicotinic acetylcholine receptor gene family of *Drosophila melanogaster*. *Bioessays* 27:366–376.
- Shirai Y, Jiang Y, Yoshioka S, Aizono Y. 2001. The release of an insect neuropeptide hormone, bombyxin, is regulated by muscarinic transmission in the brain- corpus cardiacum-corpora allatum complex of the silkworm, *Bombyx mori* (Lepidoptera: Bombycidae). *Appl Entomol Zool* 36: 431–438.
- Sprengel R, Aronoff R, Völkner M, Schmitt B, Mosbach R, Kuner T. 2001. Glutamate receptor channel signatures. *Trends Pharmacol Sci* 22:7–10.
- Stewart BA, Atwood HL, Renger JJ, Wang J, Wu CF. 1994. Improved stability of *Drosophila* larval neuromuscular preparations in haemolymph-like physiological solutions. *J Comp Physiol [A]* 175: 179–191.
- Su H, O'Dowd DK. 2003. Fast synaptic currents in *Drosophila* mushroom body Kenyon cells are mediated by α -bungarotoxin-sensitive nicotinic acetylcholine receptors and picrotoxin-sensitive GABA receptors. *J Neurosci* 23:9246–9253.
- Treherne JE, Smith DS. 1965. The metabolism of acetylcholine in the intact central nervous system of an insect (*Periplaneta americana* L.). *J Exp Biol* 43 :441–454.
- Usherwood PNR. 1994. Insect glutamate receptors. *Adv Insect Physiol* 24:309–341.
- Washio H. 2002. Glutamate receptors on the somata of dorsal unpaired median neurons in cockroach, *Periplaneta americana*, thoracic ganglia. *Zoolog Sci* 19:153–162.
- Wegener C, Hamasaka Y, Nässel DR. 2004. Acetylcholine increases intracellular Ca^{2+} via nicotinic receptors in cultured PDF-containing clock neurons of *Drosophila*. *J Neurophysiol* 91:912–923.
- Yasuyama K, Salvaterra PM. 1999. Localization of choline acetyltransferase-expressing neurons in *Drosophila* nervous system. *Microsc Res Tech* 45:65–79.
- Žitňan D, Adams ME. 2000. Excitatory and inhibitory roles of central ganglia in initiation of the insect ecdysis behavioural sequence. *J Exp Biol* 203:1329–1340.
- Žitňan D, Adams ME. 2004. Neuroendocrine regulation of insect ecdysis. In: Lawrence IG, Kostas I, Sarjeet SG, editors. *Comprehensive Molecular Insect Science*. Amsterdam: Elsevier, pp 1–60.

IV. A method for the synaptic isolation of CCAP neurons during calcium imaging experiments in the intact central nervous system of *Drosophila*

Vömel M and Wegener C. (2008).

Background	89
Results and Discussion	90
Generation of <i>shi^{ts}</i> ; CCAP-GAL4 and <i>shi^{ts}</i> ; UAS-GCaMP expressing flies	90
Control of transgene activity in <i>shi^{ts}</i> ; CCAP-GAL4/UAS-GCaMP expressing larvae and flies	91
Perspectives.....	91
Methods	92
Fly strains	92
Immunocytochemistry and microscopy.....	93
Behavioral experiments.....	93
References.....	93

A method for the synaptic isolation of CCAP neurons during calcium imaging experiments in the intact central nervous system of *Drosophila*

Matthias Vömel and Christian Wegener

Background

We previously showed by calcium imaging that the neurotransmitter acetylcholine (ACh) induces changes of the free intracellular calcium concentration ($[Ca^{2+}]_i$) in crustacean cardioactive peptide expressing neurons (N_{CCAP}) of *Drosophila* [1]. In short-term culture, ACh receptor (AChR) agonists such as nicotine and carbachol typically evoked $[Ca^{2+}]_i$ -increases in isolated N_{CCAP} . However, when applied to the intact larval ventral ganglion (VG), both AChR agonists induced $[Ca^{2+}]_i$ -rises in only few N_{CCAP} . The majority of N_{CCAP} instead responded with a pronounced $[Ca^{2+}]_i$ -decrease. These findings suggest that most N_{CCAP} of the larval VG receive inhibitory input from as yet unidentified central neurons [1]. Presumably, the inhibitory input restricts the activation of specific N_{CCAP} subsets to defined developmental stages, and in this way ensures the precisely timed progress of ecdysis-related processes [1,2]. During *in situ* calcium imaging experiments, systemically applied AChR agonists may act on both the putative inhibitory central neurons and the N_{CCAP} . Consequently, certain N_{CCAP} may receive transient inhibitory input during AChR agonist application. Such N_{CCAP} may not respond with $[Ca^{2+}]_i$ -increases to AChR agonists although they express functional AChRs. It is also possible that some N_{CCAP} lack AChRs, but receive excitatory input from AChR-expressing presynaptic neurons and, therefore, show $[Ca^{2+}]_i$ -increases upon systemic application of AChR agonists. To identify the AChR-expressing N_{CCAP} of the VG by calcium imaging, all N_{CCAP} need to be separated from their presynaptic network contacts during the systemic application of AChR agonists. Since the VG should not be mechanically damaged, we decided to disrupt the synaptic transmission between the N_{CCAP} and their input neuron(s).

In *Drosophila*, several genetic tools provide the opportunity to interfere with synaptic transmission. The GAL4/UAS system [3], for instance, allows the targeted expression of transgenes that induce cell death (e.g. [4–6]), disturb synaptic transmission (e.g. [7–9]), or suppress electrical activity (e.g. [10–12]). However, for these genetic approaches, it is a prerequisite to know the neurons that provide synaptic input onto N_{CCAP} . Supposing these neurons could be identified (- which is complicated due to the large number of cholinergic neurons in the *Drosophila* CNS [13] -), the generation of an appropriate GAL4 driver strain remains a critical and time-consuming task. Even if a specific GAL4 driver is immediately available, it would be desirable to control not only the spatial, but also the temporal expression of the respective transgenes. This could be achieved by utilizing a ligand- (e.g. GeneSwitch) or temperature-dependent GAL4/UAS system (e.g. TARGET), or a temperature-inducible FLP/FRT-recombinase system (see [14]). However, the slow time course of transgene induction and suppression taking hours to days are significant disadvantages of such approaches (see [14,15]).

We here present an alternative method to transiently disrupt the synaptic input onto N_{CCAP} during *in situ* calcium imaging experiments. This method is based upon transgenic flies that carry in their genome the CCAP-GAL4 driver [6] or the UAS-linked calcium indicator GCaMP 1.6 (UAS-GCaMP; [16]) together with a conditional mutant of the *shibire* (*shi*) gene. Shi encodes *Drosophila* dynamin, a GTPase involved in membrane recycling following synaptic vesicle release (see [15,17-19]). The corresponding mutant allele shi^{ts} makes the dynamin protein dysfunctional at moderately high temperatures. Consequently, shi^{ts} -expressing flies are active at the permissive temperature ($\sim 20^{\circ}C$), but show paralytic phenotypes at the restrictive temperature ($> 29^{\circ}C$) due to synaptic transmission impairment at the neuromuscular junction. In flies expressing both shi^{ts} and CCAP-GAL4-driven GCaMP, it should be possible to transiently inhibit the synaptic input onto N_{CCAP} and simultaneously monitor the $[Ca^{2+}]_i$ of the N_{CCAP} .

Results and Discussion

Generation of shi^{ts} ; CCAP-GAL4 and shi^{ts} ; UAS-GCaMP expressing flies

To obtain double mutant shi^{ts} ; CCAP-GAL4 and shi^{ts} ; UAS-GCaMP expressing flies, we initially generated flies that were homozygous for shi^{ts} and carried the dominant negative markers Curly of Oster (CyO) and Glazed (Gla) on the second chromosome pair (Figure 1). In subsequent crosses, the marked chromosomes were exchanged for those with the CCAP-GAL4 or the UAS-GCaMP transgene (Figure 1). The resulting homozygous shi^{ts} ; CCAP-GAL4 and shi^{ts} ; UAS-GCaMP fly strains were then crossed to generate flies that were homozygous for shi^{ts} and expressed CCAP-GAL4-driven UAS-GCaMP.

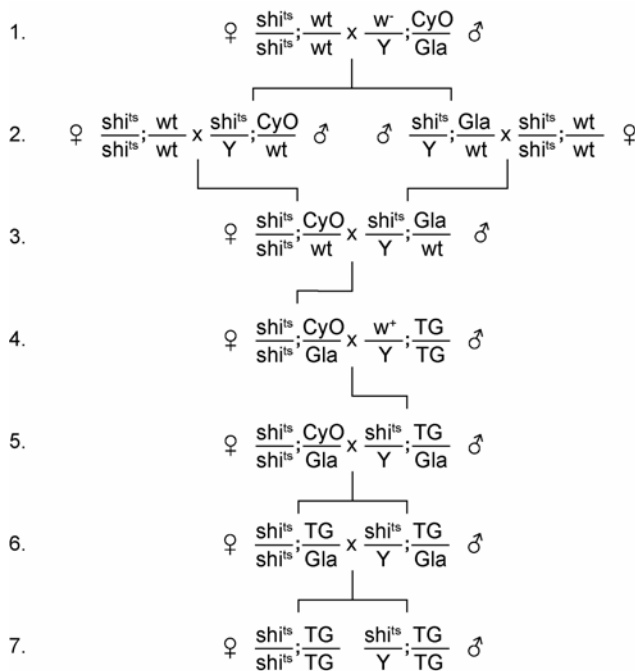


Figure 1. Generation of shi^{ts} ; CCAP-GAL4 and shi^{ts} ; UAS-GCaMP expressing flies.

Crossing scheme. The initial crosses (1-3.) resulted in transgenic flies that were homozygous for shi^{ts} and carried the dominant negative markers CyO (curly wings) and Gla (eyes reduced to one-fourth of the normal area) on the second chromosome pair. In the subsequent crosses (4-7.), the marked chromosomes were successively exchanged for those with the CCAP-GAL4 or the UAS-GCaMP transgene (TG). The shi^{ts} ; CCAP-GAL4 and shi^{ts} ; UAS-GCaMP flies were crossed to obtain shi^{ts} ; CCAP-GAL4/UAS-GCaMP progeny (not shown). w^+ : wild-type eye color; w^- : white eye color; wt: wild-type chromosome.

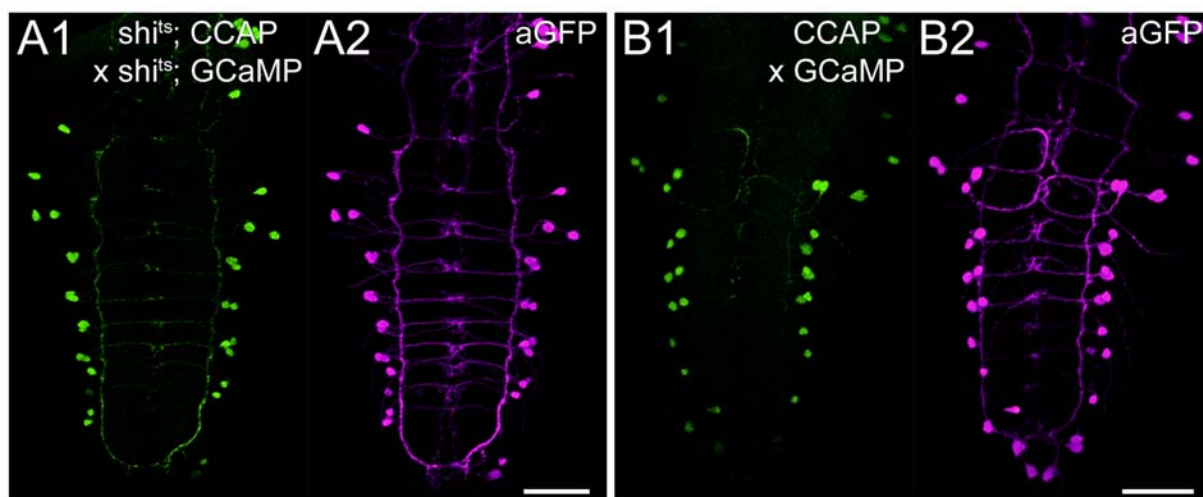


Figure 2. CCAP-GAL4-driven GCaMP expression in *shi^{ts}* expressing larvae.

Dorsal view of 3D image stacks showing A1) the GCaMP expression and A2) GFP immunoreactivity in the ventral ganglion of a *shi^{ts}; CCAP-GAL4/UAS-GCaMP* larva. B1) GCaMP expression and B2) GFP immunoreactivity in the ventral ganglion of a *CCAP-GAL4/UAS-GCaMP* larva. Scale bars: 50 μ m.

Control of transgene activity in *shi^{ts}; CCAP-GAL4/UAS-GCaMP* expressing larvae and flies

To test whether third instar larvae of the genotype *shi^{ts}; CCAP-GAL4/UAS-GCaMP* synthesize CCAP-GAL4-driven GCaMP, we immunostained the GCaMP-expressing neurons in the VG with a specific GFP antiserum. As assumed, the GFP immunolabeling pattern in the VG of *shi^{ts}; CCAP-GAL4/UAS-GCaMP* larvae matched with that of larvae expressing CCAP-GAL4-driven UAS-GCaMP (Figure 2). Thus, in the *shi^{ts}; CCAP-GAL4/UAS-GCaMP* larvae, the CCAP-GAL4 driver specifically targets UAS-GCaMP expression to N_{CCAP} .

In a second set of experiments, we examined whether flies of the genotypes *shi^{ts}; CCAP-GAL4*, *shi^{ts}; UAS-GCaMP*, or *shi^{ts}; CCAP-GAL4/UAS-GCaMP* show paralytic phenotypes at restrictive temperatures. As expected, *shi^{ts}* transgenic flies were active at the permissive temperature of 20°C, but rapidly showed severe locomotion defects at the restrictive temperature of 35°C. After 1 min at restrictive temperature, some *shi^{ts}* flies began to stagger, and within ~ 4 min all flies completely stopped moving (Figure 3). When the paralyzed flies were returned to permissive temperature, some flies started to move after 1 min, and within ~ 6 min all flies regained their activity (Figure 3). Control flies which lacked the *shi^{ts}* mutation and carried either the CCAP-GAL4 or the UAS-GCaMP transgene alone, or expressed CCAP-GAL4-driven GCaMP, did not show locomotion defects at the restrictive temperature (Figure 3). These findings indicate that the conditional *shi^{ts}* mutation is functional in *shi^{ts}; CCAP-GAL4/UAS-GCaMP* flies.

Perspectives

We generated double mutant flies of the genotypes *shi^{ts}; CCAP-GAL4* and *shi^{ts}; UAS-GCaMP*. When these fly strains are crossed, the progeny express *shi^{ts}* as well as CCAP-GAL4-driven GCaMP. Thus, in the *shi^{ts}; CCAP-GAL4/UAS-GCaMP*-expressing flies, it is possible to transiently inhibit synaptic transmission in the

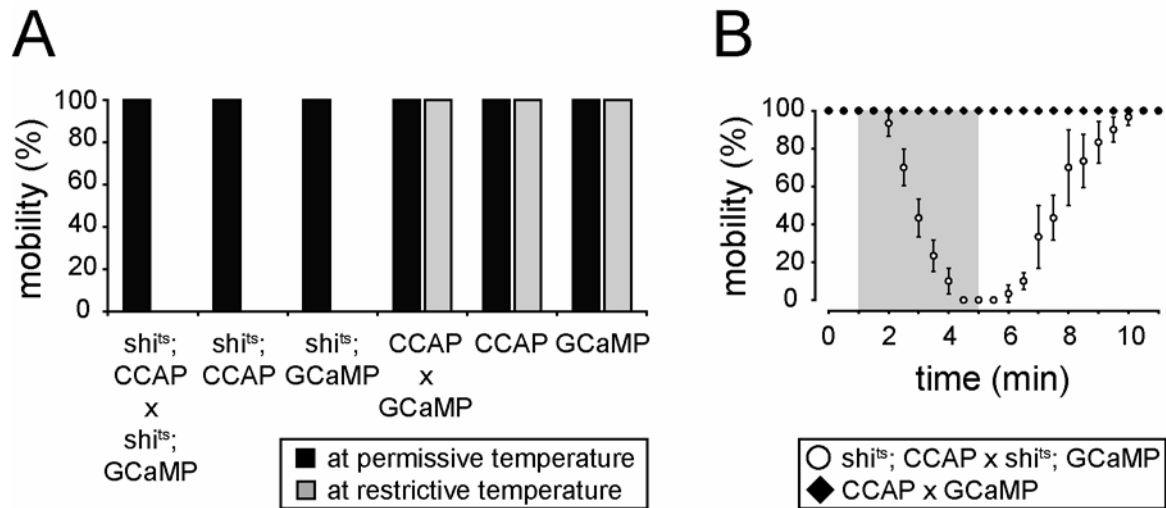


Figure 3. Temperature-dependent locomotion of shi^{ts} expressing flies.

A) Percentage of mobile shi^{ts} and control flies at permissive (20°C) and restrictive temperature (35°C). B) Time course of shi^{ts} induction and suppression. Percentage of mobile shi^{ts} and control flies (\pm SD) during a transient shift from permissive to restrictive temperature (highlighted in gray). See text for details.

CNS and at the same time monitor the effects of systemic transmitter application on the $[Ca^{2+}]_i$ of N_{CCAP} . In future experiments, we will utilize the shi^{ts}; CCAP-GAL4/UAS-GCaMP flies to investigate the following questions: Do N_{CCAP} within the intact VG of shi^{ts}; CCAP-GAL4/UAS-GCaMP larvae show similar AChR agonist-induced $[Ca^{2+}]_i$ -responses at restrictive temperature as isolated N_{CCAP} in cell culture? Which N_{CCAP} express functional AChRs at a particular developmental stage? Can an inhibitory input prevent the activation of certain N_{CCAP} ?

Acknowledgements

We thank John Ewer and Susanne Önel for the kind gift of fly lines. We are also grateful to Franz Grolig for maintaining the confocal microscope, Renate Renkawitz-Pohl for providing fly housing, and Uwe Homberg for general support. This work was supported by the Deutsche Forschungsgemeinschaft (DFG We 2652/2-2,3) to CW.

Methods

Fly strains

Double mutant shi^{ts}; CCAP-GAL4 and shi^{ts}; UAS-GCaMP fly strains were generated using flies of the genotypes shi^{ts} ([19]; kind gift of S. Önel, Marburg, Germany), w^+ ; CCAP-GAL4 ([6]; kind gift of J. Ewer, Cornell, NY), w^+ ; UAS-GCaMP 1.6 (Reiff et al., 2005; kind gift of D. Reiff, Martinsried, Germany), and yw ; CyO/Gla (Figure 1). All flies were raised on standard cornmeal agar medium and yeast at 18 or 25°C under a 12:12 h light:dark cycle.

Immunocytochemistry and microscopy

Immunostainings on larval whole mount CNS were performed as previously described [1]. To label CCAP-GAL4-driven GCaMP, a primary rabbit-anti-GFP antiserum (MBL International, Woburn, MA) was applied at a dilution of 1:500, and detected with a Cy3-conjugated AffiniPure goat-anti-rabbit secondary antibody (Jackson ImmunoResearch, West Grove, PA) at a dilution of 1:300. Fluorescence was recorded on a confocal laser scanning microscope (Leica TCS SP2, Leica Microsystems, Wetzlar, Germany) with a 40x objective (HCX PL APO 40x, N.A. 1.25) at 512 x 512 pixel resolution in 1 μ m steps along the z-axis. Confocal stacks were processed with AMIRA 3.1 software (Indeed-Visual Concepts, Berlin, Germany) and Adobe Photoshop 7.0 (Adobe Systems Inc., San Jose, CA) as previously described [1].

Behavioral experiments

At the beginning of each test series (n=5), 6 adult flies (3 female and 3 male) of each genotype were collected in a small plastic cell culture dish (with a volume of ~ 8.5 cm³). The dishes were kept for 10 min at the permissive temperature of 20°C and then exposed to the restrictive temperature of 35°C. After 4 min, the dishes were returned to 20°C. During all test series, the number of paralyzed flies was determined every 30 sec. Flies were considered as paralyzed when they were immobile and in supine position. The mobility index was calculated as the percentage of flies that were not paralyzed.

References

1. Vömel M, Wegener C (2007) Neurotransmitter-induced changes in the intracellular calcium concentration suggest a differential central modulation of CCAP neuron subsets in *Drosophila*. *Dev Neurobiol* 67: 792-808.
2. Baker JD, McNabb SL, Truman JW (1999) The hormonal coordination of behavior and physiology at adult ecdysis in *Drosophila melanogaster*. *J Exp Biol* 202: 3037-3048.
3. Brand AH, Perrimon N (1993) Targeted gene expression as a means of altering cell fates and generating dominant phenotypes. *Development* 118: 401-415.
4. Clark AC, del Campo ML, Ewer J (2004) Neuroendocrine control of larval ecdysis behavior in *Drosophila*: complex regulation by partially redundant neuropeptides. *J Neurosci* 24: 4283-4292.
5. McNabb SL, Baker JD, Agapite J, Steller H, Riddiford LM, Truman JW (1997) Disruption of a behavioral sequence by targeted death of peptidergic neurons in *Drosophila*. *Neuron* 19: 813-823.
6. Park JH, Schroeder AJ, Helfrich-Förster C, Jackson FR, Ewer J (2003) Targeted ablation of CCAP neuropeptide-containing neurons of *Drosophila* causes specific defects in execution and circadian timing of ecdysis behavior. *Development* 130: 2645-2656.
7. Murphey RK, Froggett SJ, Caruccio P, Shan-Crofts X, Kitamoto T, Godenschwege TA (2003) Targeted expression of shibire ts and semaphorin 1a reveals critical periods for synapse formation in the giant fiber of *Drosophila*. *Development* 130: 3671-3682.
8. Pitman JL, McGill JJ, Keegan KP, Allada R (2006) A dynamic role for the mushroom bodies in promoting sleep in *Drosophila*. *Nature* 441: 753-756.
9. Sakai T, Kitamoto T (2006) Differential roles of two major brain structures, mushroom bodies and central complex, for *Drosophila* male courtship behavior. *J Neurobiol* 66: 821-834.
10. Luan H, Peabody NC, Vinson CR, White BH (2006) Refined spatial manipulation of neuronal function by combinatorial restriction of transgene expression. *Neuron* 52: 425-436.
11. Mosca TJ, Carrillo RA, White BH, Keshishian H (2005) Dissection of synaptic excitability phenotypes by using a dominant-negative Shaker K⁺ channel subunit. *Proc Natl Acad Sci U S A* 102: 3477-3482.
12. White BH, Osterwalder TP, Yoon KS, Joiner WJ, Whim MD, Kaczmarek LK, Keshishian H (2001) Targeted attenuation of electrical activity in *Drosophila* using a genetically modified K(+) channel. *Neuron* 31: 699-711.
13. Yasuyama K, Salvaterra PM (1999) Localization of choline acetyltransferase-expressing neurons in *Drosophila* nervous system. *Microsc Res Tech* 45: 65-79.

Chapter IV

14. McGuire SE, Roman G, Davis RL (2004) Gene expression systems in *Drosophila*: a synthesis of time and space. Trends Genet 20: 384-391.
15. Kitamoto T (2002) Targeted expression of temperature-sensitive dynamin to study neural mechanisms of complex behavior in *Drosophila*. J Neurogenet 16: 205-228.
16. Reiff DF, Ihring A, Guerrero G, Isacoff EY, Joesch M, Nakai J, Borst A (2005) *In vivo* performance of genetically encoded indicators of neural activity in flies. J Neurosci 25: 4766-4778.
17. De Camilli P, Takei K, McPherson PS (1995) The function of dynamin in endocytosis. Curr Opin Neurobiol 5: 559-565.
18. Urrutia R, Henley JR, Cook T, McNiven MA (1997) The dynamins: redundant or distinct functions for an expanding family of related GTPases? Proc Natl Acad Sci U S A 94: 377-384.
19. Grigliatti TA, Hall L, Rosenbluth R, Suzuki DT (1973) Temperature-sensitive mutations in *Drosophila melanogaster*. XIV. A selection of immobile adults. Mol Gen Genet 120: 107-114.

V. A method for the genetic silencing of nicotinic acetylcholine receptors on the CCAP neurons of *Drosophila*

Vömel M and Wegener C. (2008).

Background	97
Results and Discussion	98
α -BgT inhibits the ACh-induced calcium increase in most but not all CCAP neurons	98
Tethered α -BgT for silencing nAChRs in CCAP neurons <i>in vivo</i>	98
Perspectives.....	99
Methods	100
Fly strains	100
Cell culture and calcium imaging.....	100
References.....	100

A method for the genetic silencing of nicotinic acetylcholine receptors on the CCAP neurons of *Drosophila*

Matthias Vömel and Christian Wegener

Background

We recently provided evidence that crustacean cardioactive peptide expressing neurons (N_{CCAP}) of the *Drosophila* larval ventral ganglion (VG) express functional acetylcholine (ACh) receptors (AChRs) [1]. In short-term culture, almost all N_{CCAP} showed an increase of the free intracellular calcium concentration ($[Ca^{2+}]_i$) upon application of the nicotinic AChR agonist nicotine, while only few N_{CCAP} responded to the muscarinic AChR (mAChR) agonist pilocarpine [1]. Thus, like several other peptidergic neurons of the larval VG [2], N_{CCAP} appear to primarily receive cholinergic input via nicotinic AChRs (nAChRs). It is unclear, however, whether cholinergic input actually influences the secretory activity of N_{CCAP} .

To approach this question, we intended to specifically turn off the ACh-induced $[Ca^{2+}]_i$ -rises in the N_{CCAP} . Both pre- and postsynaptic manipulations can be used to suppress cholinergic input to N_{CCAP} , but most of the applicable genetic tools target the neurotransmitter release machinery at the presynapse. Particularly powerful, for example, is the targeted expression of a temperature-sensitive dynamin protein that allows transient inhibition of synaptic vesicle release *in vivo* (see [3]; Chapter IV). Other approaches are based on the targeted expression of ion channels (such as $K_{ir}2.1$ or EKO), which alter the excitability of the target neuron [4], or naturally occurring toxins (such as botulinum or tetanus toxin), which cleave critical proteins in the transmitter release machinery (see [4,5]). However, all these tools do not allow specific modulation of cholinergic transmission and - even more importantly - can only be employed if the neurons which provide synaptic input to the target neuron(s) are known. Since afferent neurons of N_{CCAP} have not been identified so far, we decided to inhibit ACh-induced $[Ca^{2+}]_i$ -increases in N_{CCAP} by manipulating the reception of cholinergic signals at the postsynapse.

To disrupt cholinergic input to N_{CCAP} *in vivo*, we intended to permanently silence the nAChRs in the N_{CCAP} . The multitude of nAChR subunits and the uncertainty about the subunit composition of nAChRs in *Drosophila* (see [6,7]), however, greatly complicate direct genetic manipulations (“knock-out” or “knock-down”). Thus, we set out to identify competitive nAChR antagonists that effectively inhibit insect nAChRs and can be targeted to the N_{CCAP} by GAL4/UAS. Particularly interesting were the naturally occurring peptide toxins α -bungarotoxin (α -BgT) from the venomous snake *Bungarus multicinctus* and α -conotoxin Iml (α -CTx Iml) from the vermivorous cone snail *Conus imperialis*, since these toxins have been shown to block specific types of insect nAChRs (see [8–10]). In *Locusta migratoria*, for example, α -BgT nonselectively inhibited several types of nAChRs, whereas α -CTx Iml specifically blocked $\alpha 7$ -like nAChRs [8,11]. In *Periplaneta Americana*, α -CTx Iml

inhibited an α -BgT-insensitive nAChR [12]. Thus, we assumed that at least one of these toxins, either α -BgT or α -CTx ImI, would act as an antagonist on the nAChRs of N_{CCAP} .

While data on α -CTx ImI-sensitive nAChRs are missing for *Drosophila*, the first report on an α -BgT-sensitive nAChR has been published ~ 30 years ago [13]. Accordingly, α -BgT has been applied to block nAChRs *in vitro*, e.g. those on Kenyon cells [14,15] or cholinergic neurons [16]. α -BgT has also been used to block nAChRs on Kenyon cells *in situ* [17]. We here tested if systemic application of α -BgT or α -CTx ImI affects the ACh-induced $[Ca^{2+}]_i$ -increase in N_{CCAP} *in vitro*.

Results and Discussion

α -BgT inhibits the ACh-induced calcium increase in most but not all CCAP neurons

In a first set of Ca^{2+} -imaging experiments, we monitored the effect of ACh on $[Ca^{2+}]_i$ of acutely dissociated N_{CCAP} in the absence and presence of α -BgT. Initial application of 10 μ M ACh alone (- N_{CCAP} respond to ACh at a threshold concentration of 0.5 – 1 μ M; [1] -) induced a fast and strong rise of $[Ca^{2+}]_i$ in all N_{CCAP} tested (n=11; Figure 1). When the N_{CCAP} were exposed to 1 μ M α -BgT (- a dose commonly used for Ca^{2+} -imaging experiments; [14,16] -), a subsequent ACh application caused $[Ca^{2+}]_i$ -increases in only 5 of 11 (~ 45 %) N_{CCAP} (Figure 1). The remaining 6 (~ 55 %) N_{CCAP} did not respond to ACh or showed a highly reduced ACh-mediated $[Ca^{2+}]_i$ -increase in the presence of α -BgT. After α -BgT has been washed out, all N_{CCAP} again responded with $[Ca^{2+}]_i$ -rises upon ACh application, demonstrating that the N_{CCAP} were excitable during the complete experiments. These results show that α -BgT can prevent ACh-dependent $[Ca^{2+}]_i$ -increases in some but not all N_{CCAP} . Noteworthy, N_{CCAP} which showed ACh-induced $[Ca^{2+}]_i$ -increases in the presence of α -BgT, also responded to the mAChR agonist pilocarpine (Figure 1). Thus, some N_{CCAP} appear to exclusively express α -BgT-sensitive nAChR, whereas other N_{CCAP} seem to express muscarinic AChRs - probably in combination with nAChRs [1].

In a second set of Ca^{2+} -imaging experiments, we tested whether α -CTx ImI also acts as a competitive antagonist on nAChRs of N_{CCAP} . In all N_{CCAP} tested (n=3), application of 1 μ M α -CTx ImI did not inhibit ACh-induced $[Ca^{2+}]_i$ -increases (data not shown). Consequently, N_{CCAP} seem to express α -CTx ImI-insensitive nAChRs.

We did not investigate if α -BgT specifically inhibits nicotine-induced $[Ca^{2+}]_i$ -rises in N_{CCAP} , because N_{CCAP} strongly desensitize upon repeated application of nicotine (data not shown; [1]).

Tethered α -BgT for silencing nAChRs in CCAP neurons *in vivo*

Since α -BgT effectively inhibited nAChRs of N_{CCAP} *in vitro*, we decided to ectopically express α -BgT in the N_{CCAP} to investigate if cholinergic input through nAChRs is necessary for a regular secretory activity of N_{CCAP} . panneuronal expression of α -BgT is not sufficiently disruptive to cholinergic transmission [18] we intended to apply the “tethered toxin approach” by Ibañez-Tallon et al. [19]. In this approach, a naturally occurring neurotoxin is fused to the lynx1 GPI membrane anchor to irreversibly inhibit the corresponding target receptor

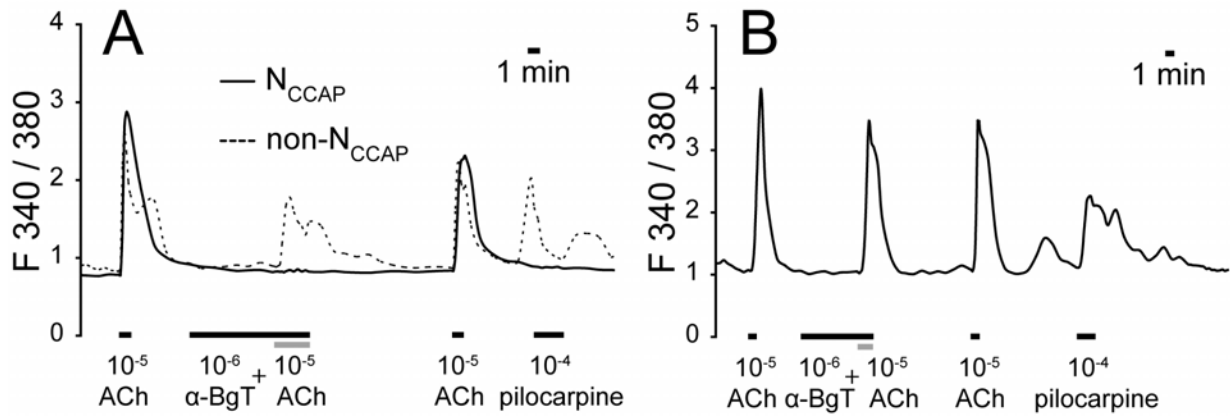


Figure 1: Responses of N_{CCAP} to ACh in the absence and presence of α -BgT.

(A) Original traces from Ca^{2+} -imaging experiments showing the $[Ca^{2+}]_i$ -responses of a N_{CCAP} (solid line) and a non- N_{CCAP} (dashed line). Application of α -BgT inhibited the ACh-induced $[Ca^{2+}]_i$ -increase in the N_{CCAP} , but not in the non- N_{CCAP} . Noteworthy, the non- N_{CCAP} responded to the mACh receptor agonist pilocarpine. (B) A N_{CCAP} showed an ACh-induced $[Ca^{2+}]_i$ -rise in the presence of α -BgT, and also responded to pilocarpine. Bars below the traces indicate the time drugs were present in the bathing solution. Concentrations are given in M.

in a cell-autonomous manner [19]. By combining the “tethered toxin approach” with the GAL4/UAS system, we planned to specifically silence the nAChR-dependent processes in the N_{CCAP} .

Recently, our collaborating partner Justin Blau (New York University, NY) generated a cDNA construct encoding a membrane-tethered α -BgT and introduced the respective construct into the *Drosophila* genome under UAS control (unpublished). The corresponding transgenic flies were used to express tethered α -BgT in the visual system of *Drosophila* larvae and - as expected - the tethered α -BgT disrupted cholinergic transmission (personal communication J. Blau). Accordingly, tethered α -BgT also promises to be helpful for the genetic silencing of the nAChRs on the N_{CCAP} .

Perspectives

We showed that N_{CCAP} in the *Drosophila* VG express α -BgT-sensitive nAChRs. Since α -BgT completely inhibited ACh-induced $[Ca^{2+}]_i$ -increases in at least some N_{CCAP} , we intend to use transgenic flies expressing tethered α -BgT under control of the UAS promotor to specifically disrupt the cholinergic input via nAChRs to N_{CCAP} *in vivo*. Unfortunately, we currently do not have the legal permission to keep or perform experiments with tethered α -BgT-expressing flies at the Philipps-Universität Marburg. Provided that we can get the legal permission to use tethered α -BgT-expressing flies, we will examine whether nAChRs are necessary for a regular secretory activity of N_{CCAP} .

Acknowledgments

We thank Justin Blau for collaboration on tethered α -BgT-expressing flies, Renate Renkawitz-Pohl for providing fly housing, and Uwe Homberg for general support. This work was supported by the Deutsche Forschungsgemeinschaft (DFG We 2652/2-2,3) to CW.

Methods

Fly strains

Ca²⁺-imaging experiments were performed with N_{CCAP} from L3 larvae expressing CCAP-GAL4-driven UAS-GFP.S65T. These larvae were generated by crossing flies of a CCAP-GAL4 strain ([20]; kind gift of J. Ewer, Cornell, NY) with flies of a w⁺;P(w⁺mC=UAS-GFP.S65T)T10 strain (Bloomington Stock Center, donated by C. Goodman). Flies were raised at 18 or 25°C on standard cornmeal agar medium and yeast under a 12:12 h light:dark regime.

Cell culture and calcium imaging

Cell dissociation and culture were performed as previously described [1]. Prior to Ca²⁺-imaging, neurons were incubated for 30 min in 1 ml sterile Leibovitz L-15 medium (PAA, Cölbe, Germany) containing 10 % heat-treated fetal calf serum, 12 mg/ml mannitol, and 2 µM Fura-2 acetoxymethylester (Molecular Probes, Leiden, The Netherlands). Neurons were washed for 5 min with standard J+J saline [21] containing (in mM): 128 NaCl, 2 KCl, 4 MgCl₂, 1.26 CaCl₂, 36 Sucrose, and 5 HEPES, pH 7.1. Then, saline was exchanged for J+J saline with 0.18 mM CaCl₂, and neurons were kept for ~ 35 min in the dark. N_{CCAP} were identified by GFP-expression and imaging was started. In each imaging experiment, N_{CCAP} were exposed three times to 10 µM ACh. After the first application of ACh (, which served as a control), N_{CCAP} were incubated for 6 min in standard J+J saline containing 1 µM α-BgT or α-CTx ImI (purchased from Sigma-Aldrich). To examine if α-BgT or α-CTx ImI prevents the ACh-induced [Ca²⁺]_i-rise in the N_{CCAP}, 1 ml standard J+J saline containing 10 µM ACh and 1 µM α-BgT or α-CTx ImI was added. In case the N_{CCAP} did not immediately show an increase of [Ca²⁺]_i, it was kept for at least 3 min in the saline containing both the ACh and the toxin. Thereafter, N_{CCAP} were thoroughly washed, and ACh was applied for a third time (as a control). Solutions were pipetted directly into the bath. Imaging data were processed using OpenLab 4.0 software (Improvision, Warwick, UK), Microsoft Excel, and Adobe Illustrator CS (Adobe Systems Inc., San Jose, CA).

References

1. Vömel M, Wegener C (2007) Neurotransmitter-induced changes in the intracellular calcium concentration suggest a differential central modulation of CCAP neuron subsets in *Drosophila*. *Dev Neurobiol* 67: 792-808.
2. Wegener C, Hamasaka Y, Nässel DR (2004) Acetylcholine increases intracellular Ca²⁺ via nicotinic receptors in cultured PDF-containing clock neurons of *Drosophila*. *J Neurophysiol* 91: 912-923.
3. Kitamoto T (2002) Conditional disruption of synaptic transmission induces male-male courtship behavior in *Drosophila*. *Proc Natl Acad Sci U S A* 99: 13232-13237.
4. White B, Osterwalder T, Keshishian H (2001) Molecular genetic approaches to the targeted suppression of neuronal activity. *Curr Biol* 11: R1041-R1053.
5. Martin JR, Keller A, Sweeney ST (2002) Targeted expression of tetanus toxin: a new tool to study the neurobiology of behavior. *Adv Genet* 47: 1-47.
6. Jones AK, Brown LA, Sattelle DB (2007) Insect nicotinic acetylcholine receptor gene families: from genetic model organism to vector, pest and beneficial species. *Invert Neurosci* 7: 67-73.
7. Sattelle DB, Jones AK, Sattelle BM, Matsuda K, Reenan R, Biggin PC (2005) Edit, cut and paste in the nicotinic acetylcholine receptor gene family of *Drosophila melanogaster*. *Bioessays* 27: 366-376.
8. McIntosh JM, Santos AD, Olivera BM (1999) *Conus* peptides targeted to specific nicotinic acetylcholine receptor subtypes. *Annu Rev Biochem* 68: 59-88.
9. Tomizawa M, Casida JE (2001) Structure and diversity of insect nicotinic acetylcholine receptors. *Pest Manag Sci* 57: 914-922.

10. Tomizawa M, Millar NS, Casida JE (2005) Pharmacological profiles of recombinant and native insect nicotinic acetylcholine receptors. *Insect Biochem Mol Biol* 35: 1347-1355.
11. van den Beukel I, van Kleef RGDM, Zwart R, Oortgiesen M (1998) Physostigmine and acetylcholine differentially activate nicotinic receptor subpopulations in *Locusta migratoria* neurons. *Brain Res* 789: 263-273.
12. Courjaret R, Lapied B (2001) Complex intracellular messenger pathways regulate one type of neuronal alpha-bungarotoxin-resistant nicotinic acetylcholine receptors expressed in insect neurosecretory cells (dorsal unpaired median neurons). *Mol Pharmacol* 60: 80-91.
13. Dudai Y (1977) Demonstration of an alpha-bungarotoxin-binding nicotinic receptor in flies. *FEBS Lett* 76: 211-213.
14. Campusano JM, Su H, Jiang SA, Sicaeros B, O'Dowd DK (2007) nAChR-mediated calcium responses and plasticity in *Drosophila* Kenyon cells. *Dev Neurobiol* 67: 1520-1532.
15. Su H, O'Dowd DK (2003) Fast synaptic currents in *Drosophila* mushroom body Kenyon cells are mediated by alpha-bungarotoxin-sensitive nicotinic acetylcholine receptors and picrotoxin-sensitive GABA receptors. *J Neurosci* 23: 9246-9253.
16. Jepson JE, Brown LA, Sattelle DB (2006) The actions of the neonicotinoid imidacloprid on cholinergic neurons of *Drosophila melanogaster*. *Invert Neurosci* 6: 33-40.
17. Gu H, O'Dowd DK (2006) Cholinergic synaptic transmission in adult *Drosophila* Kenyon cells *in situ*. *J Neurosci* 26: 265-272.
18. Yang H, Kunes S (2004) Nonvesicular release of acetylcholine is required for axon targeting in the *Drosophila* visual system. *Proc Natl Acad Sci U S A* 101: 15213-15218.
19. Ibañez-Tallon I, Wen H, Miwa JM, Xing J, Tekinay AB, Ono F, Brehm P, Heintz N (2004) Tethering naturally occurring peptide toxins for cell-autonomous modulation of ion channels and receptors *in vivo*. *Neuron* 43: 305-311.
20. Park JH, Schroeder AJ, Helfrich-Förster C, Jackson FR, Ewer J (2003) Targeted ablation of CCAP neuropeptide-containing neurons of *Drosophila* causes specific defects in execution and circadian timing of ecdysis behavior. *Development* 130: 2645-2656.
21. Jan LY, Jan YN (1976) Properties of the larval neuromuscular junction in *Drosophila melanogaster*. *J Physiol* 262: 189-214.

VI. Venus-tagged peptides for the visualization of neuropeptide transport and release in *Drosophila*

Vömel M and Wegener C. (2008).

Background	105
Results and Discussion	106
Structure of preproANF- and preproCAPA-1-Venus	106
Generation of preproANF- and preproCAPA-1-Venus expressing flies	107
ANF- and CAPA-1-Venus localize to peptidergic vesicles	107
PreproANF- and preproCAPA-1-Venus are processed in peptidergic <i>Drosophila</i> neurons	108
PreproANF-EMD is differentially cleaved in <i>Drosophila</i> neurons	111
PreproANF- and preproCAPA-1-Venus accumulate at peptide release sites	114
Perspectives	114
Methods	116
Plasmid construction	116
Fly strains	116
Immunocytochemistry and microscopy	117
Western blot analysis	117
References	118

Venus-tagged peptides for the visualization of neuropeptide transport and release in *Drosophila*

Matthias Vömel and Christian Wegener

Background

Neuropeptides are neuronal signaling molecules that regulate diverse physiological processes such as growth, ion homeostasis, learning, memory, reproduction, and circadian rhythmicity in both vertebrates and invertebrates. They are synthesized in the neuron soma as prepropeptides, processed to propeptides in the endoplasmic reticulum, and transported in vesicles from the trans-Golgi network to sites of secretion. At the release sites, exocytosis of peptidergic vesicles requires an increase of the free intracellular calcium concentration ($[Ca^{2+}]_i$) and typically occurs over minutes in response to repetitive depolarization. Accordingly, several *in vitro* and *in situ* studies relied on calcium imaging to identify potential release factors of peptidergic *Drosophila* neurons [1–5]. It is unknown, however, whether such putative release factors indeed influence the secretory activity of peptidergic neurons.

One possibility to test a presumed peptide release factor is to visualize its effect on the peptidergic vesicles of the target neuron. If the putative peptide release factor prompts the target neuron to release its peptides, the amount of visible peptidergic vesicles should decrease. Previously, Burke et al. [6] generated a fusion protein composed of the rat atrial natriuretic factor prepropeptide (preproANF) and the green fluorescent protein emerald green (EMD). The resulting preproANF-EMD allowed direct detection of peptidergic vesicles in cultured neurosecretory cells [7–12]. In transgenic flies expressing preproANF-EMD under UAS control [13], preproANF-EMD appeared to be processed, transported, and released like an endogenous *Drosophila* neuropeptide [14]. Consequently, several studies used preproANF-EMD to monitor peptide release from the neuromuscular junction [15–18], the female genital tract [19], circadian clock neurons [20,21], or neurons involved in ecdysis [21]. With preproANF-EMD, however, it is difficult to monitor peptide release in neurons that secrete small amounts of vesicles, since these neurons lack an obvious decrease in EMD fluorescence. Thus, the visualization of peptide release highly depends on the properties of the fluorophore in the reporting peptide fusion.

We here describe the generation and the characteristics of two peptide fusions that are based on the improved yellow fluorescent protein variant Venus [22]. Compared to enhanced green fluorescent protein (eGFP), Venus matures more efficiently and shows an about 10 times higher fluorescence intensity in the acidic environment of mammalian peptidergic vesicles [22]. Since secretory vesicles at the *Drosophila* neuromuscular junction are nearly neutral [23], Venus and eGFP may exhibit only slight differences in the fluorescence intensity when targeted to peptidergic *Drosophila* neurons. However, because excitation of Venus at ~ 514 nm causes less auto-fluorescence of surrounding tissue (e.g. the cuticle) than excitation of eGFP/EMD at ~ 487 nm, Venus-tagged peptide fusion proteins promise an improved “signal-to-noise” ratio for imaging peptidergic vesicles *in vivo*.

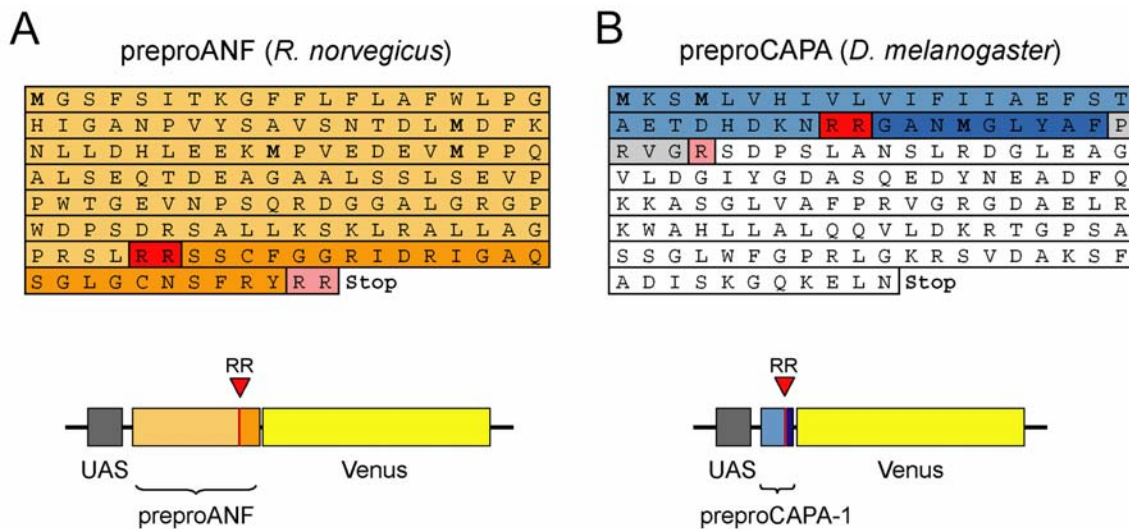


Figure 1. Structure of preproANF- and preproCAPA-1-Venus.

(A) Amino acid sequence of preproANF (top) and schematic representation of the corresponding preproANF-Venus transgene (bottom). The transgene comprises five UAS elements (grey) and the cDNA encoding the signal peptide and amino-terminal part of preproANF (beige), the amino-terminal processing site of ANF (red), the putative ANF peptide (orange), and Venus (yellow). To prevent proteolytical splitting of the preproANF-Venus fusion protein, the nucleotides encoding the carboxy-terminal processing site of ANF (pink) are not included in the transgene. (B) Amino acid sequence of preproCAPA (top) and schematic representation of the preproCAPA-1-Venus transgene (bottom). The transgene comprises five UAS elements (shown as one in grey) and the cDNA encoding the signal peptide and amino-terminal part of preproCAPA (light-blue), the amino-terminal processing site of CAPA-1 (red), a large part of the putative CAPA-1 peptide (dark-blue), and Venus (yellow). The nucleotides which encode the amino acids PRVG (light-grey) at the carboxyl terminus of CAPA-1, the adjacent processing site (pink), and the remaining preproCAPA part (white) are not included in the transgene.

Results and Discussion

Structure of preproANF- and preproCAPA-1-Venus

We generated two peptide-Venus fusion constructs: Analogous to preproANF-EMD, the first construct is composed of rat preproANF (gi|158341690) fused to Venus (Figure 1). Since the *Drosophila* genome does not contain any peptide with significant sequence similarity to ANF [14], preproANF-Venus, like preproANF-EMD, was predicted to have no deleterious effect when expressed panneurally. However, previous findings suggested that preproANF-EMD might interfere with the secretion of endogenous neuropeptides [21]. Thus, we generated a second construct composed of the *Drosophila* preproCAPA-1 and the Venus cDNA (Figure 1). The resulting preproCAPA-1-Venus fusion has a considerably smaller size than preproANF-Venus (Figure 1), and hence might influence endogenous peptide release to a lesser extent. As opposed to preproANF-Venus, preproCAPA-1-Venus is based on the endogenous *Drosophila* CAPA precursor (encoded by the *capability* gene; CG15520). Consequently, preproCAPA-1-Venus should be fully processed to CAPA-1-Venus, when expressed in the *Drosophila* CNS.

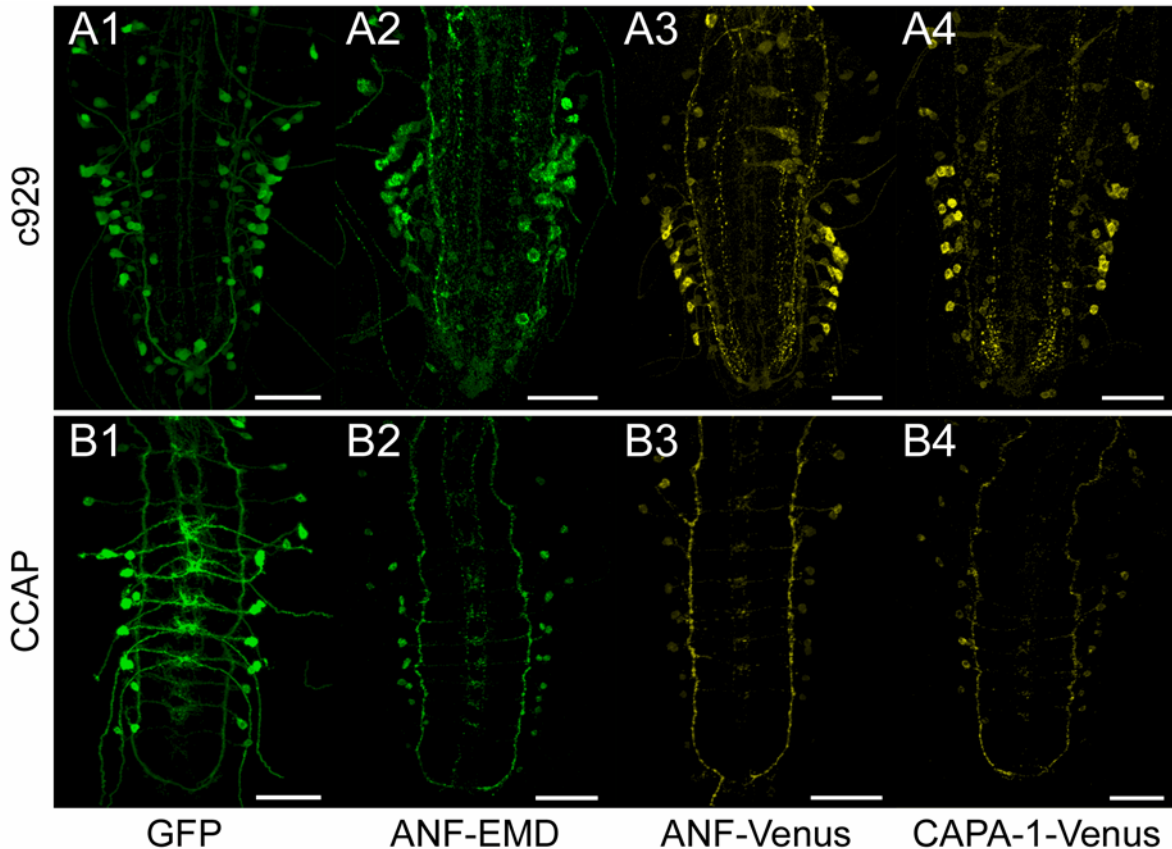


Figure 2. Targeted expression of GFP, preproANF-EMD, preproANF- and preproCAPA-1-Venus in c929- and CCAP-GAL4 expressing neurons of the *Drosophila* larval ventral ganglion.

(A1-4) Confocal images showing the GFP immunoreactivity in the VG of larvae expressing c929-GAL4-driven GFP (A1), preproANF-EMD (A2), preproANF-Venus (A3), and preproCAPA-1-Venus (A4). (B1-4) GFP immunoreactivity in larvae expressing CCAP-GAL4-driven GFP (B1), preproANF-EMD (B2), preproANF-Venus (B3), and preproCAPA-1-Venus (B4). Ectopically expressed GFP uniformly labels somata and neurites. In contrast, expression of preproANF-EMD, preproANF-Venus, and preproCAPA-1-Venus results in a punctate labeling pattern (see text for details). Scale bars: 50 μ m.

Generation of preproANF- and preproCAPA-1-Venus expressing flies

To target the expression of preproANF- and preproCAPA-1-Venus to specific peptidergic neurons, we introduced the corresponding cDNA constructs into the *Drosophila* genome under UAS control [13]. Then, we established homozygous fly strains and determined the chromosomal locations of the inserted cDNA constructs. To increase the ectopical expression of preproANF- and preproCAPA-1-Venus, we also generated transgenic flies that carry the respective cDNA constructs on both the first and second chromosome.

ANF- and CAPA-1-Venus localize to peptidergic vesicles

To examine if UAS-driven preproANF- and preproCAPA-1-Venus mature properly and emit fluorescence in peptidergic *Drosophila* neurons, the respective fusions were targeted to c929-GAL4- (*dimmed*; [24–26]) and CCAP-GAL4 expressing neurons [27] in the third instar larval CNS. The distribution patterns of c929- and CCAP-GAL4-driven GFP or preproANF-EMD served as controls. The c929-GAL4 driver induces gene

expression in ~ 200 neurosecretory cells that produce several amidated neuropeptides and peptide hormones [24,25]. CCAP-GAL4 restricts gene expression to ~ 50 neurons that synthesize crustacean cardioactive peptide (CCAP) and partly co-express myoinhibiting peptides or bursicon [3,4,27,28]. Both CCAP and bursicon play important roles for ecdysis [27,29].

In the larval ventral ganglion (VG), c929- and CCAP-GAL4-driven GFP uniformly labeled somata and neurites (Figure 2). In contrast, c929- and CCAP-GAL4-driven preproANF- or preproCAPA-1-Venus localized as fluorescent punctae to somata and neuronal projections, and showed a labeling pattern similar to that of c929- and CCAP-GAL4-driven preproANF-EMD (Figure 2). When targeted to c929-GAL4 expressing neurons, preproANF- and preproCAPA-1-Venus primarily labeled somata, longitudinal intermedial and lateral tracts, and the thoracic perisymphathetic organs. The abdominal neuromeres a6-7 contained a particularly high concentration of fluorescent punctae in the lateral neuropil, whereas the neuropil at the tip of the VG (“terminal plexus”) showed only faint preproANF- and preproCAPA-1-Venus labeling (Figure 2). In CCAP-GAL4 expressing neurons, preproANF- and preproCAPA-1-Venus localized in punctate patterns to somata, segmentally reiterated neurite arborizations in the central neuropil, and in a particularly high concentration to lateral longitudinal tracts (Figure 2). Thus, preproANF- and preproCAPA-1-Venus showed the same distribution as CCAP-GAL4-driven preproANF-EMD [21] and CCAP immunoreactivity [4,27,30]. The high concentration of preproANF- and preproCAPA-1-Venus in lateral tracts corresponds to the finding that these tracts represent major peptide release sites during pupal ecdysis [21]. Furthermore, in both the c929- and CCAP-GAL4 expressing neurons, the distribution of preproANF- and preproCAPA-1-Venus mimicked that of ectopically expressed synaptobrevin-eGFP [31]. Since synaptobrevin-eGFP locates to the membrane of several types of secretory vesicles [31–33], both preproANF- and preproCAPA-1-Venus appear to accumulate in peptidergic vesicles.

PreproANF- and preproCAPA-1-Venus are processed in peptidergic *Drosophila* neurons

The detection of fluorescent punctae in peptidergic neurites indicated that both preproANF- and preproCAPA-1-Venus were packaged into peptidergic vesicles. Thus, the overall structural features of preproANF- and preproCAPA-1-Venus were recognized by the sorting machinery, and some type of processing occurred. Since the *Drosophila* genome does not encode any peptide precursor with analogy to preproANF [14], we wondered whether preproANF-Venus is completely processed to ANF-Venus. As opposed to preproANF-Venus, preproCAPA-1-Venus is based on the endogenous *Drosophila* CAPA precursor. Accordingly, at least some neurons of the *Drosophila* CNS should be able to convert preproCAPA-1-Venus to CAPA-1-Venus.

To investigate the proteolytical processing of preproANF- and preproCAPA-1-Venus in peptidergic *Drosophila* neurons, we performed Western blots with CNS extracts from larvae expressing c929-GAL4-driven preproANF- or preproCAPA-1-Venus, and three control groups: The first group carried the c929-GAL4 driver, but lacked the reporting UAS-preproANF- or CAPA-1-Venus transgene. The second group carried the UAS-preproANF- or CAPA-1-Venus transgene, but lacked a source of GAL4 to drive its expression. The last group expressed c929-GAL4-driven GFP, which was used as a specificity control for the GFP immunolabeling.

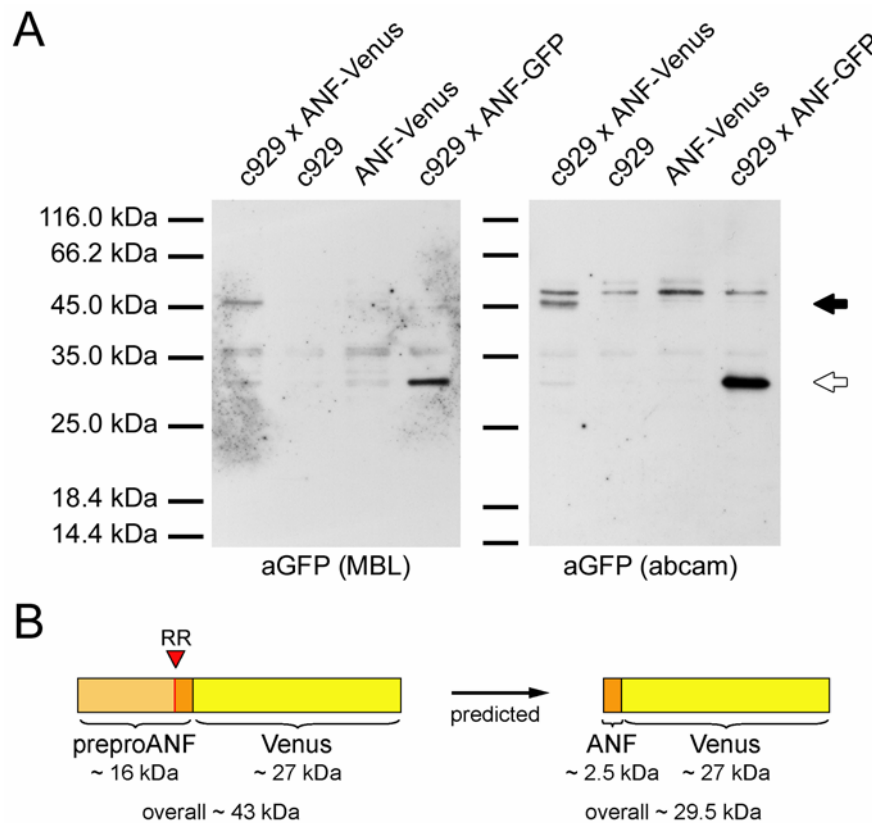


Figure 3. Western blot of CNS extracts from larvae expressing preproANF-Venus.

(A) aGFP (MBL, left)- and aGFP (abcam, right)-immunoreactive protein fractions in the CNS extracts from larvae expressing c929-GAL4-driven preproANF-Venus and controls carrying only the c929-GAL4 or the UAS-preproANF-Venus transgene, or expressing c929-GAL4-driven GFP. Both GFP antisera specifically labeled a protein fraction of ~46 kDa (black arrow) in the CNS extracts from larvae expressing c929-GAL4-driven preproANF-Venus, and a fraction of ~30 kDa (white arrow) in the CNS extracts from larvae expressing c929-GAL4-driven GFP (see text for details). (B) Schematic representation of the putative preproANF-Venus fusion protein and its predicted proteolytical fragment ANF-Venus. The fusion comprises the signal peptide and amino-terminal part of preproANF (beige), the amino-terminal processing site of ANF (red), the putative ANF peptide (orange), and the Venus fluorophore (yellow).

Since GFP (~27 kDa) has approximately the same molecular weight (MW) as fully processed ANF (~29.5 kDa) and CAPA-1-Venus (~28 kDa), we used GFP as a MW reference in the Western blots. To avoid misleading interpretations due to unspecific GFP immunolabeling, we probed all blots with two aliquots of each CNS extract, and then applied two different rabbit-anti-GFP sera, aGFP (MBL) and aGFP (abcam), to detect the GFP-immunoreactive proteins in the respective samples.

In CNS extracts from larvae expressing c929-GAL4-driven preproANF-Venus, both aGFP sera labeled a protein fraction of ~46 kDa that was missing in the CNS extracts from the control larvae (Figure 3). The ~46 kDa fraction had about the predicted MW of the proANF-Venus fusion protein (~43 kDa; proANF ~16 kDa, Venus ~27 kDa), and the same MW as a GFP-immunoreactive protein fraction in the extract from PC12 cells transfected with preproANF-eGFP [6]. A protein fraction with the predicted MW of ANF-Venus (~29.5 kDa) could not be detected (Figure 3). The GFP antisera instead labeled other protein fractions of ~48 or 36 kDa.

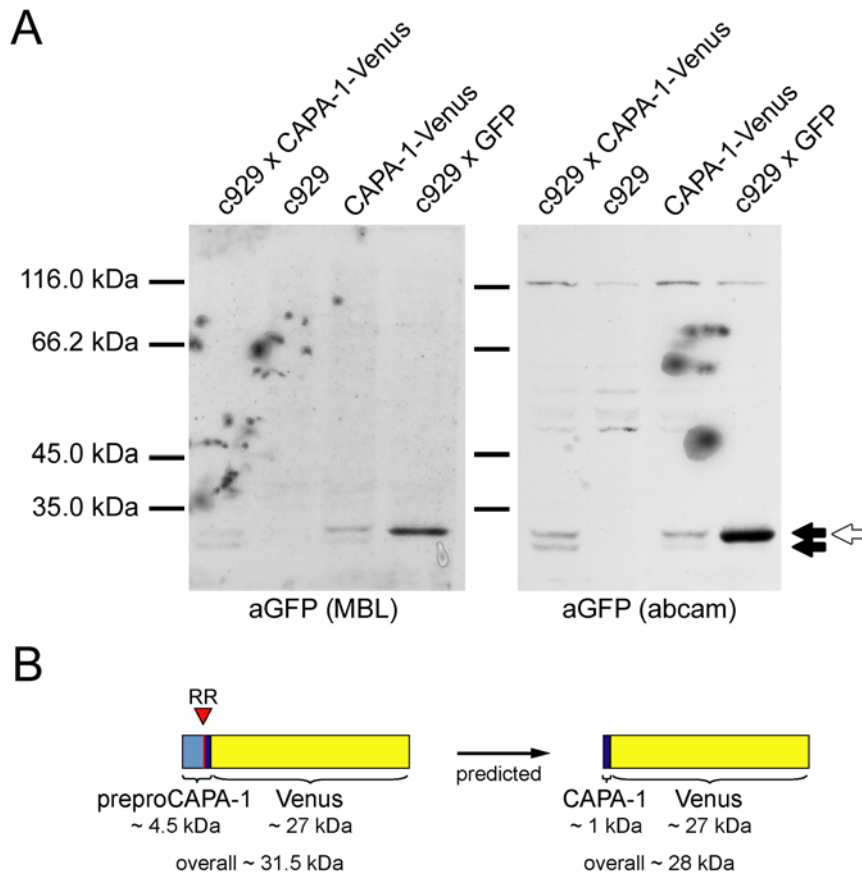


Figure 4. Western blot of CNS extracts from larvae expressing *preproCAPA-1-Venus*.

(A) aGFP (MBL, left)- and aGFP (abcam, right)-immunoreactive protein fractions in the CNS extracts from larvae expressing c929-GAL4-driven *preproCAPA-1-Venus* and controls carrying only the c929-GAL4 or the UAS-*preproCAPA-1-Venus* transgene, or expressing c929-GAL4-driven GFP. Both GFP antisera specifically labeled two protein fraction of ~ 31 and 28 kDa (black arrows) in the CNS extracts from larvae expressing c929-GAL4-driven *preproCAPA-1-Venus*, and a fraction of ~ 30 kDa (white arrow) in the CNS extracts from larvae expressing c929-GAL4-driven GFP (see text for details). (B) Schematic representation of the putative *preproCAPA-1-Venus* fusion protein and its predicted proteolytical fragment *CAPA-1-Venus*. The fusion comprises the signal peptide and amino-terminal part of *preproCAPA-1* (light-blue), the amino-terminal processing site of *CAPA-1* (red), a large part of the putative *CAPA-1* peptide (dark-blue), and the Venus fluorophore (yellow).

These fractions, however, also occurred in the CNS extracts from control larvae. Consequently, the ~ 48 or 36 kDa protein fractions did not contain a proteolytical fragment of *preproANF-Venus*. In CNS extracts from control larvae expressing c929-GAL4-driven GFP, both GFP antisera strongly labeled a protein fraction of ~ 30 kDa. This fraction was missing in the CNS extract from larvae carrying only the c929-GAL4 or the *preproANF-Venus* transgene, or expressing c929-GAL4-driven *preproANF-Venus* (Figure 3). Thus, the ~ 30 kDa likely derived from GFP, which has a predicted MW of ~ 27 kDa. Taken together, in c929-GAL4 expressing neurons, *preproANF-Venus* appeared to be processed to *proANF-Venus*, but not to the final *ANF-Venus* fusion protein.

In CNS extracts from larvae expressing c929-GAL4-driven preproCAPA-1-Venus, both GFP antisera strongly labeled two protein fractions of ~ 31 and 28 kDa. These fractions were missing in the CNS extracts from control larvae carrying only the c929-GAL4 driver. However, the ~ 31 and 28 kDa protein fractions were present in the CNS extracts from control larvae carrying the UAS-preproCAPA-1-Venus transgene alone, probably due to background expression of the transgene (Figure 4). While the ~ 31 kDa fraction had the predicted MW of proCAPA-1 (~ 4.5 kDa) fused to Venus (~ 27 kDa), the ~ 28 kDa fraction had the predicted MW of CAPA-1-Venus. Both protein fractions also showed approximately the same MW as the highly GFP-immunoreactive ~ 30 kDa protein fraction in the CNS extracts from larvae expressing c929-GAL4-driven GFP (Figure 4). Besides the putative proCAPA-1-Venus, CAPA-1-Venus, and GFP, the GFP antisera labeled several other protein fractions of ~ 48, 50, 55 or 117 kDa. These fractions were present in all CNS extracts including those of the control groups, and hence did not come from a proteolytical fragment of preproCAPA-1-Venus (Figure 4). Thus, at least in the c929-GAL4 expressing neurons, the preproCAPA-1-Venus fusion appeared to be processed to proCAPA-1-Venus as well as CAPA-1-Venus.

PreproANF-EMD is differentially cleaved in *Drosophila* neurons

In c929-GAL4 expressing neurons, preproANF-Venus appeared to be processed into one proteolytical fragment of ~ 46 kDa, the proANF-Venus fusion. However, previous findings suggested that preproANF-EMD gives rise to three proteolytical fragments of 70, 41, and 26 kDa [14], when expressed in the whole nervous system of *Drosophila* larvae. Since the amino acid sequences and the overall structural features of preproANF-Venus and preproANF-EMD are almost identical, we wondered whether preproANF-Venus might give rise to three proteolytical fragments, when panneurally expressed. Vice versa, preproANF-EMD might be processed into a single proteolytic fragment, when targeted to the c929-GAL4 expressing neurons. To test these hypotheses, we performed Western blots with CNS extracts from larvae expressing preproANF-Venus or preproANF-EMD under control of the c929- and the embryonic lethal abnormal visual system (elav)-GAL4 driver [34], respectively. While c929-GAL4 restricts gene expression to several peptidergic neurons (see above), the elav-GAL4 driver was generated for targeting gene expression to all neurons of the *Drosophila* nervous system [34]. Thus, at least the CNS extracts from larvae expressing elav-GAL4-driven preproANF-Venus or preproANF-EMD should contain all possible proteolytic fragments of the respective peptide fusions.

In the CNS extracts from larvae expressing c929- or elav-GAL4-driven preproANF-Venus, the GFP (abcam) antiserum labeled two protein fractions of ~ 48 and 46 kDa (Figure 5). The ~ 48 kDa fraction was present in the CNS extracts from all larvae groups, including those expressing c929- or elav-GAL4-driven preproANF-EMD (Figure 5). Since a comparable protein fraction also occurred in the CNS extracts from control larvae either expressing the c929-GAL4 driver or the preproANF-Venus transgene alone (see above), the ~ 48 kDa fraction likely did not come from preproANF-Venus. In view of our previous results, only the ~ 46 kDa protein fraction appeared to contain a proteolytical fragment of preproANF-Venus. This fraction had about the predicted MW of proANF-Venus (~ 43 kDa). Therefore, all neurons of the *Drosophila* CNS which express the appropriate enzymes, appear to process preproANF-Venus to proANF-Venus, but do not process proANF-Venus to other proteolytical fragment such as ANF-Venus.

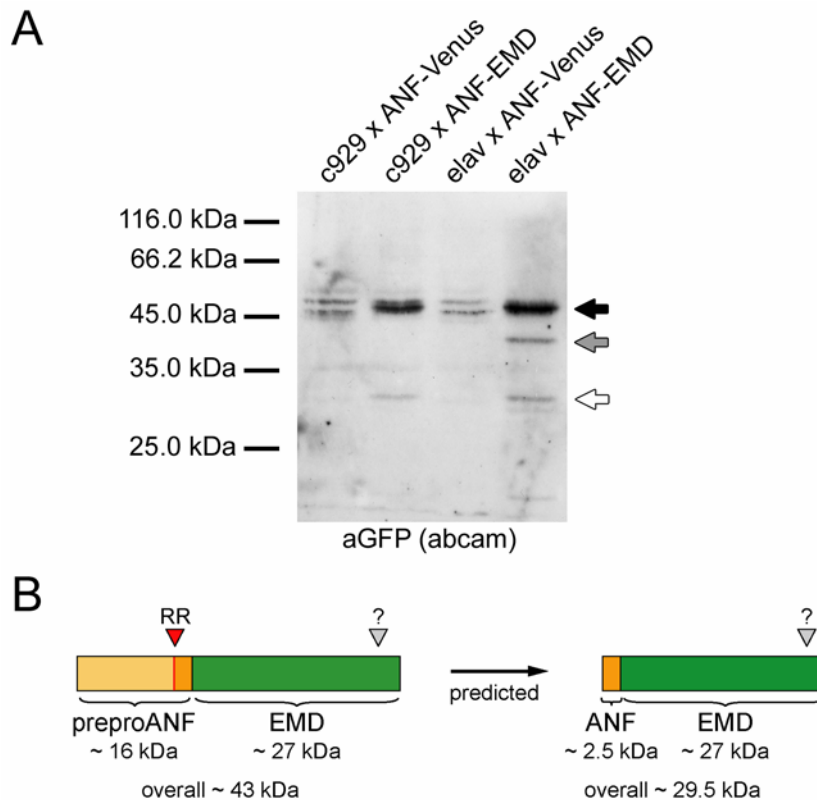


Figure 5. Western blot of CNS extracts from larvae expressing preproANF-Venus or preproANF-EMD in peptidergic neurons or all neurons of the larval CNS.

(A) aGFP (abcam)-immunoreactive protein fractions in the CNS extracts from larvae expressing c929- or elav-GAL4-driven preproANF-Venus and preproANF-EMD, respectively. The GFP antiserum specifically labeled a protein fraction of ~ 46 kDa (black arrow) in the CNS extracts from larvae expressing c929- or elav-GAL4-driven preproANF-Venus. However, two specific aGFP-immunoreactive protein fractions of ~ 47 and 30 kDa (white arrow) occurred in the CNS extracts from larvae expressing c929-GAL4-driven preproANF-EMD, whereas the CNS extracts from larvae expressing elav-GAL4-driven preproANF-EMD contained an additional fraction of ~ 40 kDa (grey arrow; see text for details). (B) Schematic representation of the putative preproANF-EMD fusion protein and its predicted proteolytical fragment ANF-EMD. The fusion comprises the signal peptide and amino-terminal part of preproANF-EMD (beige), the amino-terminal processing site of ANF (red), the putative ANF peptide (orange), and the EMD fluorophore (green). Note that the EMD protein may possess a proteolytical processing site at its carboxyl terminus (grey).

In the CNS extracts from larvae expressing c929-GAL4-driven preproANF-EMD, the GFP (abcam) antiserum strongly labeled three protein fractions of ~ 48, 47, and 30 kDa (Figure 5). Unlike the ~ 48 kDa protein fraction (see above), the ~ 47 and 30 kDa fractions appeared to contain proteolytical fragments of preproANF-EMD. However, the ~ 47 kDa fraction had a slightly higher MW than the fractions with the putative proANF-EMD and -Venus fusion proteins (~ 43 kDa). The ~ 30 kDa protein fraction had the predicted MW of the ANF-Venus fusion (~ 29.5 kDa). Thus, in the c929-GAL4 expressing neurons, preproANF-EMD appeared to be processed to proANF-EMD and ANF-EMD.

The CNS extracts from larvae expressing elav-GAL4-driven preproANF-EMD contained the three protein fractions observed in the CNS extracts from larvae expressing c929-GAL4-driven preproANF-EMD (see above)

EMD	1	MVSKGEELFTGVVPIVLVELDGDVNGHKFSVSGEGEGDATYGKLTLEFICTTGKLPVPWPT
Venus	1	MVSKGEELFTGVVPIVLVELDGDVNGHKFSVSGEGEGDATYGKLTLEFICTTGKLPVPWPT
consensus	1	*****
EMD	61	LVTTFYGVQCFARYPDHMRQHDFFKSAMPEGYVQERTIFFKDDGNYKTRAEVKFEGDTL
Venus	61	LVTTLGYGVQCFARYPDHMRQHDFFKSAMPEGYVQERTIFFKDDGNYKTRAEVKFEGDTL
consensus	61	****
EMD	121	VNRIELKGIDFKEDGNILGHKLEYNYNSHKVVYITADKQKNGIKVNFKTRHNIEDGSSVOLA
Venus	121	VNRIELKGIDFKEDGNILGHKLEYNYNSHNVYITADKQKNGIKANFKTRHNIEDGGSVOLA
consensus	121	*****
▽		
EMD	181	DHYQQNTPIGDGPVLLPDNHYLSYQSALS KDPNEKRDHMLLEFVTAAGITLGMDELYK
Venus	181	DHYQQNTPIGDGPVLLPDNHYLSYQSALS KDPNEKRDHMLLEFVTAAGITLGMDELYK
consensus	181	*****

Figure 6: Amino acid similarity between the EMD and the Venus fluorophore.

EMD and Venus differ at the amino acids 46, 64, 65, 79, 149, 163, 175, and 203. The carboxyl terminus of both EMD and Venus contains a putative processing site at 215R (grey triangle). Stars below the alignments indicate amino acids which are identical in EMD and Venus, while the point at amino acid 79 corresponds to a conservative change.

and an additional GFP-immunoreactive fraction of ~ 40 kDa (Figure 5). Thus, some neurons that are contained in the elav-GAL4, but not in the c929-GAL4 expression pattern, presumably express specific proteases that cleave preproANF-EMD. The resulting ~ 40 kDa fragment had a higher MW than the predicted proANF (~ 16 kDa) or EMD fragment (~ 27 kDa), or than the fully processed ANF-EMD fusion protein (~ 29.5 kDa), but a lower MW than proANF-EMD (, which has a predicted MW ~ 43 kDa, but showed ~ 47 kDa in the gel). Thus, the ~ 40 kDa fraction contained an unpredicted proteolytical fragment of preproANF-EMD. Noteworthy, a comparable protein fraction did not occur in the CNS extracts from larvae expressing elav-GAL4-driven preproANF-Venus (Figure 5). These findings suggest that prepro-ANF-EMD possesses a proteolytical cleavage site in the EMD part of the peptide fusion, while preproANF-Venus lacks a comparable site.

In comparison to Venus, EMD carries the amino acid substitutions L46F, L64F, G65T, R79K, N149K, A163V, G175S, and Y203T (Figure 6). Since the presumed truncated proANF-EMD had a MW of ~ 40 kDa, particularly the amino acids 175S and 203T in the EMD sequence might play a decisive role in the cleavage of elav-GAL4-driven proANF-EMD. Thus, we searched the EMD sequence for putative processing sites for prohormone convertases with the bio-informatics tool “NeuroPred” ([35]; UIUC Neuroproteomics Center on Cell to Cell Signaling, public domain: <http://neuroproteomics.scs.uiuc.edu/neuropred.html>). While potential processing sites could not be detected near 175S and 203T, the carboxyl terminus of EMD was predicted to contain a processing site at 215R (Figure 6). Proteolytical cleavage of EMD at this site should result in two fragments with the MW of ~ 24.5 and 2.5 kDa, respectively. Accordingly, processing of the preproANF-EMD fusion should produce a fragment of ~ 40.5 kDa comprising proANF (~ 16 kDa) and the large fragment of EMD (~ 24.5 kDa). However, the putative cleavage site at 215R is present in both the EMD and Venus protein, and hence can not account for the differential cleavage of elav-GAL4-driven preproANF-EMD and preproANF-Venus. Thus, the origin of the ~ 40 kDa GFP-immunoreactive protein fraction remains unclear.

Chapter VI

Based on the assumption that the ~ 40 kDa protein fraction in the CNS extracts from larvae expressing elav-GAL4-driven preproANF-EMD contains a truncated proANF-EMD fusion protein, two additional fragments should also occur: The first fragment should have a MW of ~ 22.5 kDa and comprise the fully processed ANF peptide (~ 2.5 kDa) fused to the truncated EMD protein (~ 20 kDa). Indeed, a weakly GFP-immunoreactive protein fraction with a MW of ~ 20 kDa occurred in the CNS extracts from larvae expressing elav-GAL4-driven preproANF-EMD. This fraction was missing in the CNS extracts from larvae expressing c929-GAL4-driven preproANF-EMD or c929-/elav-GAL4-driven preproANF-Venus (Fig. 5). Thus, the ~ 20 kDa fraction might contain the truncated ANF-EMD fusion protein. The second putative proteolytical fragment should comprise the carboxyl terminus of EMD, a protein of ~ 7 kDa. This fragment did not occur in the Western Blots, probably due to its low MW.

Taken together, our results suggest that preproANF-EMD is differentially cleaved in the nervous system of *Drosophila* larvae, whereas preproANF-Venus is not. At least in some neurons, the processing of preproANF-EMD appears to result in a peptide fusion with an incomplete EMD fluorophore. This so far unnoticed property of ANF-EMD might interfere with the visualization of peptidergic vesicles and the “signal-to-noise” ratio in live cell imaging experiments. Our results disagree with the previous finding of Rao et al. [14] that neurons expressing elav-GAL4-driven preproANF-EMD produce three proteolytical fragments of ~ 70, 41, and 26 kDa. Except for the ~ 41 kDa protein fraction, which likely came from an truncated proANF-EMD fusion protein, we observed totally different GFP-immunoreactive protein fractions (see above). However, the observed fractions fit better with the predicted fragments of proteolytically processed preproANF-EMD than those reported by Rao et al. [14].

PreproANF- and preproCAPA-1-Venus accumulate at peptide release sites

Our results suggested that the proteolytical fragments of preproANF- and preproCAPA-1-Venus localize to secretory vesicles. To investigate whether peptidergic vesicles containing preproANF- or preproCAPA-1-Venus are transported to secretory sites, we targeted the respective fusions to the CCAP-GAL4 expressing neurons and looked for fluorescent vesicles at the presumed neurohemal CCAP release sites at the body wall muscles [4,36]. In filleted larvae, both preproANF- and preproCAPA-1-Venus localized to the putative release sites of CCAP-GAL4 expressing neurites, while the neurites themselves contained only few fluorescent vesicles (Figure 7). Thus, the distribution patterns of preproANF- and preproCAPA-1-Venus correspond to that of preproANF-EMD (Figure 7). These results show that preproANF- and preproCAPA-1-Venus accumulate at the release sites of peptidergic neurons.

Perspectives

We generated two Venus-tagged peptide reporters, preproANF- and preproCAPA-1-Venus, and demonstrated that these reporters are expressed and transported as naturally occurring neuropeptides in larval peptidergic neurons of *Drosophila*. Our results further suggest that preproANF-Venus is processed to proANF-Venus, but not to ANF-Venus. Since preproCAPA-1-Venus appears to be completely processed, the CAPA-1-Venus fusion

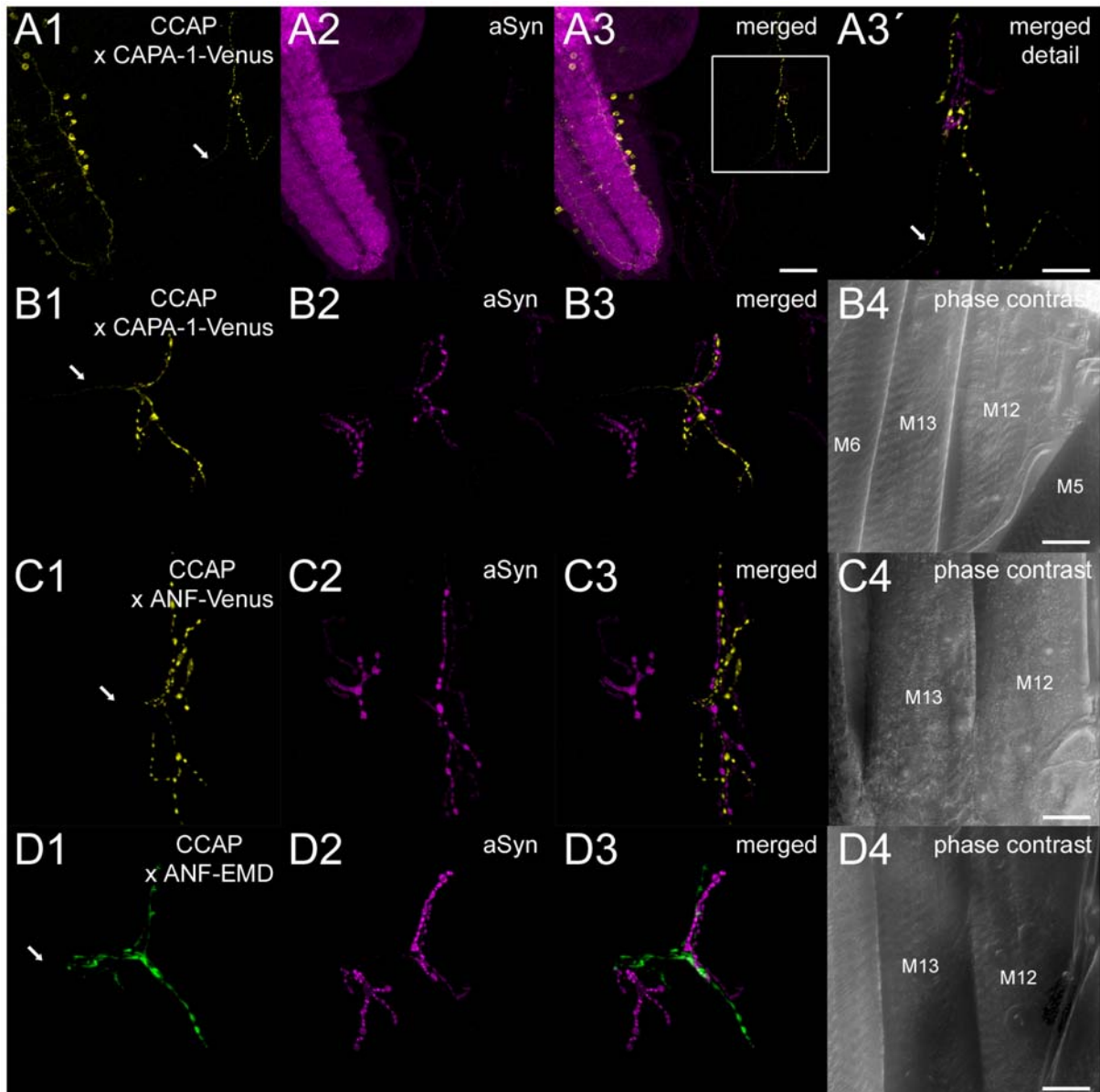


Figure 7: CCAP-GAL4-driven CAPA-1-Venus, ANF-Venus, and ANF-EMD at the body wall muscles of *Drosophila* larvae.

(A1-4) Confocal images showing CCAP-GAL4-driven CAPA-1-Venus in a filleted larvae (A1) immunolabeled against the presynaptic protein synapsin (aSyn; A2). A distinct subset of CCAP-GAL4 expressing neurons projects to the periphery and innervates the larval body wall muscles (A3). (A3') Enlargement of the boxed area in A3. (B1-4) CAPA-1-Venus-containing vesicles accumulate in peripheral endings close to synapsin-immunoreactive type I terminals at the body wall muscle M12. (C1-4) CCAP-GAL4-driven ANF-Venus and (D1-4) ANF-EMD in peripheral endings. Note that all of the peptide fusions primarily localize to the peripheral endings, while the peripheral projections themselves contain a comparatively low concentration of fluorescent vesicles (white arrows). Original images are maximum pixel intensity projections of confocal stacks. Scale bars in A1-A3: 50 μm ; others: 25 μm .

protein may require fewer space in the peptidergic vesicles than preproANF-based reporters, and thus allow a better visualization of peptidergic vesicles. In future experiments, we will use preproANF- and preproCAPA-1-Venus to monitor neuropeptide release *in vitro* and *in vivo*.

Acknowledgments

We are particularly grateful to Hannah Craig and Sean Sweeney for the kind gift of plasmids, and to John Ewer for the CCAP-GAL4 fly strain. We also thank Franz Grolig for maintenance of the confocal microscope, Renate Renkawitz-Pohl for providing fly housing, and Elwyn Issac and Uwe Homberg for general support. This work was supported by the Marie Curie Fellowship Association (Early stage training in Advanced Genetic Analyses) to MV and the Deutsche Forschungsgemeinschaft (DFG We 2652/2-2,3) to CW.

Methods

Plasmid construction

To generate pUAST_preproANF-Venus, a preproANF-EGFP cDNA fusion [6] in the pEGFP-N1 vector (Clontech, Saint-Germain-en-Laye, France) was used to amplify the preproANF cDNA by PCR using the following primer pair (Sigma-Aldrich, Haverhill, UK): 5'-GTCAGATCCGCTAGCGCTAC-3' (forward) and 5'-GTACCGGAAGCTGTTGCAG-3' (reverse). The resulting 535 bp preproANF PCR product comprised the EcoRI site of the pEGFP-N1 vector and the preproANF cDNA sequence encoding the amino acids SSCFGGRIDRIGASGLGCNSFRY. To prevent proteolytical cleavage of the ectopically expressed preproANF-Venus fusion protein, the PCR product did not include the nucleotides encoding the two carboxy-terminal amino acids Arg-Arg of ANF. These amino acids can act as cleavage sites for neuropeptide processing enzymes [37]. The preproANF PCR product was TA-cloned in-frame into the XcmI-digested pFX_Venus vector (kind gift of H. Craig, Leeds, UK; [38]) to obtain pFX_preproANF-Venus. For subcloning, the preproANF-Venus cDNA fusion into the pUAST vector [13], pFX_preproANF_Venus had to be restricted with BglII although the preproANF cDNA includes two internal BglII cleavage sites. Thus, pFX_preproANF-Venus was restricted with EcoRI and NotI to obtain the preproANF cDNA fragment, and with NotI and BglII to obtain the Venus cDNA fragment, respectively. Both the preproANF and the Venus cDNA fragments were then simultaneously cloned into the EcoRI- and BglII-restricted pUAST vector to generate pUAST_preproANF-Venus.

To obtain pUAST_preproCAPA-1-Venus, a cDNA clone in the pOT2 vector (GH28004; Berkeley *Drosophila* Genome Project Gold Collection, kind gift of Sean Sweeney, York, UK) served as template to amplify CAPA-1 by PCR using the following primer pair: 5'-AAATTCCCGGGTACTGCAGCC-3' (forward) and 5'-GAAGGCATAGAGCCCCATGTTG-3' (reverse). The resulting 316 bp preproCAPA-1 PCR product comprised the BglII site of the pOT2 vector and a partial CAPA-1 cDNA sequence encoding the amino acids GANMGLYAF. The GC-rich carboxyl terminus of the CAPA-1 cDNA which encodes the amino acids PRV (- essential for receptor binding -) was not included in the PCR product to improve PCR conditions and to prevent disadvantageous physiological effects of the final fusion protein. The resulting preproCAPA-1 PCR product was TA-cloned in-frame into the XcmI-digested pFX_Venus vector to obtain pFX_preproCAPA-1-Venus. Then, the preproCAPA-1-Venus cDNA fusion was excised from pFX_preproCAPA-1-Venus by BglII restriction, and inserted into the BglII- linearized and dephosphorylated pUAST vector.

Finally, both pUAST_preproANF-Venus and pUAST_preproCAPA-1-Venus were completely sequenced to check the exact orientation and sequence of the inserted cDNA fusions.

Fly strains

To generate transgenic flies, pUAST_preproANF-Venus or pUAST_preproCAPA-1-Venus were microinjected into *w1118* embryos by VANEDIS injection service (Oslo, Norway). After obtaining the injected larvae, 50 surviving flies of

each injection series were individually crossed to three *w¹¹¹⁸* flies of the appropriate gender. The resulting flies were checked for *w⁺*, an eye color marker indicative of transformation. To eliminate multiple P element insertions, all transgenic fly strains were backcrossed to *w¹¹¹⁸* flies for four successive generations. Then, homozygous stocks were established and the chromosomal locations of the P element insertions were determined by segregation analysis.

To obtain flies which carry the pUAST_preproANF-Venus or pUAST_preproCAPA-1-Venus transgene on the first and second chromosome, we generated homozygous flies that carried the P-element insertion on the first chromosome pair and the dominant negative markers *cyo* (curly wings) and *sp* (extra bristles on the sternopleurite) on the second chromosome pair. In subsequent crosses, the marked chromosomes were successively exchanged for those with the corresponding P-element insertion (a comparable crossing scheme is shown in Chapter IV). Progeny from crosses of *c929-*, *CCAP-* or *elav-GAL4* flies with UAS-preproANF-Venus, -preproCAPA-1-Venus, -preproANF-EMD ([14]; Bloomington Stock Center, donated by D. Deitcher), or UAS-GFP (Bloomington Stock Center, donated by C. Goodman) flies were used for immunocytochemistry and Western blot. All flies were reared on standard cornmeal agar medium and yeast under a 12:12 h light:dark regime at 18 or 25°C.

Immunocytochemistry and microscopy

For whole-mount immunocytochemistry, CNS of third instar larvae were dissected in ice-cold 0.1 M sodium phosphate buffered saline (PBS; pH 7.2) and fixed with 4 % paraformaldehyde in PBS for 2 h at 4°C. After several washes with PBS containing 1 % TritonX (PBT), tissue was incubated with rabbit-anti-GFP primary antiserum (MBL International, Woburn, MA) at a dilution of 1:500, and 5 % normal goat serum (NGS) in PBT for 1-3 days at 4°C. The tissue was then washed repeated times with PBT, followed by overnight incubation with Cy3- or Cy5-conjugated AffiniPure goat-anti-rabbit secondary antibody (Jackson ImmunoResearch, West Grove, PA) at a dilution of 1:300, and 1 % NGS in PBT at 4°C. The following day, tissue was washed several times with PBT, twice with 0.01 M phosphate buffered saline (PBS) and mounted in glycerol:PBS (80:20).

Confocal stacks were acquired on a confocal laser scanning microscope (Leica TCS SP2, Leica Microsystems, Wetzlar, Germany) with a 40x objective (HCX PL APO 40x, N.A. 1.25) at 512 x 512 pixel resolution in 0.5 - 1 µm steps along the z-axis. A false color map was applied to the maximum pixel intensity projections, and brightness and contrast were adjusted. Snapshots were taken in Leica CSL (Leica Microsystems, Wetzlar, Germany) and further processed with Adobe Photoshop 7.0 (Adobe Systems Inc., San Jose, CA) or ImageJ 1.34s (NIH, public domain: <http://rsb.info.nih.gov/ij/>).

Western blot analysis

The CNS of ~50 third instar larvae were homogenized in ice-cold 10 mM Tris-HCl (pH 7.4) containing 10 mM NaVO₃ (phosphatase inhibitor) and 10 mM phenylmethylsulfonyl fluoride (protease inhibitor). Total protein concentration of each sample was determined after Bradford [39], and then 10 µg were boiled for 3 min in an equal volume of reducing sample buffer (500 mM Tris-HCl, pH 6.8, containing 4% sodium dodecyl sulfate (SDS), 5% 2-mercaptoethanol, 20% glycerol, and 0.2% bromophenol blue). Samples were run on a discontinuous SDS-12.5% polyacrylamide gel and blotted onto Optitran BA-S 83 nitrocellulose membranes (Carl Roth GmbH & CoKG, Karlsruhe, Germany). Blots were blocked in 0.1 M phosphate-buffered saline (PBS; pH 7.4) plus 0.1% Tween 20, and 5% SlimFast vanilla powder (SlimFast, Englewood, NJ) for 2 h at room temperature (RT). Then, the blots were incubated with a 1:500 dilution of the polyclonal rabbit-anti-GFP (MBL International, Woburn, MA) antiserum or with a 1:3000 dilution of the polyclonal rabbit-anti-GFP (abcam, Cambridge, UK) antiserum in PBS containing 0.05% Tween 20 overnight at 4° C. The next day, the blots were washed in PBS containing 0.05% Tween 20, 1% Triton X-100, and 1% SDS (PBT) for 45 min, and incubated with a 1:5000 dilution of HRP-conjugated goat-anti-rabbit antibody (Jackson ImmunoResearch, West Grove, PA) in PBS containing 0.05% Tween 20

Chapter VI

for 2 h at RT. After several washes in PBT, the blots were incubated with chemiluminescent substrate according to the SuperSignal instructions (PIERCE, Rockford, IL), and exposed to Fuji Super RX film (FUJIFILM, Düsseldorf, Germany). Pictures were processed with Adobe Photoshop 7.0 (Adobe Systems Inc., San Jose, CA) and schematic drawings were created with Adobe Illustrator CS (Adobe Systems Inc., San Jose, CA).

References

1. Hamasaka Y, Wegener C, Nässel DR (2005) GABA modulates *Drosophila* circadian clock neurons via GABA(B) receptors and decreases in calcium. *J Neurobiol* 65: 225-240.
2. Hamasaka Y, Nässel DR (2006) Mapping of serotonin, dopamine, and histamine in relation to different clock neurons in the brain of *Drosophila*. *J Comp Neurol* 494: 314-330.
3. Kim YJ, Žitňan D, Galizia CG, Cho KH, Adams ME (2006) A command chemical triggers an innate behavior by sequential activation of multiple peptidergic ensembles. *Curr Biol* 16: 1395-1407.
4. Vömel M, Wegener C (2007) Neurotransmitter-induced changes in the intracellular calcium concentration suggest a differential central modulation of CCAP neuron subsets in *Drosophila*. *Dev Neurobiol* 67: 792-808.
5. Wegener C, Hamasaka Y, Nässel DR (2004) Acetylcholine increases intracellular Ca²⁺ via nicotinic receptors in cultured PDF-containing clock neurons of *Drosophila*. *J Neurophysiol* 91: 912-923.
6. Burke NV, Han W, Li D, Takimoto K, Watkins SC, Levitan ES (1997) Neuronal peptide release is limited by secretory granule mobility. *Neuron* 19: 1095-1102.
7. Abney JR, Meliza CD, Cutler B, Kingma M, Lochner JE, Scalettar BA (1999) Real-time imaging of the dynamics of secretory granules in growth cones. *Biophys J* 77: 2887-2895.
8. Han W, Ng YK, Axelrod D, Levitan ES (1999) Neuropeptide release by efficient recruitment of diffusing cytoplasmic secretory vesicles. *Proc Natl Acad Sci U S A* 96: 14577-14582.
9. Lu X, Ellis-Davies GC, Levitan ES (2003) Calcium requirements for exocytosis do not delimit the releasable neuropeptide pool. *Cell Calcium* 33: 267-271.
10. Ng YK, Lu X, Levitan ES (2002) Physical mobilization of secretory vesicles facilitates neuropeptide release by nerve growth factor-differentiated PC12 cells. *J Physiol* 542: 395-402.
11. Ng YK, Lu X, Watkins SC, Ellis-Davies GC, Levitan ES (2002) Nerve growth factor-induced differentiation changes the cellular organization of regulated peptide release by PC12 cells. *J Neurosci* 22: 3890-3897.
12. Ng YK, Lu X, Gulacsi A, Han W, Saxton MJ, Levitan ES (2003) Unexpected mobility variation among individual secretory vesicles produces an apparent refractory neuropeptide pool. *Biophys J* 84: 4127-4134.
13. Brand AH, Perrimon N (1993) Targeted gene expression as a means of altering cell fates and generating dominant phenotypes. *Development* 118: 401-415.
14. Rao S, Lang C, Levitan ES, Deitcher DL (2001) Visualization of neuropeptide expression, transport, and exocytosis in *Drosophila melanogaster*. *J Neurobiol* 49: 159-172.
15. Shakiryanova D, Tully A, Hewes RS, Deitcher DL, Levitan ES (2005) Activity-dependent liberation of synaptic neuropeptide vesicles. *Nat Neurosci* 8: 173-178.
16. Shakiryanova D, Tully A, Levitan ES (2006) Activity-dependent synaptic capture of transiting peptidergic vesicles. *Nat Neurosci* 9: 896-900.
17. Shakiryanova D, Klose MK, Zhou Y, Gu T, Deitcher DL, Atwood HL, Hewes RS, Levitan ES (2007) Presynaptic ryanodine receptor-activated calmodulin kinase II increases vesicle mobility and potentiates neuropeptide release. *J Neurosci* 27: 7799-7806.
18. Levitan ES, Lanni F, Shakiryanova D (2007) *In vivo* imaging of vesicle motion and release at the *Drosophila* neuromuscular junction. *Nat Protoc* 2: 1117-1125.
19. Heifetz Y, Wolfner MF (2004) Mating, seminal fluid components, and sperm cause changes in vesicle release in the *Drosophila* female reproductive tract. *Proc Natl Acad Sci U S A* 101: 6261-6266.
20. Kula E, Levitan ES, Pyza E, Rosbash M (2006) PDF cycling in the dorsal protocerebrum of the *Drosophila* brain is not necessary for circadian clock function. *J Biol Rhythms* 21: 104-117.

21. Husain QM, Ewer J (2004) Use of targetable gfp-tagged neuropeptide for visualizing neuropeptide release following execution of a behavior. *J Neurobiol* 59: 181-191.
22. Nagai T, Iyata K, Park ES, Kubota M, Mikoshiba K, Miyawaki A (2002) A variant of yellow fluorescent protein with fast and efficient maturation for cell-biological applications. *Nat Biotechnol* 20: 87-90.
23. Sturman DA, Shakiryanova D, Hewes RS, Deitcher DL, Levitan ES (2006) Nearly neutral secretory vesicles in *Drosophila* nerve terminals. *Biophys J* 90: L45-L47.
24. Gauthier SA, Hewes RS (2006) Transcriptional regulation of neuropeptide and peptide hormone expression by the *Drosophila dimmed* and *cryptocephal* genes. *J Exp Biol* 209: 1803-1815.
25. Hewes RS, Park D, Gauthier SA, Schaefer AM, Taghert PH (2003) The bHLH protein Dimmed controls neuroendocrine cell differentiation in *Drosophila*. *Development* 130: 1771-1781.
26. O'Brien MA, Taghert PH (1998) A peritracheal neuropeptide system in insects: release of myomodulin-like peptides at ecdysis. *J Exp Biol* 201: 193-209.
27. Park JH, Schroeder AJ, Helfrich-Förster C, Jackson FR, Ewer J (2003) Targeted ablation of CCAP neuropeptide-containing neurons of *Drosophila* causes specific defects in execution and circadian timing of ecdysis behavior. *Development* 130: 2645-2656.
28. Luan H, Lemon WC, Peabody NC, Pohl JB, Zelensky PK, Wang D, Nitabach MN, Holmes TC, White BH (2006) Functional dissection of a neuronal network required for cuticle tanning and wing expansion in *Drosophila*. *J Neurosci* 26: 573-584.
29. Ewer J, Reynolds S (2002) Neuropeptide control of molting in insects. In: Pfaff DW, Arnold AP, Fahrbach SE, Etgen AM, Rubin RT, editors. *Hormones, Brain and Behavior*. San Diego, CA: Academic Press. pp. 1-92.
30. Ewer J, Truman JW (1996) Increases in cyclic 3', 5'-guanosine monophosphate (cGMP) occur at ecdysis in an evolutionarily conserved crustacean cardioactive peptide-immunoreactive insect neuronal network. *J Comp Neurol* 370: 330-341.
31. Santos JG, Vömel M, Struck R, Homberg U, Nässel DR, Wegener C (2007) Neuroarchitecture of peptidergic systems in the larval ventral ganglion of *Drosophila melanogaster*. *PLoS ONE* 2: e695.
32. Löhr R, Godenschwege T, Buchner E, Prokop A (2002) Compartmentalization of central neurons in *Drosophila*: a new strategy of mosaic analysis reveals localization of presynaptic sites to specific segments of neurites. *J Neurosci* 22: 10357-10367.
33. Sykes PA, Condron BG (2005) Development and sensitivity to serotonin of *Drosophila* serotonergic varicosities in the central nervous system. *Dev Biol* 286: 207-216.
34. Yao KM, White K (1994) Neural specificity of elav expression: defining a *Drosophila* promoter for directing expression to the nervous system. *J Neurochem* 63: 41-51.
35. Southey BR, Amare A, Zimmerman TA, Rodriguez-Zas SL, Sweedler JV (2006) NeuroPred: a tool to predict cleavage sites in neuropeptide precursors and provide the masses of the resulting peptides. *Nucleic Acids Res* 34: W267-W272.
36. Hodge JJ, Choi JC, O'Kane CJ, Griffith LC (2005) Shaw potassium channel genes in *Drosophila*. *J Neurobiol* 63: 235-254.
37. Veenstra JA (2000) Mono- and dibasic proteolytic cleavage sites in insect neuroendocrine peptide precursors. *Arch Insect Biochem Physiol* 43: 49-63.
38. Gengyo-Ando K, Yoshina S, Inoue H, Mitani S (2006) An efficient transgenic system by TA cloning vectors and RNAi for *C. elegans*. *Biochem Biophys Res Commun* 349: 1345-1350.
39. Bradford MM (1976) A rapid and sensitive method for the quantitation of microgram quantities of protein utilizing the principle of protein-dye binding. *Anal Biochem* 72: 248-254.

Acknowledgments

I am particularly grateful to Dr. Christian Wegener for scientific guidance during my doctoral thesis and the possibility to follow own ideas.

I am also grateful to Prof. Dr. Elwyn Isaac and Dr. Josie Thomas for their excellent support during my stay in Leeds and the opportunity to improve my English.

I thank Prof. Dr. Uwe Homberg and Prof. Dr. Joachim Schachtner for surveying my thesis and continuous support during my scientific career, and Prof. Dr. Renate Renkawitz-Pohl and Prof. Dr. Monika Hassel for their participation in the examination commission.

Furthermore, I thank Prof. Dr. Renate Renkawitz-Pohl and Ruth Hyland for providing fly housing, Franz Grolig for maintenance of the confocal microscope, and various donors of fly lines and antibodies, which are listed in the corresponding chapters.

I am happy about spending my time with the people in the labs of Uwe Homberg, Elwyn Isaac, Joachim Schachtner, Monika Stengl, and Christian Wegener.

Most of all, I thank Steffi, my family, and my friends for their assistance and moral support.

Erklärung

Ich versichere, dass ich meine Dissertation

Neuroarchitecture and central regulation of peptidergic systems in the ventral ganglion of *Drosophila melanogaster*

selbständig, ohne unerlaubte Hilfe angefertigt und mich dabei keiner anderen als der von mir ausdrücklich bezeichneten Quellen und Hilfen bedient habe.

Die Dissertation wurde in der jetzigen oder einer ähnlichen Form noch bei keiner anderen Hochschule eingereicht und hat noch keinen sonstigen Prüfungszwecken gedient.

Marburg, den

(Matthias Vömel)

Curriculum vitae

Matthias Vömel

address : FB Biologie, Tierphysiologie
Karl-von-Frisch Straße
35032 Marburg
Germany

phone : +49 6421 28 23416

email : Voemel@students.uni-marburg.de

Personal

Date and place of birth : 30.09.1977, Seeheim-Jugenheim (Germany)

Marital status : Single

CV

2004 – present Doctoral thesis, Philipps-Universität Marburg, Germany

2003.12. Diploma, Philipps-Universität Marburg, Germany;
Title of diploma thesis: Expression of different guanylyl cyclases in the brain of the sphinx moth *Manduca sexta* during metamorphosis

1998 – 2003 Undergraduate, Philipps-Universität Marburg, Germany

1997 – 1998 Military service, Speyer, Germany

1988 – 1997 High School, Tilemannschule Limburg, Germany

Academic appointment

2007 – 2008 Research assistant, Philipps-Universität Marburg, Germany

Special training

2006.10. – 2007.1. Early stage training in Advanced Genetic Analysis, University of Leeds, UK.
This work was supported by the Marie Curie Fellowship Association to MV.

Teaching

Tutor in undergraduate courses:

- Animal physiology (muscle physiology, nerve physiology, and chronobiology)
- Zoology (morphology of vertebrates)

Publications

Reviewed articles:

- Vömel M, Wegener C. (2008). Neuroarchitecture of aminergic systems in the larval ventral ganglion of *Drosophila melanogaster*. PLoS ONE 3(3): e1848.
- Utz S, Huetteroth W, Vömel M, Schachtner J. (2008). Mas-allatotropin in the developing antennal lobe of the sphinx moth *Manduca sexta*: distribution, time course, developmental regulation, and colocalization with other neuropeptides. Dev Neurobiol 68: 123-142.

- Santos JG, Vömel M, Struck R, Homberg U, Nässel DR, Wegener C. (2007). Neuroarchitecture of peptidergic systems in the larval ventral ganglion of *Drosophila melanogaster*. PLoS ONE 2(8): e695.
- Vömel M, Wegener C. (2007). Neurotransmitter-induced changes in the intracellular calcium concentration suggest a differential central modulation of CCAP neuron subsets in *Drosophila*. Dev Neurobiol 67: 792-809.

Abstracts:

- Wegener C, Vömel M. (2007). Calcium imaging in primary cell culture and *in situ* suggests a differential transmitter-mediated regulation of CCAP neuron subsets in *Drosophila*. 7th NWG meeting, Göttingen (Germany), T9-4B.
- Vömel M, Wegener C. (2006). *In vitro* and *in situ* characterization of transmitter-induced Ca²⁺-responses in CCAP-expressing neurons of *Drosophila melanogaster*. 11th European *Drosophila* Neurobiology Conference, Leuven (Belgium), P93.
- Gonzáles-Santos J, Vömel M, Homberg U, Nässel D, Wegener C. (2006). Three-dimensional charting of peptidergic neurons in the larval ventral nerve cord of the fruit fly, *Drosophila melanogaster*. 11th European *Drosophila* Neurobiology Conference, Leuven (Belgium), P83.
- Vömel M, Wegener C. (2005). Acetylcholine and glutamate trigger intracellular Ca²⁺-rises in CCAP-expressing neurons of *Drosophila melanogaster*. IVth International Conference on Arthropods, Zakopane (Poland), P47.
- Wegener C, Gonzáles-Santos J, Vömel M, Predel R. (2005). Chemical and morphological characterization of peptidergic systems in the larval ventral ganglion of *Drosophila melanogaster*. 98th DZG meeting, Bayreuth (Germany), 1_V_1.01, p18.
- Winterhagen P, Vömel M, Schachtner J. (2002). Various guanylyl cyclases might be involved in cGMP regulation in the developing antennal lobe of the sphinx moth *Manduca sexta*. 95th DZG meeting, Halle (Germany), Zoology 105 Suppl. V, p47.